Imaging the cellular dynamics of morphogenesis: from early cleavage stages to embryogenesis

PhD thesis submitted for the degree of Doctor of Philosophy in Cell and Developmental Biology

University College London

Adam A. Moverley

Declaration

I, Adam Moverley confirm that the work presented in this thesis is my own. Where information has been derived from other sources, I confirm that this has been indicated in the thesis.

Abstract

Throughout the history of developmental biology, the microscope has consistently proven one of the most powerful tools available to researchers. Here we use high resolution microscopy to probe cellular behaviours during tissue patterning, using the preimplantation mouse and chicken embryos as model systems.

During preimplantation development the segregation of cells into inner and outer positions of the embryo is key to establishing the inner cell mass (ICM) and trophectoderm. Using the mouse embryo as a model, we found that the nuclear lamina links to the cell cortex via an F-actin meshwork, and Lamin-A levels are upregulated in response to actomyosin contractility. When cells internalise, cells lose their contractile apical cortex and Lamin-A is downregulated. This causes the localisation of Formin-2 to the cytoplasm and increases cytoplasmic F-actin. This, in turn stabilises Amot, causing Yap phosphorylation and acquisition of ICM identity. In outer cells, Lamin-A levels remain high, preventing Yap phosphorylation, leading to Cdx2 expression and trophectoderm identity.

Later in development, the axis of the embryo is laid down in head-to-tail order. During this time, the somites form in pairs on either side of the midline. Somites are transient blocks of tissue that form as the mesenchymal cells of the presomitic mesoderm (PSM) undergo mesenchymal-to-epithelial transition (MET). Using scanning electron microscopy (SEM), immunofluorescence, and confocal microscopy we show that cells of the PSM undergo a gradual MET that begins earlier than previously reported. Epithelialisation began in the dorsal and medial PSM, progressing to the anterior and finally the lateral PSM. Inhibition of Notch signalling stops the oscillatory expression of clock genes but does not change epithelialisation dynamics in the PSM. Finally, live imaging was used to examine the relationship between cell cycle timing and segmentation and demonstrate the presence of a stem cell population in the posterior part of the node.

Impact statement

The nuclear lamina plays numerous roles in the proper function of the nucleus. This includes structural roles ensuring its integrity, size and shape, as well as shaping chromatin organization and gene expression. Recent research has explored the potential of the nuclear lamina to behave as a mechanosensor. However, much of this work has been performed in tissue culture. Here we show a novel function of the nuclear lamina behaving as a mechanosensor during preimplantation development of the intact mouse embryo. A robust understanding of preimplantation development is essential for successful IVF and assisted reproduction techniques. These new insights into the specification of the ICM and trophectoderm may lead to culture supplements and protocol adaptations that support proper mechano-signalling in vitro, thereby increasing embryo viability. Furthermore, this deepens our understanding of the formation of pluripotent embryonic stem cells which has implications for research into organoids and regenerative medicine. By modulating substrate stiffness or cytoskeletal properties in culture this might assist in maintaining pluripotency by more accurately mimicking conditions *in vivo*.

Somitogenesis lays down the foundation for the vertebral column and parts of the nervous system. Failures in this process can lead to numerous congenital disorders, including scoliosis, kyphosis and lordosis, caused by the formation of hemivertebrae or wedge vertebrae. Improper somite border formation may result in vertebral synostosis and incorrect expression of Hox genes can lead to homeotic transformations, such as cervical ribs in Klippel-Feil syndrome. A deeper understanding of these processes is therefore of medical significance. We also characterized the formation and behaviour of a novel stem cell niche residing in the posterior node, which has implications for regenerative medicine. In carrying out this research we developed a modified variant of New's culture method for high resolution live imaging. This could be employed by future researchers to study many aspects of axial development beyond somite formation, such as the formation of the neural tube and notochord and neural crest migration.

UCL Research Paper Declaration Form: referencing the doctoral candidate's own published work(s)

1. **For a research manuscript that has already been published** (if not yet published, please skip to section 2):
   (a) **What is the title of the manuscript?** The nuclear lamina couples mechanical forces to cell fate in the preimplantation embryo via actin organization
   (b) **Please include a link to or doi for the work**: https://doi.org/10.1038/s41467-023-38770-5
   (c) **Where was the work published**? Nature Communications
   (d) **Who published the work**? Nature Portfolio
   (e) **When was the work published**? 29th May 2023
   (f) **List the manuscript's authors in the order they appear on the publication**: Robin M. Skory* Adam A. Moverley* Goli Ardestani, Yanina Alvarez, Ana Domingo-Muelas, Oz Pomp, Blake Hernandez, Piotr Tetlak, Stephanie Bissiere, Claudio D. Stern, Denny Sakkas & Nicolas Plachta
   *These authors contributed equally: Robin M. Skory, Adam A. Moverley
   (g) **Was the work peer reviewed**? Yes
   (h) **Have you retained the copyright**? Creative Commons Attribution 4.0 International License
   (i) **Was an earlier form of the manuscript uploaded to a preprint server (e.g.medRxiv)? If 'Yes', please give a link or doi. If 'No', please seek permission from the relevant publisher and check the box next to the below statement**: No.
   ☒ I acknowledge permission of the publisher named under 1d to include in this thesis portions of the publication named as included in 1c.
2. **For a research manuscript prepared for publication but that has not yet been published (if already published, please skip to section 3):**
3. **For multi-authored work, please give a statement of contribution covering all authors (if single-author, please skip to section 4):** R.M.S. and A.A.M. wrote the manuscript. R.M.S., A.A.M., Y.A., O.P., P.T., B.H., A.D.-M. and S.B. performed the mouse work. G.A., and D.S. performed the human embryo work. D.S. supervised the human studies and C.D.S. and N.P. supervised the mouse studies. R.M.S. and A.D.-M. designed and created figure schemes.

4. **In which chapter(s) of your thesis can this material be found?** Chapter 2

e-Signatures confirming that the information above is accurate (this form should be co-signed by the supervisor/ senior author unless this is not appropriate, e.g. if the paper was a single-author work):

Candidate: Adam Moverley

Date: 18/03/2025

Supervisor/Senior Author signature (where appropriate): Nicolas Plachta

Date: 18/03/2025

UCL Research Paper Declaration Form: referencing the doctoral candidate's own published work(s)

1. **For a research manuscript that has already been published** (if not yet published, please skip to section 2):
   (a) **What is the title of the manuscript?** Sequential changes in cellular properties accompanying amniote somite formation
   (b) **Please include a link to or doi for the work**: https://doi.org/10.1111/joa.13791
   (c) **Where was the work published**? Journal of Anatomy
   (d) **Who published the work**? Wiley
   (e) **When was the work published**? 24th November 2022
   (f) **List the manuscript's authors in the order they appear on the publication**: Agnieszka M. Piatkowska, Kaustubh Adhikari, Adam A. Moverley, Mark Turmaine, James A. Glazier, Nicolas Plachta, Susan E. Evans, Claudio D. Stern
   (g) **Was the work peer reviewed**? Yes
   (h) **Have you retained the copyright**? Creative Commons Attribution 4.0 International License
   (i) **Was an earlier form of the manuscript uploaded to a preprint server (e.g.medRxiv)? If 'Yes', please give a link or doi. If 'No', please seek permission from the relevant publisher and check the box next to the below statement**: No.

   ☒ I acknowledge permission of the publisher named under 1d to include in this thesis portions of the publication named as included in 1c.
2. **For a research manuscript prepared for publication but that has not yet been published (if already published, please skip to section 3):**
3. **For multi-authored work, please give a statement of contribution covering all authors (if single-author, please skip to section 4):** A.M.P., A.A.M and C.D.S. wrote the manuscript. A.M.P and A.A.M. performed experiments. K.A performed data analysis. M.T assisted with SEM imaging. J.A.G., N.P., and S.E.E. advice and comments. C.D.S. acquired funding and supervised project.
4. **In which chapter(s) of your thesis can this material be found?** Chapter 3

e-Signatures confirming that the information above is accurate (this form should be co-signed by the supervisor/ senior author unless this is not appropriate, e.g. if the paper was a single-author work):

Candidate: Adam Moverley

Date: 18/03/2025

Supervisor/Senior Author signature (where appropriate): Claudio Stern

Date: 18/03/2025

UCL Research Paper Declaration Form: referencing the doctoral candidate's own published work(s)

1. **For a research manuscript that has already been published** (if not yet published, please skip to section 2):
   (a) **What is the title of the manuscript?** The embryonic node behaves as an instructive stem cell niche for axial elongation
   (b) **Please include a link to or doi for the work**: https://doi.org/10.1073/pnas.2108935119
   (c) **Where was the work published**? PNAS
   (d) **Who published the work**? United States National Academy of Sciences
   (e) **When was the work published**? 31st January 2022
   (f) **List the manuscript's authors in the order they appear on the publication**: Tatiana Solovieva, Hui-Chun Lu, Adam Moverley, Nicolas Plachta, and Claudio D. Stern
   (g) **Was the work peer reviewed**? Yes
   (h) **Have you retained the copyright**? Creative Commons Attribution 4.0 International License
   (i) **Was an earlier form of the manuscript uploaded to a preprint server (e.g.medRxiv)? If 'Yes', please give a link or doi. If 'No', please seek permission from the relevant publisher and check the box next to the below statement**: Yes. https://doi.org/10.1101/2020.11.10.376913
   ☐ I acknowledge permission of the publisher named under 1d to include in this thesis portions of the publication named as included in 1c.
2. **For a research manuscript prepared for publication but that has not yet been published (if already published, please skip to section 3):**
3. **For multi-authored work, please give a statement of contribution covering all authors (if single-author, please skip to section 4):** T.S. and C.D.S. designed research; T.S. and A.M. performed research; N.P. contributed new reagents/analytic tools; T.S. and H.-C.L. analyzed data; N.P. guided A.M. with microscopy and analysis software for movies; T.S. and C.D.S. wrote the paper; and C.D.S. obtained funding and provided overall supervision of the team and project.
4. **In which chapter(s) of your thesis can this material be found?** Chapter 3

e-Signatures confirming that the information above is accurate (this form should be co-signed by the supervisor/ senior author unless this is not appropriate, e.g. if the paper was a single-author work):

Candidate: Adam Moverley

Date: 18/03/2025

Supervisor/Senior Author signature (where appropriate): Claudio Stern

Date: 18/03/2025

Acknowledgements

This thesis would not exist if it wasn't for the talented researchers I had the privilege of working alongside.

At the bench, this includes Yanina Alvarez, Agnieszka Piatkowska, Tatiana Solovieva, Ana Domingo-Muelas, and Robin Skory.

In their supervisory roles, Claudio Stern and Nicolas Plachta provided constant support and insight. In particular, I would like to thank Claudio, from which supernatural realm he conjured the patience to meet with me each week while I wrote this thesis, I will never know.

The mouse work in this study would not have been possible without the steady hands of Piotr Tetlak harvesting embryos and performing microinjections every week.

Thanks to any friends and family who supported me through this process, and thanks to my parents, who put a roof over my head while I wrote this.

Contents

List of figures

Chapter 1. General Introduction

1.1. Tissue patterning during development

The development of a complex organism from a single cell requires the emergence of intricate spatial patterns. To produce these patterns, cells must behave appropriately based on limited information, namely, their current internal state, determined by lineage history, and signals confined to their immediate environment and from neighbouring cells. How cells are able to coordinate given these limitations is a fascinating question central to developmental biology. Broadly speaking, the mechanisms that have been proposed to coordinate tissue patterning can be divided into two categories: (a) those using long range signalling to relay positional information and define boundaries or regions of cellular behaviour, and (b) self-organising patterns that rely on short range, local signalling and direct cell-cell interactions.

1.1.1. Positional information and boundaries

The concept of positional information was first proposed by Lewis Wolpert (1969), where he outlined the French Flag problem and described how patterns might be specified across a field of cells in the embryo. Shortly afterwards, Francis Crick (1970) outlined how this might be achieved through the diffusion of a morphogen to produce a gradient and estimated this may be sufficient to relay positional information over distances up to 1mm, or 100 cells. Since then, this concept has become central to many models of pattern formation and molecular evidence for morphogen gradients has been shown in a variety of contexts, including Bicoid's role in establishing the anterior-posterior axis of the Drosophila blastoderm (Driever and Nüsslein-Volhard, 1988), a BMP gradient in the dorsal-ventral patterning of the frog embryo (Piccolo et al., 1996; Sasai et al., 1995), Sonic hedgehog (Shh) in the antero-posterior patterning of the vertebrate limb (Riddle et al., 1993) and dorsal-ventral patterning of the neural tube (Dessaud et al., 2010).

Despite the number of developmental models that rely on morphogen gradients, as well as the numerous gradients observed experimentally in embryos, Kerszberg and Wolpert (2007) argue that it is unlikely that gradients created by morphogens diffusing through extracellular space are sufficient to specify boundaries with the precision and robustness we observe in development, and it is likely that additional mechanisms are at play. An example that illustrates this is the well characterised, exponential gradient

of the transcription factor Bicoid in the Drosophila blastoderm (Driever and Nüsslein-Volhard, 1988). Unlike most other proposed morphogen gradients, this gradient is produced in a syncytium, meaning it does not have to contend with the additional complications introduced by having to diffuse through extracellular space. Despite this, the expression pattern of gap gene Hunchback, a target gene of Bicoid, is specified with greater accuracy than the gradient of Bicoid itself, suggesting it is determined by more than the concentration of Bicoid at a given point in space (Houchmandzadeh et al., 2002). Later studies showed that this is likely to be achieved by communication between nuclei to further coordinate boundary position (Gregor et al., 2007a, 2007b).

In Drosophila, Wingless provides positional information necessary for patterning the wing disc. However, rather than diffusing freely, a gradient of Wingless is established through a restricted diffusion mechanism, binding to the glypicans Dally and Dally-like protein and migrating along the epithelial surface by 'hopping' from one glypican to another (Han et al., 2005). Another study examining Wingless in the imaginal disc found that Wingless associates with lipophorins, facilitating its movement over longer distances (Panáková et al., 2005). Together, this suggests that patterning of the imaginal disc requires at least two additional mechanisms to modulate the diffusion of Wingless in order to pattern the wing correctly. It has been suggested that rather than measuring the concentration of morphogen, cells respond to total signalling over a period of time, which may reduce the amount of noise in the signal (Meinhardt, 1978).

Evidence for this has been demonstrated in the patterning of the vertebrate limb, where the identity of digits, particularly digits 4 and 5, are determined not only by the concentration of Shh, but also the duration of exposure of Shh. Experiments demonstrated that a high concentration of Shh alone was not sufficient to change digit identity and that multiple, short exposures to Shh suggests that cells retain a 'memory' of previous stimulation (Harfe et al., 2004). Similarly, in the neural tube, where it was previously thought that domains are specified by the concentration of Shh produced by the notochord, it has been shown that response the Shh is dynamic and varies with the duration of the signal. Exposure to Shh in the ventral neural tube initially leads to expression of OLIG2, associated with motor neuron progenitors, in both the motor neuron progenitor domain and the V3 domain. It is only after exposure to a high concentration of Shh for an extended period that cells of the V3 domain lose expression of OLIG2 and begin expressing their expected marker NKX2.2 (Dessaud

et al., 2007). Further evidence has recently demonstrated in cultured cells, using optogenetics to stimulate FGF signalling dynamics. In this system, pluripotent embryonic stem cells retained a 'memory' of previous signals and were agnostic to different signalling intensities and dynamics, instead integrating the total signal received over a period of time (Arekatla et al., 2023). Another mechanism by which this could be achieved was recently proposed and outlines how cells of the chick epiblast might interpret a morphogen gradient through interactions with neighbouring cells (Lee et al., 2022). This model, referred to as the 'neighbourhood watch' model, suggests that instead of determining their position by assessing morphogen concentration autonomously, instead cells may sense the concentration collectively by relating the concentration of morphogen observed by themselves to the concentration observed by their neighbours.

1.1.2. Scaling in pattern formation

Despite natural variation in the size of organisms, patterning can scale and remain proportional. The ability of patterns to scale has been challenged further through experimentation, with organisms showing the ability to scale after more extreme perturbations that alter the size of an organism beyond naturally occurring size variation (Cooke, 1975; Driesch, 1892; Holtfreter, 1938; Spemann, 1903). An early question explored by developmental biologists was that of mosaic versus regulative development. Mosaic development suggests that the fate of each cell is predetermined, and that loss of part of the embryo will mean a corresponding loss in the final organism. Regulative development proposes that cells can change their behaviour according to their environment and show plasticity, meaning loss of a part of an organism may be compensated for by other cells. Han Driesch (1892) showed that by separating the blastomeres of a 2-cell sea urchin embryo, each cell was able to give rise to a smaller, but complete and properly proportioned organism. This supported the theory of regulative development and showed that sea urchins were capable of size-invariant patterning even when the size of the organism was reduced by half.

The ability for organisms to size-regulate had been well established for many years before any mechanism was proposed to explain it. Renewed discussion of the mechanisms behind pattern scaling came with the publication of highly influential models of pattern formation, including reaction diffusion systems (Gierer and

Meinhardt, 1972; Turing, 1952) and the concept of positional information and the French flag model (Wolpert, 1969). While these models could explain how patterns might be achieved, their inability to scale suggested they were likely incomplete (a fact highlighted by Wolpert in his original paper). Since Wolpert's original proposal, several mechanisms have been proposed by which a morphogen gradient may be regulated in order to achieve size invariant patterning.

Models have outlined how two morphogen gradients in opposing directions could create patterning that can adjust to the size of the field, with cells measuring the ratio between the two signals (McHale et al., 2006). It has also been proposed that a highly diffusible moderator could regulate the activity of a morphogen (Rasolonjanahary and Vasiev, 2018, 2016). Assuming the total amount of moderator produced is invariant with respect to tissue size, then the mean concentration of the moderator would be higher in smaller tissues and more diffuse in larger tissues. This could allow for regulation of a morphogen by mechanisms such as sequestration or competitive binding to a receptor, producing the correct scaling. Finally, it has been proposed that scaling could be controlled with a feedback mechanism (Ben-Zvi and Barkai, 2010). In this model there is an expander that regulates the activity of the morphogen gradient. The range of the morphogen can be increased by the expander molecule, by modulating the diffusion or degradation of the morphogen. In turn, the expander is negatively regulated by the presence of the morphogen. In smaller embryos, high concentrations of the morphogen suppress the expander activity, and in larger embryos, where the morphogen is more diffuse, increased activity of the expander extends the range of the morphogen gradient.

Experimental evidence consistent with the expander model has been obtained in the dorsal-ventral patterning of Xenopus embryos, in which BMP interacting with anti-dorsalising morphogenetic protein (ADMP) creates a self-regulating feedback system that shapes the BMP gradient (Reversade and De Robertis, 2005). It has also been demonstrated that Sizzled, a highly diffusible BMP target, acts to stabilise Chordin by inhibiting its degradation (Inomata et al., 2013). This behaviour also matches the expander model, with Sizzled acting to expand Chordin expression at the dorsal side of the embryo if the BMP gradient extends too far. It has been proposed ADMP and Sizzled work in tandem, regulating BMP and Chordin in a 'double-expander' mechanism (Ben-Zvi et al., 2014).

1.1.3. Self-organising patterns

Perhaps the most famous model describing a self-organising system is the reaction-diffusion model proposed by Alan Turing (1952). Turing's original model consisted of two components, a self-enhancing, slow diffusing 'activator' and a fast diffusing 'inhibitor' that is both produced by, and suppresses, the activator. Turing's equations showed that a small fluctuation in an otherwise homogeneous system could become amplified, spontaneously generating patterns in what he termed 'diffusion-driven instability' (Turing, 1952). By adjusting parameters such as the diffusion coefficients of the activator and inhibitor, as well as their production and decay rates, this simple, two component system has been shown to produce a remarkable number of the patterns seen in nature (Meinhardt, 2009, 1982; Murray, 2002). Despite this ability, for a long time there was little molecular evidence to support their existence in biological systems. The first compelling molecular evidence was the demonstration that a reaction-diffusion system is responsible for the pattern of hair follicle formation in mice (Sick et al., 2006). Here it was shown that Wnt and its inhibitor DKK interact to produce evenly spaced regions of stable Wnt expression where hair follicles form. Shortly afterwards it was demonstrated that skin pigmentation in zebrafish is coordinated by a reaction-diffusion mechanism (Yamaguchi et al., 2007). This study also demonstrates the ability of self-organising systems to repair themselves when part of the pattern is lost.

It has been argued that the prevalence of reaction-diffusion systems in biological patterning may be underestimated because there is a perceived gap between the complex signalling networks observed experimentally and the idealised two component mathematical model presented by Turing (Kondo and Miura, 2010). Despite the apparent complexity of many biological networks, they may, in essence, function as reaction-diffusion systems. Similarly, there are examples of self-organising systems acting in confined regions that do not generate fields of a pattern, but instead generate a single boundary using the same mechanism. For example, the system of self-enhancement and lateral inhibition is used to generate left right asymmetry in the mouse embryo (Nakamura et al., 2006).

It has been suggested that many developmental processes are governed by interactions between positional information and self-organising systems (Green and Sharpe, 2015; Lander, 2011). As described above, a Bicoid gradient provides

positional information to guide gap gene expression in the Drosophila blastoderm (Driever and Nüsslein-Volhard, 1988). More recent studies have shown that perturbing the Bicoid gradient by flattening the gradient (Ochoa-Espinosa et al., 2009) or mixing the syncytium by heating it unevenly (Lucchetta et al., 2008) did not cause the changes in gap gene expression that models would predict. It was later demonstrated that there are cross-regulatory interactions between gap genes that generate dynamic attractor states to position the expression patterns in a self-organising manner (Manu et al., 2009). This suggests that the role of Bicoid may be to provide the initial positional input for a system that then generates robust patterning through self-organisation.

1.2. Microscopy as a method to explore development

Since the light microscope was invented in the 17th century it has remained central to the fields of cell and developmental biology. Early light microscopes enabled Antonie van Leeuwenhoek (1679) to describe sperm cells and allowed us to visualize fertilisation, showing the fusion of gametes (Hertwig, 1876). Most modern imaging of development relies on fluorescence microscopy, both for fixed samples using fluorescently tagged antibodies or probes, and for live imaging, using genetically encoded fluorescent proteins. This, combined with confocal microscopy, allowing for optical sectioning and 3D reconstruction of samples, have become standard techniques in developmental biology.

Since the isolation of GFP from the jellyfish *Aequorea victoria* (Prasher et al., 1992) and dsRed from *Discosoma sp.* (Matz et al., 1999) numerous fluorescent proteins have been engineered with different properties useful for live imaging. In addition to proteins with varied excitation and emission spectra, proteins with specific characteristics have also been engineered, including bright and stable proteins such as tdTomato (Shaner et al., 2004) and StayGold (Hirano et al., 2022), and proteins that mature rapidly, making them effective reporters for genes with dynamic expression patterns, such as mVenus (Kremers et al., 2006) and Achilles (Yoshioka-Kobayashi et al., 2020). Photoactivatable and photo-switchable proteins such as paGFP (Patterson and Lippincott-Schwartz, 2002) and Dendra (Gurskaya et al., 2006) allow sub-populations of cells to be labelled and tracked. Photoactivatable fluorescent proteins can also be used to refine noise sensitive techniques such as fluorescence correlation spectroscopy by selectively illuminating only a small pool of the fluorescently tagged protein, reducing background signal (Zhao et al., 2017).

1.2.1. Confocal microscopy

Laser scanning confocal microscopes produce sharp, high contrast images by using a pinhole to remove out of focus light from above and below the intended focal point. This allows the acquisition of thin optical sections and allows for 3D reconstruction of samples by acquiring ‘stacks’ of optical sections. Although they provide excellent spatial resolution, they have several limitations when used for live imaging. The sequential scanning is relatively slow and harsh on living samples, causing phototoxicity. They are also unsuitable for imaging larger living samples, and struggle to penetrate beyond 100μm due to light scattering.

Some of these limitations can be overcome using a spinning disk confocal microscope, which uses a rotating disk with many pinholes to illuminate each point in the sample rapidly. They offer greatly increased imaging speed and reduced phototoxicity due to distributed illumination, although this is often at the cost of spatial resolution. This makes them well suited for imaging short lived, dynamic events such as calcium signalling and cytoskeletal dynamics, as well as 4D imaging, allowing for rapid acquisition of confocal stacks. Recently, the use of resonant scanners on traditional confocal microscopes have provided improved scanning speeds, allowing for the acquisition of 10s of frames per second and gentler imaging. This has made them more viable for live imaging, but they are still unable to achieve the same temporal resolution as spinning disks.

1.2.2. Multiphoton excitation

Multiphoton imaging uses longer wavelengths to illuminate the sample, typically in the infrared range, and relies on two or more lower energy photons being absorbed by the same fluorophore. This can only occur when photons arrive almost simultaneously and only provides significant excitation with a high density of photons, meaning that only a tiny region at the focal point of the laser is illuminated. The use of longer, infrared wavelengths allow much deeper penetration into living samples that cannot be optically cleared. It causes less phototoxicity as only a tiny focal volume of the sample is illuminated and, since a pinhole is not required for optical sectioning, more light can be collected while imaging meaning that less radiation is needed to illuminate the sample. Being gentle and able to penetrate further into tissues means that multiphoton imaging is particularly suited to live imaging large samples. However, a drawback of

multiphoton imaging is the requirement of specialised femtosecond lasers, which typically limits imaging to a single wavelength, with the laser needing to repeatedly retune if imaging needs to be done at multiple wavelengths to visualise different components.

1.2.3. Selective Plane Illumination Microscopy (SPIM, or light-sheet microscopy)

This technique uses a thin sheet of light, rather than a laser point, to illuminate the specimen. This light sheet illuminates an optical plane of the sample which is captured by an objective orthogonal to the light-sheet. Because an entire optical plane is illuminated and captured simultaneously, out of focus regions of the sample are not illuminated. This considerably reduces bleaching and phototoxicity compared to confocal and widefield techniques. It also allows for the entire sample to be scanned rapidly by moving the specimen or the light sheet back and forth. The ability to scan with high temporal resolution and minimal phototoxicity makes light-sheet microscopy potentially ideal for live imaging. However, many light sheet systems require samples to be mounted in specific ways, such as agarose embedded or suspended in media, which makes live imaging certain organisms such as chick embryos particularly difficult. However, recent attempts have been made to adapt light-sheet imaging for chick embryos (Bango Da Cunha Correia, 2018).

1.2.4. Super resolution techniques

Recent advances in other light microscopy techniques such as stimulated emission depletion microscopy (STED) and structured illumination microscopy (SIM), as well as sample preparation techniques such as expansion microscopy (Zhuang and Shi, 2023), have allowed for visualisation of structures beyond the 200nm diffraction limit of light. Recently this has allowed imaging of actomyosin dynamics in Drosophila (Moore et al., 2022) and combining SIM with expansion microscopy has allowed imaging of the nanoscale structure of the nuclear lamina (Mäntylä et al., 2023). While super resolution techniques are powerful, they often require fixed samples and intense illumination, meaning they are poorly suited to longer term live imaging. SIM is perhaps the best suited for live imaging, but it is still highly dependent on sample preparation and best suited to thin samples, with any resolution gains quickly being lost due to light scattering in thicker tissues.

1.3. Model systems for studying morphogenesis

1.3.1. The mouse as a model for studying preimplantation development

The preimplantation mouse embryo represents an interesting system to study mechanobiology, with a number of mechanically driven events occurring at these early stages. These include apical constriction, which allocates cells to inner positions of the embryo (Samarage et al., 2015), expansion of the blastocyst cavity and hatching (Violette et al., 2006), and sorting of epiblast and primitive endoderm cells, which has been proposed to result from active cell movements (Meilhac et al., 2009), differential cell surface properties (Yanagida et al., 2022) and oscillations in the blastocyst cavity (Guo et al., 2025). It has been suggested that Lamin-A may act as a “mechanostat”, that is able to scale with tissues stiffness and allow the nucleus to respond to and resist mechanical stresses (Swift et al., 2013). Examination of Lamin-A expression across a range of tissues revealed low levels of Lamin-A in soft tissues such as fat and brain and high levels in bone and cartilage. Similarly, in cultured mesenchymal stem cells, the stiffness of the matrix correlated with Lamin-A levels. Further research has demonstrated that cytoskeletal tension generated by myosin II can regulate Lamin-A phosphorylation (pSer22), with inhibition of myosin II resulting in increased phosphorylation, localisation of Lamin-A to the nucleoplasm and increased turnover (Buxboim et al., 2014). Taken together, this suggests that Lamin-A may be able to respond to the mechanical properties of a cell’s environment. We therefore investigated whether the nuclear lamina functions as a mechanosensor in the preimplantation mouse embryo. The mouse embryo has a number of features that make it an attractive model system. Its small size means it is easy to image the entire embryo with high spatial resolution. It is also easy to culture many embryos in the same dish, allowing multiple embryos to be imaged simultaneously with high temporal resolution. The embryo is also easy to manipulate using small molecular inhibitors and microinjection, allowing expression of fluorescently tagged proteins and targeted knockdown via siRNA. Although the presence of the zona pellucida surrounding the embryo is convenient when culturing and manipulating embryos, it means that direct measurements of membrane stiffness with techniques such as atomic force microscopy or micropipette aspiration are difficult.

1.3.2. The chick as a model for studying axial development and somitogenesis

Somite formation is a fascinating example of tissue patterning that has been proposed to involve many of the tissue patterning mechanisms outlined above. This includes positional information relayed through morphogen gradients (Slack, 1983), self-organisation (Cotterell et al., 2015; Dias et al., 2014) and mechanical forces (Mongera et al., 2018). Somites are transient blocks of epithelial tissue that form on each side of the midline during axial development. They form as the mesenchymal cells of the presomitic mesoderm (PSM) undergo mesenchymal-to-epithelial transition, forming epithelial blocks of tissue at regular intervals. There are numerous features of the chick embryo that make it a powerful model for studying somite formation and much of our current understanding of somitogenesis was established by experiments in the chick. This includes the first evidence for oscillating genes in the PSM (Palmeirim et al., 1997), as well as FGF and Wnt morphogen gradients in the PSM (Aulehla et al., 2003; Dubrulle et al., 2001) and somite boundary formation (Kulesa and Fraser, 2002; Sato et al., 2002; Sato and Takahashi, 2005).

Some of the features that make the chick an attractive model include its robust and granular staging systems, both for pre-primitive streak (Eyal-Giladi and Kochav, 1976) and primitive streak onwards (Hamburger and Hamilton, 1951). Developmental processes are dynamic, with events occurring over narrow time windows, making these staging systems essential for performing targeted manipulations reproducibly. This is further aided by extensive lineage tracing studies of the epiblast, primitive streak and node (Garcia-Martinez et al., 1993; Hatada and Stern, 1994; Psychoyos and Stern, 1996; Schoenwolf et al., 1992; M. A. Selleck and Stern, 1991; Stern et al., 1988). These experiments provide a detailed understanding of the cellular precursors that give rise to somites, enabling targeted manipulation. The chick embryo grows as a flat disc, which has allowed for convenient *ex ovo* culture techniques to be developed, including New's method (New, 1955) and the 'EC' method which utilises a filter paper carrier (Chapman et al., 2001). These culture techniques, along with the embryo's flat disc morphology and transparency mean there is excellent potential for live imaging. In this study we use both mouse and chick embryos to explore the molecular and cellular mechanisms behind tissue patterning using high resolution microscopy and live imaging.

Chapter 2. Exploring a novel role for the nuclear lamina during the first lineage segregation event in mammalian development

2.1. Introduction

2.1.1. The nuclear lamina: structure and function

The nuclear lamina is a network of intermediate filaments found adjacent to the inner membrane of the nuclear envelope. In somatic cells, the lamina predominantly consists of four proteins encoded for by three genes: Lamin-B1 and Lamin-B2, encoded by the genes LMNB1 and LMNB2 and Lamin-A and Lamin-C, splice variants of the gene LMNA (Peter et al., 1989; Vorburger et al., 1989). A number of minor splice variants exist in certain contexts, such as Lamin-B3 and Lamin-C2 found in the testes (Furukawa and Hotta, 1993; Lin and Worman, 1993). The lamina plays a variety of roles related to the structure and function of the nucleus, including the regulation of nuclear size and shape (Cantwell and Dey, 2022; Lele et al., 2018), integrity (Harada et al., 2014; Shin et al., 2013), chromatin organization (Shevelyov and Ulianov, 2019; Van Steensel and Belmont, 2017) and gene expression (Andrés and González, 2009; Ho and Lammerding, 2012). It couples the nucleus to the cytoskeleton via the LINC complex (Hieda, 2017; Wong et al., 2021), facilitating nuclear position (Razafsky et al., 2014) and mechanosensing (Lityagina and Dobreva, 2021; Osmanagic-Myers et al., 2015). Additionally, it has been shown to play roles in RNA splicing (Kumaran et al., 2002), DNA replication (Dorner et al., 2006; Shumaker et al., 2008) and DNA repair (Lambert, 2019). Many of these functions are intimately connected, for example the lamina's role in organising chromatin structure impacts both gene expression and nuclear integrity. Similarly, the LINC complex establishes a connection between the lamina and cytoskeleton, which can facilitate mechanosensing, nuclear positioning, and microtubule dependent double-strand break repair.

2.1.2. Cytoskeletal coupling via LINC complex

The nuclear lamina is connected to the cytoskeleton via the 'linker of nucleoskeleton and cytoskeleton' (LINC) complex (Figure 2.1). The LINC complex typically consists of both a SUN protein and a KASH protein, with the former residing in the inner nuclear membrane and interacting with lamins directly, and the latter residing in the outer nuclear membrane and interacting with components of the cytoskeleton. There are 5 SUN proteins found in mammals, but most somatic cells express only SUN1 and 2

(Crisp et al., 2006), with SUN3, 4 and 5 primarily being restricted to germ cells (Frohnert et al., 2011; Göb et al., 2010). SUN proteins contain a transmembrane domain that resides in the inner nuclear membrane, an N-terminal, nucleoplasmic domain that can interact with lamins and chromatin, and a C-terminal SUN domain that resides in the perinuclear space between the inner and outer nuclear membranes (Haque et al., 2006; Hodzic et al., 2004). In the perinuclear space the SUN domain can interact with the KASH domain of KASH proteins. Similar to SUN proteins, KASH proteins contain a transmembrane domain and a C-terminal domain that extends into the perinuclear space. In contrast, the N-terminal domain extends into the cytoplasm where it can interact with numerous components of the cytoskeleton (Starr and Fischer, 2005; Starr and Han, 2002). There are 6 KASH proteins in the human genome. The most widely expressed and best characterised are nesprins 1 to 4. Nesprin-1 and -2, depending on the isoform, can interact directly with actin filaments or indirectly with microtubules via kinesin and dynein. Nesprin-3 interacts with intermediate filaments indirectly via plectin. Nesprin-4 interacts indirectly with microtubules via kinesin-1 (Bone and Starr, 2016; Wilhelmsen et al., 2006). The lamina-cytoskeletal interactions established by the LINC complex enable the regulation of a variety of cellular processes, such as nuclear positioning (Wilhelmsen et al., 2006), chromatin organisation (Wong et al., 2021) and mechanosensing (Hao and Starr, 2019).

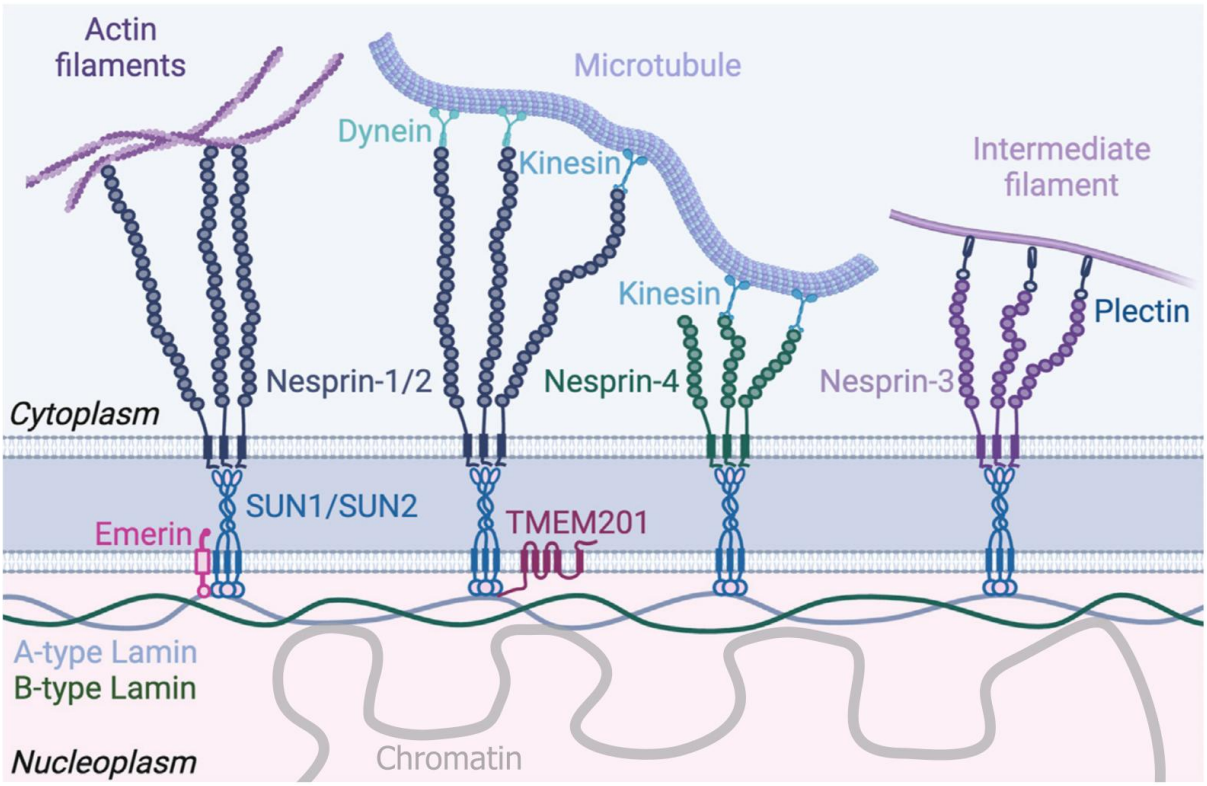

Figure 2.1 The LINC complex

The LINC (Linker of Nucleoskeleton and Cytoskeleton) complex couples the nucleoskeleton to the three major components of the cytoskeleton: actin, microtubules, and intermediate filaments. SUN1 and SUN2 reside at the inner nuclear membrane and interact with A-type and B-type lamins. Nesprins 1-4 reside in the outer nuclear membrane and interact directly with actin filaments and indirectly with microtubules via kinesin and dynein and indirectly with intermedia filaments via plectin. Adapted from (Bougaran and Bautch, 2024), Frontiers in Physiology, licensed under CC BY 4.0.

2.1.3. Mechanosensing

This physical connection between nucleoskeleton and cytoskeleton has been shown to cause conformational changes in the lamina in response to mechanical stimuli. Levels of Lamin-A in different cell types has been shown to scale with tissue stiffness (Swift et al., 2013) and matrix elasticity during tissue culture affects Lamin-A phosphorylation and turnover (Buxboim et al., 2014). More direct evidence for a nuclear mechanosensing pathway has been demonstrated, with the nuclear membrane protein emerin being phosphorylated in a lamin-dependent manner in responses to forces applied to nesprin-1 using magnetic tweezers (Guilluy et al., 2014). It is believed that changes in cytoskeletal tension cause conformational changes in Lamin-A/C, affecting the accessibility of epitopes for phosphorylation and other interactions (Ihalainen et al., 2015). Mechanical forces can promote Lamin-A localisation to the nuclear periphery, where it constitutes a major component of the nuclear lamina (Shumaker et al., 2005). In contrast, Lamin-A phosphorylation causes disassembly from the lamina and localisation to the nucleoplasm where there is increased turnover (Buxboim et al., 2014; Kochin et al., 2014; Swift et al., 2013).

2.1.4. Specification of ICM and Trophectoderm identity

During preimplantation mammalian development, the totipotent blastomeres that make up the cleavage stage embryo begin diverging into two lineages, leading to the formation of the pluripotent inner cell mass (ICM) and the trophectoderm (Johnson and Ziomek, 1981). At the 8-cell stage, the embryo undergoes compaction and the blastomeres begin to polarise. At this stage, the surface of each of the 8 blastomeres comprises an apical domain facing the perivitelline space and a basolateral domain in contact with neighbouring blastomeres. At the 16-cell stage the cells of the embryo are numerous enough to be arranged such that some blastomeres are completely enclosed by other blastomeres. It is these ‘inner’ cells that will form the ICM while the ‘outer’ cells form the trophectoderm. The differences between these lineages are first identified by the nuclear localisation of Yap and expression of Cdx2 in the trophectoderm (Strumpf et al., 2005) and later by expression of Oct4, Sox2, and Nanog in the ICM (Dietrich and Hiiragi, 2007; Palmieri et al., 1994; Wicklow et al., 2014). This begs the question of how spatial segregation of cells into inner and outer positions is related to changes in gene expression. Cell polarity is thought to be key in

translating the differences in position between inner and outer cells into changes in gene expression associated with ICM and trophectoderm identity.

An important event in the establishment of these two cell lineages is the physical segregation of blastomeres into inner and outer positions of the 16-cell embryo. Blastomeres located at the cortex of the embryo at this stage polarise, forming distinct apical and basolateral domains. Data currently published suggests a model where Hippo pathway member Angiomotin (Amot) localises to the basolateral membrane in inner cells (Figure 2.2). Here it promotes Yap phosphorylation and retention in the cytoplasm. In contrast, outer cells have a polarised, F-actin-rich apical cortex that sequesters Amot, preventing Yap phosphorylation. This results in shuttling of Yap into the nucleus where it drives Cdx2 expression and outer cell identity. (Hirate et al., 2013; Leung and Zernicka-Goetz, 2013; Nishioka et al., 2009). Yap signalling and Hippo pathway activation can be regulated by extracellular matrix stiffness, which influences cytoskeletal tension and can induce differentiation of mesenchymal stem cells (Dupont et al., 2011), proliferation in sheets of mammary epithelial cells (Aragona et al., 2013) and changes in cell volume in fibroblasts (Gonzalez et al., 2018). It has also been shown that forces applied across the nucleus, transmitted from the extracellular matrix via mechanical coupling of the cytoskeleton and nucleoskeleton, can regulate the shuttling of Yap between the nucleus and cytoplasm (Elosegui-Artola et al., 2017). This, along with recent research demonstrating the potential for the nuclear lamina to play a role in mechanotransduction (Buxboim et al., 2014; Swift et al., 2013) prompted us to explore whether the nuclear lamina might play a role in establishing ICM and trophectoderm identity during preimplantation development.

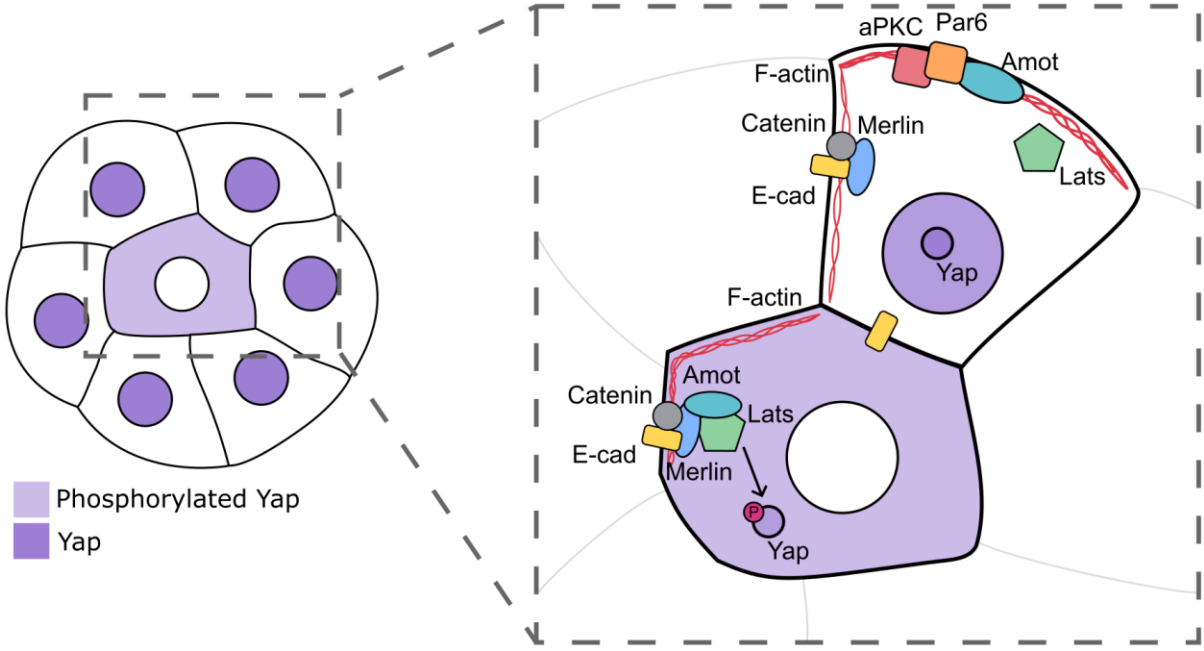

Figure 2.2 Polarity model of inner-outer cell identity specification

The cell polarity model describes how differential phosphorylation and localisation of Yap is established between inner and outer cells to drive ICM and TE identity. In inner cells, a complex of E-cadherin, Merlin and Amot forms at the basolateral cortex. This leads to the activation of Lats kinase, phosphorylation of Yap by Lats, and confinement of Yap to the cytoplasm. In outer cells, Amot is sequestered at the polarised apical cortex, meaning Lats is not activated and Yap is not phosphorylated, allowing nuclear localisation of Yap. Adapted from (Ajduk and Zernicka-Goetz, 2016).

2.2. Methods

2.2.1. Ethics approval

This research complies with all relevant ethical regulations. This includes a review and approval of the mouse work from the Institutional Animal Care and Use Committee (IACUC) of the University of Pennsylvania (Protocol #806983) and a review and approval of all donated human embryo work by the New England Institutional Review Board (WO 16450-1).

2.2.2. Mouse embryo collection and culture

Following all animal ethics guidelines of the University of Pennsylvania IACUC, 8 week old wild-type female mice were super ovulated. For each experimental replicate 5 female mice were used. 5 international units (IU) of pregnant mare serum (PMS, National Hormone and Peptide Program) were used for super ovulation. 5 IU of recombinant chorionic gonadotrophin (CG, National Hormone and Peptide Program) were administered intraperitoneally 48 hours and immediately prior to mating. Four mouse strains were used with distinct genetic background. Two inbred (FVB/NTac and C57BL/6JInv) and two outbred (Hsd:NSA(CF-1) and IcrTac:ICR). All mouse lines were purchased from approved vendors (Jackson Laboratory, Envigo, or Charles Rivers Laboratories). A BSL2 animal facility based at the University of Pennsylvania was used to maintain these mouse lines in pathogen-free conditions with access to water and food ad libitum. Temperature was maintained at 68 °F − 76 °F and humidity at 30% − 70% and a 12-hour dark / 12-hour light cycle between 07:00 and 19:00 was used.

2.2.3. Microinjection

M2 medium (Merck) was used to flush embryos from oviducts. Embryos were then cultured at 37 °C and 5% CO_2 in KSOM + AA (Merck) covered by mineral oil (Sigma). 0.1 to 0.3 pL of RNA diluted in injection buffer (5 mM NaCl, 5 mM Tris, 0.1 mM EDTA) was microinjected using a FemtoJet (Eppendorf). A pCS2+ backbone was used for all mRNA transcription. After DNA constructs were cloned into PCS2+, plasmids were linearised and SP6 mMESSAGE mMACHINE® kits (Ambion) were used to perform *in vitro* transcription, following manufacturer's instructions. RNA was purified using RNA Cleanup (New England Biolabs) or RNAeasy (Qiagen) kits, following manufacturer's instructions. mRNA was microinjected using the following concentrations: mRuby-Lamin-A at 50 ng μl^{-1}; H2B-RFP at 5 ng μl^{-1}; GFP-Utrophin at 70 ng μl^{-1}; H2B-GFP at

5 ng μl^{-1}; memb-GFP at 70ng μl^{-1}; RhoAQ63L at 50 ng μl^{-1}; Keratin8-Emerald at 150ngμl^{-1}; Keratin 18-Emerald at 150 ng μl^{-1}; GFP-MAP2c at 70 ng μl^{-1}; Emerald-Amot at 100 ng μl^{-1}; Emerald-Formin2 at 100 ng μl^{-1}; VCA-mRuby at 100 ng μl^{-1}. siRNA (Qiagen) was microinjected at 200 nM. In each experiment a subset of 5-10 embryos were isolated in order to confirm the efficiency of the siRNA knockdown. The following siRNAs were used:

Lamin-A:

Mm_Lmna_5: AACAGGCTACAGACGCTGAAG (SI02655450),

Mm_Lmna_6: AAGGACCTCGAGGCTCTTCTC (SI02655457),

Ctrl_Lmna_1: AACTGGACTTCCAGAAGAACA (SI03650332).

SUN1:

Mm_Unc84a_1: GACCTTAAAGGTGGAAATAAA (SI01462363),

Mm_Unc84a_2: AAGTCGAGGTTTCCTATATTA (SI01462370),

Mm_Unc84a_3: TGGAGATATTTCAAATATTA (SI01462377).

SUN2:

Mm_Rik_1: CCGGTTAGTGTTCGGGTGAAA (SI00912751),

Mm_Rik_2: CACGTAGAACTCCCTGCATAA (SI00912758),

Mm_Rik_3: CAGGTGTATATATGTAGCATA (SI00912765),

Mm_Rik_4: CAGGATTGGAATGGTGGATT (SI00912772).

AllStars negative control: sequence not disclosed by Qiagen (SI03650318)

Embryos showing signs of arrested or abnormal development (~ 15%) were excluded from the study using previously published criteria (Fierro-González et al., 2013; Kaur et al., 2013). We have demonstrated in previous studies that embryos microinjected and imaged for similar durations can produce viable offspring after being transferred to pseudopregnant mice (Domingo-Muelas et al., 2023; Kaur et al., 2013). Drug treatments were performed by diluting each drug in KSOM to the following concentrations: nocodazole (Sigma, M1404) at 10 μM; H-1152 (Tocris, 2414) at 50 μM; azidoblebbistatin (Opto-Pharma, DR-A-081) at 10 μM; SMIFH2 (Sigma, S4826) at 250 mM; leptomycin B (Sigma, L2913) at 100 nM; CK-666 (Sigma, SML0006) at 250 mM. In each experiment control embryos were cultured using the vehicle drugs were diluted in KSOM to provide the same concentration. Azidoblebbistatin was

activated by targeting a 3 μm × 5 μm region of interest using a 405 nm laser at 20% power for 60s. All drug treatments were performed for 4 hours after which embryos were immediately fixed as described in the immunofluorescence protocol below.

2.2.4. Immunofluorescence

Embryos were fixed in 4% paraformaldehyde in PBS for 30 minutes at room temperature. They were then washed twice for 5 minutes in PBS containing 0.1% Triton X-100 (PBS-T) and permeabilised for 30 minutes in PBS containing 0.5% Triton X-100. After permeabilization block was performed by incubating in 10% fetal bovine serum (FBS) in PBS for 2 hours. Primary antibodies were diluted in 10% FBS solution, at the following concentrations: Lamin-A/C (Santa Cruz, sc-376248) at 1:200, Lamin-A (Abcam, ab26300) at 1:200; Phospho-Lamin-A/C (Ser22) (Cell Signaling, 2026) at 1:200; Lamin-B1 (Protein Tech, 66095-1-Ig) at 1:200; phospho-myosin II (3671 P, Cell Signaling) at 1:200; Keratin 8 (DSHB, TROMA-I) at 1:20; Yap (Cell Signaling, 8418 S) at 1:200; Phospho-Yap (Cell Signaling 13008) at 1:200; Amot (gift from H. Sasaki) at 1:200; Cdx2 (Abcam, 88129) at 1:200; α-tubulin (Sigma, T6199) at 1:500; Formin-2 (Invitrogen, PA5-65632). Embryos were incubated with primary antibodies overnight at 4°C. Afterwards, embryos were washed 5 times in PBS-T for 5, 10, 15, 20 then 25 minutes. Embryos were then incubated in secondary antibodies conjugated with Alexa-Fluor fluorophores (Invitrogen, A32723, A32731, A32733, A11006 and A32728), in blocking solution (1:1000) for 2 hours and washed in PBS-T 3 times for 5 minutes. For F-actin labelling, embryos were incubated with Phalloidin-Alexa Fluor 555 (Invitrogen, A34055), at 1:500, Phalloidin-Rhodamine (Molecular Probes, R415) at 1:500 or SPY555-actin (Spirochrome, SC202) at 1:1000. For nuclear labelling, embryos were incubated with DAPI (Sigma, 10236276001) at 1:1000 or NucBlue-Hoechst 33342 (Invitrogen, R37605) using 2 drops per 1 ml.

2.2.5. Live embryo imaging

For live-imaging, embryos were cultured in LabTek chambers (Nunc) or μ-Slide 18 Well (Ibidi). A specialised stage top incubator for each microscope system (Leica SP8, Carl Zeiss LSM780, LSM880 or Nikon A1RHD25) was used to maintain 37 °C and 5% CO_2. Embryos were imaged using an Apochromat 40×1.1 NA objective. Embryos were imaged every 5 minutes for long term imaging and every 2 minutes when capturing cleavage divisions.

2.2.6. Image analysis

Embryos were visualised and analysed using Imaris 8.2 or 9.7 (Bitplane). The surface tool was used for cell segmentation based on the phalloidin signal to define the cortex of each cell. When analysing expression in the cytoplasm and cell cortex, the segmented surface was converted into a binary mask and a minimum filter was used to shrink the mask by 1 μm to create a region representing the cytoplasm. The original mask was then enlarged by 1 μm using a maximum filter and the cytoplasmic mask was subtracted from the enlarged mask to create a mask representing the cell cortex. Measurements of immunofluorescence were performed in Imaris and ImageJ by measuring mean fluorescence intensity in a region of interest, except when calculating the nuclear:cytoplasmic ratios, where total signal through the nucleus and cytoplasm was used To account for variations in signal intensity due light scattering at different sample depths, measurements were normalised by dividing the signal by the intensity of the DAPI or Hoechst signal from the same cell. To identify inner cells, each cell of the embryo was segmented and the segmented regions used to confirm that no part of the cell cortex was in contact with the surface of the embryo.

2.2.7. FRAP

FRAP was performed at 3.5x zoom targeting a 5 μm by 10 μm region of interest. This region was photobleached using a 405 nm laser at 100% power and a pixel dwell time of 6 μs. For analysis, the mean fluorescence intensity in the photobleached region of interest was measured and normalised to a control region of the same size that had not been photobleached. The mean fluorescence intensity prior to photobleaching was set to 100% and the mean fluorescence intensity immediately after bleaching was set as 0%. An exponential curve was then fitted to the fluorescence intensities measured over time. The immobile fraction was calculated as $1 - I_\infty$, where I_∞ is fluorescence intensity that is reached after recovering to a plateau. Exponential fitting was performed using Python 3.6.12 and SciPy 1.7.3.

2.2.8. Statistics and reproducibility

Statistical analyses were performed GraphPad Prism. Data were first tested for normality using the D'Agostino-Pearson omnibus test. If variables displayed a normal distribution, an unpaired, Student's t-test was used when comparing two groups, and an ANOVA with Dunnett's multiple comparisons test when comparing more than two

groups. If variables did not appear to follow a normal distribution, the Mann-Whitney U-test was used when comparing two groups, and the Kruskal-Wallis test with Dunn's multiple comparisons test when comparing more than two groups. All tests were performed two-tailed.

2.3. Results

2.3.1. Lamin-A scales with actomyosin contractility during cleavage stages

We hypothesised that mechanical forces may play a role in determining cell identity during preimplantation development and the nuclear lamina may act as a mechanosensor, detecting forces generated by apical constriction and cells polarising. Therefore, we began by characterising the expression of Lamin-A/C during the early stages of preimplantation development. Embryos at the 2-cell, 4-cell, pre-compaction 8-cell and post-compaction 8-cell stages were immunostained for Lamin-A/C. It has been demonstrated previously that mechanical forces can promote Lamin-A localisation to the nuclear periphery, where it constitutes a major component of the nuclear lamina (Shumaker et al., 2005). In contrast, Lamin-A phosphorylation causes disassembly from the lamina and localisation to the nucleoplasm where there is increased turnover (Buxboim et al., 2014; Kochin et al., 2014; Swift et al., 2013). We therefore decided to characterise the ratio of Lamin-A/C between lamina and nucleoplasm and developed a computational pipeline to segment each nucleus and divide it into lamina and nucleoplasm sub-compartments. Nuclei were segmented automatically based on DAPI or Hoechst staining, then this region of interest was expanded and eroded as necessary to create regions corresponding to the nuclear lamina and nucleoplasm (Figure 2.3). Examining the ratio of Lamin-A/C between the lamina and nucleoplasm (hereafter referred to as “Lamin-A/C L:N”) shows that Lamin-A becomes increasingly concentrated at the nuclear lamina as the embryo develops from 2 to 4 to 8 cell stages (Figure 2.4A, C). In the same, period we observed that total Lamin-A/C levels throughout the nucleus decrease slightly after progressive cleavage divisions, showing a small but significant 4% decrease during the transition from 2-cell to 8-cell stage (Figure 2.4B). Levels remain constant during compaction, suggesting that changes observed are due to changes in Lamin-A localisation.

The nuclear staining also revealed significant changes to nuclear shape, with nuclei becoming more spherical and less invaginated (Figure 2.4D, E). At the 2-cell stage, nuclei are irregular in shape with invaginations and blebbing (Figure 2.4F). As embryos transition from the 2-cell to the 4-cell stage nuclei become largely spherical, with a sharp increase in measurements of sphericity and solidity, as well as an aspect ratio approaching 1. Beyond the 4-cell stage there is little change in nuclear shape, with nuclei maintaining a spherical structure. It is also possible that these changes are the

result of changes in chromatin organisation rather than mechanical forces, as cells of the embryo are undergoing zygotic genome activation during these stages.

Lamin-A has been shown to respond to changes in matrix elasticity, which in turn can be regulated by changes in actomyosin contractility (Buxboim et al., 2014). We therefore decided to examine levels of phosphorylated myosin II at different cleavage stages. The amount of p-myosin II increased from the 2-cell stage to the 8-cell stage, with a further increase observed between pre and post compaction embryos (Figure 2.5). In addition to total of p-myosin II increasing, it also becomes more concentrated at the cell cortex. This suggests that actomyosin contractility at the cell cortex increases during this time. This observation is consistent with previous research showing the importance of actomyosin contractility in facilitating compaction (Fierro-González et al., 2013; Maître et al., 2015). During mitosis, cells adopt a rounded shape, driven by hydrostatic forces and balanced by actomyosin contractility (Stewart et al., 2011). During this time the stiffness of the cortex affects the cell shape and deformability (Grill, 2011; Ramkumar and Baum, 2016). As the embryo transitions from the 4-cell stage to the 8-cell stage, during cleavage divisions cell shape is dynamic and cells deform easily in response to the forces of cytokinesis, suggesting lower membrane stiffness (Figure 2.6, Supplementary Movie 1). In contrast, during cleavage divisions between the 8-cell and 16-cell stages, cells remain more spherical, consistent with a more rigid cell cortex.

Taken together, these results suggest that as embryos progress from the 2-cell to the 8-cell stage, actomyosin contractility increases and the cell cortex becomes and stiffer. We attempted to perturb these changes by treating embryos with H-1152, a ROCK inhibitor (Ikenoya et al., 2002). ROCK is a downstream effector of Rho-GTPases and can play a variety of roles in cytoskeletal organisation, including the stabilisation of actin stress fibres via LIM-kinase activation (Maekawa et al., 1999; Ohashi et al., 2000) and increased phosphorylation of myosin light chain (Amano et al., 1996; Kimura et al., 1996). Treatment with H-1152 at the 8-cell stage lowered Lamin-A levels, as well as nuclear sphericity (Figure 2.7B). Similar treatments at the 2-cell stage have no effect on any parameters we measured (Figure 2.7A). These results suggest that rising actomyosin contractility during cleavage stage divisions leads to changes in nuclear morphology and Lamin-A/C L:N.

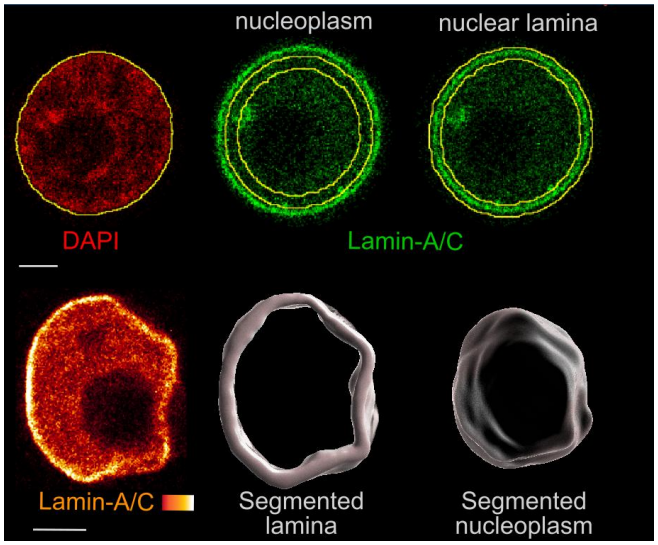

Figure 2.3 Segmentation of the nucleus into lamina and nucleoplasm subcompartments

Examples of computational segmentation of the nuclear lamina and nucleoplasm for quantification of Lamin-A/C levels in each subnuclear compartment. This begins with initial segmentation of the nucleus by thresholding the DAPI signal. Then expanding and eroding this region of interest to create regions corresponding to the lamina and nucleoplasm. The first row shows a 2D cross section of the segmentation based on a single confocal section and second row shows a 3D reconstruction of a final segmentation based on an entire confocal stack. Scale bars, 10 μm.

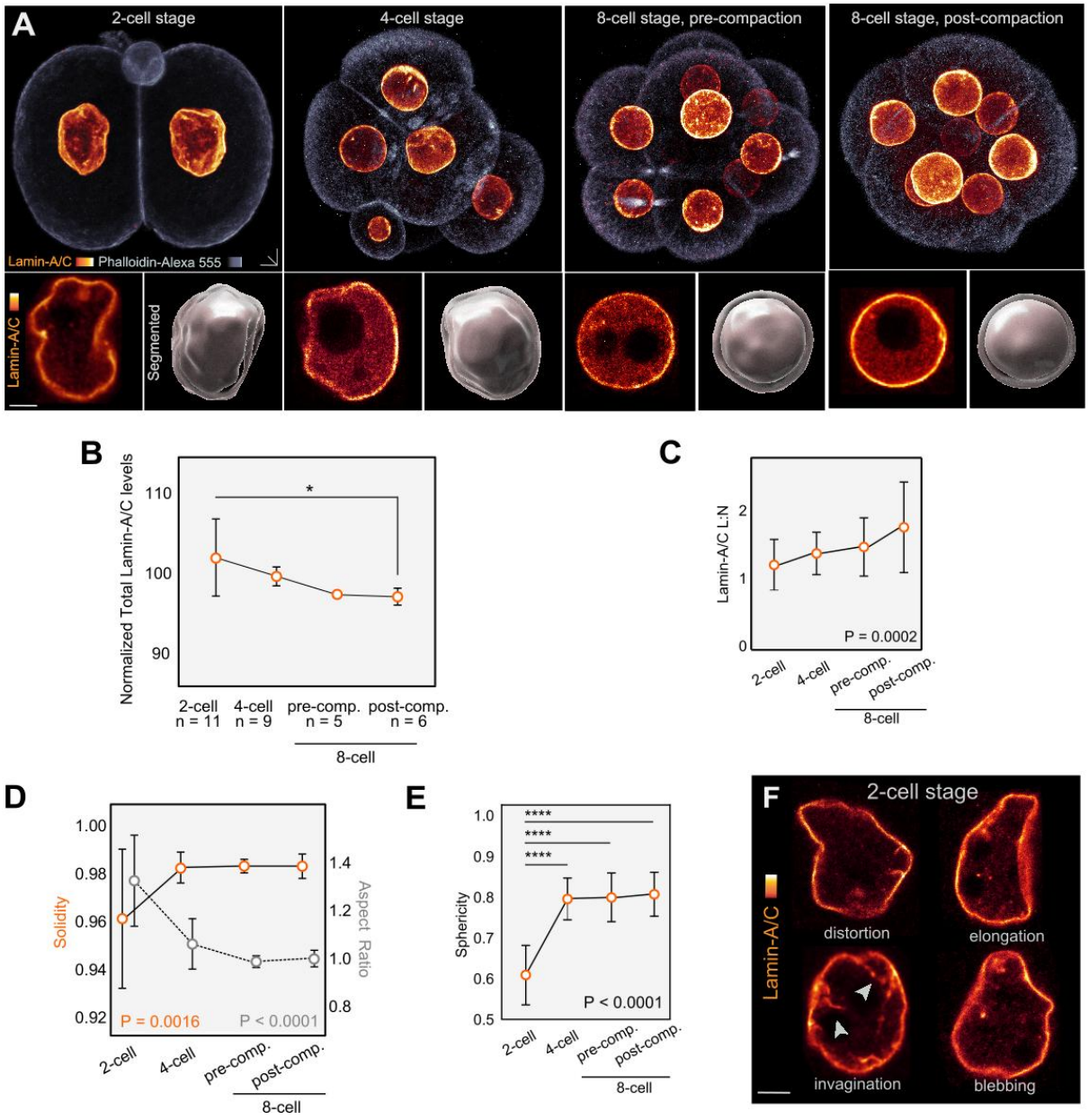

Figure 2.4 Lamin-A concentration increases at the nuclear lamina as embryos undergo successive cleavage divisions

A. 3D immunofluorescence images of preimplantation mouse embryos at progressive cleavage stages stained for Lamin-A/C and F-actin. Lower left insets show a single confocal section through a representative nucleus, lower right insets show 3D segmentation of the same nucleus with both nucleoplasm (opaque) and lamina (transparent). **B-C.** Analysis of Lamin-A/C levels, both as total levels throughout the nucleus (B) and as a ratio between lamina and nucleoplasm (C) (Lamin-A/C L:N) *P=0.0032, Kruskal-Wallis test. Dots represent the mean and error bars represent SD **D-E.** Descriptors of nuclear shape at different developmental stages calculated using 3D segmentation data. Dots represent the mean and error bars represent SD. Kruskal-

Wallis test **F.** 2D confocal sections highlighting a variety of features observed in nuclei at the 2-cell stage. For B-E n=11 for 2-cell, n=9 for 4-cell, n=5 for pre-comp. n=6 for post-comp. Scale bars, 10 μm.

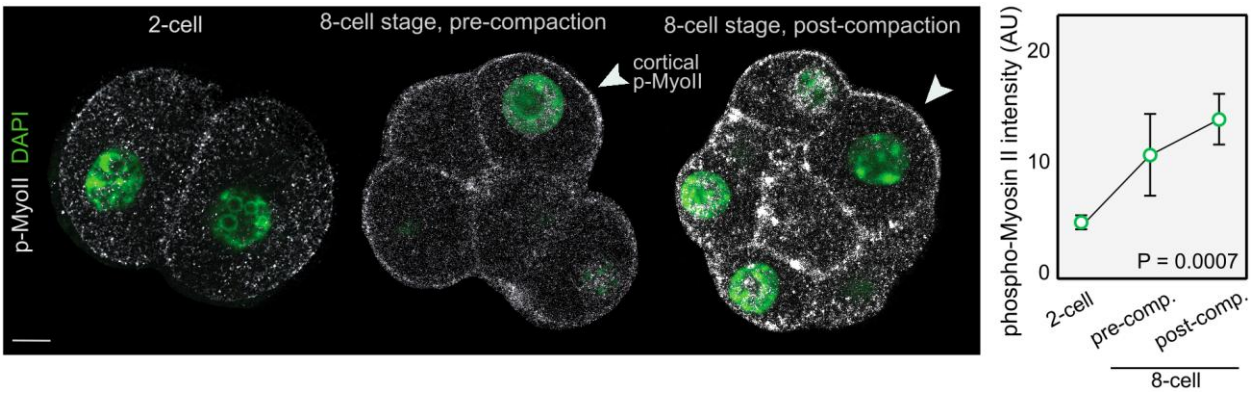

Figure 2.5 Levels of pMyoII increase during cleavage stages and post-compaction

2D confocal sections of embryos immunostained for phosphorylated myosin II at the 2-cell, 8-cell pre-compaction and 8-cell post-compaction stages. Quantification shows phosphorylated myosin II across the different stages. n=4 for 2-cell, n=14 for 8 cell pre-compaction, and n=16 for 8-cell post-compaction. P=0.0007, Kruskal-Wallis test, dots represent the mean and error bars represent SD. Scale bars, 10 μm.

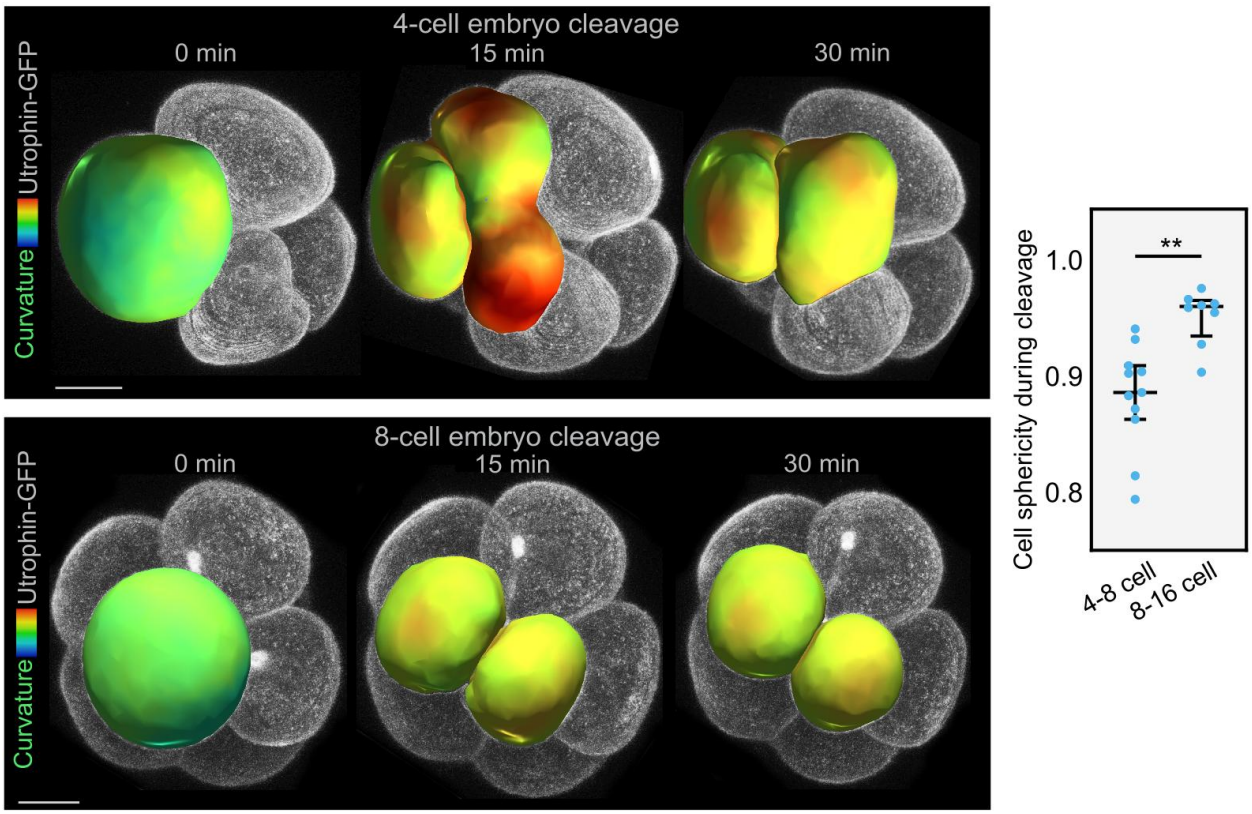

Figure 2.6 Blastomeres deform less during cytokinesis at later stages

Stills from Supplementary Movie 1. Live-imaging of cleavage divisions during the transition from 4-cell to 8-cell stage and from 8-cell to 16-cell stages. Embryos were microinjected with mRNA encoding Utrophin-GFP allowing for 3D segmentation and calculation of cell sphericity. 3D segmentation is overlaid with a colour map of local curvature. n=11 for 4-8 cell, n=8 for 8-16 cell, **P=0.006, Mann-Whitney U test. Bars on dot plots represent median and interquartile range. Scale bars, 20 μm.

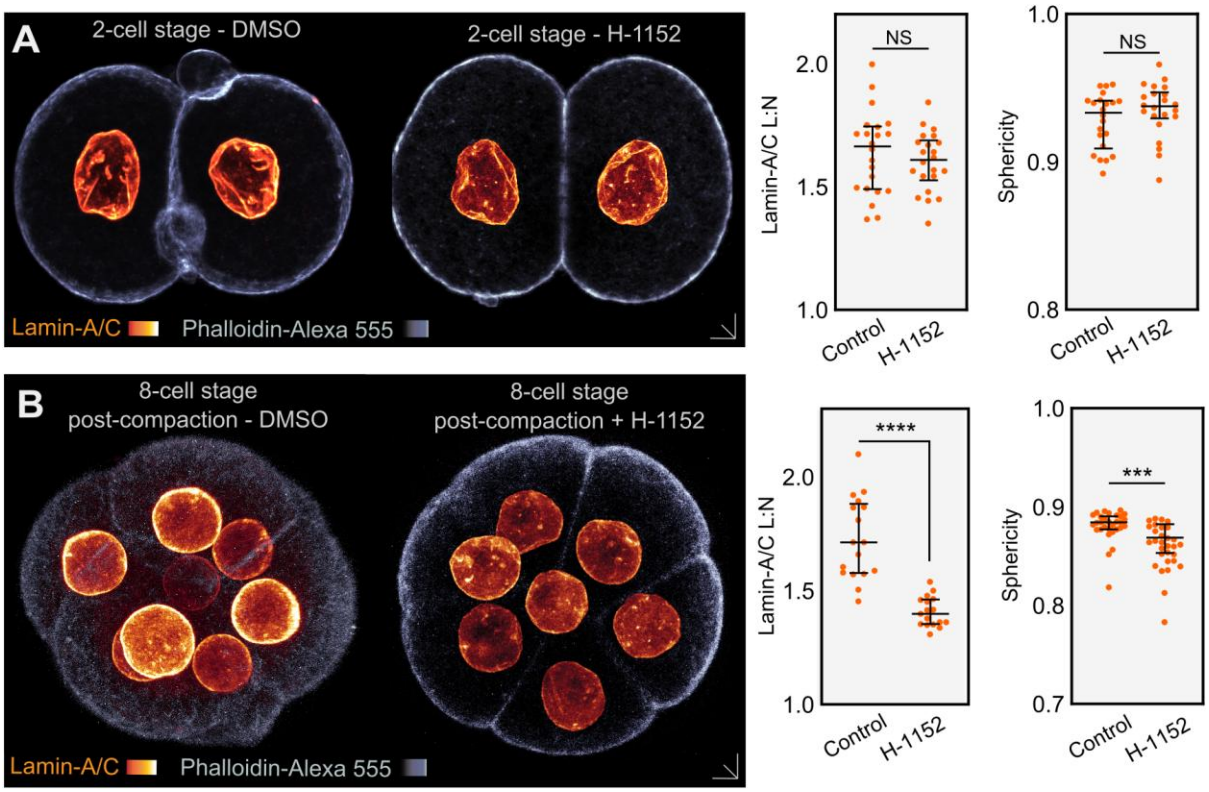

Figure 2.7 Treatment with H-1152 causes a reduction in Lamin-A/C L:N in post compaction embryos

A-B. 3D immunofluorescence images showing embryos treated with rho-kinase inhibitor H-1152 as well as quantification and comparison of Lamin-A/C L:N and nuclear sphericity between control and treatment groups. **A.** Embryos treated at the 2-cell stage. n=22 for DMSO and H-1152. NS: p=0.26 for Lamin-A/C levels, p=0.226 for sphericity, Mann-Whitney U test. **B.** Embryos treated at the 16-cell stage. n=17 for DMSO and H-1152. ****P<0.0001, ***P=0.0008, Mann-Whitney U test. All statistical tests are two-tailed. Bars on dot plots represent median and interquartile range. Scale bars, 10 μm.

2.3.2. Lamin-A responds to mechanical stimuli via F-actin

After observing that rising actomyosin contractility correlates with increased Lamin-A/C L:N, we began to explore how forces occurring at the cell cortex may be transmitted to the nucleus. The LINC complex facilitates interaction between the nuclear lamina and all three major components of the cytoskeleton: actin, microtubules and intermediate filaments (Crisp et al., 2006). It is currently unknown which lamina–cytoskeletal interactions occur in preimplantation embryos. However, all known physical interactions between cytoskeleton and nucleoskeleton occur via the Sun1/2 complex in the perinuclear space. To examine the possibility that changes in Lamin-A may be the result of interactions between the lamina and cytoskeleton, we microinjected siRNAs targeting Sun1 and Sun2 into one blastomere of 2-cell embryos. Knockdown of Sun1/2 caused a downregulation of Lamin-A L:N in injected cells (Figure 2.8). However, this result should be interpreted with caution as we were unable to obtain a reliable antibody for Sun1/2 meaning the efficacy of the siRNA knockdown was not confirmed.

To investigate this hypothesis further, we imaged each component of the cytoskeleton and attempted to perturb them in order, assessing the effect on Lamin-A. Immunostaining for α-tubulin revealed that microtubules form a network of filaments that extends from the cell cortex to the nucleus and could be responsible for mechanotransduction (Figure 2.9A). However, despite the presence of a dense microtubule network, upon treatment with microtubule depolymerising drug nocodazole, there were no observable changes in Lamin-A levels or distribution, suggesting that microtubules do not play a significant role in the regulation of Lamin-A (Figure 2.9B). Staining for Keratins 8 and 18, which are the first keratins observed to form filaments in the preimplantation embryo (Lim et al., 2020; Lu et al., 2005), showed that although filaments are present, they are sparse and do not form dense networks until the blastocyst stage (Figure 2.10A). At the blastocyst, stage keratin filaments can be seen extending from the cortex to the nucleus, particularly from the apical cortex. At the 16-cell stage however, the limited number of keratin filaments present remain confined to the cell cortex. Consistent with these observations, embryos injected with siRNAs targeting Keratin 8 and 18 showed no changes in Lamin-A L:N (Figure 2.10B).

After examining microtubules and intermediate filaments we performed similar experiments targeting actin. Staining with phalloidin at the 2-cell and 8-cell stages revealed a continuous actin meshwork that extends from the cell cortex to the nucleus (Figure 2.11A and B). Presence of an F-actin meshwork spanning from the nucleus to the cortex was also observed in a 10-cell human embryo (Figure 2.11C). Our staining for p-myosin II showed that it is also present throughout the cytoplasm (Figure 2.5). This suggests there could be a continuous, contractile actomyosin network through the cytoplasm. To test this, we used spatiotemporally confined manipulations of myosin II activity using azidoblebbistatin, which, upon stimulation with an 860 nm laser, becomes cross linked with myosin II, blocking its actin-binding domain. Inactivation of myosin II between the nucleus and apical cortex resulted in a decrease in mRuby-Lamin-A L:N over a period of 30 minutes post stimulation (Figure 2.12). When the same experiment was performed targeting the basolateral cortex, a significantly smaller reduction in Lamin-A L:N was observed. This is consistent with the high levels for p-myosin observed at the apical cortex. Together, these results suggest Lamin-A/C may be regulated by mechanical forces at the apical cortex which are transmitted to the nucleus by a contractile actomyosin network.

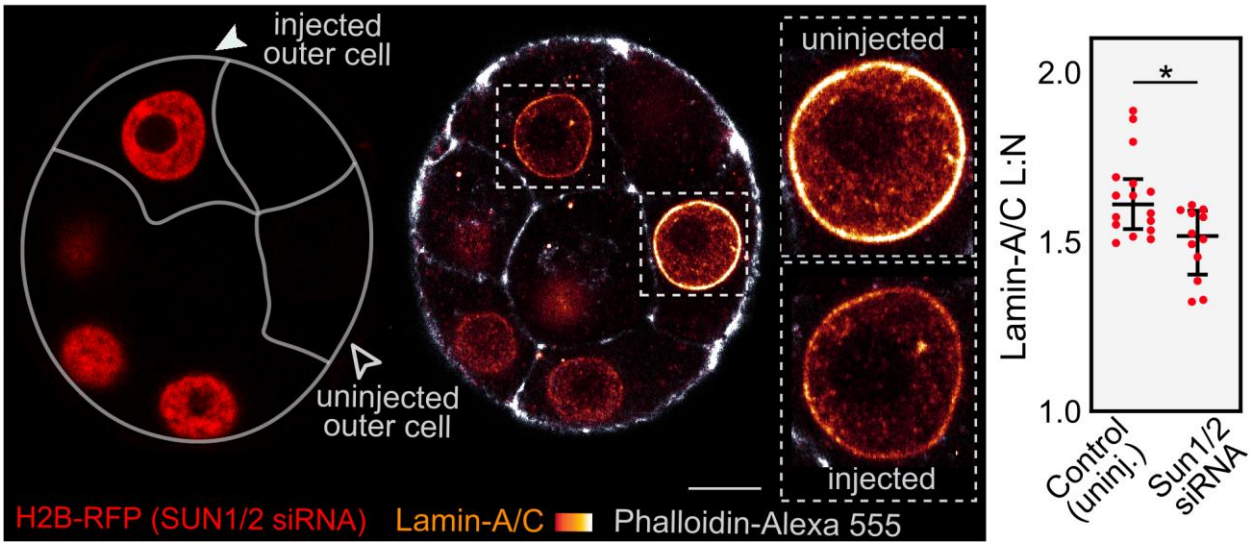

Figure 2.8 Knockdown of SUN1/2 causes changes in Lamin-A/C L:N

One blastomere of 2-cell stage embryos was microinjected with siRNA targeting SUN1 and SUN2. These were co-injected with mRNA encoding H2B-RFP to label the manipulated cells. 2D confocal sections show labelled cells and immunostaining for Lamin-A/C. Quantification compares Lamin-A/C L:N between the two groups. n=16 for control, n=12 for SUN1/2 siRNA. *P=0.024, Mann-Whitney U test. Bars in dot plots represent median and interquartile range. Scale bars, 10 μm.

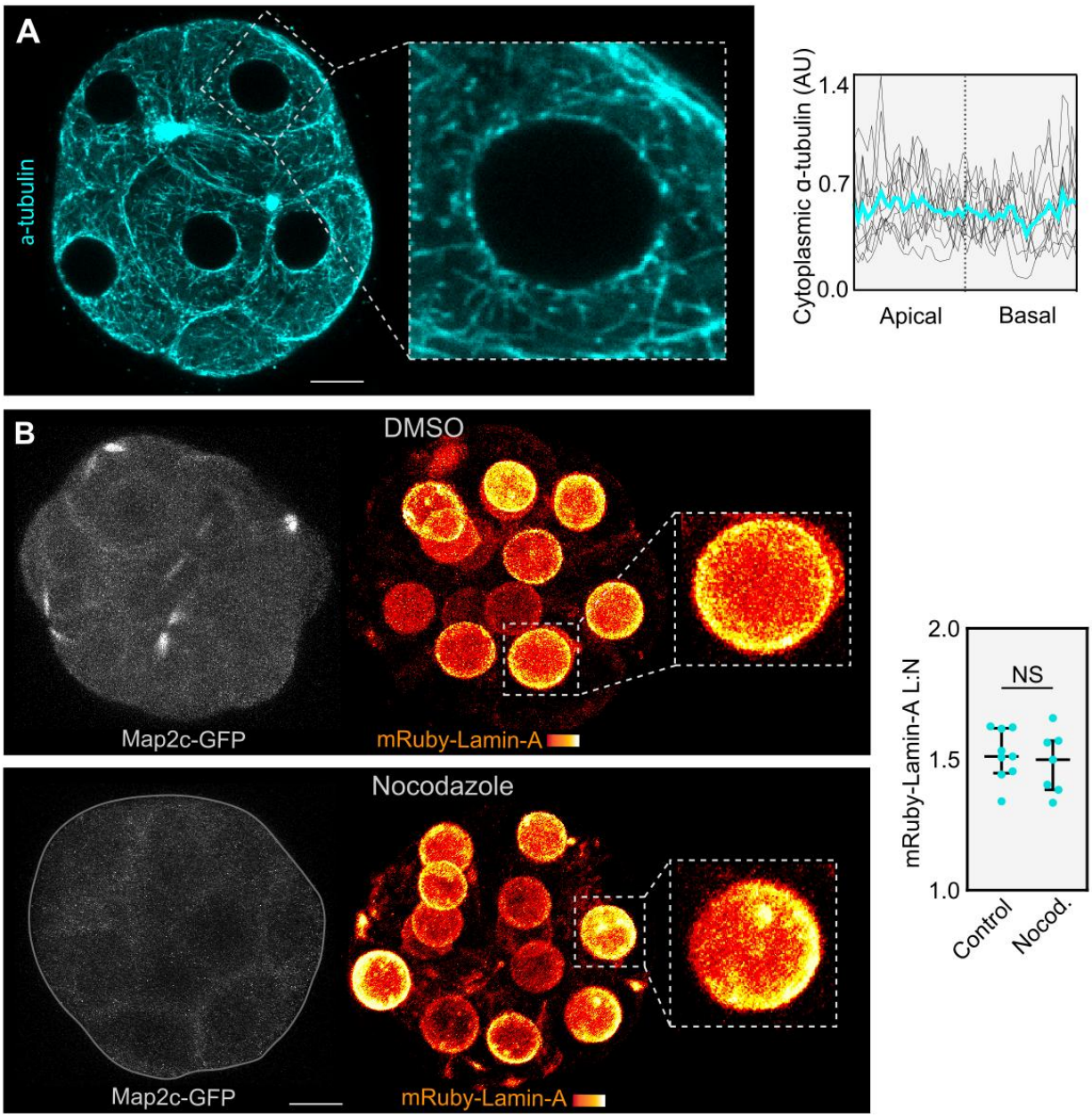

Figure 2.9 Microtubules span the cytoplasm from the nucleus to the cortex but do not appear to interact with Lamin-A/C

A. 2D confocal section showing immunstaining for α-tubulin. Plot shows intensity profiles of α-tubulin fluorescence around the nucleus. Intensity profiles of blastomeres from 12 embryos are stacked together with a mean intensity profile shown in cyan. **B.** 3D fluorescence image of live of embryos microinjected with mRNA encoding mRuby-Lamin-A and Map2c-GFP. Embryos were treated with microtubule depolymerising drug nocodazole. Quantification shows comparison of mRuby-Lamin-A L:N between treatment groups. n=9 for DMSO, n=7 for nocodazole. NS=0.607, Mann-Whitney U test. Bars on dot plots represent median and interquartile range. Scale bars, 10 μm. Data shown in panel B collected by Yanina Alvarez.

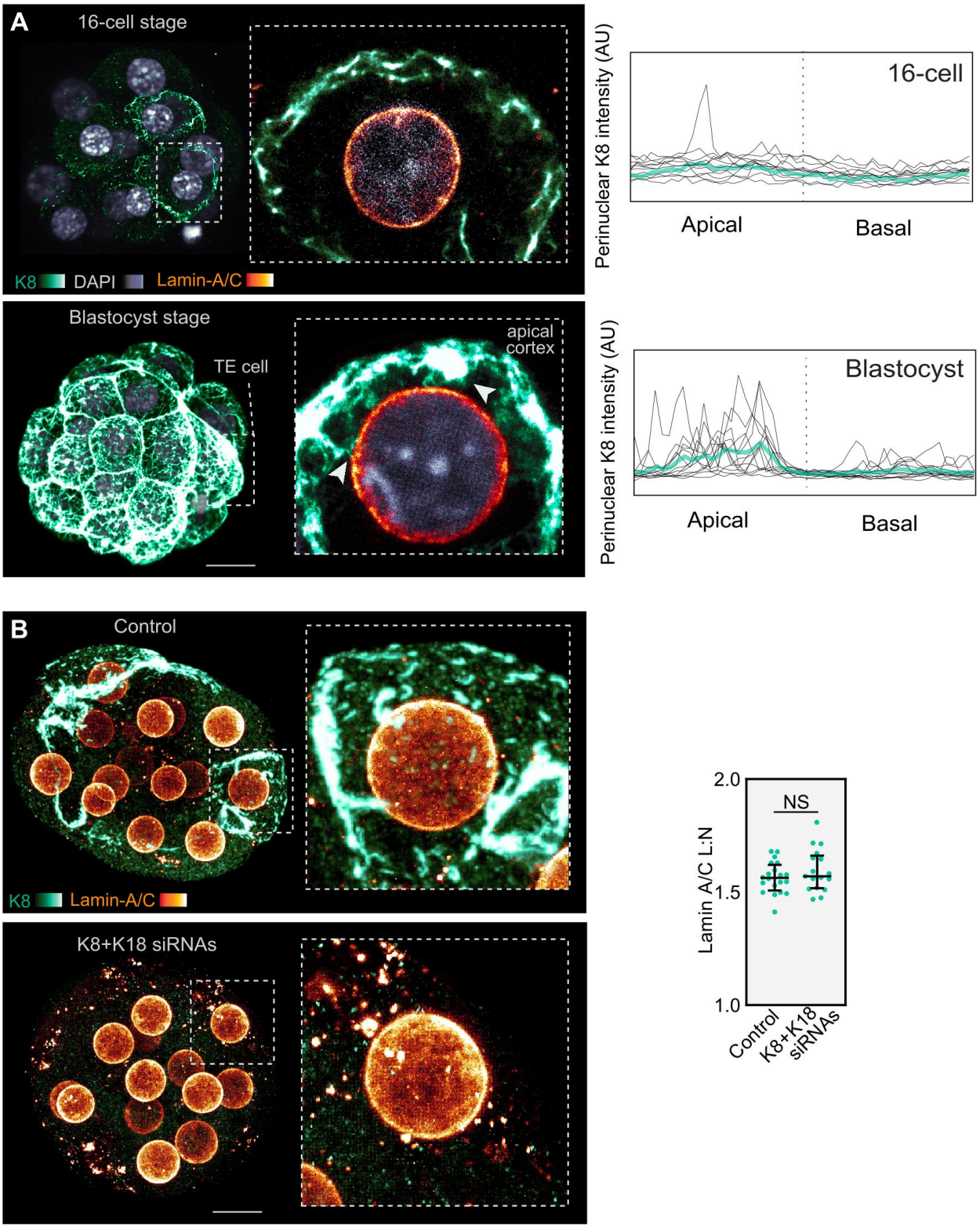

Figure 2.10 Keratin filaments are sparse at the 16 cell stage and do not appear to interact with Lamin-A/C

Figure 2.8 Keratin filaments are sparse at the 16 cell stage and do not appear to interact with Lamin-A/C

A. 3D projection of confocal stacks showing immunostaining for Keratin-8 filaments and Lamin-A/C at the 16-cell and blastocyst stage. Plots show intensity profiles of Keratin-8 fluorescence around the nucleus. Intensity profiles of blastomeres from 11 embryos at the 16-cell stage and 13 embryos at the blastocyst stage are stacked together with mean intensity profiles shown in green. **B.** Embryos were microinjected with siRNA targeting Keratin 8 and 18, 3D projection of confocal stacks show immunostaining for Lamin-A/C and Keratin 8. Quantification compares Lamin-A/C L:N between the two groups. n=20 for control, n=18 for Keratin-8 siRNA, NS P=0.612, Mann-Whitney U test. Bars on dot plots represent median and interquartile range. Scale bars, 10 μm.

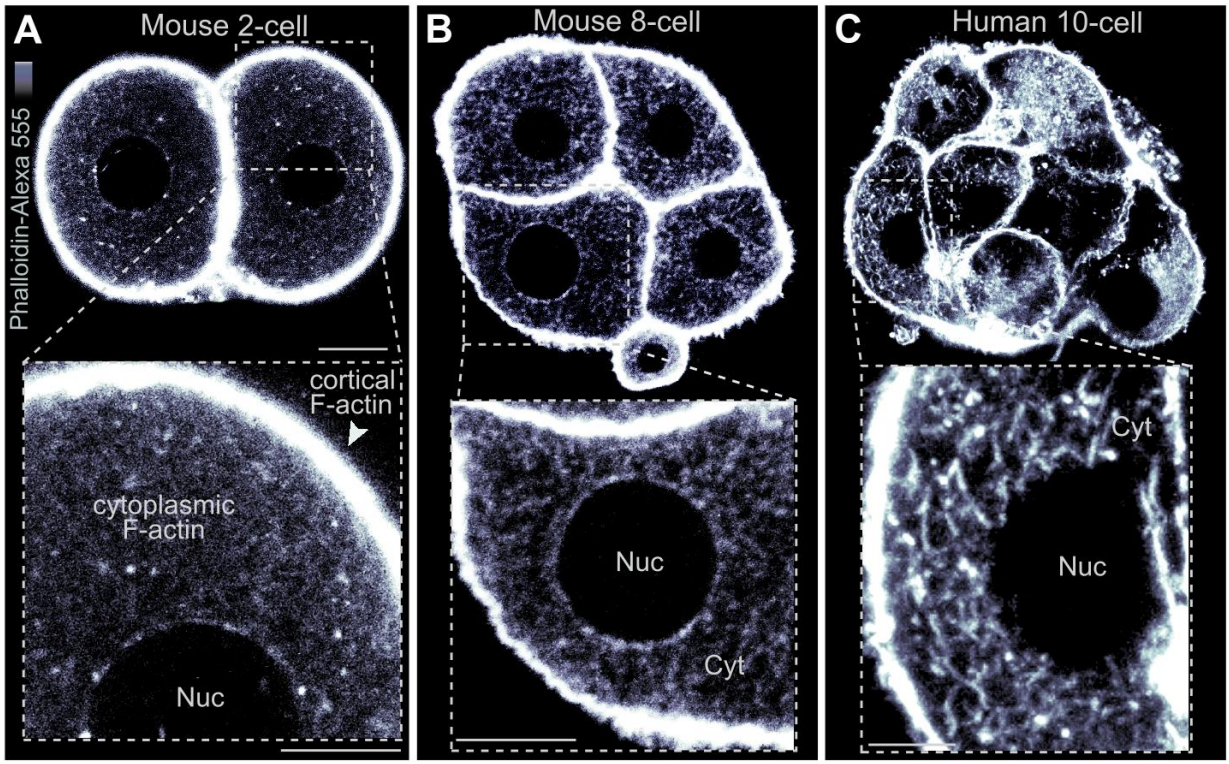

Figure 2.11 A meshwork of F-actin spans the cytoplasm from the nucleus to the cortex in mouse and human preimplantation embryos.

2D confocal sections of mouse embryos at the 2-cell and 8-cell stages as well as a 10-cell human embryo, stained with phalloidin. This shows a meshwork of F-actin throughout the cytoplasm, from the cell cortex to the nucleus. Scale bars, 10 μm.

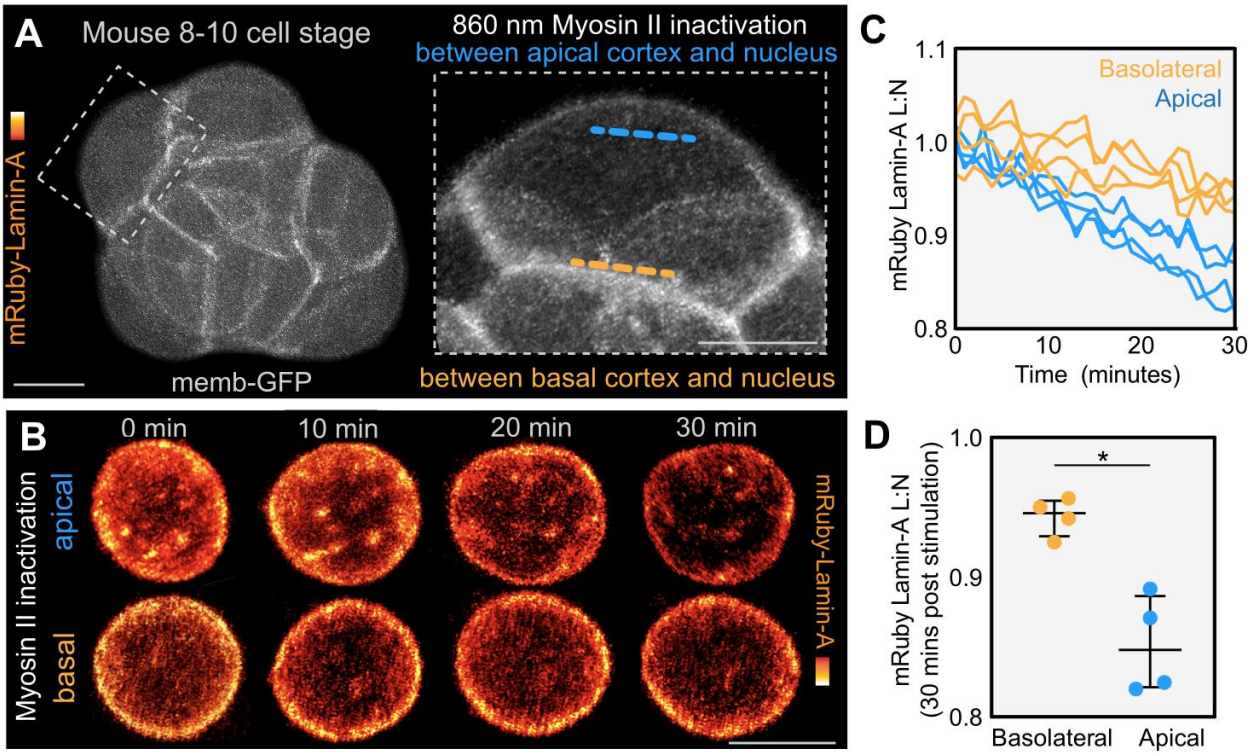

Figure 2.12 Inactivation of Myosin II activity between the nucleus and apical cortex reduces Lamin-A/C L:N.

A. Outline of experimental design. Post-compaction 8-cell embryos were microinjected with mRuby-Lamin-A and memb-GFP, then incubated with azidoblebbistatin, a derivative of blebbistatin that becomes crosslinked to myosin II upon photostimulation, inhibiting myosin II activity. Regions of the cytoplasm were photostimulated with 860nm infrared light, either between the nucleus and apical cortex or between the nucleus and the basolateral cortex. Embryos were then imaged at regular intervals for 30 minutes. **B.** 2D confocal sections showing live imaging of mRuby-LaminA in the nuclei of photostimulated embryos. **C and D.** Quantification of mRuby-LaminA L:N over time post stimulation. n=4 for apical and basolateral, p=0.0286, Mann-Whitney U test. Experiment performed by Yanina Alvarez. Bars in dot plots represent median and interquartile range. Scale bars, 10 μm

2.3.3. Lamin-A levels identify the first lineage segregation

Our initial results indicate that Lamin-A/C levels are influenced by changes in actomyosin contractility. We continued by characterising Lamin-A/C expression at later stages, particularly at the 16-cell stage, when blastomeres segregate into inner and outer positions. Immunostaining for Lamin-A/C revealed lower levels of Lamin-A/C localised to the nuclear lamina in inner cells. This effect was also observed during live imaging of embryos injected with mRNA encoding Lamin-A fused to mRuby (mRuby-Lamin-A) (Figure 2.13). These differences in Lamin-A/C remain present at the blastocyst stage, where they distinguish the ICM and trophectoderm lineages. These results were further validated by immunostaining with two different Lamin-A/C antibodies (Figure 2.14A). In contrast, immunostaining for Lamin-B reveals no differences in expression between inner and outer cells and little variation between blastomeres (Figure 2.14B). This is consistent with previous research indicating that Lamin-A/C, rather than B type lamins are responsible for mechanotransduction (Lammerding et al., 2006; Swift et al., 2013). We observed increasing levels of Lamin-A at the nuclear lamina between the 2-cell and 8-cell stages, followed by differential levels between inner and outer cells at the 16-cell stage. It is unclear whether these changes in Lamin-A/C between inner and outer cells are the result of changes in Lamin-A/C expression or localisation. To explore this, we stained with an antibody specific to Lamin-A/C phosphorylated at serine 22, which revealed higher levels of phosphorylation in the nucleoplasm of inner cells (Figure 2.15). Phosphorylation at this residue has been shown to identify non filamentous Lamin-A/C that is confined to the nucleoplasm with increased turnover (Kochin et al., 2014). Lamin-A/C pSer22 has also been shown to correlate with matrix elasticity, with cells cultured on stiffer matrices show decreased phosphorylation and cells cultured on softer matrices showing increased phosphorylation (Buxboim et al., 2014). This suggests that at least some of the observed change in Lamin-A levels between inner and outer cells is due to changes in localisation from lamina to nucleoplasm. However, this does not demonstrate that these differences are exclusively caused by changes in localisation and does not rule out changes in Lamin-A at the expression level.

To probe whether the differential localisation of Lamin-A/C between inner and outer cells is also the result of changes in actomyosin contractility, we treated 16-cell embryos with H-1152 and blebbistatin, a myosin inhibitor (Straight et al., 2003). This

resulted in a shift in Lamin-A from the lamina to the nucleoplasm, with outer cells displaying a similar phenotype to inner cells in untreated embryos (Figure 2.16). After observing the effects of ROCK inhibition, we wanted to examine the effect of ectopic ROCK activation. To achieve this, cells were injected with mRNA encoding the constitutively active RhoA mutant Q63L (Longenecker et al., 2003). This mutant has significantly reduced GTPase activity, causing a large proportion of the protein to remain in its active, GTP-bound state. Injected cells showed increased Lamin-A levels, with inner cells showing a distribution of Lamin-A mimicking that typically seen in outer cells (Figure 2.16). To test if similar mechanotransduction pathways might be present in human embryos we performed immunostainings for Lamin-A/C on human blastocysts. This revealed higher Lamin-A/C L:N in trophectoderm than ICM, similar to the patterns observed in mouse blastocysts (Figure 2.17A). Upon treatment with H-1152 human blastocysts also showed lower Lamin-A/C L:N in the trophectoderm (Figure 2.17B). Taken together, these results suggest that in mouse and human embryos, actomyosin contractility is able to regulate Lamin-A/C. Lamin-A/C L:N scales with contractility until cells internalise, at which point Lamin-A/C L:N drops.

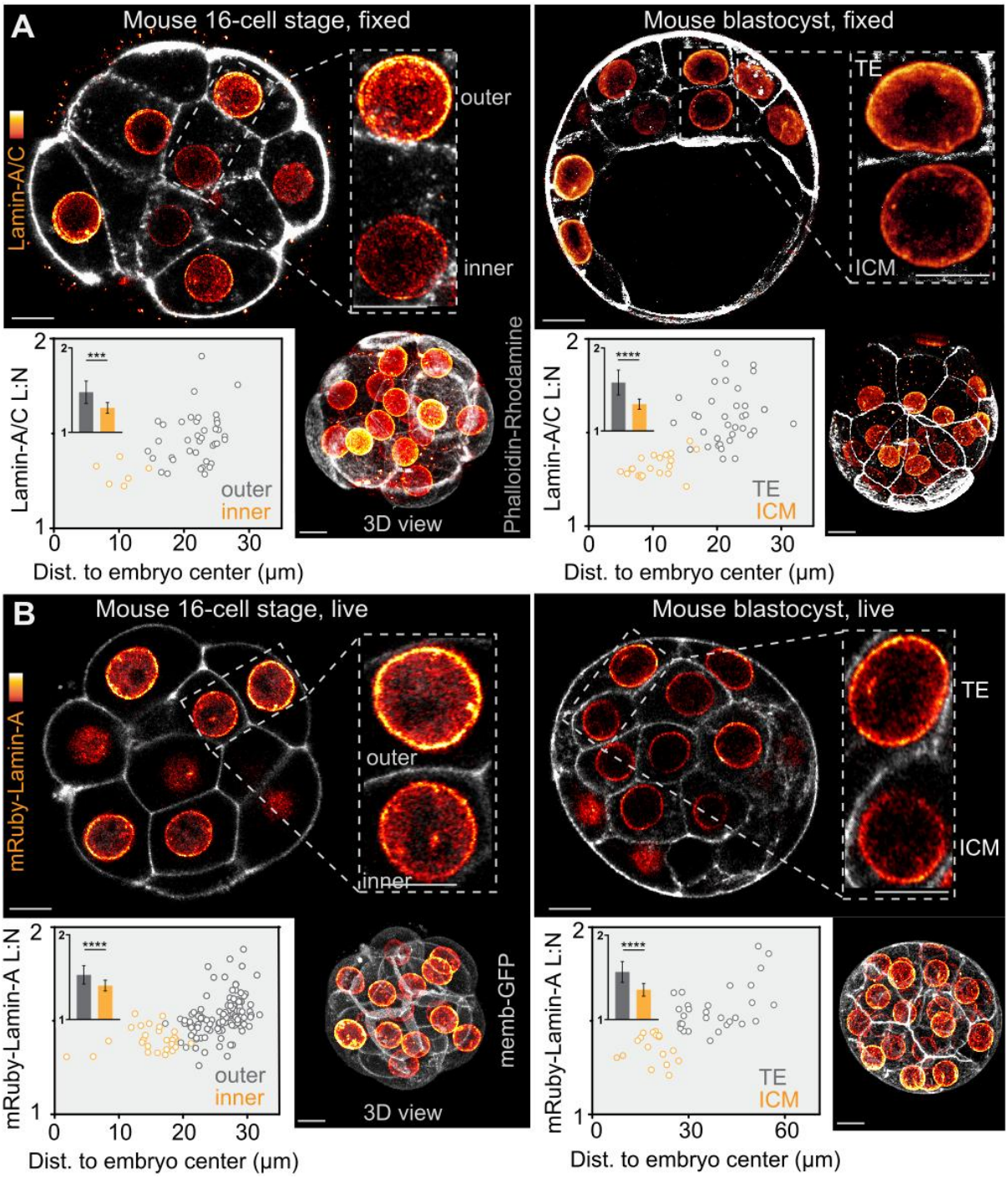

Figure 2.13 Lamin-A shows differential expression between inner and outer cells at the 16-cell and blastocyst stages

A. Immunofluorescence for Lamin-A/C in fixed mouse embryos at the 16-cell and blastocyst stages. 2D confocal sections are shown to illustrate inner-outer differences. Insets show 3D projections of confocal stacks. **B.** Live-imaging of embryos microinjected at 1-cell stage with mRNA encoding mRuby-Lamin-A and memb-GFP. For **A** n=6 for 16-cell inner, n=40 for 16-cell outer, n=21 for blastocyst ICM, n=33 for blastocyst trophectoderm. For **B** n=29 for 16-cell inner, n=48 for 16-cell outer, n=18 for

blastocyst ICM, n=32 for blastocyst trophectoderm. ***P=0.0004, ****P<0.0001, Mann-Whitney U test. Experiment performed by Yanina Alvarez. Scale bars, 10 μm.

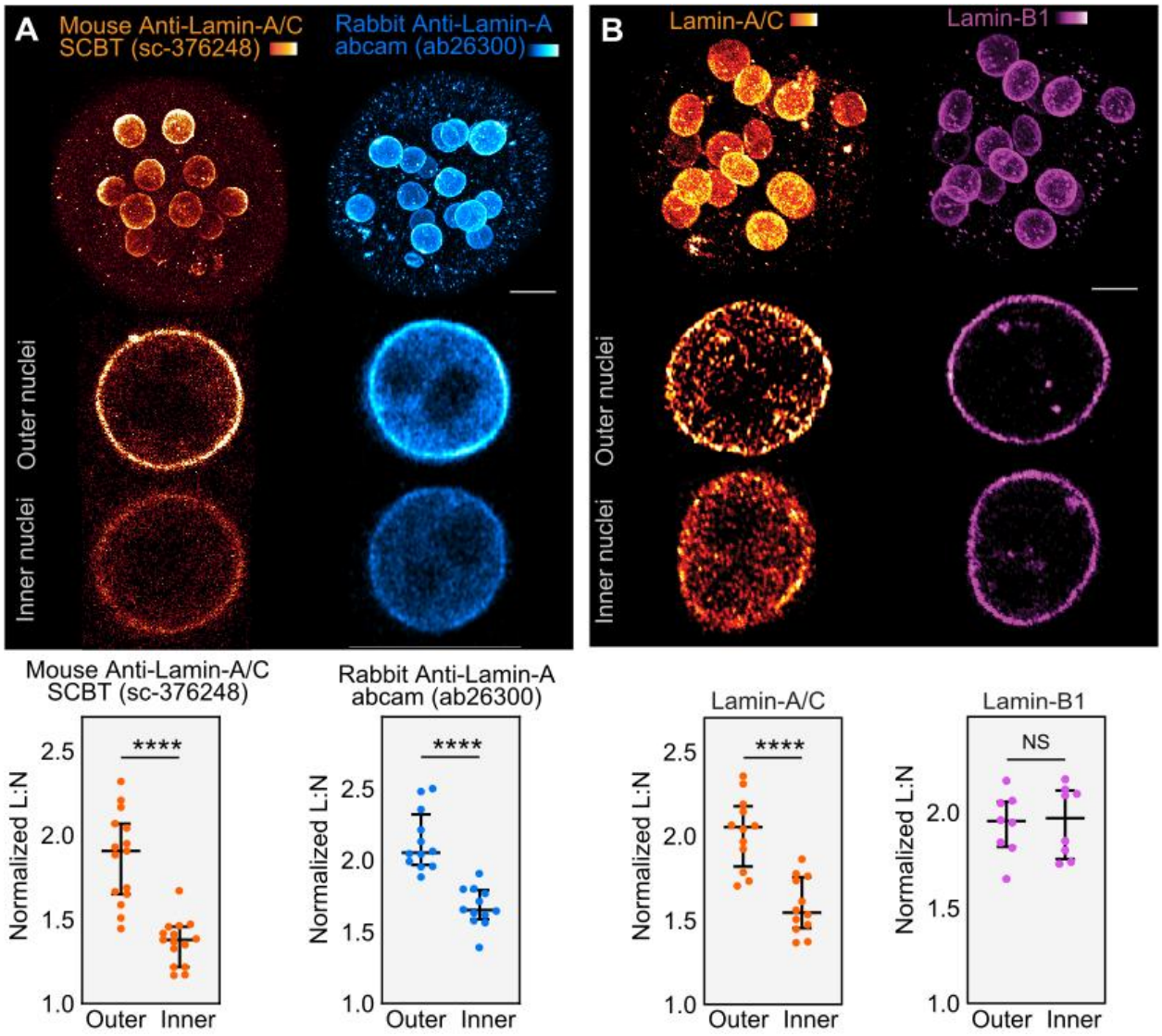

Figure 2.14 Lamin B1 shows no differences between inner and outer cells

A. 3D projections of confocal stacks showing two different Lamin-A antibodies. 2D confocal slices of representative inner and outer cell nuclei are shown below. For sc-376248 n=15 for outer and inner. For ab26300 n=12 for outer and inner. ****P<0.0001, Mann-Whitney U test. **B.** 3D projections of confocal stacks showing embryos immunostained for Lamin-A/C and Lamin-B1. 2D confocal slices of representative inner and outer cell nuclei are shown below. n=12 for Lamin-A/C outer and inner, n=8 for Lamin-B outer and inner, ****P<0.0001, NS P=0.763, Mann-Whitney U test. Data in panel B was acquired by Yanina Alvarez. Bars in dot plots represent median and interquartile range. Scale bars, 10 μm

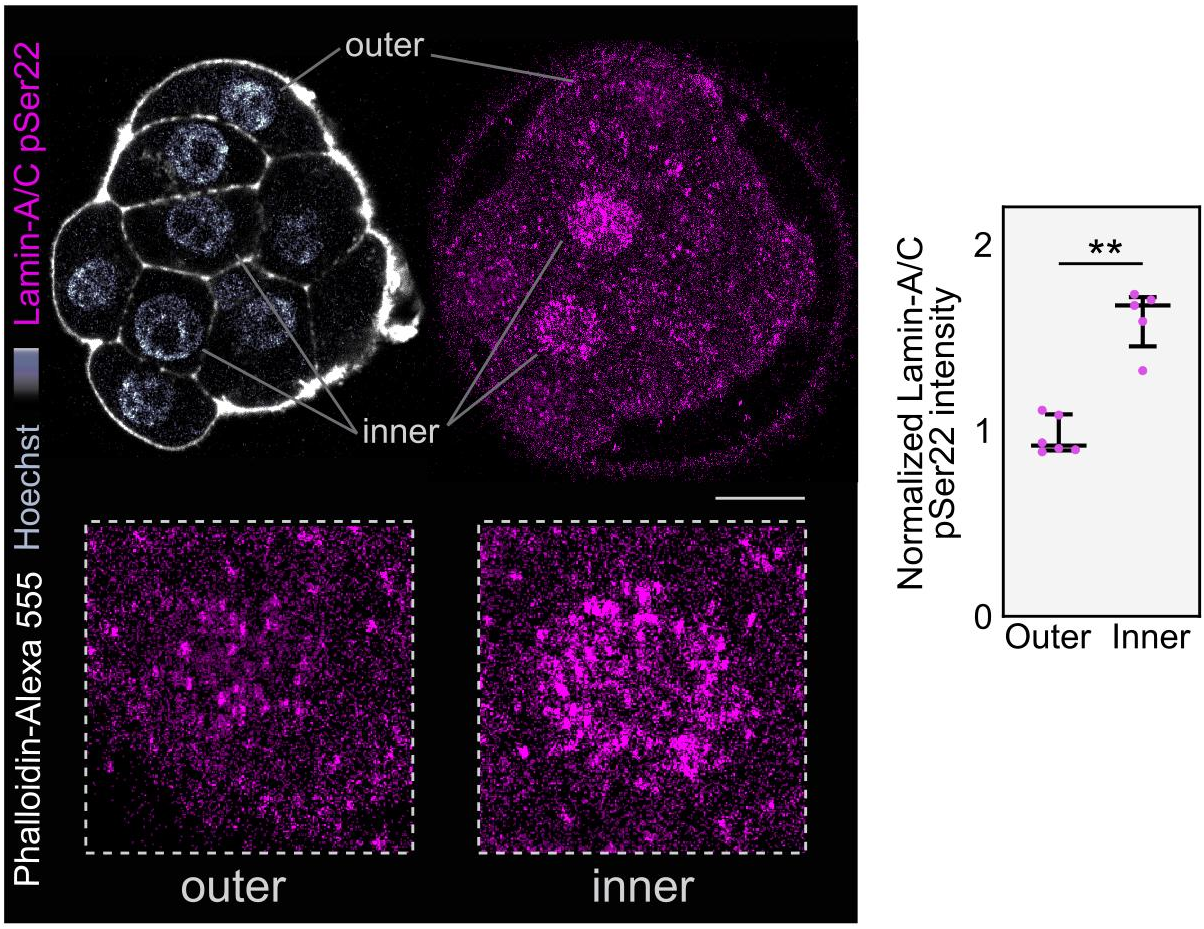

Figure 2.15 Nuclei of inner cells have higher levels of Lamin-A/C pSer22

2D confocal sections show embryos immunostained using a Lamin-A/C pSer22 phospho-specific antibody. Insets below show representative inner and outer nuclei. n=6 for outer, n=5 for inner. **P=0.0043, Mann-Whitney U test. Scale bars, 10 μm.

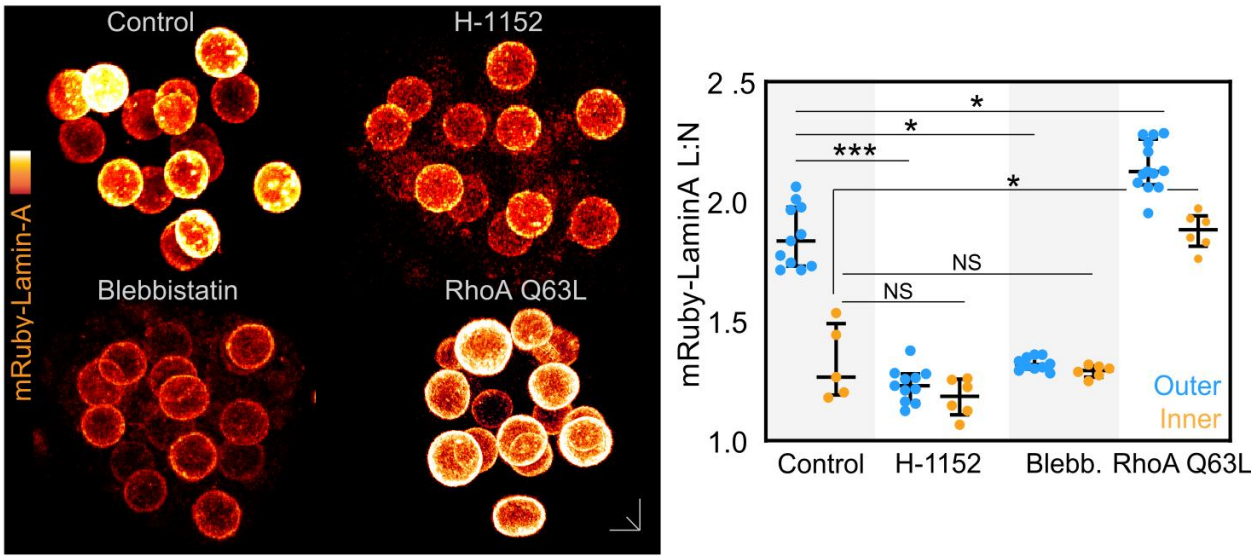

Figure 2.16 Manipulation of actomyosin contractility influences Lamin-A/C

3D projections of confocal stacks showing live embryos injected at the 1-cell stage with mRuby-Lamin-A and treated with H-1152, blebbistatin or co-injected with RhoA Q63L. n=11 for control outer, n=5 for control inner, n=11 for H-1152 outer, n=6 for H-1152 inner, n=10 for blebbistatin outer, n=6 for blebbistatin inner, n=13 for RhoA Q63L outer and n=6 for RhoA Q63L inner. ***P=0.0007, *P=0.0343 for control outer vs blebbistatin outer, *P=0.0410 for control outer vs RhoA Q63L outer. *P=0.0418 control inner vs RhoA Q63L inner. Mann-Whitney U test. Experiment performed by Yanina Alvarez. Scale bars, 10 μm.

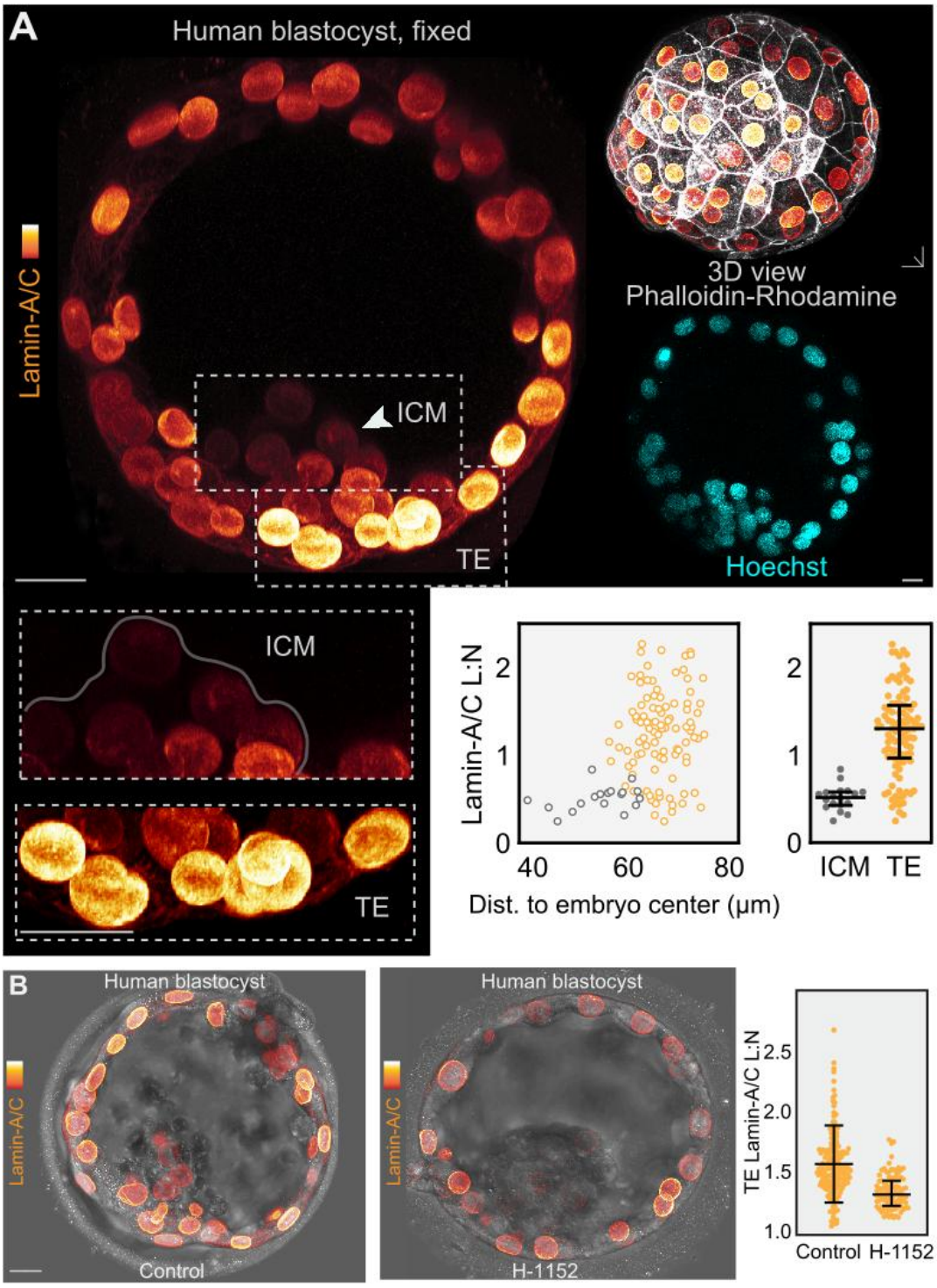

Figure 2.17 Lamin-A/C displays differential expression between ICM and trophectoderm in human blastocysts

A. Immunofluorescence for Lamin-A/C in a fixed human embryo at the blastocyst stage. 2D confocal sections are shown to illustrate ICM-trophectoderm differences. Insets show 3D projections of confocal stacks. Dots in plots represent cells from a single human embryo. **B.** Human embryo treated with H-1152. Dots in plots represent TE cells from one control embryo one treated with H-1152. Scale bars, 10 µm.

2.3.4. Lamin-A/C influences Yap and Cdx2 expression and cell identity

The changes in Lamin-A/C localisation that we observed occur in parallel with the first lineage segregation event in mammalian development. To explore whether there is a relationship between these two events, we co-stained for Lamin-A/C, phospho-Yap, and Cdx2 (Figure 2.18). Cdx2 is a marker of outer cell and trophectoderm identity, and our immunostainings revealed a strong correlation between Lamin-A/C L:N and Cdx2, with cells showing the highest Lamin-A/C L:N displaying the highest expression of Cdx2. Yap is a transcriptional co-regulator of Cdx2 and in inner cells Yap is phosphorylated and confined to the cytoplasm. After quantifying cytoplasmic levels of phosphorylated Yap we observed an inverse correlation with Lamin-A/C L:N.

To explore whether the relationship between Lamin-A/C and these markers of cell identity could be causative as well as correlative, we performed a knockdown of Lamin-A using siRNA. Microinjection of the siRNA produced an efficient, 74% reduction in Lamin-A/C protein at the 16-cell stage in embryos injected at the 1-cell stage and a 61% reduction in protein when embryos were injected at the 2-cell stage (Figure 2.19). In the outer cells of embryos injected with Lamin-A siRNA, Yap phosphorylation increased, matching the Yap phosphorylation levels normally observed in inner cells (Figure 2.20A). In contrast, Cdx2 and Yap levels decreased in the outer cells of embryos injected with Lamin-A siRNA, mimicking the levels typically observed in inner cells (Figure 2.20B and C). These stainings revealed a partial loss of nuclear Yap in response to Lamin-A siRNA and this appears to result in a complete loss of Cdx2 downstream, which is unexpected. However, Yap drives Cdx2 expression cooperatively with Tead4 (Nishioka et al., 2009), meaning Cdx2 may display a Hill-like response to Yap and scale non-linearly with its concentration. The gene regulatory network governing ICM and TE identity has also demonstrated properties of a bistable system, with Oct3/4 and Cdx2 showing reciprocal inhibition of each other (Niwa et al., 2005) and Carm1 and Cdx2 showing bistable expression patterns (Shi et al., 2015). This suggests a threshold of Yap nuclear localisation may be required before embryo ‘switches’ to a TE identity. Taken together, these results suggests that changes in Lamin-A L:N may have downstream effects on fate markers in the preimplantation embryo.

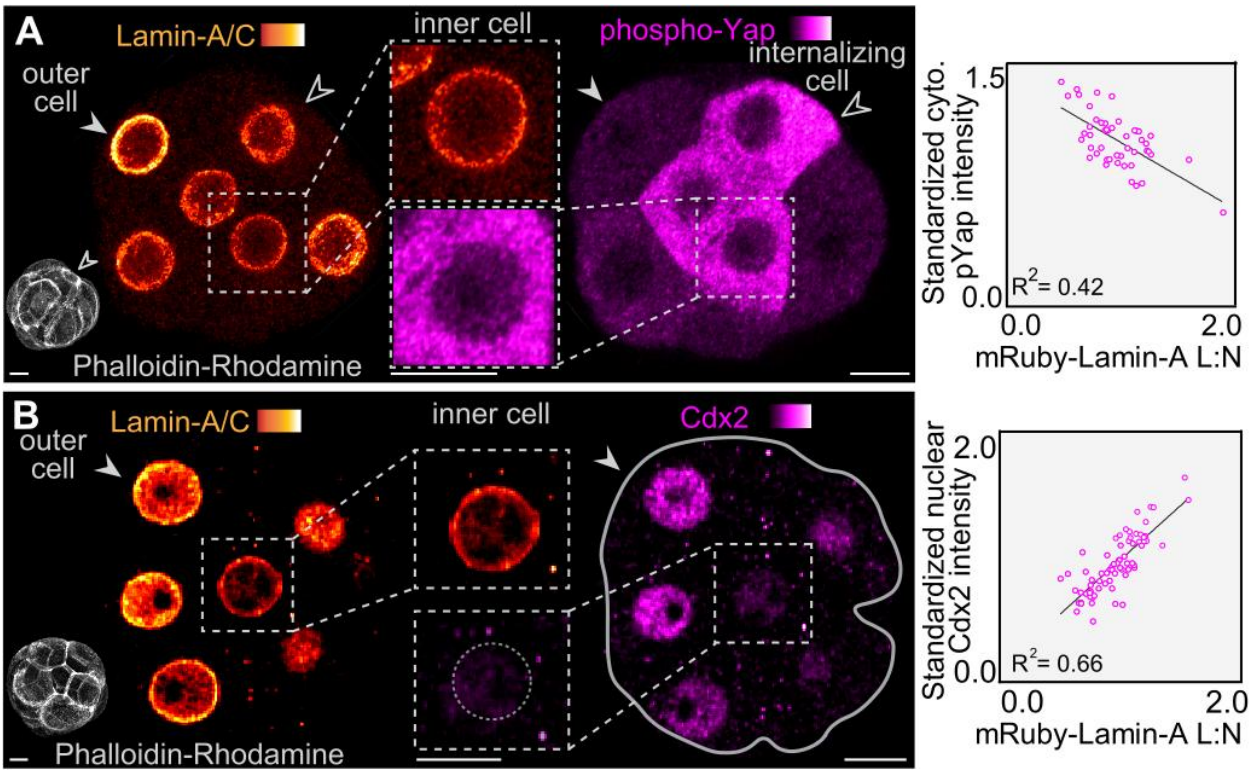

Figure 2.18 Lamin-A/C L:N correlates with markers of outer cell identity

A. 2D confocal sections of embryos immunostained for Lamin-A/C and phosphorylated Yap. Solid arrowhead indicates outer cells. Open arrowhead indicates cell undergoing internalisation via apical constriction. n=48, R^2=0.42. **B.** 2D confocal sections of embryos immunostained for Lamin-A/C and Cdx2. Solid arrowhead indicates outer cell. n=71, R^2=0.66. Experiment performed by Yanina Alvarez. Scale bars, 10 μm.

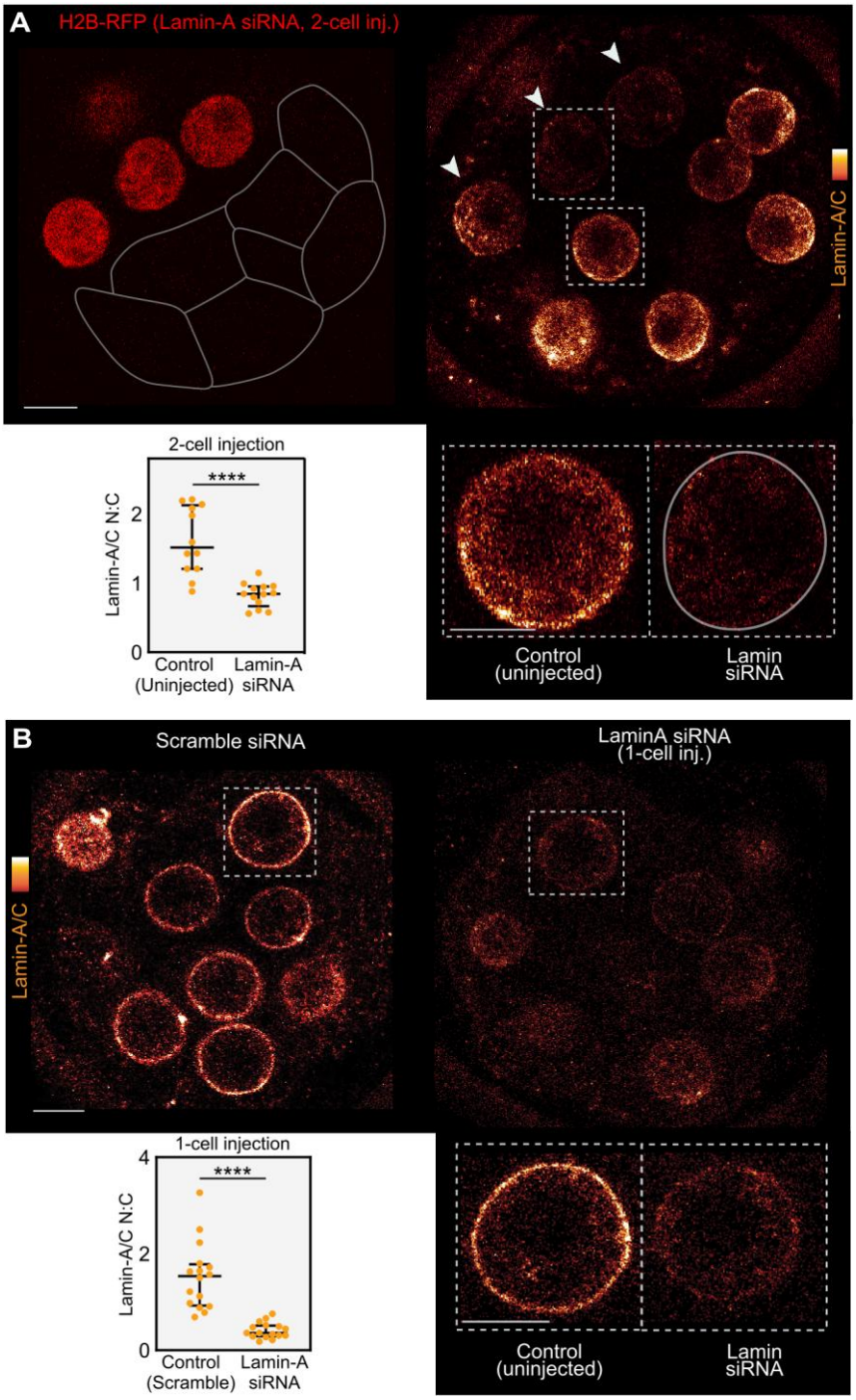

Figure 2.19 Validation of Lamin-A/C knockdown using siRNA

A. 2D confocal sections of embryos injected at the 2-cell stage with siRNA targeting Lamin-A/C and mRNA encoding H2B-RFP to label manipulated cells. Embryos were immunostained for Lamin-A/C. Insets show representative injected and uninjected nuclei. n=12 for control, n=11 Lamin-A siRNA. **B.** 2D confocal sections of embryos injected at the 1-cell stage with siRNA targeting Lamin-A/C and immunostained for Lamin-A/C. n=16 for 1-cell control and Lamin-A siRNA. ****P<0.0001, Mann-Whitney U test. Bars in dot plots represent median and interquartile range. Scale bars, 10 μm.

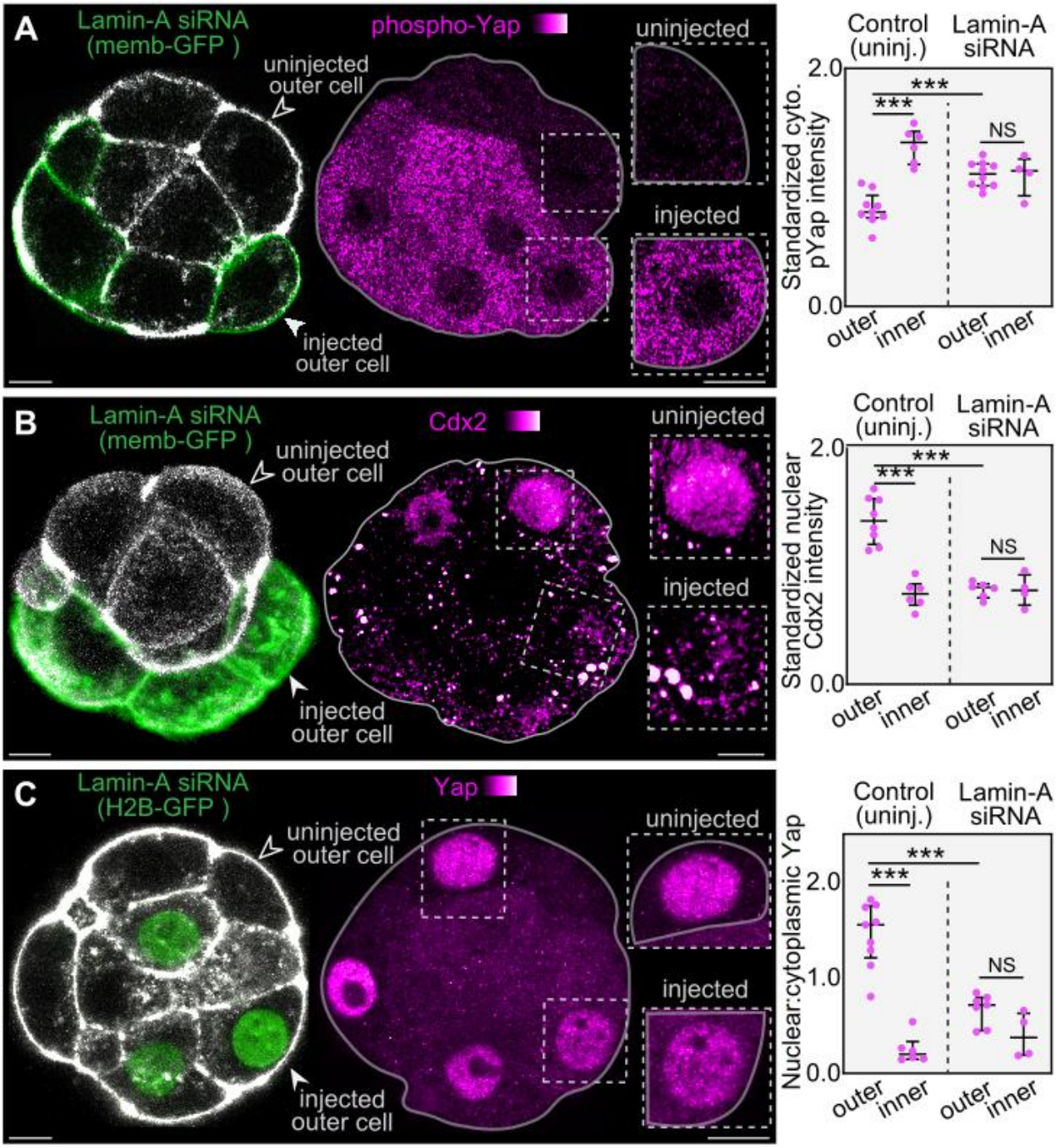

Figure 2.20 Knockdown of Lamin-A/C causes a loss of outer cell identity

A-C. 2D confocal sections of embryos injected at the 2-cell stage with siRNA targeting Lamin-A/C and either memb-GFP or H2B-RFP to label manipulated cells. Embryos were immunostained for phosphorylated Yap (A), Cdx2 (B) and Yap (C). For (A) n=9 for control outer, n=6 for control inner, n=10 for Lamin-A siRNA outer, n=4 for Lamin-A siRNA inner. ***P=0.0004 for control inner vs control outer, ***P=0.0006 for control outer vs Lamin-A siRNA outer, NS>0.999. For (B) n=8 for control outer, n=6 control inner, n=6 Lamin-A siRNA outer, n=4 Lamin-A siRNA inner. ***P=0.0007 for control

inner vs control outer, ***P=0.0007 for control outer vs Lamin-A siRNA outer, NS=0.9143. For (C) n=9 for control outer, n=6 for control inner, n=7 for Lamin-A siRNA outer, n=4 for Lamin-A siRNA inner. ***P=0.0004 for control inner vs control outer, ***P=0.0003 for control outer vs Lamin-A siRNA outer, NS=0.0727. Bars in dot plots represent median and interquartile range. Experiments performed by Yanina Alvarez. Scale bars, 10 μm

2.3.5. Changes in Lamin-A trigger actin reorganization and Amot stabilization

After observing that there may be a causal relationship between Lamin-A/C L:N and markers of cell identity, we wanted to explore possible mechanisms by which Lamin-A/C might influence their expression and localisation. A key regulator of Yap phosphorylation and localisation at this stage is Angiomotin (Amot). Current models indicate that in inner cells, Amot localises to the basolateral cortex and forms a complex with Nf2 and Lats1/2, resulting in the phosphorylation of Yap (Leung and Zernicka-Goetz, 2013). In outer cells it is believed that Amot is sequestered at the apical cortex, preventing Yap phosphorylation (Leung and Zernicka-Goetz, 2013).

We began by immunostaining embryos for Amot at the 16-cell stage using an antibody kindly donated by H. Sasaki, targeting the Amot C-terminus and recognizing both p130 and p80 isoforms (Hirate et al., 2013). This staining confirmed previous observations that Amot localises to the apical domain in outer cells and the basolateral membrane in inner cells. However, we also observed significant changes in the levels of Amot in the cytoplasm between inner and outer cells, with inner cells having significantly higher levels of Amot in the cytoplasm (Figure 2.22A). This was quantified by computationally segmenting both the cortex and cytoplasm (Figure 2.21). A similar expression pattern of Amot was observed in human blastocysts, with Amot in cells of the ICM being present in both the cytoplasm and at the basolateral cortex and Amot in outer cells being confined to the apical cortex (Figure 2.23). To test whether these changes in Amot levels between inner and outer cells might be the result of changes in Lamin-A/C, we performed a knockdown of Lamin-A/C using siRNA. Reducing the expression of Lamin-A/C in outer cells led to increased Amot in the cytoplasm, producing a phenotype similar to that of the unmanipulated inner cells (Figure 2.22B).

In endothelial cells it has been shown that the N-terminal domain of the p130 isoform of Amot co-localizes with F-actin in mouse aortic endothelial cells (Ernkvist et al., 2006). This, along with our observation of an extensive F-actin meshwork throughout the cytoplasm of blastomeres at these stages (Figure 2.11) prompted an investigation into potential differences in actin organisation at these stages. Staining with phalloidin revealed a significantly denser F-actin meshwork in the cytoplasm of inner cells, consistent with the higher levels of Amot observed there (Figure 2.24). In contrast, the F-actin meshwork in outer cells is relatively sparse in the cytoplasm and concentrated at the apical cortex, also matching the expression pattern of Amot observed there.

Staining for F-actin was also performed on human blastocysts and revealed similar patterns of actin organisation to those we observed in the mouse embryo (Figure 2.25). At the blastocyst stage, human embryos showed high levels of F-actin in the cytoplasm of inner cells, as well as high concentrations of F-actin at the apical cortex of outer cells.

Experiments in mutant mice deficient in Lamin-A/C show that loss of Lamin-A/C results in altered actin dynamics in cardiac tissues and embryonic fibroblasts, due to a loss of emerin localisation to the inner nuclear membrane (Ho et al., 2013). To explore whether the differences in actin organisation we observed are Lamin-A/C dependent we injected one cell of 2-cell stage embryos with siRNA targeting Lamin-A/C. This resulted in a significant increase in the levels of cytoplasmic F-actin throughout the embryo, suggesting that the dense F-actin meshwork observed in the cytoplasm of inner cells may be the result of changes in the nuclear lamina that occur as cells internalise (Figure 2.24). If Amot observed in the cytoplasm of inner cells is binding to actin its mobility is likely reduced. To assess the mobility of Amot, a FRAP experiment was performed using a fluorescently tagged Amot (Emerald-Amot). This revealed a significantly larger immobile fraction of Amot in inner cells (Figure 2.27). This is in line with increased Actin binding to the denser meshwork observed there. To explore a potential interaction between actin and Amot in more detail, we treated embryos with Latrunculin-A, which binds to actin monomers, preventing polymerisation. Rather than a redistribution of Amot, loss of F-actin resulted in a global decrease in Amot levels throughout the embryo, including the apical cortex of outer cells and the cytoplasm of inner cells (Figure 2.28). These results suggest that actin binding may affect the stability and turnover of Amot, in addition to localisation. In previously published research, where Amot was demonstrated to colocalise with actin cables, Amot redistributed into puncta upon treatment with Latrunculin A (Ernkvist et al., 2006). However, the authors did not attempt to quantify changes in the total levels of Amot, so it unclear whether stability was also affected. Ernkvist et al. also treated with Latrunculin A for a shorter duration (1 hr vs 4 hrs in this study), suggesting that Amot may immediately redistribute upon loss of actin with total protein decreasing over a longer duration.

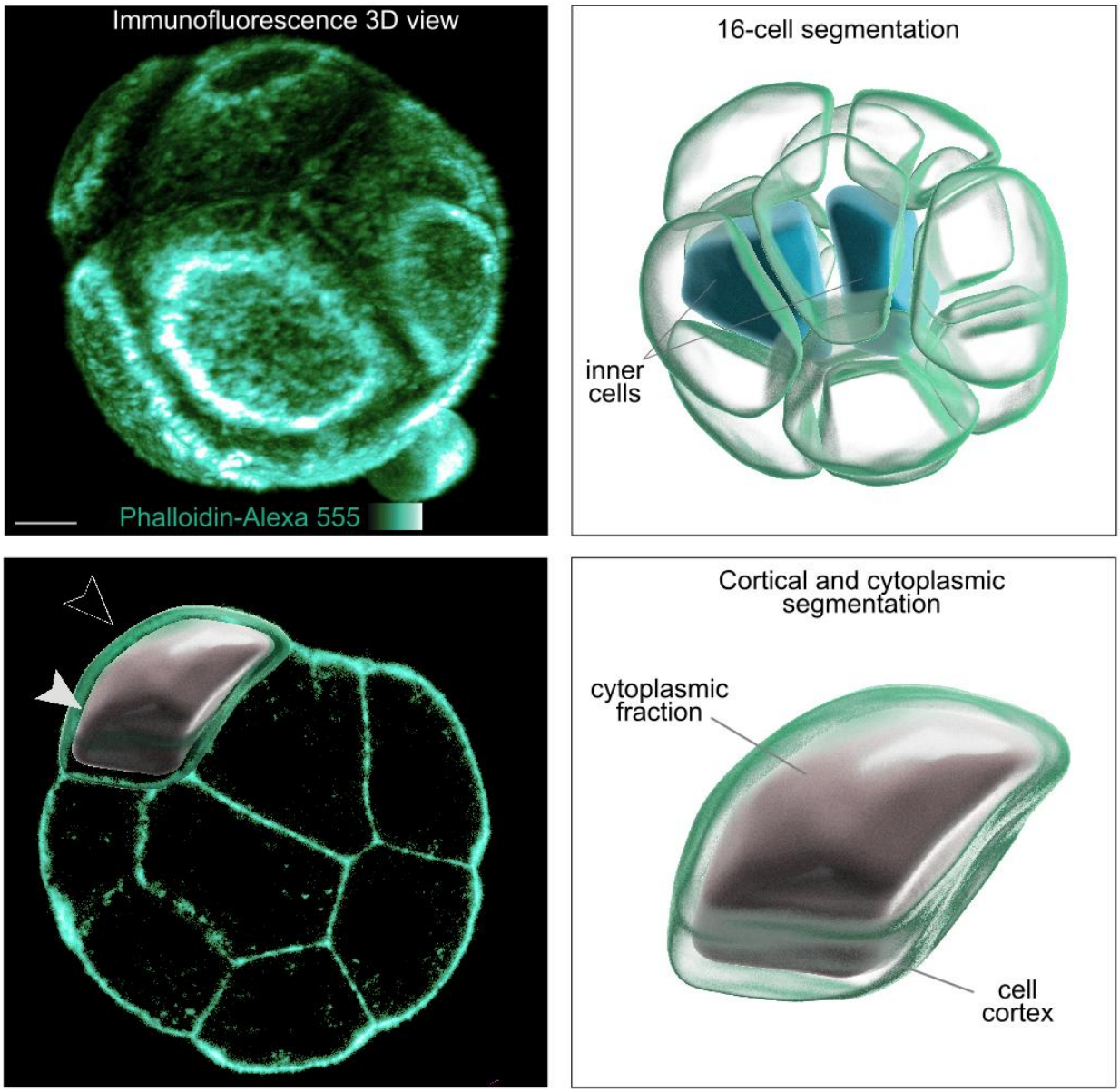

Figure 2.21 3D segmentation of embryos, defining inner and outer cells as well as cytoplasm and cell cortex

3D projection of embryo stained with phalloidin along with examples of an embryo are segmented based on this signal. Cells can then be segmented into cytoplasm (opaque) and cell cortex (transparent). Using these segmentations cells are then grouped as inner (blue) or outer (green). Scale bars, 10 μm.

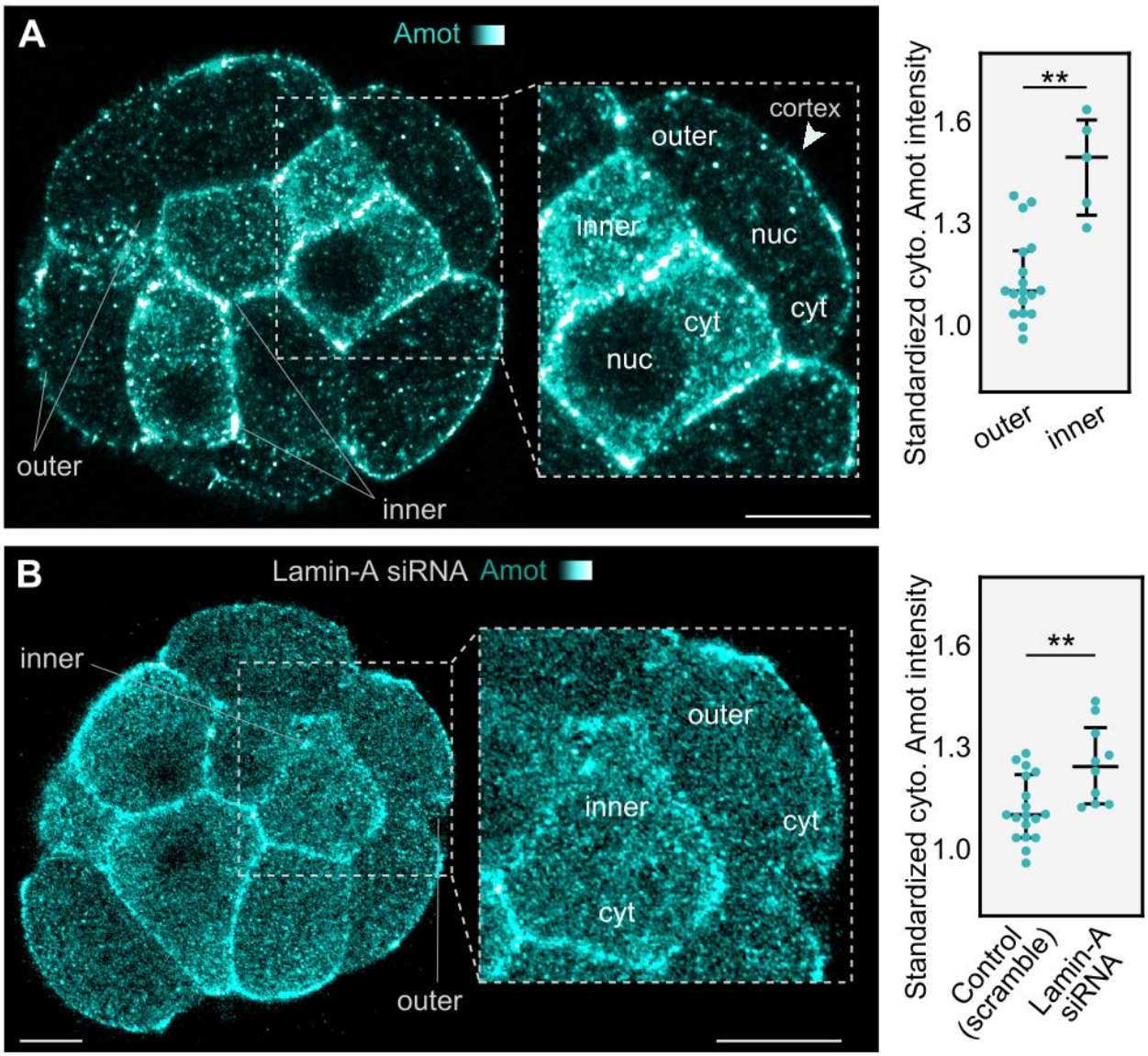

Figure 2.22 Amot is differentially expressed in the cytoplasm between inner and outer cells in a Lamin-A/C dependent manner

A. 2D confocal sections an of embryo immunostained for Amot. Inset highlights differences between inner and outer cells. n=18 for outer, n=5 for inner **P=0.0011, Mann-Whitney U test. **B.** 2D confocal sections of embryos injected at the 1-cell stage with siRNA targeting Lamin-A/C and immunostained for Amot. n=18 for control, n=10 for Lamin-A siRNA **P=0.003, Mann-Whitney U test. Bars in dot plots represent median and interquartile range. Scale bars, 10 μm

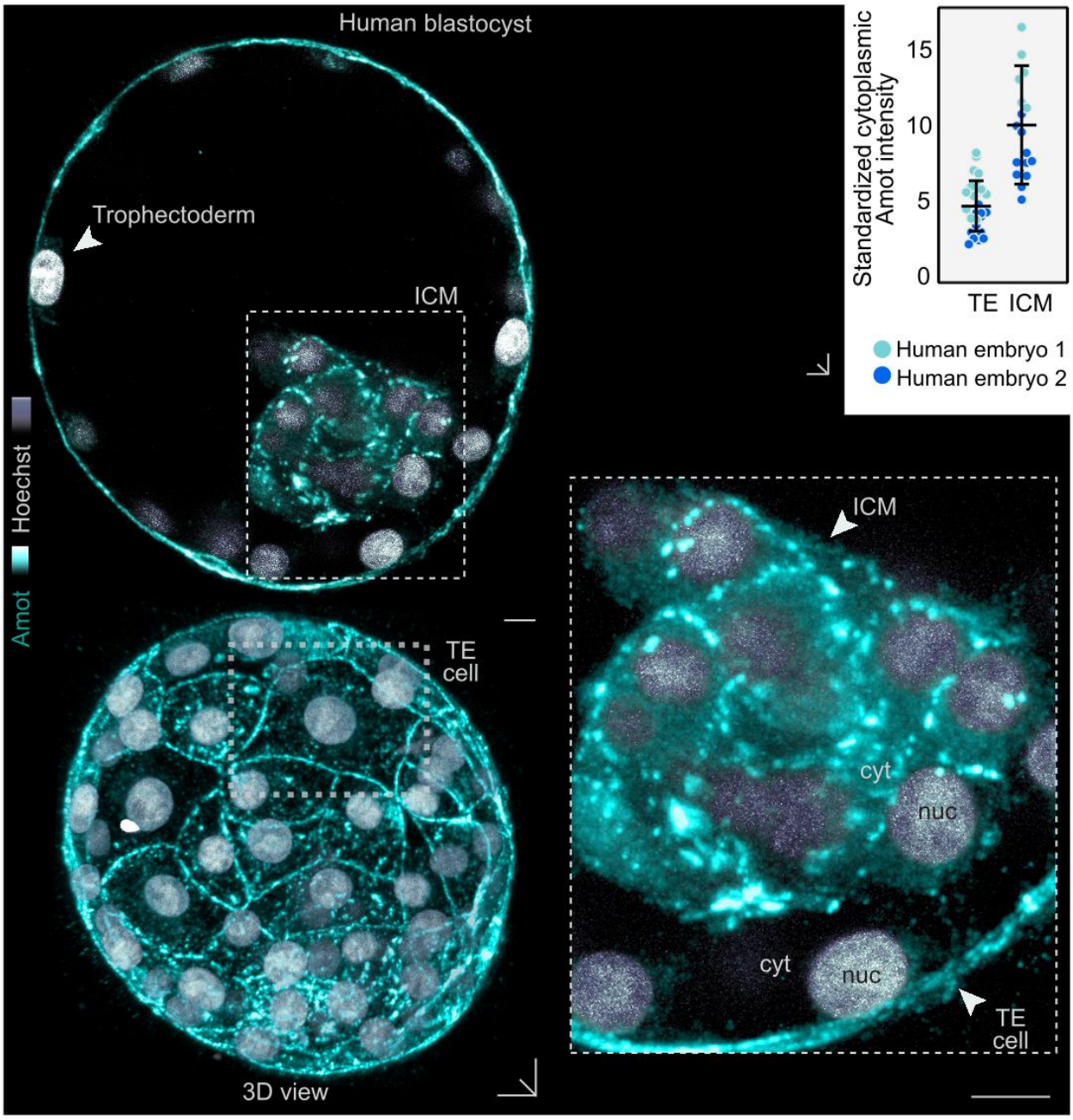

Figure 2.23 Amot is differentially expressed between the cytoplasm of cells of TE and ICM in human blastocysts.

Image of a human blastocyst immunostained for Amot. A 2D confocal section along with inset shows differences between ICM and TE. n=2. Bars in dot plots represent median and interquartile range. Scale bars, 10 μm.

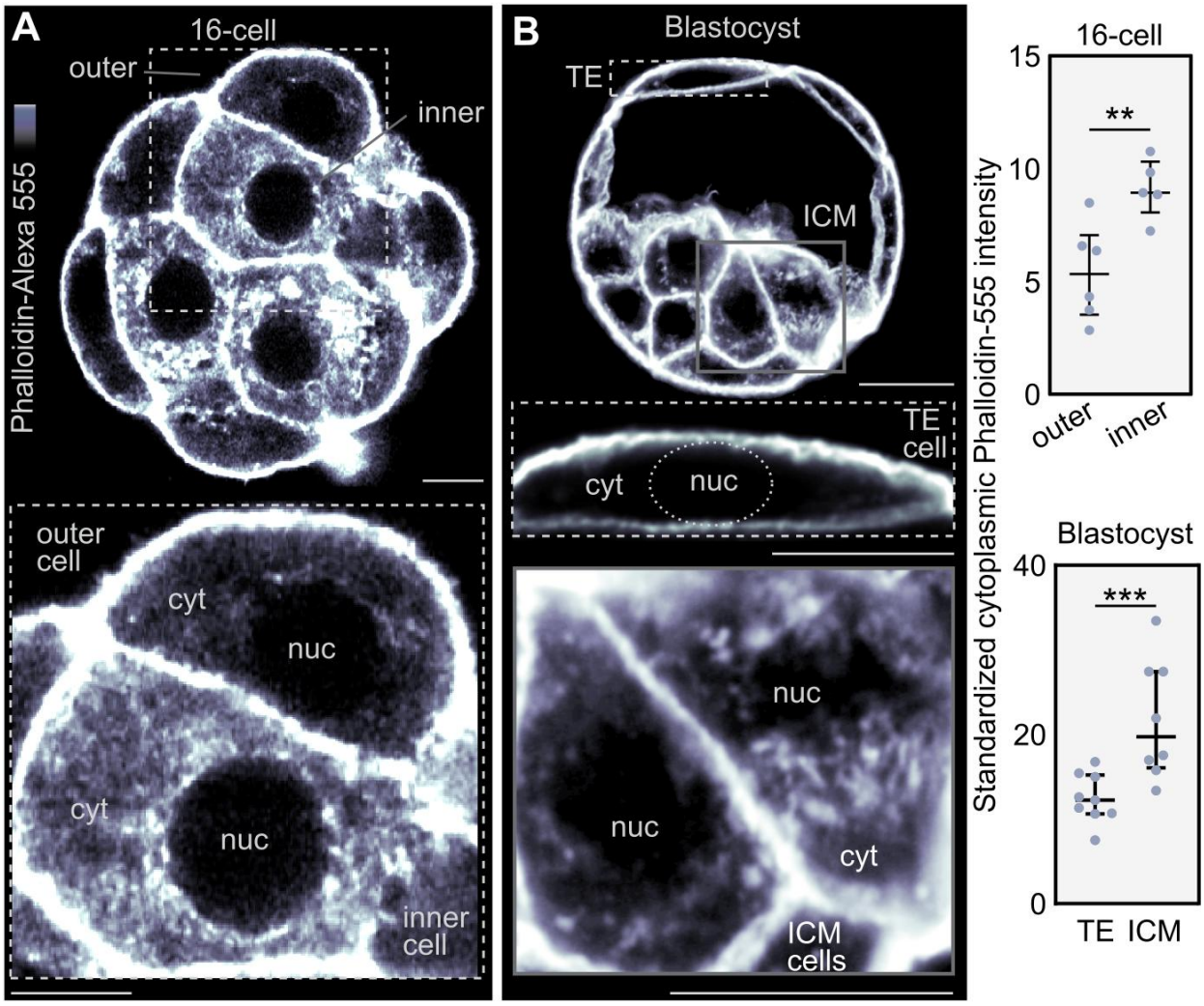

Figure 2.24 F-actin is differentially organised in the cytoplasm between inner and outer cells at the 16-cell stage

A. 2D confocal sections of a 16-cell embryo stained with phalloidin. Inset highlights differences between inner and outer cells. n=5 for 16-cell inner, n=6 for 16-cell outer, **P=0.0087, Mann-Whitney U test. **B.** 2D confocal sections a blastocyst stained with phalloidin. Inset highlights differences between ICM and TE cells. n=8 for blastocyst ICM, n=25 for blastocyst trophectoderm, ***P=0.001, Mann-Whitney U test. Experiment performed by Yanina Alvarez. Scale bars, 10 μm.

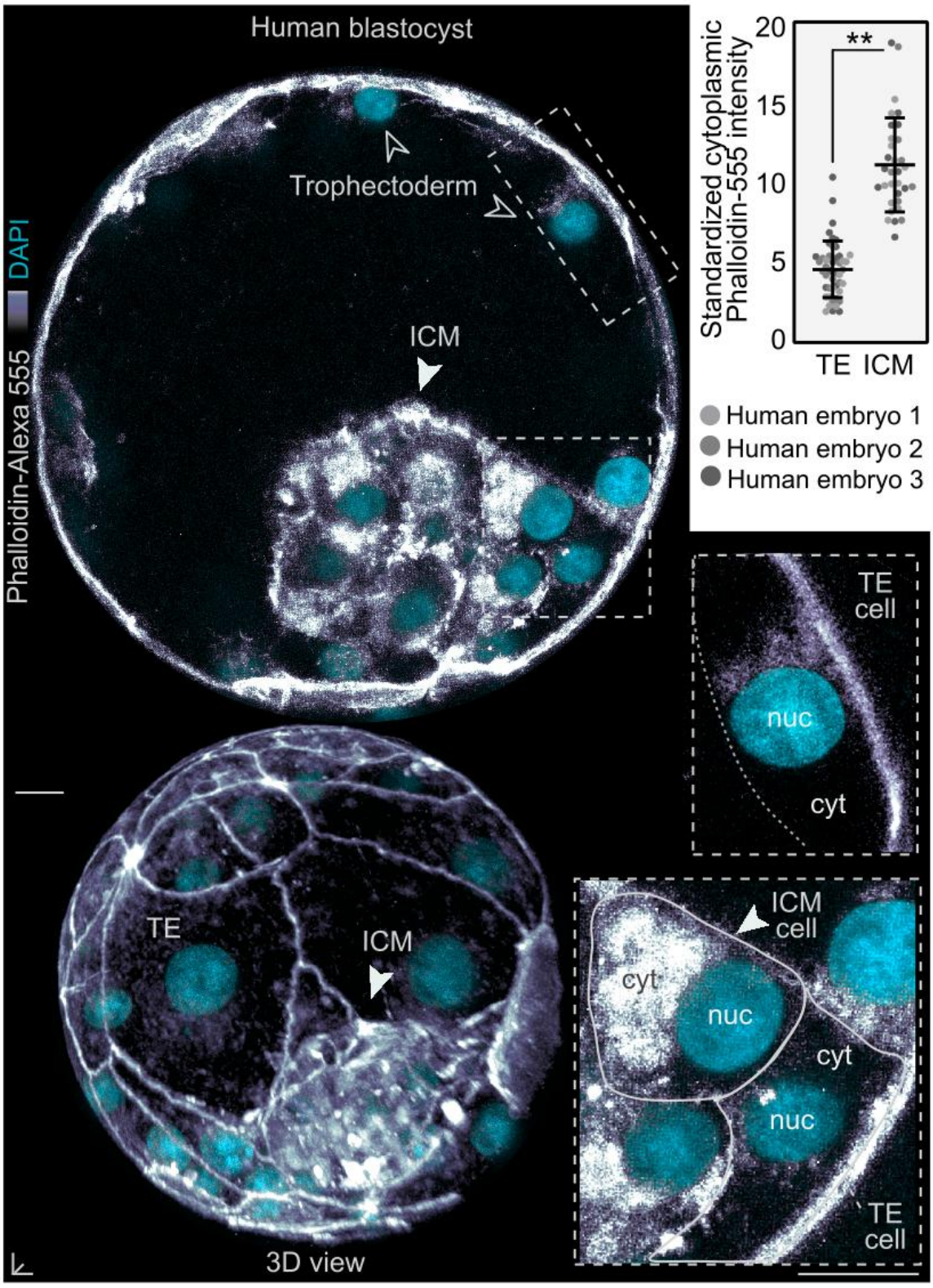

Figure 2.25 F-actin is differentially organised between the cytoplasm of cells of TE and ICM in human blastocysts.

Image of a human blastocyst stained with phalloidin. A 2D confocal section along with inset shows differences between ICM and TE. n=3, P=0.0025, Mann-Whitney U test. Bars in dot plots represent median and interquartile range. Scale bars, 10 μm.

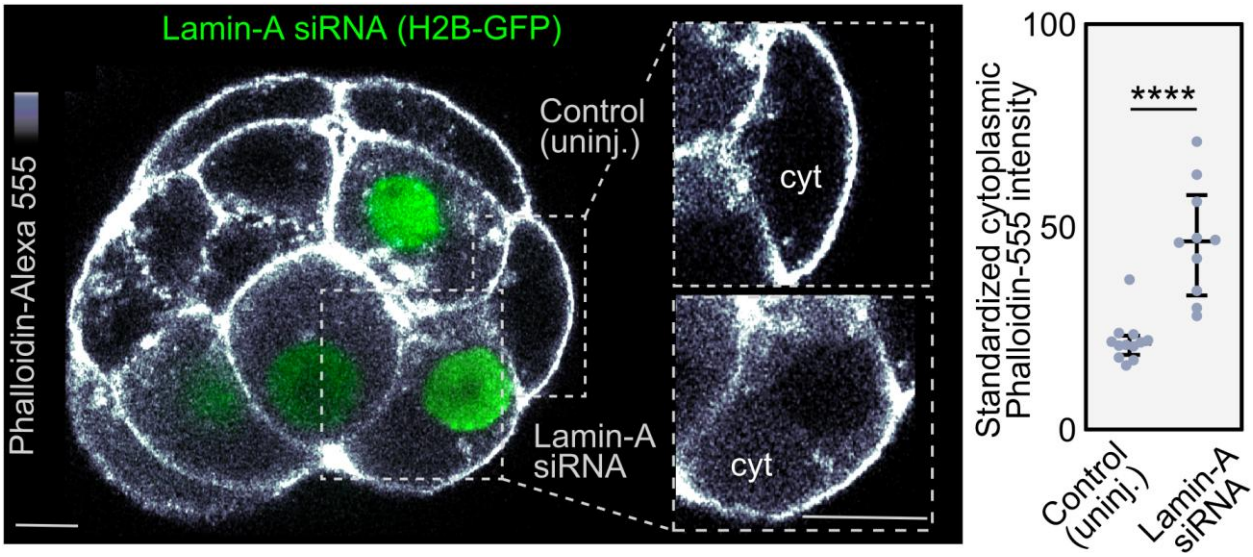

Figure 2.26 Differential actin organisation between inner and outer cells at the 16-cell stage is Lamin-A/C dependent

2D confocal sections an of embryo injected at the 2-cell stage with siRNA targeting Lamin-A/C and H2B-GFP to label manipulated cells. Embryos were stained with phalloidin. Insets highlight differences between injected and uninjected outer cells. n=12 for control, n=10 for Lamin-A siRNA. ****P<0.0001, Mann-Whitney U test. Bars in dot plots represent median and interquartile range. Experiment performed by Yanina Alvarez. Scale bars, 10 μm

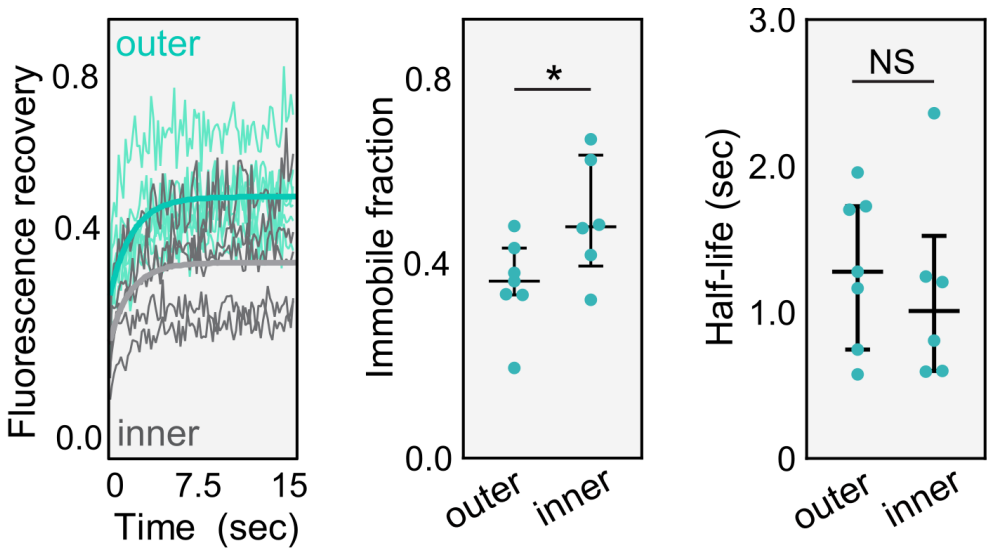

Figure 2.27 FRAP reveals that inner cells have a larger immobile fraction of Amot in the cytoplasm than outer cells

Embryos were injected at the 2-cell stage with mRNA encoding Emerald-Amot. n=6 for inner cells, n=7 for outer cells. *P=0.022, Mann-Whitney U test. Bars in dot plots represent median and interquartile range.

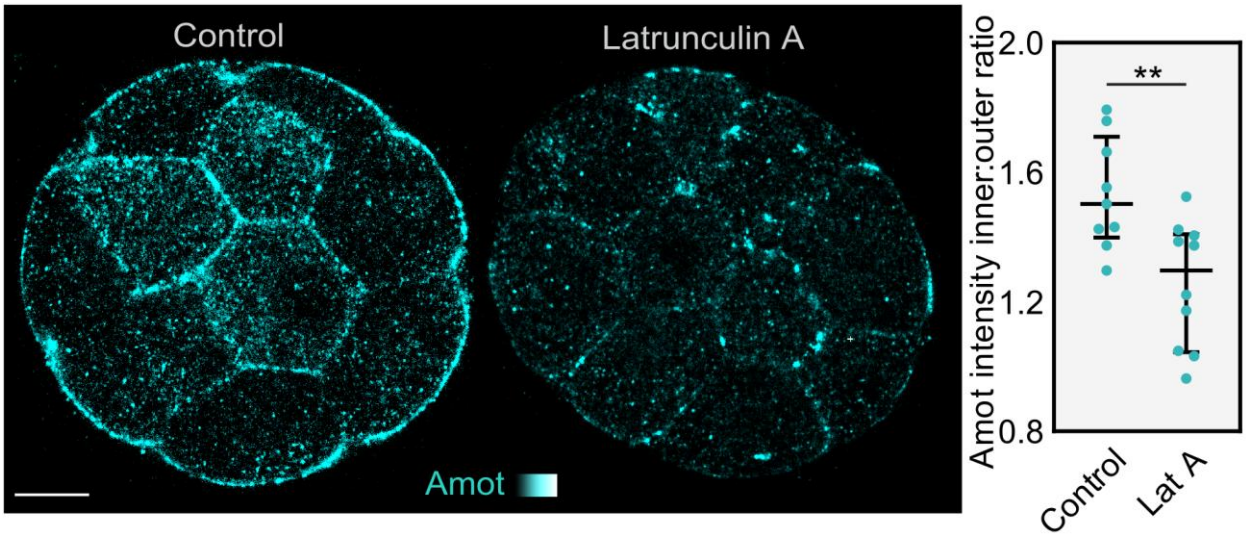

Figure 2.28 Treatment with Latrunculin A results in a loss of differential Amot organisation between inner and outer cells.

2D confocal sections showing 16-cell embryos immunostained with Amot after treatment with Latrunculin A. n=9 for control, n=10 Latrunculin A, **P=0.0061 Mann-Whitney U test. Bars in dot plots represent median and interquartile range. Scale bars, 10 μm.

2.3.6. Lamin-A regulates the F-actin meshwork via Formin-2 localisation

To investigate the mechanism by which Lamin-A may establish differences in actin organisation between inner and outer cells we examined the expression of actin nucleators. While Formin-2 has been demonstrated to play a number of roles in meiosis (Almonacid et al., 2019; Dumont et al., 2007; Schuh, 2011), it has yet to be demonstrated to play a role in preimplantation development. Immunostaining for Formin-2 revealed changes in localisation, which could be responsible for changes in actin organisation between inner and outer cells. Here we observed that Formin-2 becomes increasingly concentrated in the nucleus as embryos progress to the 16-cell stage (Figure 2.29). Formin-2 is present in both the cytoplasm and nucleus at the 2-cell stage, then is increasingly confined to the nucleus as cells reach the 16-cell stage. However, at the 16-cell stage, as cells segregate into inner and outer positions, the nuclear concentration of Formin-2 drops in inner cells. These events are consistent with the formation of a dense F-actin meshwork in the cytoplasm of inner cells. This led us to hypothesise that Lamin-A/C regulates actin organisation via changes in Formin-2 localisation.

To test this, we performed another knockdown of Lamin-A/C using siRNA delivered by microinjection, this time at 1-cell stage. Treated embryos showed a change in Formin-2 localisation in outer cells, shifting from the nucleus to the cytoplasm, displaying similar localisation to inner cells in control embryos (Figure 2.30). Treatment with Leptomycin B, a selective inhibitor of nuclear export, resulted in a loss of differential localisation of Formin-2 between inner and outer cells (Figure 2.31), suggesting that Lamin-A/C may regulate nuclear transport to establish differences in actin organisation between inner and outer cells. To further explore the role of Formin-2 in establishing inner and outer cell identities we treated embryos with SMIFH2, an inhibitor of FH2 domain activity, to inhibit Formin-2 activity (Figure 2.32). This resulted in a loss of the dense, cytoplasmic F-actin meshwork we previously observed in inner cells, as well as a loss of inner cell identity, as indicated by increased nuclear localisation of Yap. We then attempted to induce ectopic actin nucleation in outer cells by injecting a high concentration of mRNA encoding Formin-2 tagged with emerald (Figure 2.33). Expression of the emerald tagged Formin-2 was primarily cytoplasmic, with a relatively small nuclear fraction compared to endogenous Formin-2 observed by immunostaining. This may be a result of the fluorescent tag interfering with nuclear

localisation or the level of overexpression causing ectopic localisation. However, this overexpression succeeded in producing additional F-actin in the cytoplasm of outer cells. This resulted in ectopic stabilisation of Amot, and a significant reduction in Yap nuclear localisation, suggesting a partial loss of outer cell identity.

In addition to Formin-2, we explored the possibility other actin nucleators regulate the actin reorganisation seen in these stages including the Arp2/3 complex. Although we were unable to obtain antibodies or produce a fusion protein that displayed a consistent expression pattern, treatment with the Arp2/3 inhibitor CK-666 disrupted the formation of a dense F-actin meshwork in inner cells (Figure 2.34). The resulting phenotype was similar to what was observed after treatment with SMIFH2 and inner cells showed similar ectopic nuclear localisation of Yap. The VCA domain of WASP proteins is a key activator of the Arp2/3 complex (Campellone and Welch, 2010; Chaigne et al., 2015), promoting nucleation of new actin filaments. Microinjection of mRNA encoding the VCA domain tagged with mRuby (VCA-mRuby) caused the formation of a dense actin meshwork in outer and a reduction in nuclear Yap (Figure 2.35).

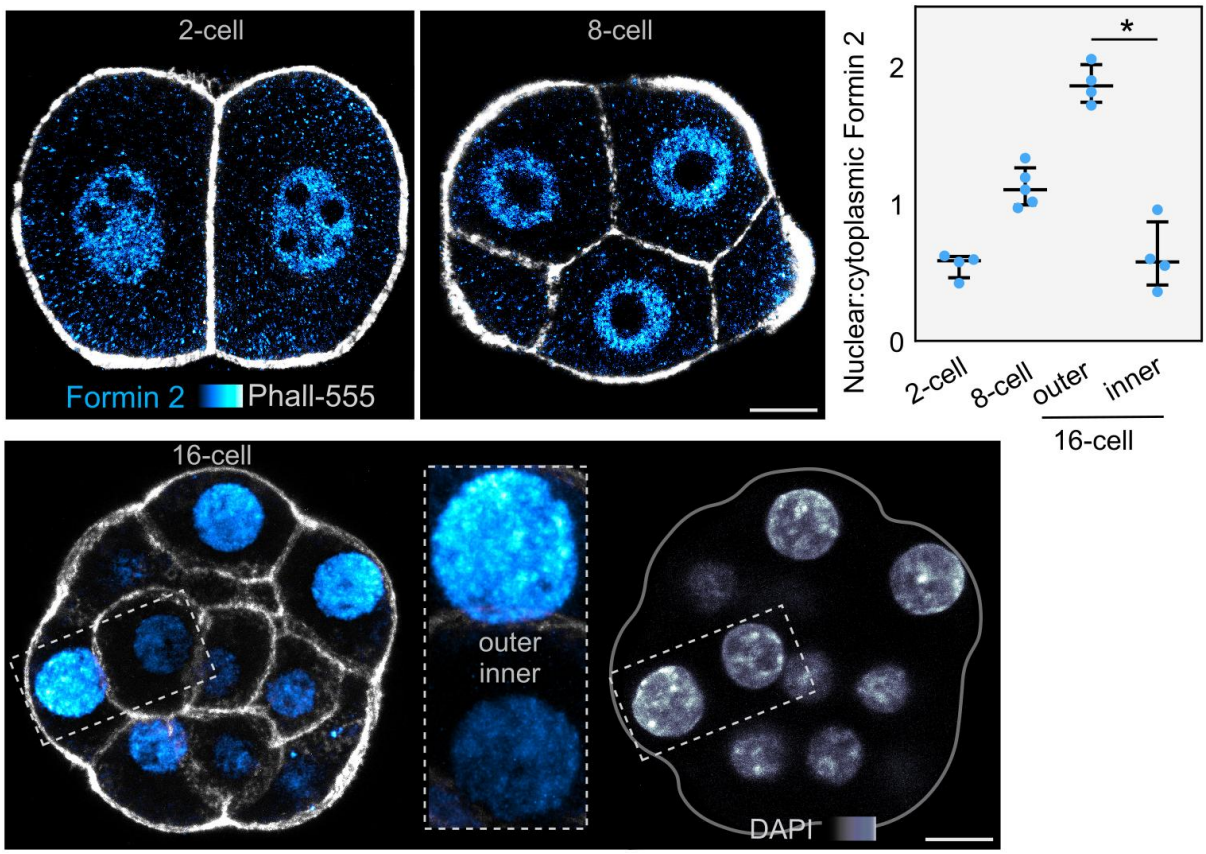

Figure 2.29 Formin-2 is localised to the nucleus and is differentially expressed between inner and outer cells

2D confocal sections showing embryos at different cleavage stages immunostained for Formin-2. Insets highlight differential expression of Formin-2 between inner and outer cells. n=4 for all stages. *P=0.0286, Mann-Whitney U test. Bars in dot plots represent median and interquartile range. Scale bars, 10 μm

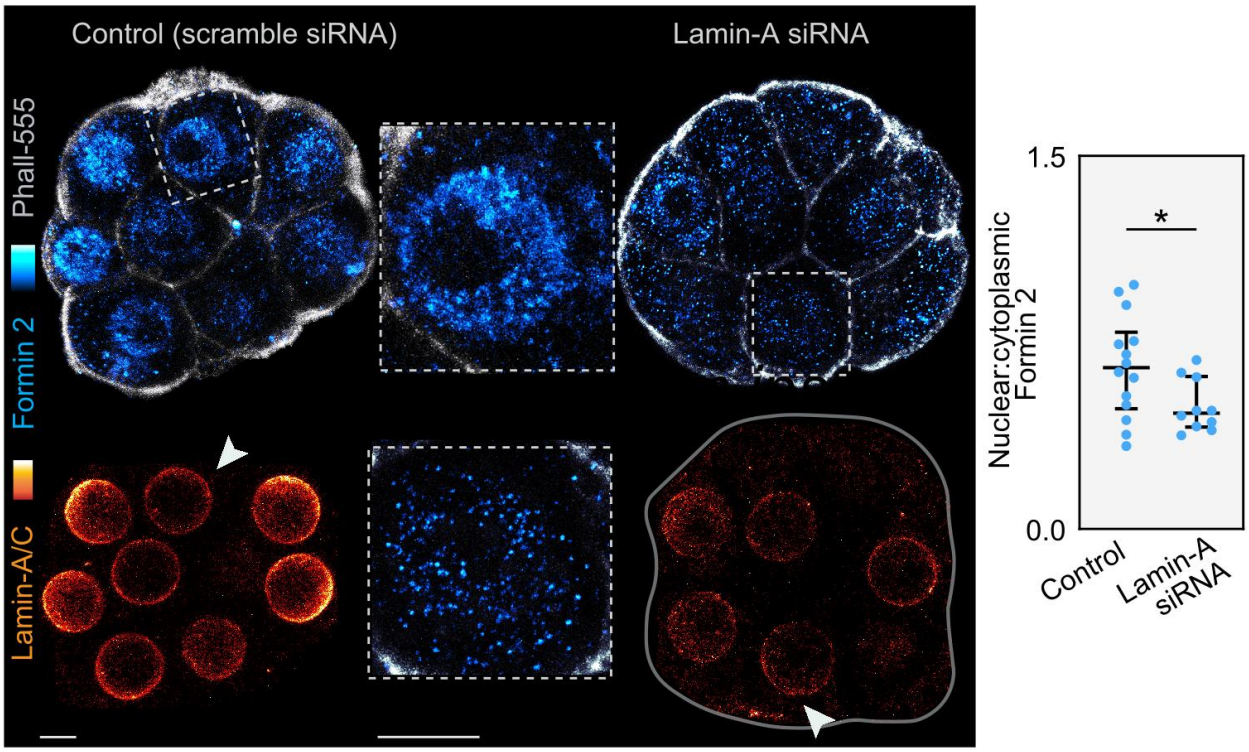

Figure 2.30 Differential Formin-2 localisation between inner and outer cells is Lamin-A/C dependent

2D confocal sections of embryos inected at the 1-cell stage with siRNA targeting Lamin-A/C and immunostained for Formin-2 and Lamin-A/C. Insets highlight differences between inner and outer nuclei. n=14 for control, n=10 for Lamin-siRNA. *P=0.0470, Mann-Whitney U test. Bars in dot plots represent median and interquartile range. Scale bars, 10 μm

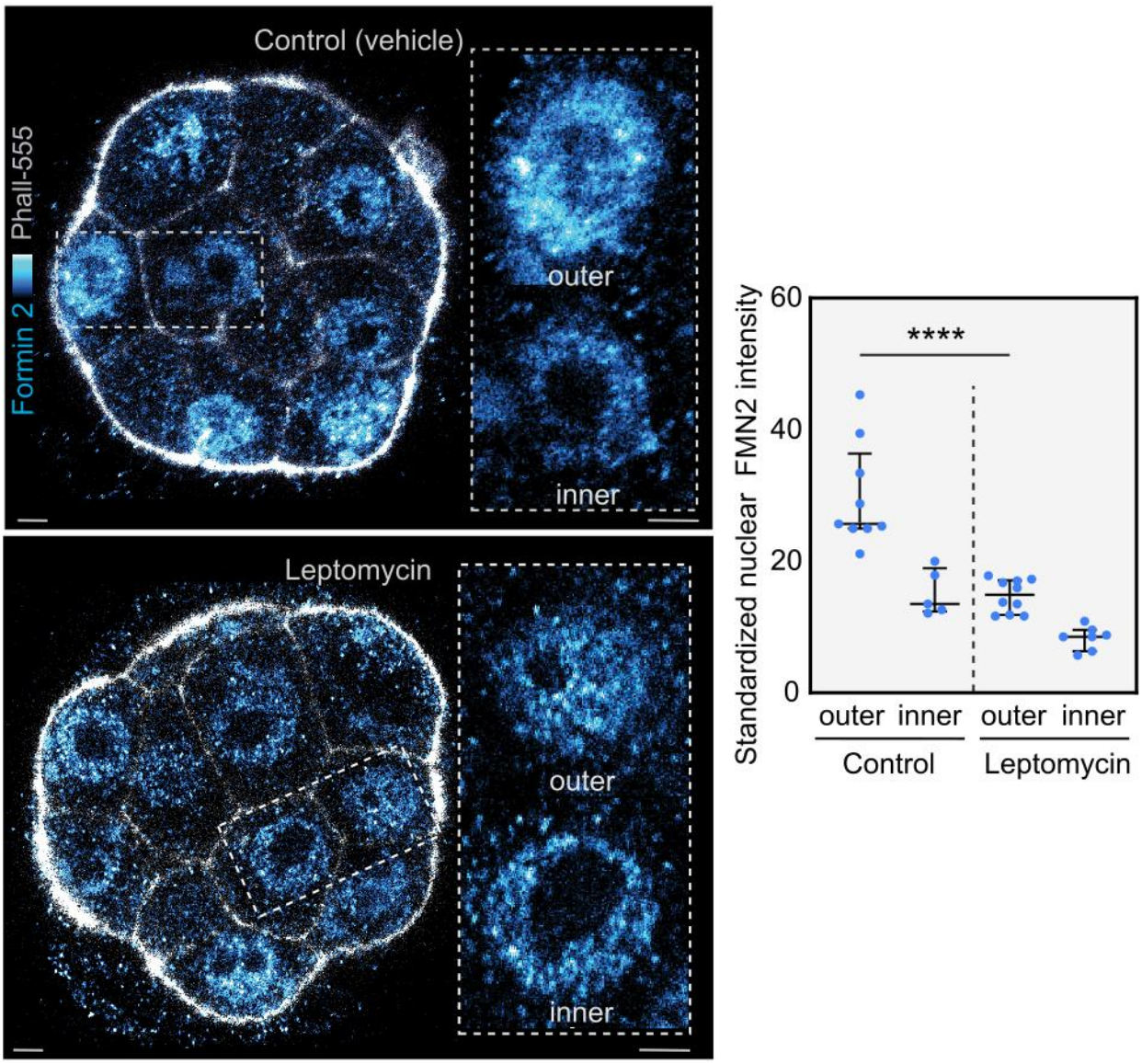

Figure 2.31 Treatment with Leptomyocin causes a loss of differential Formin-2 localisation between inner and outer cells

2D confocal sections of 16-cell embryo immunostained for Formin-2 after treatment with DMSO (control) or Leptomyocin B (100 nM). Insets highlight differences between inner and cell nuclei for each treatment group. n=9 for control outer, n=5 for control inner, n=10 for leptomycin B outer, n=7 for leptomycin B inner. ****P<0.0001, Kruskal-Wallis test. Bars in dot plots represent median and interquartile range. Scale bars, 10 µm

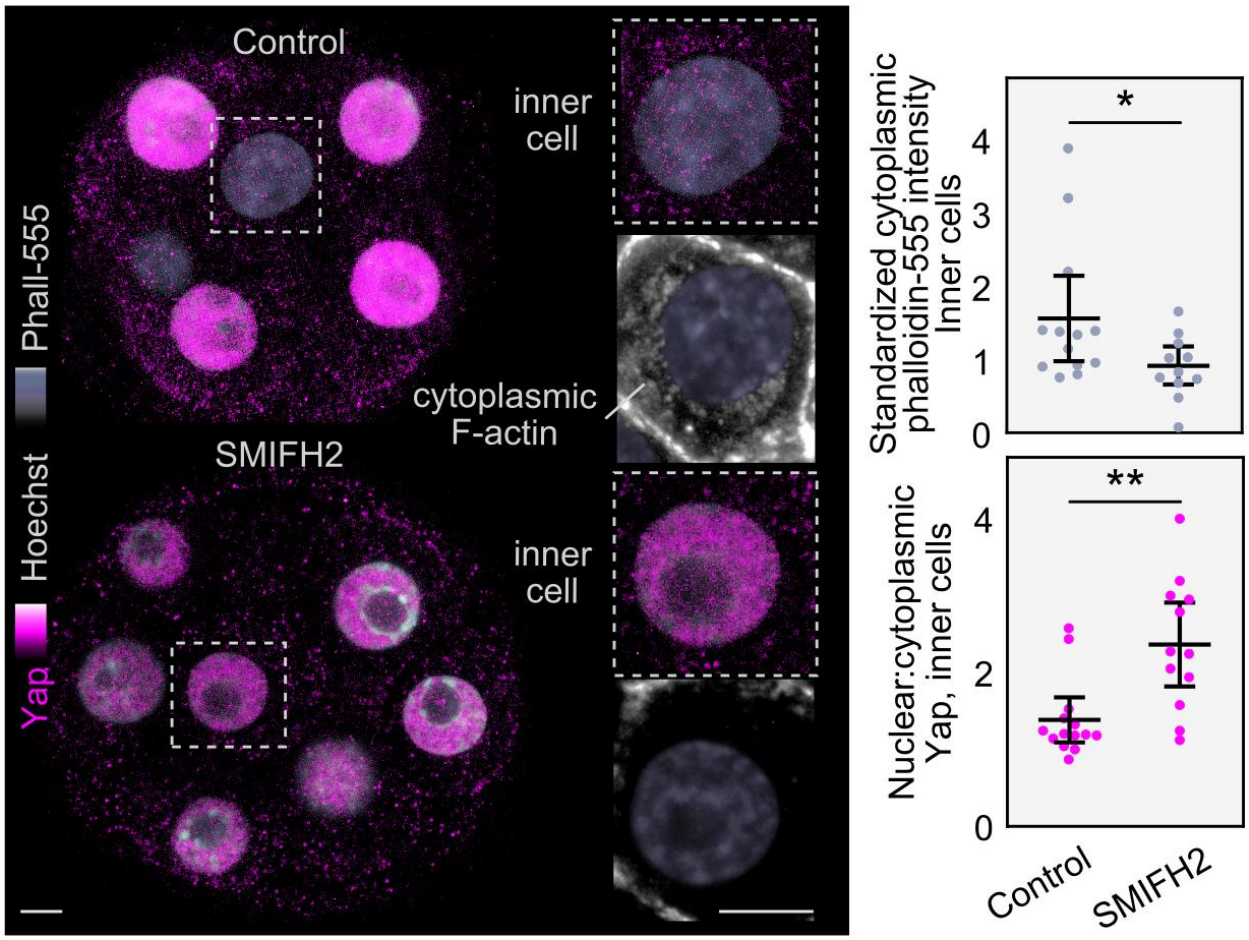

Figure 2.32 Treatment with SMIFH2 causes a loss of inner-outer cell identity

2D confocal sections of a 16-cell embryo immunostained for Yap after treatment with DMSO (control) or 250 µM SMIFH2. Insets highlight differences between inner cell nuclei in control and treatment groups as well as differences in cytoplasmic F-actin. n=13 for control, n=11 for SMIFH2, *P=0.0364, **P=0.0024, Mann-Whitney U test. Bars in dot plots represent median and interquartile range. Scale bars, 10 µm

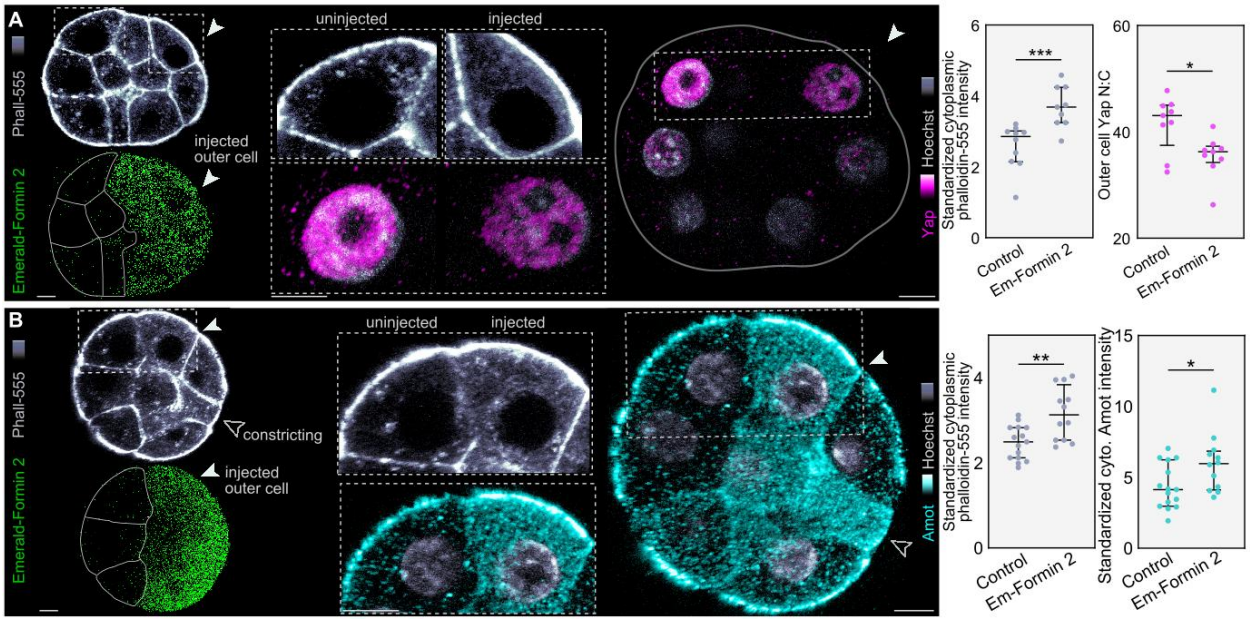

Figure 2.33 Overexpression of Formin-2 causes loss of outer cell identity

A-B. 2D confocal sections of embryos injected at the 2-cell stage with mRNA encoding Emerald-Formin2 and immunostained for Yap (A) or Amot (B). Insets highlight differences between nuclear Yap (A), cytoplasmic Amot (B) and cytoplasmic F-actin (A and B) between injected and uninjected outer cells. n=10 for Emerald-Formin-2 (injected cells), n=9 for control (uninjected cells). ***P=0.0006, **P=0.0063, *P=0.0244 (A), *P=0.0414 (B), Mann-Whitney U test. Bars in dot plots represent median and interquartile range. Scale bars, 10 μm

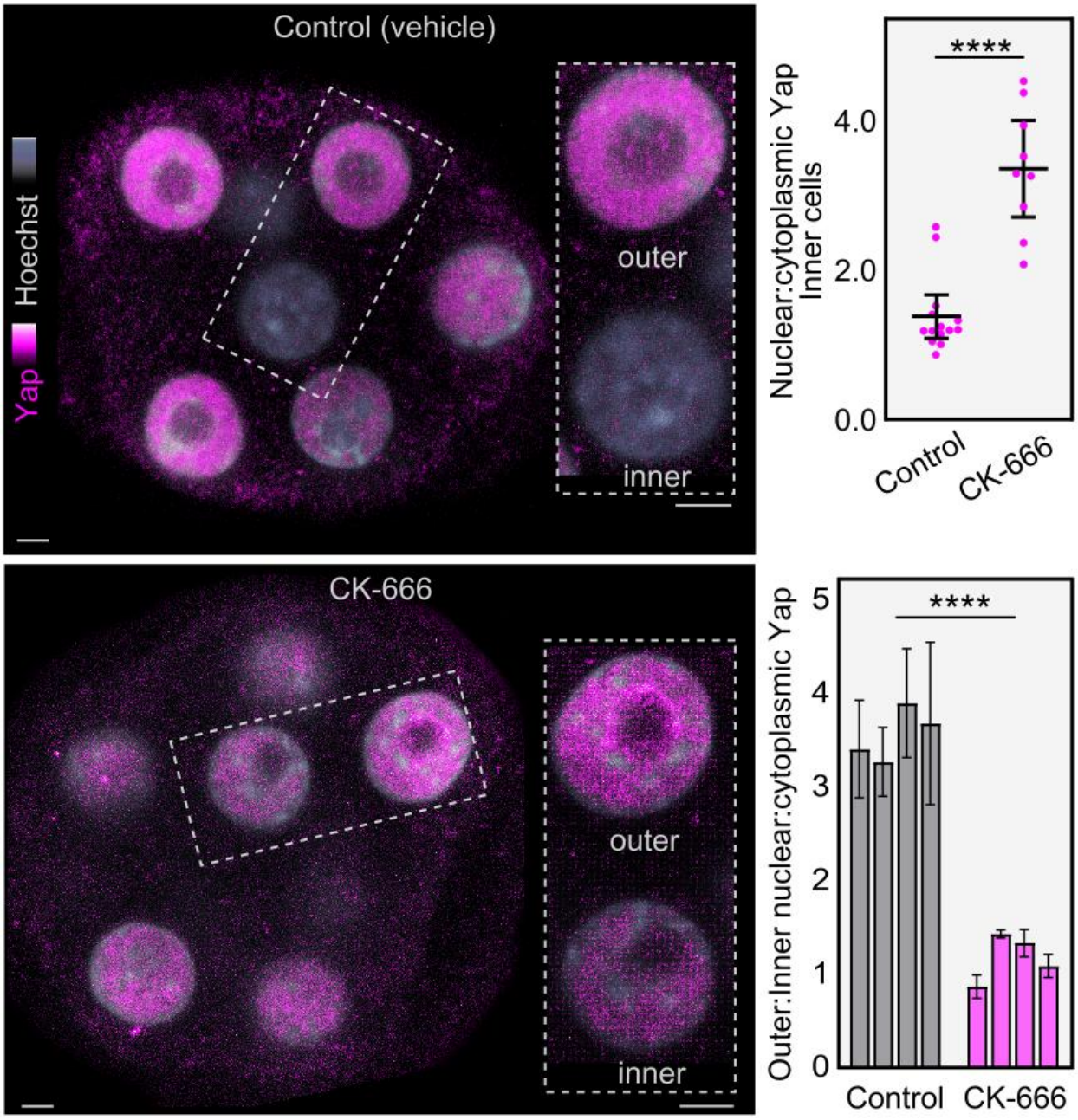

Figure 2.34 Treatment with CK666 causes a loss of inner-outer cell identity

2D confocal sections of a 16-cell embryo immunostained for Yap after treatment with DMSO (control) or CK666 (250 nM). Insets highlight differences between inner and outer cell nuclei in the different treatment groups. Bar graph shows the ratio of nuclear to cytoplasmic Yap between outer to inner cells. Each bar represents one embryo, errors bars represent SD. n=14 for control, n=9 for CK666. ****P<0.0001, Mann-Whitney U test comparing group means. Bars in dot plots represent median and interquartile range. Scale bars, 10 μm

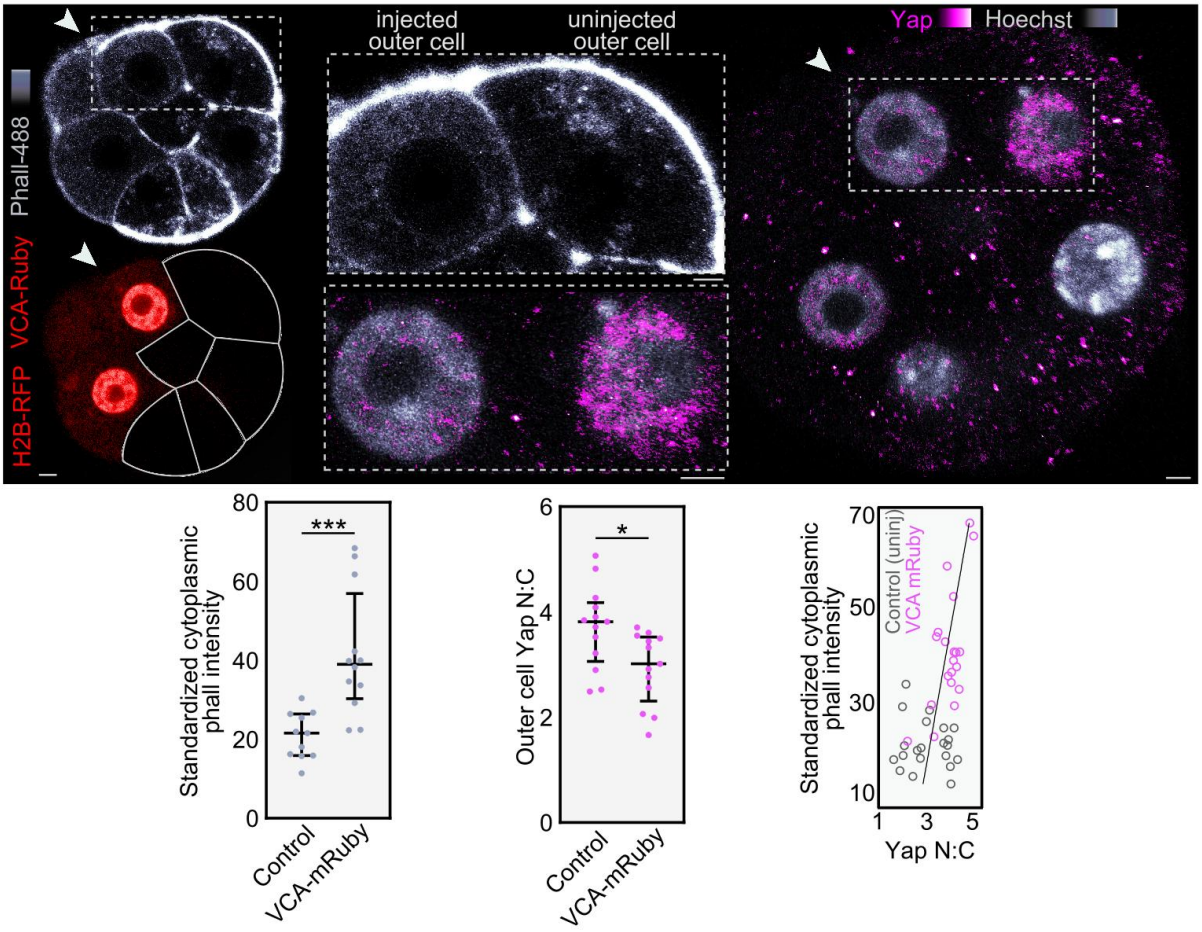

Figure 2.35 Expression of VCA causes loss of outer cell identity

2D confocal sections of embryos injected at the 2-cell stage with mRNA encoding VCA-Ruby and H2B-RFP to label manipulated cells. Embryos were then immunostained for Yap. Insets highlight differences between nuclear Yap and cytoplasmic F-actin between injected and uninjected outer cells. n=11 for control (uninjected outer cells), n=12 for VCA-Ruby (injected outer cells), ***P=0.0001, *P=0.014, Mann-Whitney U test. Bars in dot plots represent median and interquartile range. Scale bars, 10 μm.

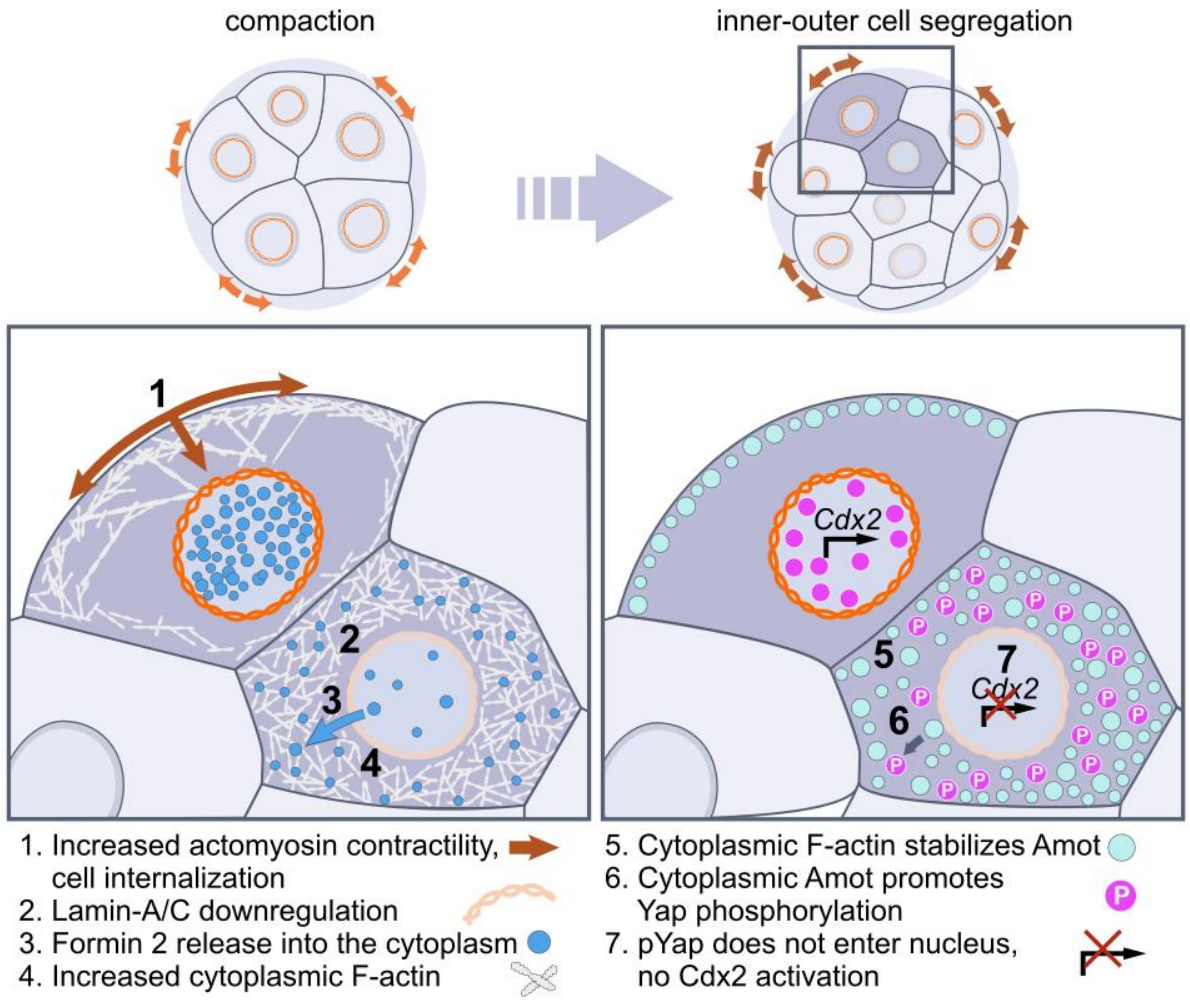

Figure 2.36 Scheme of proposed pathway by which Lamin-A/C links mechanical forces to changes in cell identity.

2.4. Discussion:

The data presented suggest that the nuclear lamina may allow blastomeres of the preimplantation embryo to change their identity in response to the mechanical forces they are subjected to (Figure 2.36). These mechanical forces are transmitted via an F-actin meshwork that spans from the cell cortex to the nucleus. In response to different levels of mechanical stimulation, Lamin-A/C localisation changes, eliciting downstream changes in the localisation of the actin nucleator Formin-2. In inner cells, this triggers the release of Formin-2 from the nucleus, causing actin nucleation in the cytoplasm and stabilisation of Amot. Increased Amot stabilisation results in Yap phosphorylation and its exclusion from the nucleus, favouring an inner cell identity. In outer cells, higher levels of actomyosin contractility prevents the release of Formin-2, reducing actin polymerisation in the cytoplasm, resulting in less Amot stabilisation, less Yap phosphorylation, and the adoption of outer cell identity.

Proteomics performed on a variety of mouse tissues and human mesenchymal stem cells and fibroblasts cultured on gels with tuneable stiffness has shown that Lamin-A abundance and phosphorylation scale with respect to matrix stiffness (Buxboim et al., 2014; Swift et al., 2013). This suggests that the nucleus is has the potential as a mechanosensor. However, the importance of nuclear mechanosensing in vivo has not been established (Lomakin et al., 2020; Venturini et al., 2020). Similarly, Yap has been demonstrated to be a component of mechanosensing pathways (Dupont et al., 2011; Panciera et al., 2017), but whether the Hippo pathway may be involved in mechanotransduction during preimplantation development is unknown (Sasaki, 2017).

2.4.1. Measuring cortical tension and forces transmitted to the nucleus

We observed that levels of phosphorylated myosin II increase during the early stages of preimplantation development and infer from this that actomyosin contractility is also likely to increase over this period. The majority of the p-Myosin II observed is at the cell cortex, suggesting that cortical tension increases over time. However, these forces would act perpendicular to the nucleus-membrane axis and it is not immediately clear how changes in cortical tension would influence forces transmitted to the nucleus. Based on how blastomeres deform during divisions at different stages of development we hypothesised this increase in cortical tension leads to increased membrane stiffness and more efficient transmission of forces to the nucleus. Inferring membrane stiffness from deformations during cell division is also imprecise and the mitotic spindle

is atypical during preimplantation development meaning the changes in deformation could be the result of changes in the forces generated during chromosome segregation rather than membrane stiffness. How cortical tension and membrane stiffness change over time may be explored more effectively using atomic force microscopy or micropipette aspiration. However, both of these techniques require the removal of the zona pellucida, which could introduce other confounding factors.

Although a larger proportion of phosphorylated myosin II resides at the cell cortex, we still observed phosphorylated myosin II throughout the cytoplasm, suggesting there is a continuous contractile F-actin meshwork between the cortex and nucleus. Mechanical tethering between the nucleus and cortex has been demonstrated previously in other systems, such as the F-actin tether observed in Drosophila nurse cells (Huelsmann et al., 2013). It has been shown that differential actomyosin activity between cells at the 16-cell stage can drive internalisation of some cells, allocating them to the inside of the embryo (Samarage et al., 2015). Our data here outline a possible pathway by which cells might sense this differential actomyosin activity via the nuclear lamina, producing changes in cell identity.

2.4.2. Manipulations of actomyosin contractility

Our manipulations of actomyosin contractility were limited to pharmacological approaches using small molecule inhibitors. There are a variety of potential off-target effects, particularly associated with perturbing cell polarity. Current models posit that inner and outer cell identity is established by cell polarity, with the different properties of the apical and basolateral domains at the cell cortex leading to differential Yap phosphorylation (Hirate et al., 2015; Korotkevich et al., 2017; Leung and Zernicka-Goetz, 2013). Comparable to our study, much of the data supporting the polarity model is in the form of pharmacological manipulations, as well as knockouts of Rho GTPases. For example, treatment with the ROCK inhibitor Y27632 causes a reduction of nuclear Yap in outer cells (Shi et al., 2017) and Cdc42 disrupted Cdx2 expression and prevents implantation (Chen et al., 2000). However, as with our own methods, these manipulations are likely to affect cortical tension and actin organisation in addition to cell polarity (Hodge and Ridley, 2016). It is therefore challenging to design experiments that exclusively target cell polarity to distinguish the precise way in which each of these mechanisms might contribute to cell identity. Nuclear mechanosensing

may be a complementary mechanism that expands the current model, providing some redundancy in the specification of inner-outer cell identity.

Previous studies have largely focused on Amot found at the cell cortex, both in inner cells where it facilitates Yap phosphorylation via Lats1/2 and in outer cells where it is sequestered at the apical cortex, preventing Yap phosphorylation (Hirate et al., 2015; Korotkevich et al., 2017; Leung and Zernicka-Goetz, 2013). Although a cytoplasmic fraction of Amot has been identified (Hirate et al., 2013), its role in establishing cell identity has not been explored. Here we imaged both Amot and F-actin at a range of fluorescence intensities, leading to the identification of differential actin and Amot organisation between the cytoplasm of inner and outer cells. Amot has been shown to associate with F-actin (Ernkvist et al., 2006) and our data shows that F-actin and Amot colocalise. We also observed that Amot has a high immobile fraction in inner cells where there is a dense F-actin meshwork and that disrupting the F-actin meshwork with Latrunculin A also disrupts Amot expression. Based on these data, we believe that Amot interacts with F-actin and that this interaction stabilises Amot in the cytoplasm. However, this conclusion is inconsistent with research showing that Amot requires phosphorylation at Ser176 in order to activate the Hippo pathway and that Amot phosphorylated at this residue does not interact with F-actin (Hirate et al., 2013). It is important for future work to characterise this cytoplasmic fraction of Amot and determine its phosphorylation status and interactions. This fraction of Amot may bind to actin indirectly, or there may be other phosphorylation states that allow both actin binding and Hippo activation, meaning the two are not mutually exclusive.

2.4.3. Formin-2

The differences in actin organisation between inner and outer cells appear to be the result of changes in the localisation of actin nucleator Formin-2. We observed that Formin-2 becomes increasingly concentrated in the nucleus as embryos progress from the 2-cell to the 8-cell stage. However, at the 16-cell stage it is differentially localised between inner and outer cells in a Lamin-A/C dependent manner. It remains sequestered in the nuclei of outer cells, while being released into the cytoplasm of inner cells, where it promotes the formation of a dense F-actin meshwork. The mechanism by which Lamin-A/C might regulate nuclear transport is unknown, but research has shown that Lamin-A mutants can result in nuclear import defects (Busch

et al., 2009). In addition, the ability of mechanical cues to regulate nuclear pore complexes in cultured cells has been previously established (Donnaloja et al., 2019).

We used SMIFH2 to examine the effect of Formin-2 inhibition on cytoplasmic F-actin and cell identity. However, these results are difficult to interpret given recent work in cultured fibroblasts showing that SMIFH2 is also a direct inhibitor of myosin II (Nishimura et al., 2021). We observed that treatment with SMIFH2 caused a reduction in cytoplasmic F-actin and an increase in nuclear Yap in inner cells. We proposed that this reduction in F-actin led to decreased Amot stabilisation, which in turn led to Yap phosphorylation and nuclear localisation. However, our proposed mechanosensing pathway suggests that changes in cortical tension as result of an off-target effect on myosin II would produce the same changes to inner cell identity and therefore the role of Formin-2 cannot be established based on this experiment alone.

In addition to Formin-2, our data also suggest the Arp2/3 complex may play a complementary role in the formation of the dense cytoplasmic F-actin meshwork observed in inner cells. This is consistent with the role of the Arp2/3 complex in the nucleation of branched actin filaments, which are typically associated with dense meshworks (Campellone and Welch, 2010). However, after testing multiple antibodies we were unable to determine its expression pattern reliably. Injection of mRNA encoding the VCA domain, an activator or Arp2/3 mediated actin branching, produced a phenotype similar to those we observed by overexpression of Formin-2.

2.4.4. The role of Actin in our proposed pathway.

When considering the entire pathway that we have proposed in this study (Figure 2.36), it is difficult to determine the precise role played by actin. This is because it appears to play a role upstream and downstream of the nuclear lamina, both in the transmission of cortical forces to the nuclear lamina, and as a downstream effector, by stabilising Amot and promoting inner cell identity. This raises the question of feedback loops between the transmission of forces and actin reorganisation, making it challenging to establish causality convincingly. It is plausible that a positive feedback loop that reinforces cell identity occurs, in which the dense F-actin meshwork observed in inner cells acts to dampen force transmission to the nucleus, triggering further actin reorganisation. This actin reorganisation may also serve to maintain the physical segregation of inner and outer cells, which have been shown not to reposition after

being allocated to the inner part of the embryo (Pomp et al., 2022; Samarage et al., 2015). This is consistent with data demonstrating the ability of cell lineages to segregate based on shared physical properties (Fagotto, 2014; Krieg et al., 2008; Steinberg, 2007).

Although Yap and Cdx2 are two well established markers of inner-outer cell identity, this study is somewhat limited by its reliance on them. Similarly, the scope is limited by focusing on the 16-cell stage, without examining how our perturbations affect the formation of the ICM and trophectoderm during the blastocyst formation. These experiments can be challenging to perform with our current experimental methods, as mRNA is diluted and degraded through successive cleavage divisions, meaning that results become increasingly difficult to interpret as embryos reach the blastocyst stage. Perturbing the nuclear lamina may only delay the establishment of inner-outer cell identity, as this would be consistent with studies showing the Lamin-A knockout mice complete preimplantation development (Wolf et al., 2008). Future research should explore additional markers and later stages of development, potentially employing stable genetic manipulations to provide more comprehensive insights into the role of the nuclear lamina throughout preimplantation development.

Chapter 3. Visualising cell dynamics during somite formation

3.1. Introduction

3.1.1. Formation of the vertebrate body plan

In vertebrates, the earliest stages of development, including cleavage patterns, gastrulation movements, and the formation of the germ layers, display surprising morphological diversity. However, despite this initial diversity, vertebrates display an equally striking convergence in their morphology at what is collectively known as the pharyngula stage. This period of development is characterised by a variety of conserved embryonic structures, including the notochord, neural tube and somites. While each of these structures is transient in nature, they are essential in laying out a blueprint for the vertebrate body plan.

Fully understanding the developmental processes that produce these structures requires multi scale investigation. This often begins at the molecular level, by observing changes in gene expression that occur during the formation of a tissue. However, these observations remain superficial without an understanding of how these patterns of gene expression are translated into changes in cellular behaviour. In turn, further insights are needed to understand how, collectively, changes in the behaviour of individual cells lead to the patterning of complex tissues.

3.1.2. The somites

Somites are transient blocks of epithelial tissue that form bilaterally on each side of the midline. The process is visually striking, with somites forming in pairs every 90 minutes in the chick embryo and with a fairly regular size. This process proceeds in an anterior to posterior direction, as the mesenchymal cells of the presomitic mesoderm (PSM) coalesce to form epithelial rosettes. The cells that give rise to the somites begin entering the node and anterior primitive streak around stage HH4 in the chick embryo (Garcia-Martinez et al., 1993; Psychoyos and Stern, 1996; M. A. Selleck and Stern, 1991) The position along the rostral-caudal axis of the primitive streak/node from which a cell emerges determines its contribution to tissues along the medial-lateral axis, with cells leaving the node contributing to the notochord and medial somite, and cells that emerge more caudally contributing to the lateral somite and eventually lateral plate mesoderm (Psychoyos and Stern, 1996; M. A. Selleck and Stern, 1991; Selleck and Stern, 1992). Cells of the somite later differentiate into

sclerotome and dermomyotome (Christ et al., 2004; Ordahl and Le Douarin, 1992), eventually giving rise to the vertebrae, ribs, skeletal muscle, cartilage and parts of the dermis. In addition, cells in each half of the somite have distinct rostral and caudal identities which play a role in neural crest migration and the patterning of the peripheral nervous system (Bronner-Fraser, 1986; Bronner-Fraser and Stern, 1991; Keynes and Stern, 1984; Rickmann et al., 1985).

3.1.3. The occipital somites

In the chick embryo, the first 5 somites are the occipital somites and form the occipital sclerotomes, which contribute to the base of the skull (Hinsch and Hamilton, 1956; Lim et al., 1987) These somites do not form sequentially, with the second pair along the anterior-posterior axis forming first, followed by the first and third pairs almost simultaneously (Hamburger and Hamilton, 1951). Segmentation continues sequentially from the fourth somite onwards and first pair of somites disappears by stage HH10 (Hamburger and Hamilton, 1951). In situ hybridisation for Uncx4.1, which marks the caudal half of somites, suggests that first two somite pairs lack rostral-caudal polarity, with the third pair being the first to express Uncx4.1 in the caudal half (Schrägle et al., 2004). Immediately caudal to this occipital region lie the atlas (C1) and axis (C2) vertebrae, together forming the atlanto-axial joint which allows head rotation. DiI/DiO labelling has demonstrated that the anterior part of the fifth somite uniquely gives rise to the atlas vertebra, making it the only vertebra originating from a single somite (Ward et al., 2017). In contrast, the axis is assembled from three somite pairs (5–7), with its odontoid process deriving from the body of the atlas (Ward et al., 2017).

3.1.4. The core cells

In amniotes, the somite consists of an epithelial rosette surrounding a central lumen called the somitocoele (Williams, 1910). The somitocoele contains mesenchymal cells, here referred to as the core cells (Bellairs, 1979). These cells have not been well characterised, and as such, their origin, behaviour and fate remain intriguing and somewhat unresolved. Historically these cells were thought to contribute to the sclerotome (Williams, 1910), but later evidence suggested they also contribute to the myotome (Mestres and Hinrichsen, 1976). Injection of lysinated fluorescein-dextran into cells of the epithelial rosette showed that the cell or its progeny can either remain

in the rosette or move to the core (Wong et al., 1993). In contrast, labelling a single core cell revealed that the cell and its descendants always remained confined within the core. However, this was later challenged by two-photon live imaging, which revealed cells from the somite core egressing into the epithelial rosette (Martins et al., 2009). Quail-chick transplantation experiments showed that core cells contribute to the lateral sclerotome, with some cells migrating toward the notochord. After a further 6 days, transplanted cells contributed to the ribs and peripheral region (annulus fibrosus) of the intervertebral discs (Huang et al., 1996, 1994). Ablation of the core population leads to fused vertebral bodies and articular processes with a lack of proper intervertebral joints and discs, suggesting that sclerotome cells originating from the rosette cannot compensate for the loss of the core cell population (Mittapalli et al., 2005). Core cells also display plasticity, as demonstrated by grafts of GFP-labelled core cells into different parts of the epithelial rosette, with the core cells contributing to different structures depending on their new position (Senthinathan et al., 2012).

3.1.5. Rostral-caudal polarity

An important property of somites is their subdivision into rostral and caudal halves. These rostral and caudal identities prevent somite halves from mixing, as demonstrated by studies transplanting quail somite halves into chick embryos to produce ‘compound somites’ (Stern and Keynes, 1987). In experiments where a rostral somite half was grafted next to another rostral half (or a caudal half next to caudal) the boundary between the somite halves collapses, resulting in cell mixing. This boundary later produces a visible border between rostral and caudal halves of the sclerotome, known as von Ebner’s fissure (von Ebner, 1888). The rostral-caudal subdivision of somites contributes to the patterning of the peripheral nervous system by guiding the migration of neural crest cells through a permissive corridor in the rostral half of the somite and preventing migration via the caudal half (Bronner-Fraser, 1986; Bronner-Fraser and Stern, 1991; Keynes and Stern, 1984; Rickmann et al., 1985). Protein disulphide isomerase (PDI) is expressed in the caudal somite half and was shown to prevent motor axon outgrowth via contact repulsion (Cook et al., 2020; Davies et al., 1990). In contrast, expression of semaphorin, neuropilin, and Ephrin/Eph are repulsive signals that prevent neural crest cells from migrating through the caudal somite (Bronner-Fraser and Stern, 1991; Davy and Soriano, 2007; Gammill et al., 2006; Koblar et al., 2000; Schwarz et al., 2009).

3.1.6. Formation of somite boundaries

Formation of a new somite requires the creation of a boundary between it and the anterior PSM. Sagittal sections in chick embryos initially suggested that border formation starts dorsally and proceeds ventrally, involving epithelialisation of core PSM cells joining a dorsal epithelial sheet (Beloussov and Naumidi, 1983). Epithelialisation of the posterior wall appeared to precede the anterior, and this was supported by subsequent studies also based on sagittal sections (Nakaya et al., 2004; Sato et al., 2002). In contrast, time-lapse imaging in the coronal plane suggests that it is the anterior border rather than the posterior border that forms first, with the medial aspect of the somite forming first and propagating to the lateral half (Kulesa and Fraser, 2002). Similar live imaging experiments in the chick corroborated the medial to lateral direction of epithelialisation, but instead observed the posterior border of the somite epithelialised first (Martins et al., 2009). Transplantation studies demonstrated that the PSM contains prospective border regions (Sato et al., 2002; Sato and Takahashi, 2005). In these studies, the authors designated the next two prospective somite boundaries ‘0’ and ‘-1’. Transplantation of the -1 prospective boundary to a region anteriorly creates an ectopic fissure and forms two smaller somites instead of one, indicating instructive boundary-forming activity (Sato et al., 2002). Further experiments grafting only the ventral cells from the ‘-1’ boundary region showed that these cells alone were sufficient to induce an ectopic boundary, suggesting that boundary formation progresses in a ventral-to-dorsal direction (Sato and Takahashi, 2005). This contradicts earlier reports of boundary formation proceeding in a dorsal to ventral direction (Beloussov and Naumidi, 1983). Replacing the ectoderm with endoderm or placing a barrier between the ectoderm and PSM did not prevent boundary formation, suggesting that the mechanism of boundary formation is intrinsic to the PSM and not influenced by the ectoderm (Sato and Takahashi, 2005).

3.1.7. Models of somite formation

Numerous models have been proposed to explain how the embryo generates regularly sized segments at regular intervals (Figure 3.1). These include pre-patterning models, which suggest that the PSM already has an underlying segmented pattern that is generated earlier in development (Christ et al., 1974; Meier, 1979), a reaction diffusion model (Meinhardt, 1982), the progressive oscillatory reaction diffusion (PORD) model (Cotterell et al., 2015), the cell cycle model (Collier et al., 2000; Keynes and Stern,

1988; Primmett et al., 1989, 1988; Stern et al., 1988), the clock and wavefront model (Cooke and Zeeman, 1976), as well as variants such as the clock and gradient (Slack, 1983) and clock and trail (Kerszberg and Wolpert, 2000).

Two fundamental questions one might ask regarding segmentation are: ‘what mechanism determines which cells will segment together?’ and ‘at what point in time and space is this grouping established?’ Do cells segment with whichever neighbours they find themselves amongst? Or is there an underlying order to the PSM which cells sort according to? Do groupings remain unstable, only becoming fixed at the point of segmentation? Or are groups of cells established early in the PSM? The clock and wavefront model, which in recent years has dominated discussion in the literature, implies the former answers to these questions, with cells lacking any intrinsic identity and the segmental pattern emerging based on position and timing.

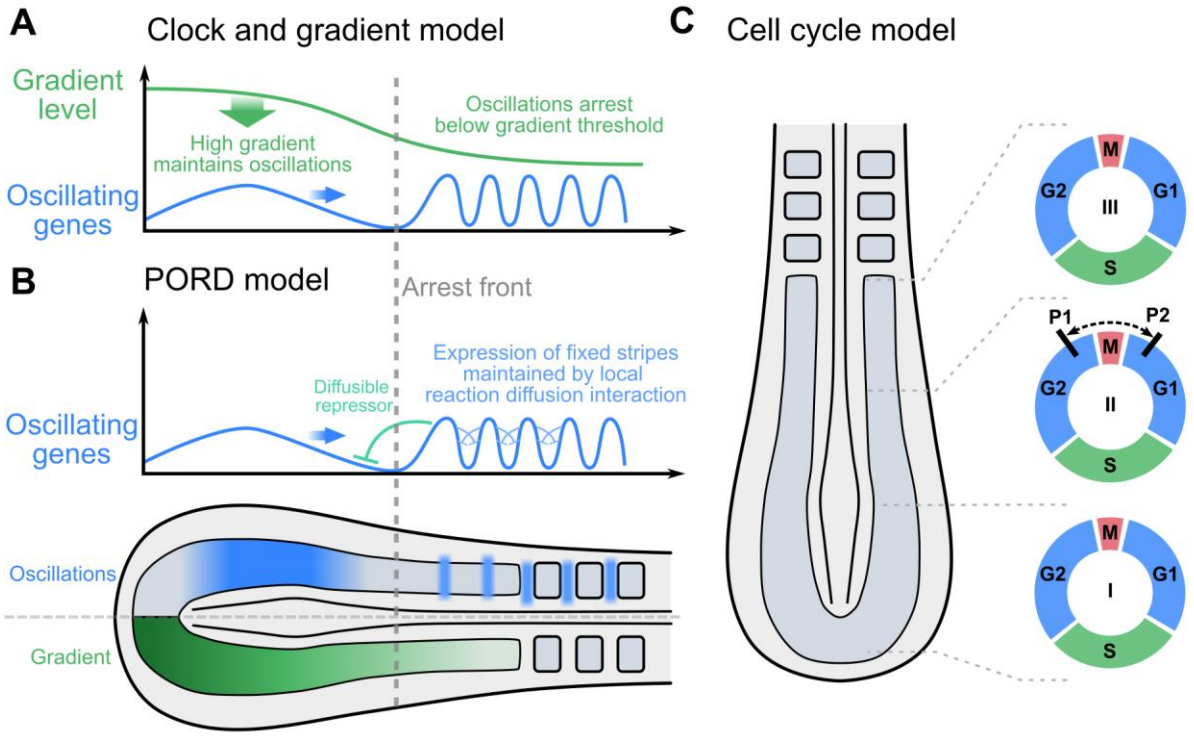

Figure 3.1 Models of somite formation

The clock and gradient and PORD models offer alternate interpretations of oscillating gene expression in the PSM and how these signals are translated into somite boundaries. **A.** The clock and gradient model suggests that gene oscillations in the PSM are maintained by a morphogen gradient that decreases anteriorly. This morphogen gradient defines an arrest front, beyond which the morphogen gradient can no longer sustain oscillations, causing them to arrest and define a somite boundary. **B.** The PORD model suggests that a morphogen gradient is not necessary, and somite boundaries can be produced by local interactions. In the PORD model oscillating gene expression in the PSM is the result of a reaction diffusion system that produces travelling waves that move anteriorly until they meet the boundary of last formed somite, where they arrest to form stable, fixed, stripes of expression. **C.** The cell cycle model suggests that groups of cells with approximately synchronised cell cycles segment together. Segmentation is gated by events in the cell cycle indicated by points P1 and P2. It is proposed that during this period cells become competent to respond to signals causing changes in cell adhesion, resulting in synchronised cells aggregating and segmenting together. Adapted from Piatkowska et al., (2021), Cotterell et al., (2015) and Primmett et al., (1989).

3.1.8. The clock and wavefront model

First described by Cooke and Zeeman (1976), the clock and wavefront model suggests that a travelling wavefront, interacting with a cellular oscillator might instruct groups of cells undergo to a synchronised, rapid segmentation. For many years both the wavefront and the cellular oscillator remained hypothetical, until oscillatory expression of c-hairy1, a member of the Notch pathway, was observed in the PSM (Palmeirim et al., 1997). Following this, several more genes from the Notch and Wnt pathways with oscillating expression in the PSM were observed, with genes in the Wnt pathway oscillating anti-phase to genes in the Notch pathway (Bénazéraf and Pourquié, 2013; Dequeant et al., 2006; Forsberg et al., 1998; Jouve et al., 2000). The expression of these molecular oscillators is not phase linked throughout the PSM as first suggested by Cooke and Zeeman (1976), rather bands of expression are seen, which start off broad posteriorly and narrow as they approach the point of segmentation. A candidate for the wavefront was proposed to exist in the form of a gradient of FGF8 (Dubrulle et al., 2001), whose expression is highest in the tailbud and posterior PSM and decreases anteriorly as a result of mRNA decay (Dubrulle and Pourquié, 2004). Later a similar gradient of Wnt was found (Aulehla et al., 2008, 2003) as well as expression of Raldh2 in the somites and anterior PSM, suggesting there may be a gradient of retinoic acid that runs in the opposite direction to the FGF and Wnt gradients (Diez del Corral et al., 2003). Cook and Zeeman's model proposed a travelling wavefront, where the time the wave takes to traverse the length of the PSM determines segment size. However, when an embryo is transected, segmentation continues as normal (Slack, 1983). For this to be compatible with the original model, there would need to be a mechanism that could sense the length of the embryo and adjust the speed of the wavefront accordingly. Since there is no known mechanism that could achieve this, Slack proposed an alternative 'clock and gradient' model (Figure 3.1A) that relies on a morphogen gradient rather than a travelling wavefront (Slack, 1983). Since most modern interpretations of the model match this description, 'clock and wavefront' is something of a misnomer, with most models in fact being 'clock and gradient' models.

3.1.9. Pre-patterning

If the clock and wavefront model suggests one extreme, that cells are grouped at the point of segmentation, based on position and timing, then pre-patterning suggests the

opposite, with cells segmenting based on an underlying pattern in the PSM that is established much earlier in development. The first evidence for pre-patterning came from Meier's study of the PSM in chick embryos using SEM. He observed regularly spaced spherical clusters of cells running the length of the PSM which he termed 'somitomeres' (Meier, 1979). Meier reported as many as 10-12 somitomeres running the entire length of the PSM (Meier, 1984, 1979; Packard and Meier, 1983). Similar cellular arrangements have been observed in several other organisms using SEM imaging, including quail (Packard and Meier, 1983), snapping turtle (Packard and Meier, 1984), newt (Jacobson and Meier, 1984) and mouse (Tam et al., 1982). In contrast, SEM imaging of three species of amphibians, *Rana*, *Ambystoma* and *Pleurodeles* revealed no such cellular arrangements in the PSM (Youn and Malacinski, 1981), as did SEM imaging of the teleost fish *Barbus conchonius* (Wood and Thorogood, 1994). This led the authors to suggest that somitomeres may be an artefact of the fixation and sample preparation used for SEM. Somitomeres have proved undetectable using light microscopy or by measuring the cell density throughout the PSM (Jacob et al., 1986). The idea of a pre-patterning of the PSM also appears to be incompatible with the extensive cell movement and mixing observed in the posterior PSM (Bénazéraf et al., 2010; Stern et al., 1988). Assuming somitomeres are not an artefact of SEM imaging, the idea of pre-patterning of the PSM raises as many questions as it answers, shifting the question to how the pre-patterning is established.

3.1.10. The cell cycle model

The cell cycle model proposes that the PSM is arranged with cells in age order, such that the cell cycle of neighbouring cells is relatively synchronous, and that some event linked to the cycle triggers cells to segment together (Figure 3.1C) (Collier et al., 2000; Keynes and Stern, 1988; Primmett et al., 1989, 1988). This was initially proposed to explain the finding that a single heat shock causes repeated anomalies. Heat shock experiments were initially performed to determine the length of time between a group of cells being instructed to segment together and the formation of the somite (Cooke, 1978; Elsdale et al., 1976). The authors assumed that if cells were being instructed by a wavefront, a brief heat shock might disrupt the progression of the wave, resulting in an anomaly when those cells segmented together. However, when similar heat shocks were performed in the chick, they resulted in repeated anomalies that occurred every

6-7 somites, or approximately 10 hours (Primmett et al., 1988). This suggested that rather than disrupting cells responding to a wavefront, the heat shock was instead disrupting a repeating event that occurred every 10 hours. Labelling of individual cells in the PSM showed that cells divide approximately every 10 hours, matching the frequency of the anomalies (Stern et al., 1988). Further observations linking segmentation to the cell cycle came in the form of pharmacological perturbations that disrupt the cell cycle, such as with treatment with L-Phenylalanine. These cell cycle perturbations induced similar, repeated segmentation anomalies as the heat shock experiments (Primmett et al., 1989). The model therefore proposes that cells enter the PSM after mitosis, meaning the PSM is organised with cells in age order, with cells that enter around the same time having synchronised cell cycles (Collier et al., 2000; Keynes and Stern, 1988; Primmett et al., 1988, 1988). At the time cells enter the PSM after cell division they are mesenchymal with low cell-cell adhesion. It has been demonstrated that cell movement and mixing occurs in the posterior PSM (Bénazéraf et al., 2010) and as a result, cells that entered together are likely to drift apart initially. Later, events in the cell cycle trigger synchronised changes in cell adhesion, resulting in groups of cells that entered the PSM sorting and segmenting together. Research published more recently has shown a link between the cell cycle and the pace of oscillating genes in the PSM (Carrieri et al., 2019; Delaune et al., 2012; Wiedermann et al., 2015). This suggests that the cell cycle may play a role in clock and wavefront style models and disruptions observed in heat shock experiments and experiments that disrupt the cell cycle may be a result of disrupting the segmentation clock.

3.1.11. Reaction diffusion models

Meinhardt (1982) proposed a reaction diffusion model that relies on a gradient moving posteriorly interacting with a molecular oscillator in the PSM. This shares features with Slack's (1983) clock and gradient model, a variant of the clock and wavefront model. Given these similarities, it is plausible that the oscillatory gene expression observed in the PSM may be part of a clock and wavefront model, clock and gradient model, or reaction diffusion model. More recently a 'progressive oscillatory reaction-diffusion' (PORD) model was proposed (Figure 3.1B), that suggests oscillations of an activator and repressor creates travelling waves that move anteriorly (Cotterell et al., 2015). However, unlike other models that include molecular oscillators, this model does not rely on a long-range morphogen gradient. Instead, the PORD model proposes that the

boundaries of formed somites consist of stable bands of ‘activator’ expression that secrete the diffusible repressor. When the anteriorly travelling wave of activator-repressor interactions meets the stable band of activator expression at the most recently formed somite boundary, the travelling wave arrests, forming another region of stable activator expression and a new somite boundary. Interestingly, the PORD model was discovered using an unbiased exploration of different possible gene regulatory network designs. Almost 10,000 different networks were tested to see if they could generate a segmented pattern and those that could matched the description of either a clock and gradient style model or the new PORD model. The authors then tested predictions made by the clock and gradient models and PORD models side by side with a series of experiments in chick embryos and concluded that the PORD model better predicted the experimental results observed.

3.1.12. Inconsistencies in the Clock and Wavefront model

Since the observation that Notch pathway members do in fact show oscillatory gene expression in the PSM (Palmeirim et al., 1997), the clock and wavefront models have come to dominate discussion in the current literature. However, several observations are not adequately explained by this model, suggesting that, at the very least, it is incomplete. In loss of function Notch mutants, segmentation is disrupted, but still occurs, with somites forming in a delayed and disorganised fashion (Conlon et al., 1995; de la Pompa et al., 1997; Oginuma et al., 2010). Given the importance of Notch signalling in driving the ‘clock’ component of the model, this calls into question the importance of these signals in triggering segmentation. They proposed a travelling wavefront, but so far, only static gradients of Wnt and FGF have been observed in the PSM (Aulehla et al., 2008, 2003; Dubrulle et al., 2001). This gradient is the result of mRNA decay (Dubrulle and Pourquié, 2004), and there is no known mechanism by which the rate of mRNA decay might scale with embryo size. Finally, it has been demonstrated that mesoderm that would typically contribute to the lateral plate, can be induced to form somites when treated with noggin (Dias et al., 2014). In these experiments the posterior third of the primitive streak was soaked in noggin then grafted into the area opaca of another developing embryo. After 10 hours the grafted tissue generated somite like structures of appropriate size and expressed somite markers but formed without oscillatory expression of molecular clock genes. Reports suggesting that there are differences in the rate of epithelialisation along the dorsal-

ventral axis (Bellairs, 1979) and the medial-lateral axis (Kulesa and Fraser, 2002; Martins et al., 2009) also appear incompatible with the clock and wavefront model. Instead, the model posits that the molecular clock triggers a rapid, synchronised segmentation and in addition, dorsal-ventral or medial-lateral expression differences in clock or wavefront genes have not been reported. The clock and wavefront model also struggles to explain how the occipital somites from, with somite 2 preceding the formation of somite 1 and somites 1 and 3 forming simultaneously. It is not clear how the clock and wavefront model could trigger somites to form out of sequence or for two pairs to form synchronously. Another observation that appears incompatible with the clock and wavefront model are the repeated segmentation anomalies produced by heat shock experiments (Primmett et al., 1989, 1988). The clock and wavefront model suggests that cells of the PSM are plastic, segmenting based on their position and timing. Heat shocks can produce as many as four repeating anomalies, which corresponds to a period of over 40 hours, in which time the entire PSM would be expected to have segmented and been replaced. Therefore, heat shock and cell cycle inhibition experiments appear to be disrupting a process not described by the clock and wavefront model.

3.1.13. Cellular aspects of somite formation

Much of the recent work published on the mechanism of somite formation has fallen into one of two categories: those that focus on the molecular intricacies of a proposed clock and wavefront model (Bhavna, 2019; Hubaud et al., 2017; Sonnen et al., 2018; Yoshioka-Kobayashi et al., 2020), and those attempting to grow organoids and embryoids that produce segmented tissues (Diaz-Cuadros et al., 2020; Matsuda et al., 2020; Miao et al., 2023; Sanaki-Matsumiya et al., 2022; Veenvliet et al., 2020; Yaman and Ramanathan, 2023). In both cases, relatively little effort has gone into understanding how molecular events seen in the PSM are translated into the cellular behaviours that generate segmented tissue. These studies tend to assume that cells of the next prospective somite receive a collective signal and undergo rapid epithelisation. Few studies have attempted to examine the cellular aspects of how the epithelial rosettes of somites are constructed (Bellairs, 1979; Duband et al., 1987; Kulesa and Fraser, 2002; Martins et al., 2009) and there are conflicting reports about the order in which epithelialisation of the PSM proceeds (Beloussov and Naumidi, 1983; Kulesa and Fraser, 2002; Martins et al., 2009; Polezhaev, 1992). Here we

attempt to examine the dynamics of cellular behaviour in the PSM using SEM imaging and high-resolution microscopy.

3.1.14. Origin of somite precursors

In the chick embryo, a region known as Hensen's node contributes to the medial somites and the notochord as the anterior-posterior axis elongates (Joubin and Stern, 1999; M. A. J. Selleck and Stern, 1991). This is of particular relevance to the cell cycle model of somite formation, as cells entering the PSM from the node and anterior streak immediately after cell division would approximately synchronise their cell cycles and could act as a mechanism to coordinate segmentation.

The node is produced as two populations of cells converge during the formation of the primitive streak, from stage EG&K XI to HH3+ (Hatada and Stern, 1994; Izpisúa-Belmonte et al., 1993; Streit et al., 2000). The first of these two populations is found in Koller's sickle and can be identified by goosecoid expression. The second population consists of cells of the epiblast, which are initially adjacent to Koller's sickle near the posterior marginal zone, before moving rostrally until they reach the centre of the blastoderm (Streit et al., 2000). It is here they are joined by the tip of the primitive streak and the cells of Koller's sickle, forming the node. After meeting, the two groups of cells are then joined by cells of the epiblast lateral to the node and streak from stage HH3+ to HH4 (Joubin and Stern, 1999; Sheng et al., 2003; Solovieva et al., 2022). Ingression of cells from the epiblast continues into the streak, but stops at the level of the node from HH4 onwards (Psychoyos and Stern, 1996; Sheng et al., 2003). Cells entering the node from stages HH4+ to 5 migrate rostrally, forming the head process and from stage HH6 onwards the node begins to regress caudally (Spratt, 1947). Cells continue to exit the node as it regresses, contributing to the notochord, medial somite, definitive endoderm and neural midline floorplate (Joubin and Stern, 1999; M. A. J. Selleck and Stern, 1991). The node is a highly dynamic region and most cells that enter the node do so transiently, exiting shortly after (Joubin and Stern, 1999). However, fate mapping individual cells injected with a fluorescent tracer suggests that some cells remain resident in the node while their descendants leave (M. A. J. Selleck and Stern, 1991), and that some regions within the node contain resident cells that are self-renewing (Charrier et al., 1999; Mathis et al., 2001; McGrew et al., 2008; Selleck and Stern, 1992). Given the functional importance of the node as an organiser and its capacity to induce a secondary axis (Spemann and Mangold, 1924; Stern, 2005), it

begs the question of whether resident, self-renewing cells are already present as the node forms, or whether this behaviour is imparted upon cells that enter the node. Considering the importance of this potential stem cell population as a source of somite precursor cells, we aim to explore these questions in this chapter.

3.2. Methods

3.2.1. Scanning electron microscopy (SEM)

Fertile hen's eggs (Brown Bovan Gold, Henry Stewart & Co.) were incubated at 38°C until stage HH11 (Hamburger and Hamilton, 1951), approximately 11-15 somites. Embryos were harvested and processed for SEM as described by Bellairs (1979), with the modification that after fixation in sodium cacodylate each embryo was sectioned once, either sagittally or transversely, using a tissue chopper (Mickle Laboratory Engineering). Embryos were dried using a critical point dryer (Leica) and CO_2 and then mounted and sputter-coated with gold/palladium. Images were acquired using a JEOL JSM-740IF Field Emission Scanning Electron Microscope with 2000x magnification at 2 KV and pressure of 5.25 10−4 Pa.

3.2.2. SEM image processing and aspect ratio analysis

Montages of the images were assembled in Photoshop CS6 (Adobe) and analysed using FIJI. A touch screen (SmartPodium 624) and pen were used to segment each cell using the 'freehand selection tool' in FIJI. Only cells in focus and not obscured by neighbouring cells were analysed. The aspect ratio of each cell was calculated in FIJI by dividing the longest dimension by the shortest dimension of the segmented region as seen in the (two-dimensional) SEM images. The regions of interest were then colour-coded using a lookup table in FIJI. For each region of the PSM the aspect ratio of cells were plotted against the PSM length, represented by a percentage, from 0% in the posterior to 100% at the anterior PSM-somite border. A sigmoid curve was then fitted using regression analysis for the sagittal sections. For transverse sections the aspect ratio of cells was plotted for each PSM length the embryos were sectioned at.

3.2.3. Whole-mount immunostaining

Embryos were harvested in PBS, pinned to a silicon-coated Petri dish and excess tissue trimmed with a blade. Embryos were fixed in 4% paraformaldehyde for 15 minutes at room temperature. Embryos were then permeabilised overnight in 1% Triton-X100 in PBS (PBS-T) with 0.02% thimerosal. Blocking was performed overnight at 4°C using 0.1% BSA (Sigma, A3803) and 5% heat-inactivated goat serum (Sigma, G6767) in PBS-T. Embryos were then incubated in GM130 antibody (BD Biosciences #610822) at 1:100 in blocking solution. Embryos were washed overnight in PBS-T three times. Embryos were then incubated in Alexa 488-conjugated secondary

antibody (Life Technologies, A21202) at 1:1000 along with ToPro3 nuclear stain (Molecular probes, T3605) at 1:2000 and 10 µg/mL RNase A (Sigma, R6513). Embryos were then dehydrated gradually, starting with a solution of PBS-T and 10% isopropanol and increasing the isopropanol concentration in 10% increments until a solution of 100% isopropanol was reached. Embryos were the cleared using BABB and mounted for imaging. For embryos treated with LY411575, eggs were incubated at 38°C until stage HH4, embryos were harvested, then placed in a solution of PBS with 1µM LY411575 for 40 minutes at room temperature. Embryos were then cultured using a modification of New's method (Stern and Ireland, 1981), with albumin containing 1µM LY411575 until stage HH11 then processed for immunostaining as described above.

3.2.4. 3D imaging, processing and analysis

Images were acquired using an Olympus Fluoview FV1000 or Zeiss LSM 780 confocal microscope and processed in FIJI. Images were computationally sectioned in the transverse plane and the PSM was divided into medial, lateral, dorsal and ventral regions, then each region was further divided into an apical and basal region. The mean fluorescence intensity difference between the apical and basal regions was then calculated and plotted against the PSM length, represented by a percentage, from 0% in the posterior to 100% at the anterior PSM-somite border. A sigmoid curve was then fitted using regression analysis.

3.2.5. Whole-mount in situ hybridization

Embryos were fixed in 4% paraformaldehyde for 30 minutes at room temperature then stored in methanol at −20°C. In situ hybridization was performed as described by Streit and Stern (2001) using digoxigenin-labelled probes for Paraxis (Burgess et al., 1996, 1995); cHairy1 (Palmeirim et al., 1997) and Uncx4.1 (Dale et al., 2003). The Uncx4.1 was probe amplified using PCR with GOTaq (Promega) using primer pairs M13F: GTAAAACGACGGCCAGT, M13R: GCGGATAACAATTTCACACAGG for 30 cycles with 1 min at 50°C for annealing.

3.2.6. Hybridization chain reaction

Embryos were fixed in 4% paraformaldehyde for 30 minutes at room temperature then stored in methanol at −20°C. Hybridization Chain Reaction (HCR) (Dirks and Pierce, 2004) was performed using the HCR v3.0 protocol for whole-mount chicken embryos

as provided by the manufacturer (Molecular Instruments). Embryos were mounted in a drop of SlowFade Gold (Initrofen) using 13 mm × 0.12 mm SecureSeal spacers (Grace Bio-Labs). Images were captured using a Leica SP8 confocal microscope and an Apochromat 40X 1.4 NA oil objective. 3D maximum projections and sagittal sections were generated using Imaris 8.2 (Bitplane).

3.2.7. Epiblast grafts

Transgenic GFP donor embryos were harvested and placed in Tyrode's solution (Stern, 1993). With the ventral side facing upwards, endodermal and mesodermal layers were removed and a piece of epiblast, consisting 20 to 50 cells was excised using a 30-G syringe needle. Each piece of epiblast was inspected to ensure that no mesoderm or endoderm cells remained before grafting, despite this, the possibility of a small number of mesoderm or endoderm cells remaining cannot be ruled out completely. A piece of epiblast of equal size was removed from the host epiblast and replaced with the donor tissue. The 'anterior' epiblast was taken from a region in the midline, approximately halfway between the tip of the streak and the area opaca. The 'lateral' epiblast was taken from a region immediately adjacent to the node.

3.2.8. Regrafts of single cells

First an anterior to lateral graft was performed as described above and the host embryo cultured to HH8-10. The embryo was then harvested and placed in Tyrode's solution. The node was excised and placed in a drop of nonenzymatic dissociation medium (Sigma, # C5914-100ML). GFP+ cells were identified by fluorescence under a dissection microscope then aspirated individually using a pulled 50µL micropipette (Drummond Scientific, Cat 2-000-050) connected to aspirator tube. A small incision was made in the node of the second host and the GFP+ cell maneuvered into the incision by gently dispensing saline using the micropipette. In some grafts the single GFP+ cell was transferred while still attached to neighbouring GFP- cells from the first host, but only one GFP+ was ever transferred. After grafting embryos were left at room temperature for 15 minutes to aid attachment of the graft cell to the host, then cultured until HH8-10.

3.2.9. Live imaging and cell tracking

An electroporation mixture was prepared with 1 mg ml^{-1} of plasmid DNA, 6% sucrose and 0.05% Fast Green FCF. This mixture was the applied to the dorsal side of HH4-

embryos, in a small region just lateral to the node, targeting ingressing cells. Embryos were electroporated with either pDsRed-Express plasmid, or a mixture of H2B-citrine and memb-Cherry. Electroporation was performed using a custom chamber, as described by Voiculescu (2008), using four pulses of 5V, 50msec pulse width and 500ms interval. Embryos were cultured using a modification of New's method (Stern and Ireland, 1981) for 6 hours to allow them to adhere to the vitelline membrane. After 6 hours embryos were transferred to a glass bottom dish for imaging. A drop of PBS was placed in the centre of the new dish, then the embryo and glass ring were inverted and placed over the drop of PBS. Albumin was then slowly added on top of the vitelline membrane until the embryo came into contact with the PBS drop, as shown in Figure 3.19A. Embryos were then imaged using a Zeiss LSM 880 and Plan-Apochromat 20x, 0.8 NA air objective, or a Leica SP8 and PL APO 20x, 0.75 NA air objective. Confocal stacks were acquired at 5 or 10 minute intervals using tiling and a 10% overlap to cover the entire embryo. Cell tracking was performed using Imaris (Bitplane) then cell tracks were exported and analysed using Python 3.10.

3.3. Results

Figures 3.2 to 3.8 were produced in collaboration with Agnieszka Piatkowska and published in Piatkowska et al. (2023).

3.3.1. Examining epithelialisation of the PSM in the sagittal plane

Given a variety of published observations that appear incompatible with the clock and wavefront model, we set out to reexamine cellular behaviours in the PSM leading up to segmentation. Rather than the rapid epithelialisation and segmentation predicted by the clock of wavefront model, we hypothesised that this process may be more gradual and set out to examine cell shape and markers of polarity along the length of the PSM. To examine how cells of the PSM epithelialise prior to segmentation, embryos at stage HH11 (~15 somites) were fractured in the sagittal plane through the middle of the PSM. The sectioned embryos were then imaged using SEM, and cells were classified as belonging to dorsal, ventral or core domains of the PSM. Cell outlines were then segmented and their aspect ratio calculated (Figure 3.2A-B, K). To compare the dynamics of epithelialisation between different subpopulations of PSM cells their aspect ratios were plotted against the relative position of each cell along the length of the PSM, from 0% at the posterior end and 100% in the anterior PSM, just adjacent to the most recently segmented somite (Figure 3.2K). To evaluate the position within the PSM at which cells undergo MET, a sigmoid curve was fitted to the data using regression analysis. We used two different metrics as a threshold for the onset of MET, the inflection points of the sigmoid curve and the point at which the curve reached 10% of its maximum height.

Using either threshold point, cells of the dorsal PSM epithelialised markedly earlier than those of the ventral PSM (Figure 3.2E-H, Figure 3.3). When using the inflection point of the curves as an indicator of the onset of MET, the ventral and dorsal regions of the PSM begin epithelialising at 70% and 44% of the length of the PSM respectively. Similarly, when comparing the point at which the curve reaches 10% of its maximum vertical height, the dorsal and ventral regions begin epithelialising at 66% and 42% respectively. This shows that different regions of the PSM epithelialise asynchronously, suggesting that cells dorsal side begin epithelialising approximately 10 hours before they segment and form a somite and approximately 4 hours before cells of the ventral PSM begin epithelialising. Cells in the core did not epithelialise at any point, instead

displaying a constant aspect ratio through the entire length of the PSM, including in recently formed somites.

3.3.2. Examining epithelialisation of the PSM on the transverse plane

To assess the timing of epithelialisation in the medial and lateral regions of the PSM, embryos at stage HH11 (~15 somites) were sectioned in the transverse plane at selected points along the length of the PSM and imaged using SEM. Cells were grouped into dorsal, ventral, medial, lateral and core regions then segmented and their aspect ratios calculated. At 100% PSM length, adjacent to the most recently formed somite (Figure 3.4A-B), all regions are epithelised with the exception of the core which remains mesenchymal. Cells of the lateral PSM appear less elongated, suggesting that they separate from the lateral plate mesoderm at around the same time as a new somite forms. The lateral PSM also shows markedly fewer elongated cells at 90% PSM length, where the other regions consist primarily of epithelialised cells (Figure 3.4C-D). At 65% PSM length the dorsal region is epithelialised and some elongated cells were observed in the medial and ventral regions, but the lateral or core regions remained mesenchymal in appearance. All regions appeared mesenchymal at 40% of the PSM length, with a limited number of elongated cells seen in the dorsal region (Figure 3.4G-H). At 10% the sections consisted almost exclusively of mesenchymal cells (Figure 3.4I-J). Taken together, this analysis suggests a progressive epithelialisation of the PSM, starting with the dorsal region, then progressing to the medial, ventral and finally lateral regions (Figure 3.5).

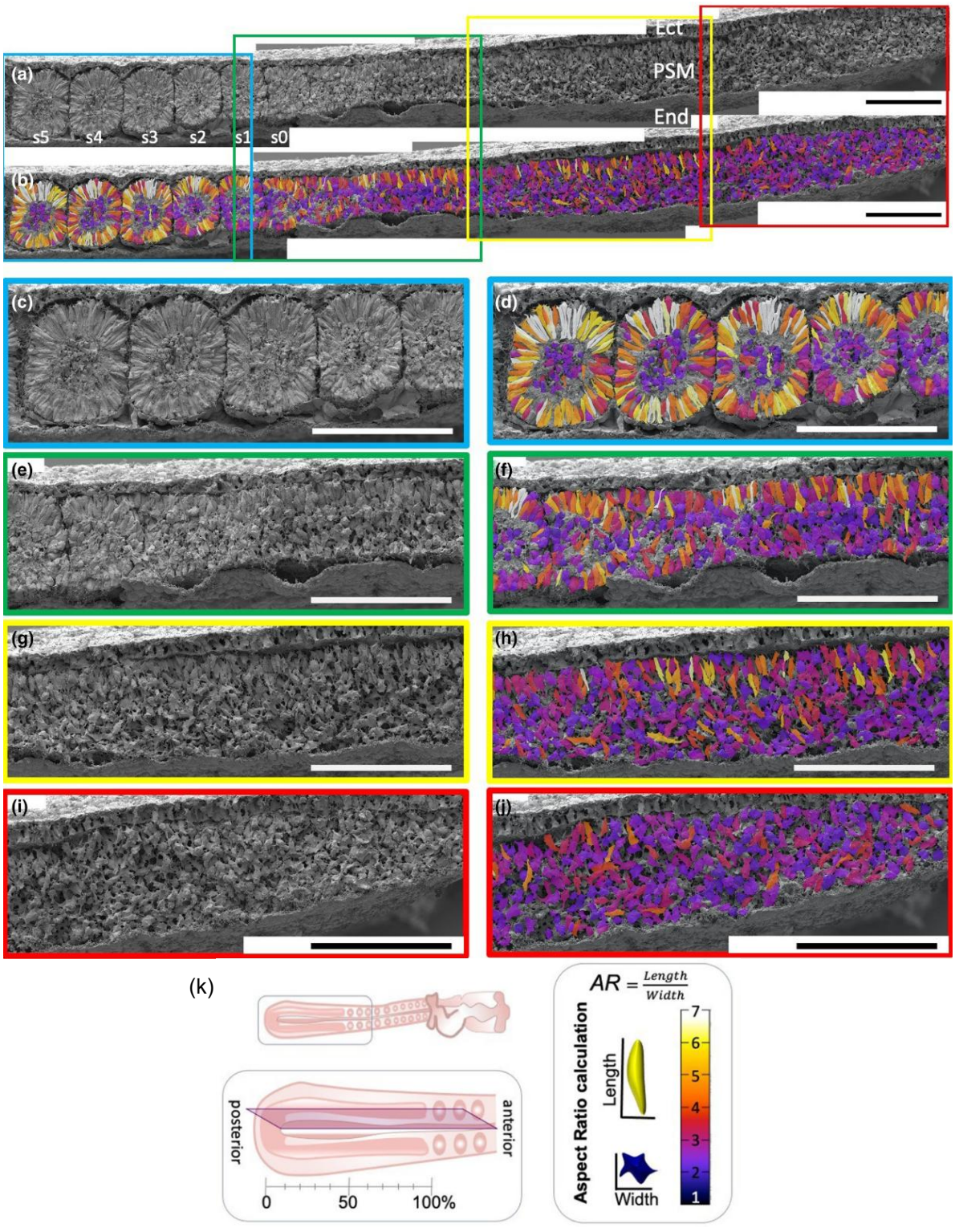

Figure 3.2 Sagittal sections reveal epithelialisation dynamics of the PSM

(a) An example of a sagittal section through middle of the PSM and somites. S1 is the 12th somite. (b) The same sagittal section with cell outlines colour coded based on their aspect ratio. (c–j) Enlargements of section shown in (a) and (b) as indicated by coloured boxes. (k) scheme showing mid sagittal section, and aspect ratio colour coding. Experiment performed by Agnieszka Piatkowska. Scale bars are 100 μm. S=somite, PSM=pre-somitic mesoderm, Ect=ectoderm, End=endoderm.

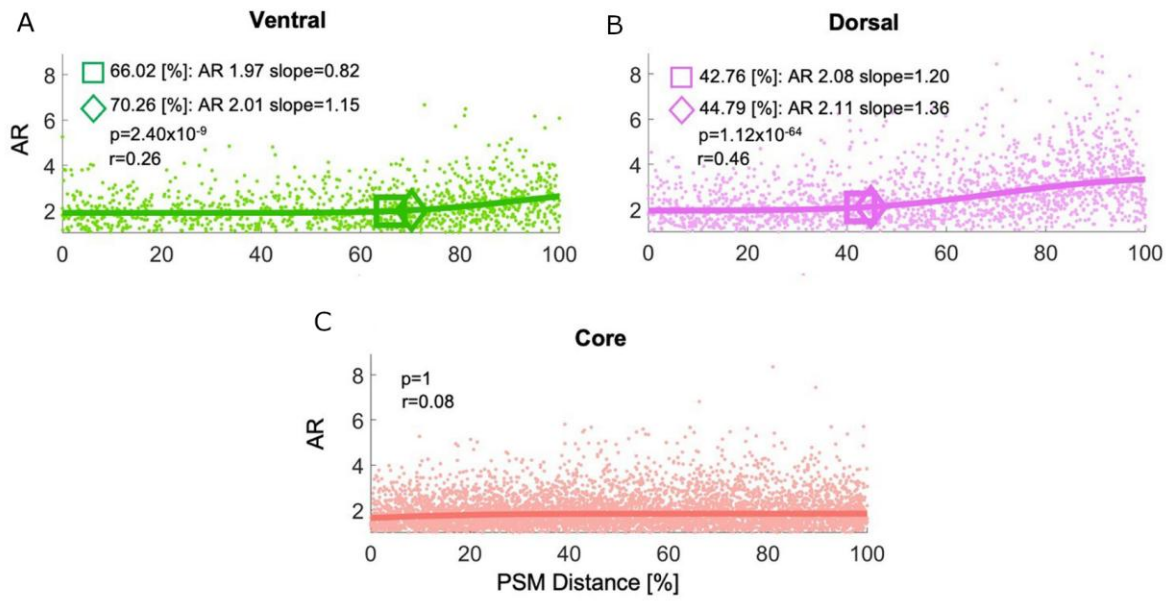

Figure 3.3 Comparison of cell elongation in different PSM regions

A-C. Aspect ratio vs distance in sagittal PSM sections. The aspect ratios of each cell from 12 embryos were plotted against distance along the PSM represented in [%]. Lines represent a sigmoid curve fitted with regression analysis. Diamonds represent the inflection point; squares represent the point where the fitted curve reaches 10% of its maximum vertical height. p-values are calculated with an F-test. Data collected by Agnieszka Piatkowska.

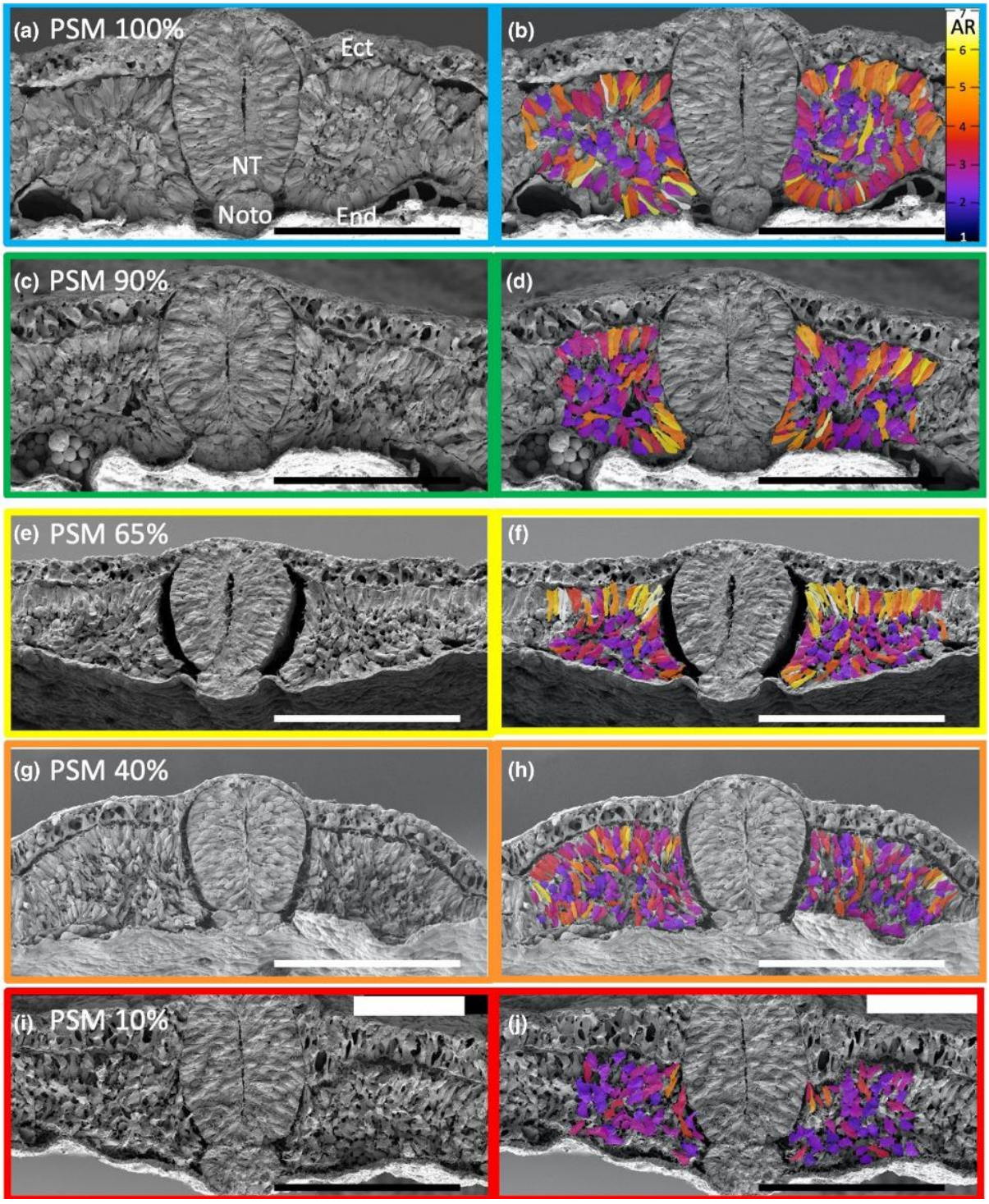

Figure 3.4 Transverse sections reveal epithelialisation dynamics of the PSM

SEM images of transversely sectioned embryos at different PSM distances. Each section is from a different embryo. (a, c, e, g, i) transverse sections at 100%, 90%, 65%, 40%, and 10% of the PSM length respectively. (b, d, f, h, j) same images with aspect ratio colour encoded. Experiment performed by Agnieszka Piatkowska. Scale bars are 100μm. Ect=ectoderm, end= endoderm, NT=neural tube, Noto=notochord.

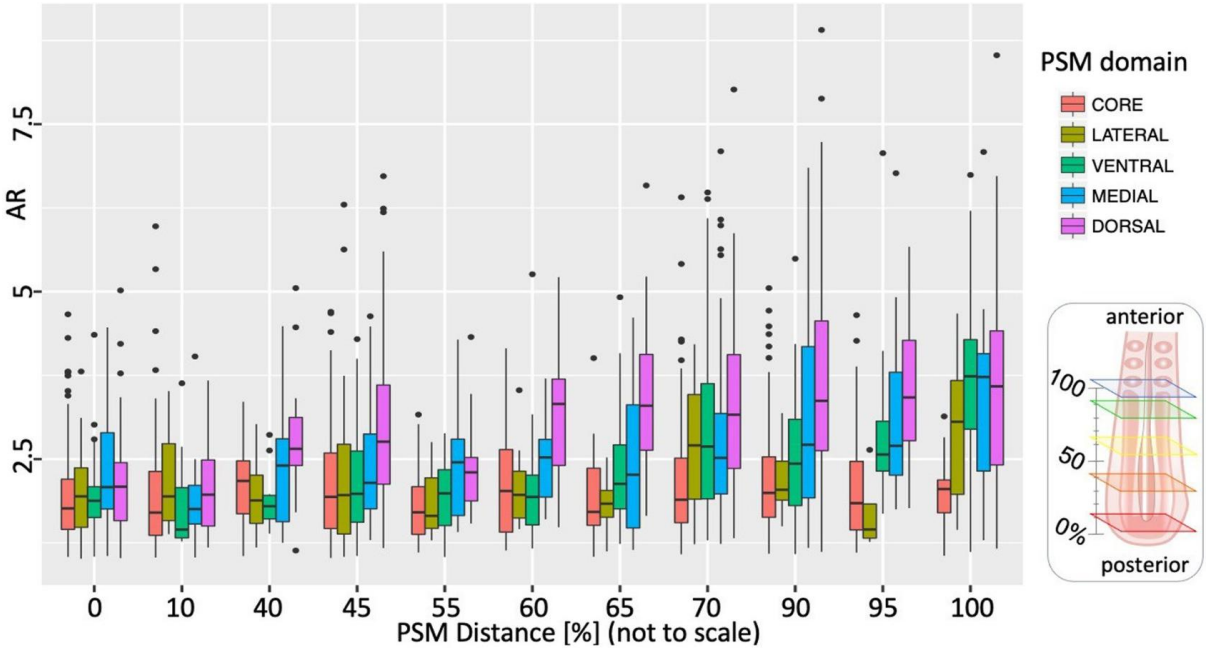

Figure 3.5 Comparison of cell elongation in different PSM regions

Box plots comparing aspect ratio in different PSM regions at each distance of transverse sections. Insert shows schematic representation of transverse sections at different distances along the PSM. Data collected by Agnieszka Piatkowska.

3.3.3. Examining expression of polarity markers along the PSM

To gain a broader understanding of the dynamics of epithelialisation throughout the PSM, embryos were stained for the cell polarity marker GM130. Embryos were then imaged using confocal microscopy, allowing computational reconstruction of sagittal and transverse sections of the PSM. As with the SEM images processed previously, the PSM was divided into dorsal, ventral, medial, lateral and core regions. In addition, each of these regions (excluding the core) was then subdivided into apical and basal regions allowing quantification of the localisation of GM130 to either apical or basal regions. GM130 is a marker of the Golgi apparatus, which is found in the perinuclear region, its exact position being determined by cell polarity. In epithelial cells it sits between the nucleus and the apical membrane, making the relative position of the nucleus and Golgi a useful marker of cell polarity and a proxy for epithelialisation. Cell density throughout the PSM meant that it was not possible to examine individual Golgi-nucleus pairs, however, by dividing the PSM into apical and basal regions it was possible to examine the organisation of the PSM at a tissue level. Mesenchymal regions are expected to have an even distribution of Golgi localised to both apical and basal regions, whereas regions that have polarised are expected to have the Golgi localised to only the apical region. The difference between the apical and basal regions was then plotted against the relative position within the PSM. This produced results that were somewhat consistent with the SEM images, but differed in a number of ways (Figure 3.6, Figure 3.7 and Figure 3.8). Similar to our observations of cell aspect ratio, the medial, ventral and lateral regions appeared to polarise sequentially, at around 60%, 70% and 90% respectively. However, based on GM130, the dorsal PSM polarises later than implied by the cell aspect ratio at 75% PSM length.

3.3.4. Notch signalling specifies somite rostral-caudal polarity

It is difficult to reconcile the gradual epithelialisation of the PSM, particularly the asynchronous epithelialisation observed in the mediolateral and dorsoventral axes, with predictions made by clock and wavefront models. To explore the possible role of Notch signalling (whose components oscillate as part of the “segmentation clock”), we inhibited Notch signalling using the γ-secretase inhibitor LY411757, and examined the effect on cell shape along the PSM. Embryos treated with LY411757 show segmented, somite-like structures complete with expression of the somite marker Paraxis (Figure 3.9C-D). These somite structures formed despite the lack of oscillations in Notch

related gene c-hairy1 (Palmeirim et al., 1997) (Figure 3.9E-F). In embryos treated with LY411757 the average somite size is slightly smaller than in control embryos, but there was also significantly more variance in the size of somites formed, with somites ranging from 32μm to 100μm in diameter in Notch inhibited embryos, compared to 52μm to 80μm in controls (Figure 3.9G). Interestingly, embryos treated with LY411757 also show absence of expression of the caudal somite marker Uncx4.1 (Figure 3.10A-B) (Schrägle et al., 2004), suggesting that the role of Notch signalling may be to ensure regular boundaries between somites, rather than epithelisation. This is consistent with a previous study (Dias et al., 2014), where cells of posterior primitive streak were induced to form somites ectopically in the absence of oscillating clock genes. These ectopic somites had an epithelial rosette structure along with expression of Paraxis, but lacked rostral-caudal polarity.

After observing increased variance in somite size and lack of rostral-caudal polarity in embryos where Notch is inhibited, we were curious to know if the somites were irregular in size at the time they segmented. The lack of rostral-caudal polarity could mean that the boundaries between somites are unstable and that the irregularity in size was the result of somites splitting and merging after they form. To answer this question, we performed live imaging of embryos treated with LY411575 and observed that somites tended to be of uniform size, but then split and merged shortly after segmentation (Figure 3.10C-H).

3.3.5. Notch inhibition does not influence the dynamics of PSM epithelialisation

Given that the PSM continues to segment in the absence of Notch signalling, we wanted to explore whether Notch inhibition influences the dynamics of PSM epithelialisation. To do this we repeated staining for Golgi marker GM130 in embryos treated with LY411575 (Figure 3.11). The apical-basal distribution of GM130 was measured in the lateral, ventral, medial and dorsal compartments of the PSM and plotted against PSM length. The order of epithelialisation followed the same radial pattern observed in SEM imaging (Figure 3.12), with the dorsal epithelialising first at 61% PSM length, followed by the medial, ventral and finally lateral domain, which epithelialised at 66%, 75% and 76% PSM length respectively.

3.3.6. Cells of the somite core display rostral-caudal polarity

Having observed that cells found within the somite core do not epithelialise, we were curious about whether they have rostral and caudal identities, as do the surrounding epithelial cells. To explore this question, hybridisation chain reaction (HCR) was used to visualise expression of rostral and caudal somite markers simultaneously (Dirks and Pierce, 2004). This allowed us to discern potential regions of overlap or mixed identity, as well as regions which lacked any rostral-caudal polarity. HCR was performed using Uncx4.1 as a caudal marker and EphA4 as a rostral marker (Schmidt et al., 2001). In somites S1 and S2 both EphA4 and Uncx4.1 are expressed (Figure 3.13A). Both markers extend to the somite core, without a gap, suggesting that all cells in the core have either a rostral or caudal identity. There appear to be a small number of cells expressing EphA4 in the caudal region and Uncx4.1 in the rostral region. This suggests that there may still be some cell mixing occurring at this time, and that these cells may subsequently sort, die, or change their identity. The rostral, EphA4 expressing domain is larger than the caudal domain, which is also true in anterior PSM where the EphA4 expression occupies a region much larger than the rostral half of the next prospective somite. The boundary between rostral and caudal halves also appears oblique, being largest in the medial half of the somite and narrower in the lateral half and the Unxc4.1 domain mirroring this. Taken together, these observations suggest that von Ebner's fissure, a physical boundary that roughly divides the somites into equal halves (Stern and Keynes, 1987), does not correspond to the boundary between rostral and caudal halves.

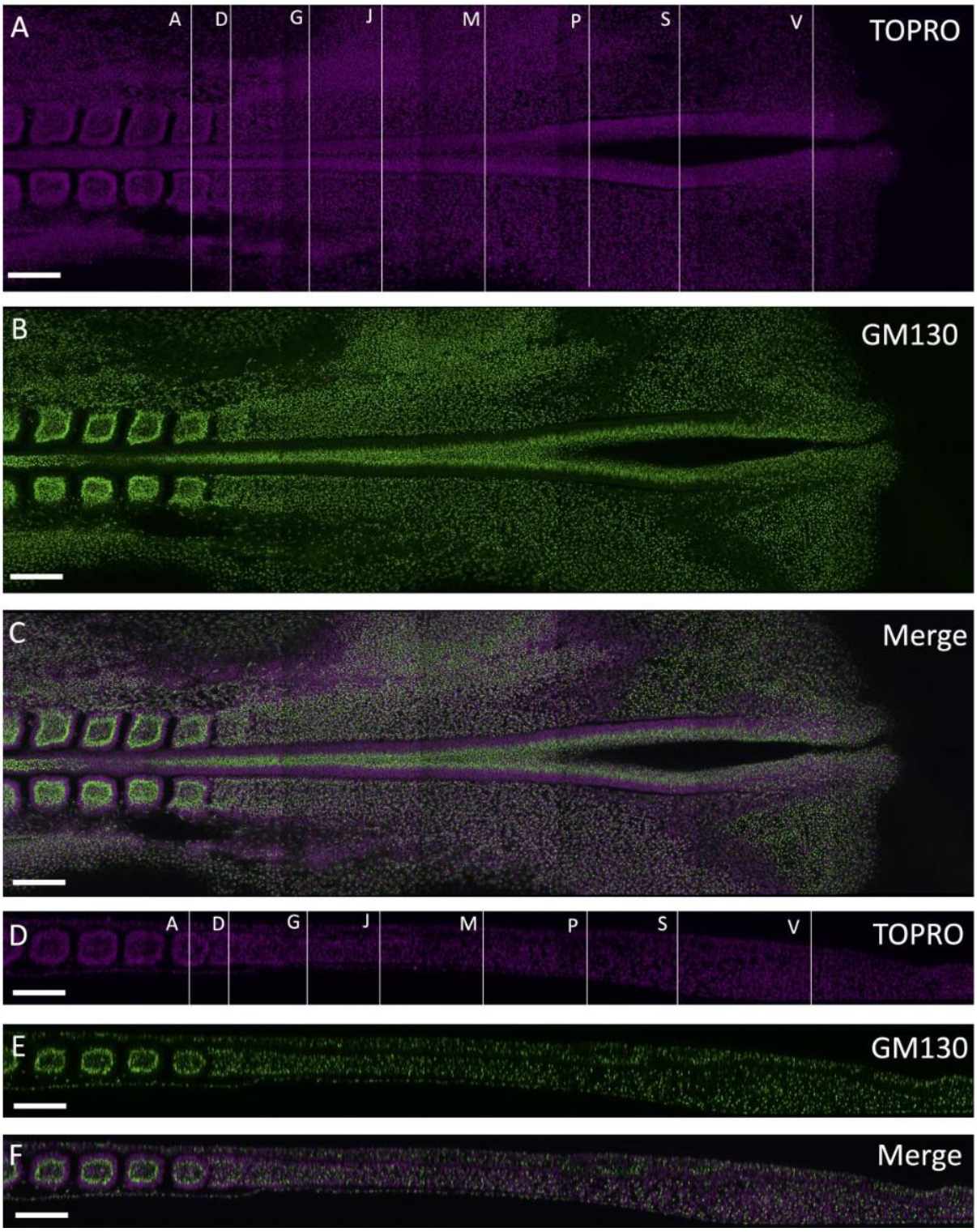

Figure 3.6 GM130 expression in the PSM

Confocal sections showing GM130 expression and TOPRO (nuclear stain) in coronal (**A-C**) and sagittal (**D-F**) planes. White lines represent transverse sections shown in Figure 3.13. Experiment performed by Agnieszka Piatkowska. Scale bars are 100μm.

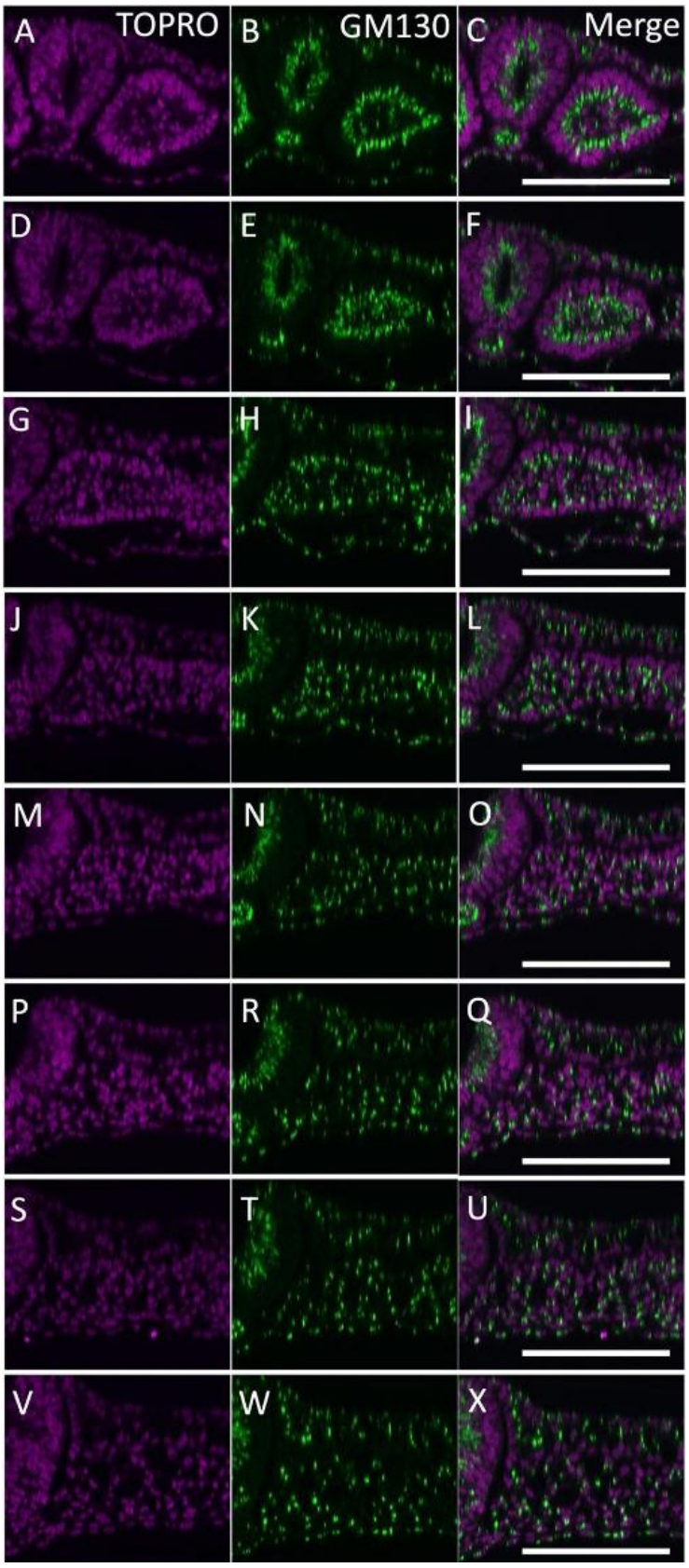

Figure 3.7 GM130 expression in transverse sections of the PSM

Transverse sections reconstructed from 3D confocal image data. The level of each transverse section is indicated in Figure 3.12A and D (white bars). Dorsal is at the top of each image. Experiment performed by Agnieszka Piatkowska. Scale bars,100μm.

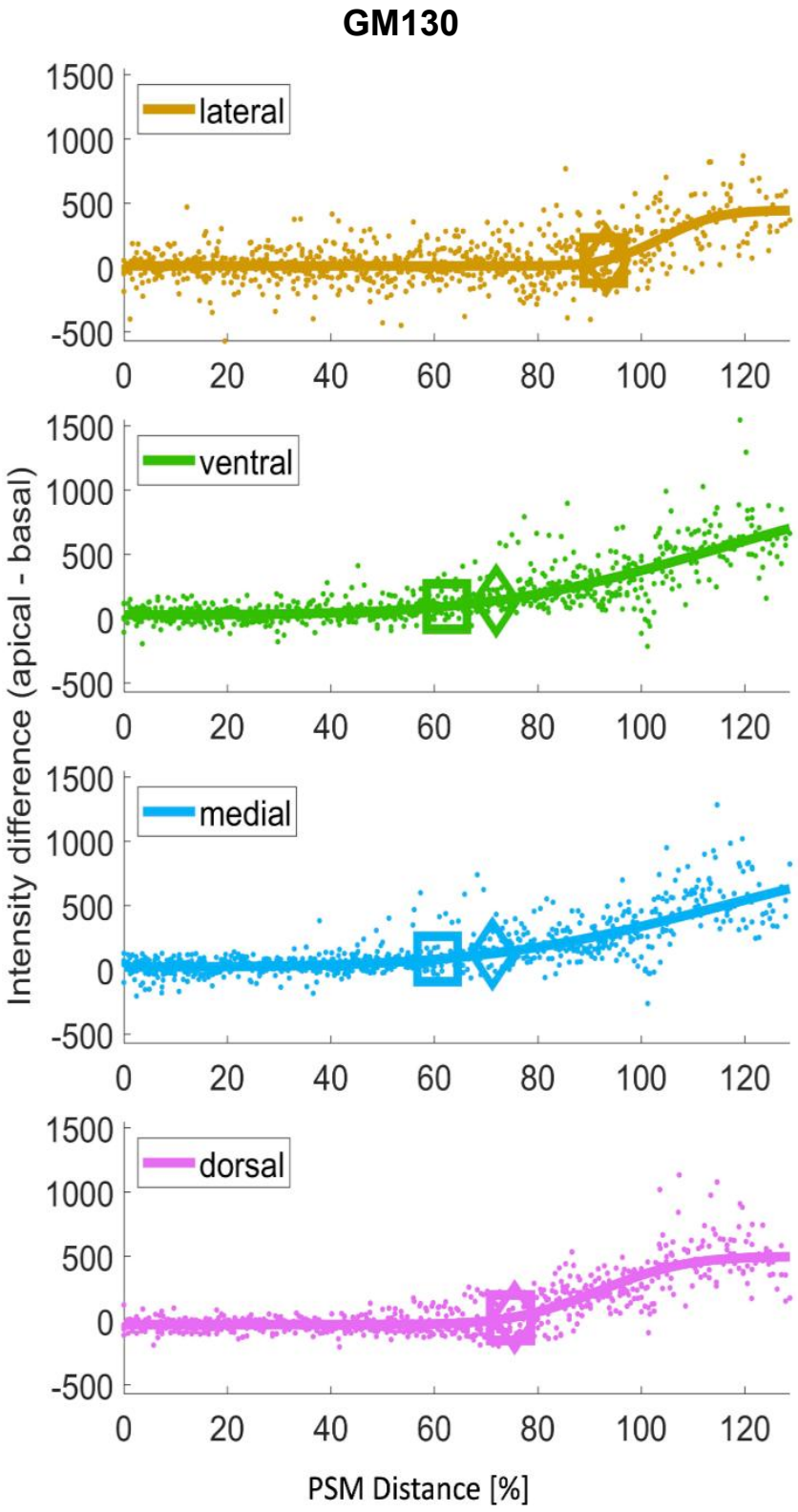

Figure 3.8 Analysis of GM130 expression in each PSM region

Pixel intensities of the basal zone were subtracted from those of the apical zone for every PSM domain and plotted against PSM distance represented in [%]. 0%–100% is PSM, whereas values above 100% represent somites. Each dot is a single data point (apical-basal). The line is a sigmoid fit from regression analysis. Squares represent 10% of vertical height of the fitted curve and diamonds are inflection points. Data collected by Agnieszka Piatkowska.

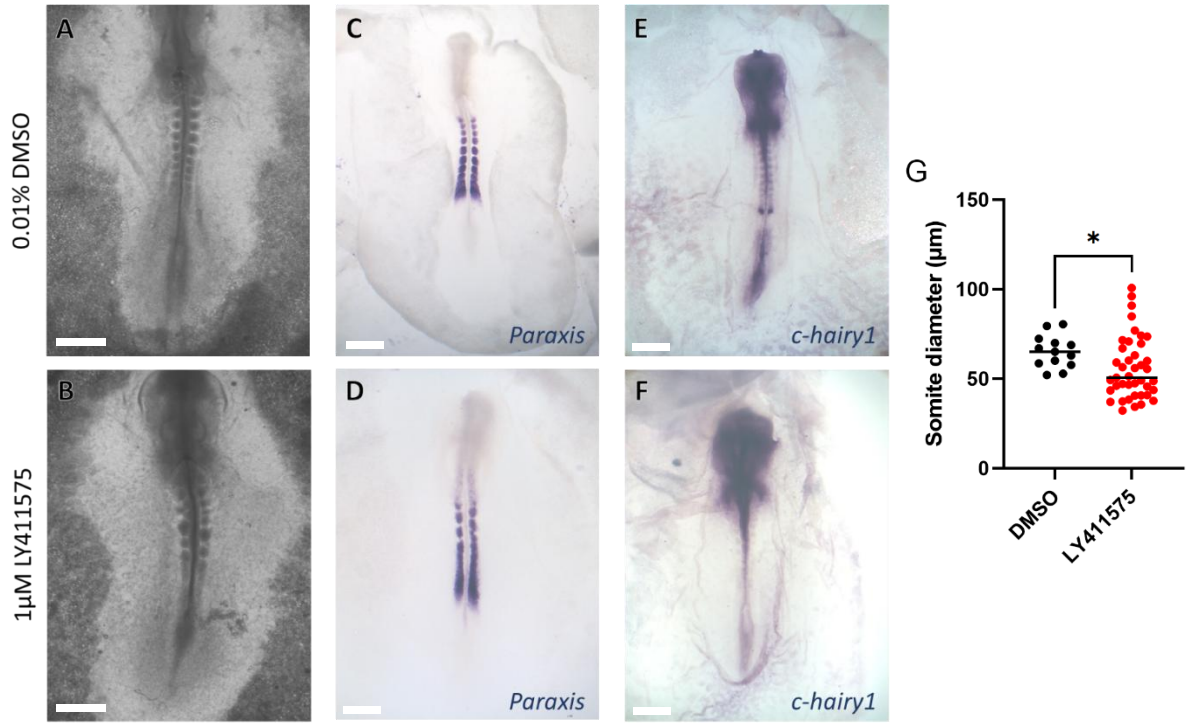

Figure 3.9 Embryos treated with Notch inhibitor form somites in absence of clock gene expression

A-B. Brightfield showing morphology of somites in control and treated embryos. **C-F.** Whole mount in situ hybridisation showing mRNA expression of Paraxis (**C-D**), c-hairy1 (**E-F**). **G.** Comparison of somite diameter in control and treated embryos P=0.0157. Scale bars, 500µm.

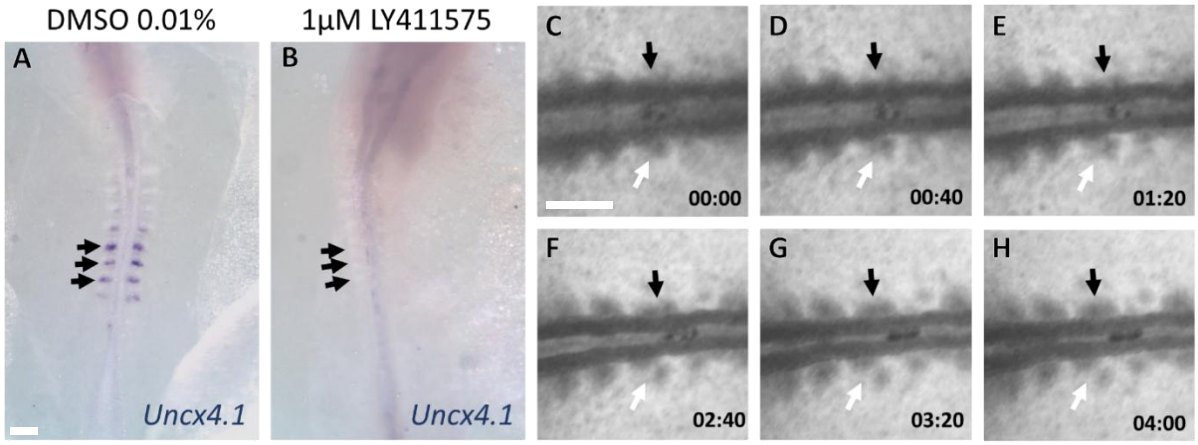

Figure 3.10 Somites in embryos treated with LY411575 lack rostral-caudal sub compartments and well-defined boundaries.

A-B. In situ hybridisation showing expression of caudal polarity marker Uncx4.1 **C-H**. Selected frames from time lapse movie showing somites merging (black arrows) and splitting (white arrows). Scale bars, 200µm.

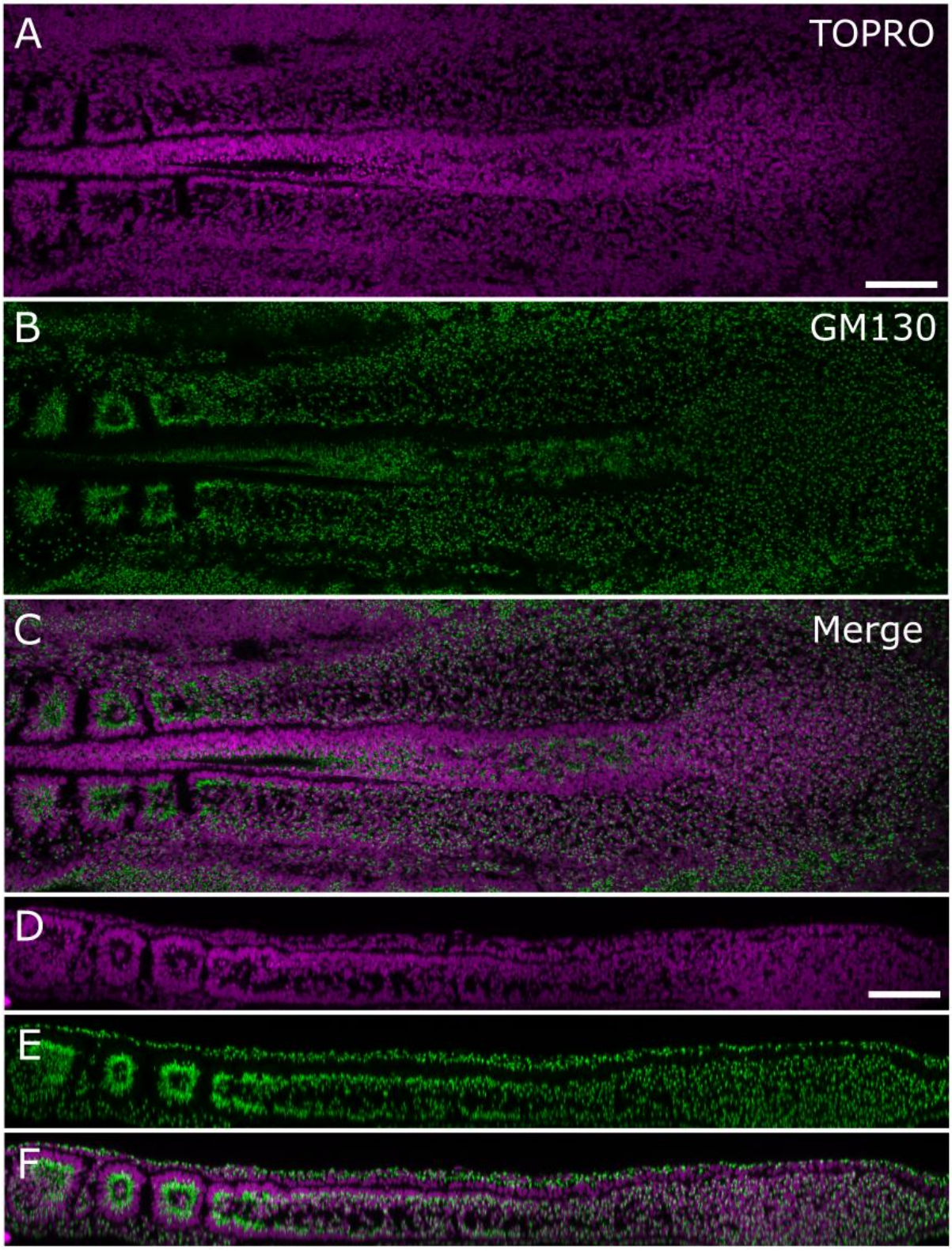

Figure 3.11 GM130 expression in PSM of embryos treated with LY411575

Confocal sections showing GM130 expression and TOPRO (nuclear stain) in coronal (**A-C**) and sagittal (**D-F**) planes. Scale bars are 100μm.

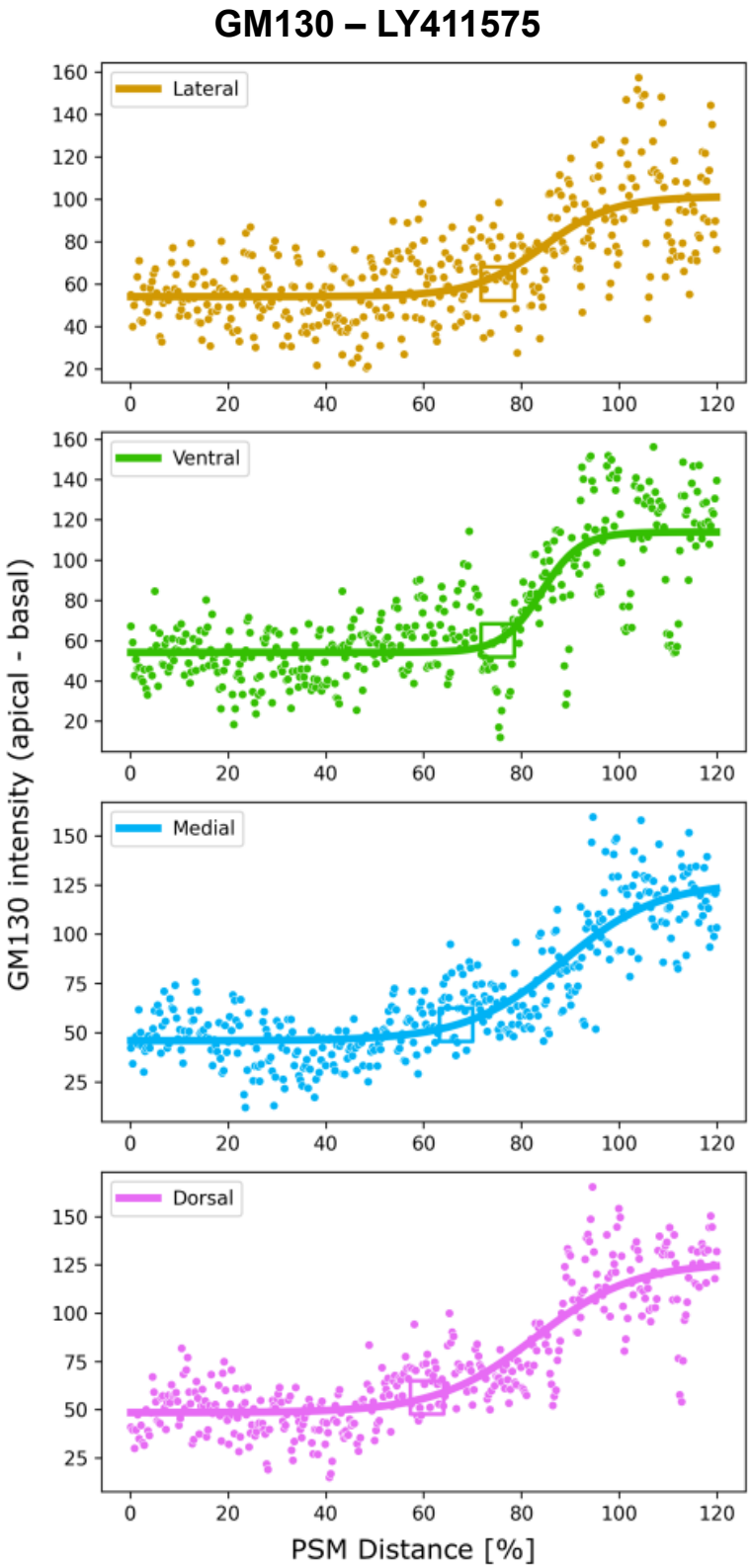

Figure 3.12 Analysis of GM130 expression in each PSM region in embryos treated with LY411575

Pixel intensities of the basal zone were subtracted from those of the apical zone for every PSM domain and plotted against PSM distance represented in [%]. 0%–100% is PSM, whereas values above 100% represent somites. Each dot is a single data point (apical-basal). The line is a sigmoid fit from regression analysis. Squares represent 10% of vertical height of the fitted curve.

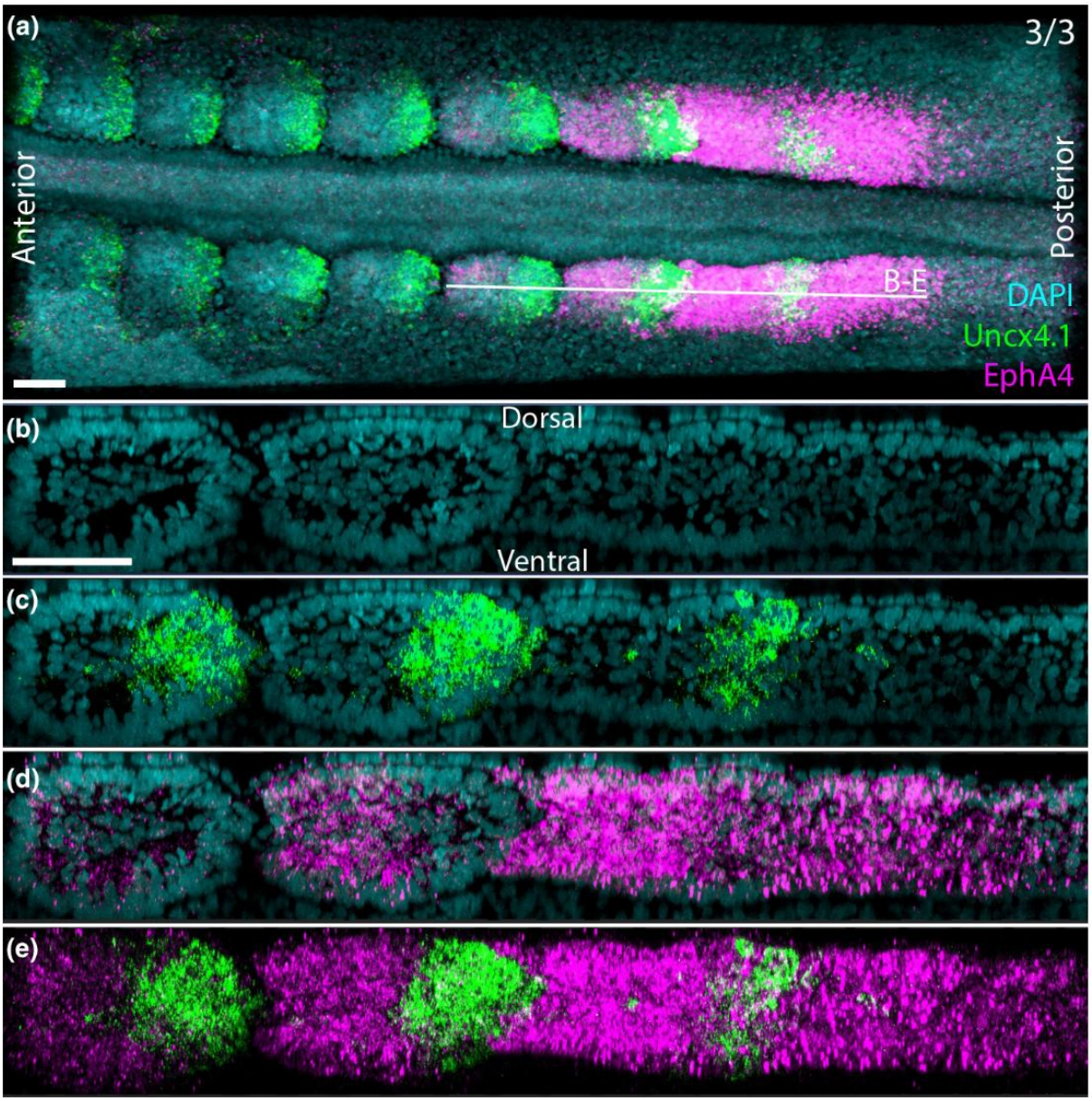

Figure 3.13 Rostral-caudal identity of core cells

Multiplexed expression of rostral and caudal somite markers. (a) Whole-mount hybridization chain reaction (HCR) for Uncx4.1 and EphA4 shown as a 3D maximum projection in the coronal plane (b–e) Sagittal sections (5μm thickness) of the same embryo generated computationally showing DAPI (b), DAPI and Uncx4.1 merged (c) DAPI and EphA4 merged (d) Uncx4.1 and EphA4 merged (e). Scale bars are 50μm.

Figures 3.14 to 3.18 were produced in collaboration with Tatiana Solovieva and published in Solovieva et al. (2022).

3.3.7. The node can instruct non-node cells to become resident

The node is a dynamic region in the early embryo with cells of the epiblast entering the node (Joubin and Stern, 1999). However, it has been demonstrated through the fate mapping of single cells that some cells that enter the node become resident (Selleck and Stern, 1992). Given evidence that the node contains resident cells that are self-renewing (Charrier et al., 1999; Mathis et al., 2001; McGrew et al., 2008; Selleck and Stern, 1992), we set out to test the hypothesis that the node is an instructive stem cell niche, capable of imparting self-renewing, stem cell behaviour on cells that transit through it. To explore this hypothesis, a series of epiblast grafts were performed. Cells from transgenic GFP donor embryos were taken from one of two regions of epiblast, either lateral to the node or anterior to the node (Figure 3.14D, F, H, J) and grafted either lateral to the node or anterior to the node of a wild type HH3+/4 host embryo. Cells taken from a position lateral to the node would normally be expected to transit through the node, giving rise to notochord, mesoderm and somite (Bortier and Vakaet, 1992; Hatada and Stern, 1994). In contrast, cells taken from a position anterior to the node would not normally pass through the node and instead give rise to head epidermis or anterior neural plate (Bortier and Vakaet, 1992; Hatada and Stern, 1994). By taking epiblast anterior to the node and grafting it to a position lateral to the node, cells that would never normally enter the node are forced to do so, testing whether the behaviour of these cells is intrinsic or if the node is instructive. Grafts were performed in four configurations, anterior to anterior, lateral to lateral, anterior to lateral and lateral to anterior (Figure 3.14D, F, H and J). Embryos were then cultured to HH8+ after which whole-mount in situ hybridization was performed and the embryos sectioned to examine the fate of grafted cells.

Cells that were transplanted from an anterior to lateral position, forcing cells that would never normally enter the node to do so, gave rise to caudal node and chordoneural hinge (88%), notochord (71%), PSM and medial somites (71%) and floorplate (44%), and expressed CHRD, TCF-15 (Paraxis) and FOXA2 (Figure 3.14L and Figure 3.15D-L). Upon being forced to enter the node some cells from the grafts exhibited resident behaviour, remaining present in the node at stage HH8+. Interestingly, cells from the anterior epiblast, which would never normally enter the node, were instructed to

display resident behaviour with the same efficiency as the lateral epiblast (Figure 3.14L, 30/34 (88%) vs 8/9 (89%), respectively). Although grafts of both anterior and lateral epiblast contributed equally to the resident cell population, their contribution to axial mesodermal tissues such as somites and notochord was slightly lower in anterior to lateral grafts compared with lateral-to-lateral grafts. The reverse was true when comparing neural derivatives such as floorplate and lateral neural plate, with cells that originated from epiblast anterior to the node making greater contributions to these tissues. This difference suggests that while the cells remain plastic, they are already biased towards certain fates before entering the node. This makes the ability of the node to impart resident behaviour on cells from the anterior epiblast with high efficiency even more notable. Lateral to anterior grafts allowed us to test if prospective node cells remain plastic before transiting through the node. After overnight culture, staining revealed that prospective node cells contributed to epidermis and anterior neural plate in the head (100%, n=10 embryos) and lacked expression of CHRD (Figure 3.16). Thus, lateral cells appear plastic and adapt their behaviour in accordance with their new position, behaving the same as donor cells in anterior-to-anterior grafts.

3.3.8. Cells that become resident in the node are able to self-renew

To characterise the properties of resident cells in the node further, additional experiments using two successive host embryos were performed to test their ability to self-renew, a defining feature of stem cells (Becker et al., 1963; Siminovitch et al., 1963; Till et al., 1964). First, anterior to lateral grafts were performed as previously outlined and cultured overnight to stage HH8-10. The node was then dissociated and a single GFP+ cell was re-grafted to a second HH3+/4 host embryo to test their ability to self-renew and contribute to axial tissues a second time (Figure 3.17A-D). The second host embryo was cultured overnight to stage HH8-10 and in 17 of 75 embryos grafted GFP+ cells were found and in 9 of those multiple GFP+ cells were observed (Figure 3.17E-H), showing that the grafted cell was able to divide successfully and demonstrating self-renewal. These cells able to contribute to a variety of tissues, including floor plate, notochord and endoderm. In three of the embryos GFP+ cells were observed in both the node and in axial tissues demonstrating both self-renewal and the ability to contribute to the axis of a second host. Here we have demonstrated the ability of the node to impart self-renewing and resident behaviour on cells that have

been forced to enter the node ectopically. This behaviour is consistent with the properties of instructive stem cell niches (Dexter et al., 1977; Li and Xie, 2005; Schofield, 1978).

3.3.9. The posterior node behaves as a stem cell niche

We then asked which part of the node behaves as a stem cell niche: is it the entire node, or are resident cells confined to a sub-region of the node? To explore this, we divided the HH8 node into left and right, anterior, middle and posterior regions (six regions) and performed fate mapping by labelling each region with a lipophilic dye (DiI). Embryos were then cultured to HH11-12. All cells labelled in each of the anterior regions had left the node and chordoneural hinge by HH12 and contributed to axial tissues, including notochord, floorplate and neural plate (Figure 3.18B, D). Cells labelled in the middle node regions had shifted to the anterior node and chordoneural hinge after culture, while also contributing to axial tissues (Figure 3.18D). In contrast, only cells that had been labelled in the posterior parts of the node displayed resident behaviour, continuing to contribute to the posterior node after culture in addition to the chordoneural hinge and axial tissues (Figure 3.18C-D). The chordoneural hinge is an important growth zone for axial elongation and through serial transplantation has been shown to be a source of self-renewing axial progenitor cells with broad potency, capable of contributing to notochord, neural tube, and somites (Cambray and Wilson, 2002). We were unable to detect asymmetries between the left and right halves of each subregion in terms of their contributions to axial tissues (Figure 3.18D).

To examine cell movements and behaviour in real time a modified, inverted *ex ovo* culture method was developed based on New's method (Figure 3.19A). Using tiling, this allowed for imaging of the entire node and PSM with sufficient spatial and temporal resolution to perform cell tracking over extended periods (Figure 3.19B-C) and track cell divisions (Figure 3.19D). To label cells of the node and PSM for tracking, spatiotemporally targeted electroporation was used to transfect cells lateral to the node at HH4. These cells were electroporated using plasmid DNA encoding dsRed, allowing them to be tracked using live imaging as they entered the node. Cells were tracked successfully over a period of 10 hours, from stage HH5 to HH9, revealing a population of cells in the posterior node that remained resident during node regression. In contrast, all cells present in the anterior node at HH5 left the node by HH9 and

contributed to the axis (Figure 3.20A-C, Supplementary Movie 2). Collectively, these data strongly indicate that the posterior node is an axial stem cell niche.

3.3.10. Tracking cellular behaviour leading up to segmentation

Cells from 18 somites from 3 embryos were tracked over a period of 12-15 hours leading up to the point of segmentation in order to explore cellular behaviours in the PSM (Example of tracking shown in Figure 3.19B-C). The amount of cell movement matched what has previously been reported (Bénazéraf et al., 2010; Stern et al., 1988), with extensive cell movement in the posterior PSM which gradually decreases as cells near the point of segmentation (Figure 3.21A). This is also consistent with our observation of gradual epithelialisation starting at 40% of the PSM length. The cell cycle model proposes that cells that will segment together enter the PSM at the same time, just after cell division. This suggests they would start in close proximity, after which it is likely they would drift apart due to the cell movement and mixing in the posterior PSM, before aggregating again leading up to segmentation due to changes in cellular adhesion triggered by their synchronised cell cycles. To examine this, the perimeter of the convex hull enclosing the cells of each somite was plotted as a measure of cell spread over time (Figure 3.21B). Between 12 and 8 hours prior to segmentation the cells of each somite appear to spread out, before gradually aggregating from 8 hours onwards leading up to segmentation. The frequency of cell divisions was also tracked relative to the time of segmentation (Figure 3.21C). This revealed two peaks in cell division that were 10 hours apart, one 8 hours prior to segmentation and one 2 hours post segmentation. This suggests that there is cell cycle synchronization among cells that segment together and the peak 8 hours prior to segmentation coincides with the onset of aggregation (Figure 3.21B).

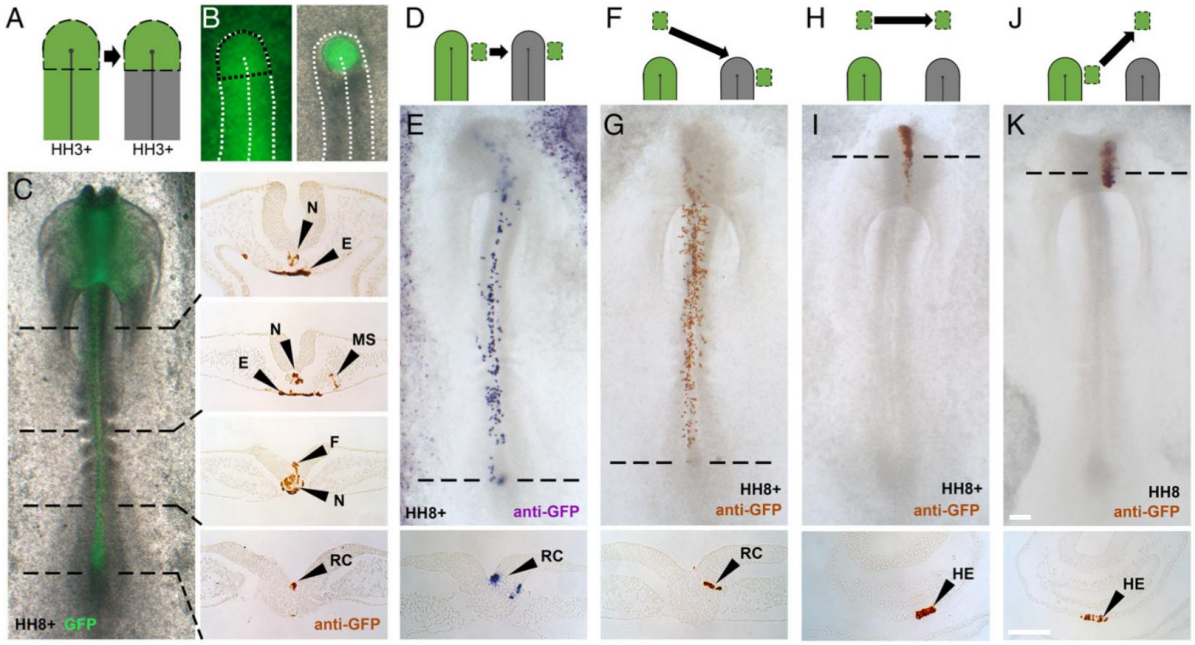

L

Epiblast graft	Tissue contribution of graft-derived cells after culture						
	Caudal node	CNH	Caudal node and/or CNH	Notochord	Floorplate	PSM/ medial somite	Lateral neural plate
Epiblast lateral to the HH3+/4 node (n = 9)	7/9 (78%)	7/9 (78%)	8/9 (89%)	8/9 (89%)	3/9 (33%)	9/9 (100%)	1/9 (11%)
Anterior epiblast placed lateral to the HH3+/4 node (n = 34)	29/34 (85%)	28/34 (82%)	30/34 (88%)	24/34 (71%)	15/34 (44%)	24/34 (71%)	9/34 (26%)

Figure 3.14 Cells that transit through the node can acquire resident behaviour. **A.** Scheme showing node transplant from transgenic GFP donor to wild type host. **B.** Widefield fluorescence images of transgenic GFP donor (left) and wild type host immediately after node transplant (right). White dashed lines identify the primitive streak and black dashed lines the node. **C.** Host embryo at stage HH8+ after overnight culture (left). Transverse sections of anti-GFP antibody stained host embryo. Dashed black lines indicate level of transverse sections. **D-E** Epiblast lateral to the node transplanted to same position in a host embryo gives rise to axial tissue and becomes resident in the node. **F-G** Epiblast anterior the node placed lateral to the node, forcing cells to transit through the node and giving rise to axial tissue and resident cells in the node. **H-I** Epiblast anterior to the node transplanted to same position in a host embryo gives rise to tissue in the head. **J-K** Epiblast lateral to the node is placed anterior to the node, meaning it no longer passes through the node and instead gives rise to head tissue instead of axial tissue. **L** Table showing the contribution of grafted cells to different tissues in lateral to lateral vs anterior to lateral grafts. N=notochord, E=endoderm, MS=medial-somite F=floorplate, RC=resident cell, CNH=chordoneural

hinge, HE=head epidermis. Experiment performed by Tatiana Solovieva. Images of wholemount embryos represent a region around 2 mm x 5mm. Scale bar, 200μm.

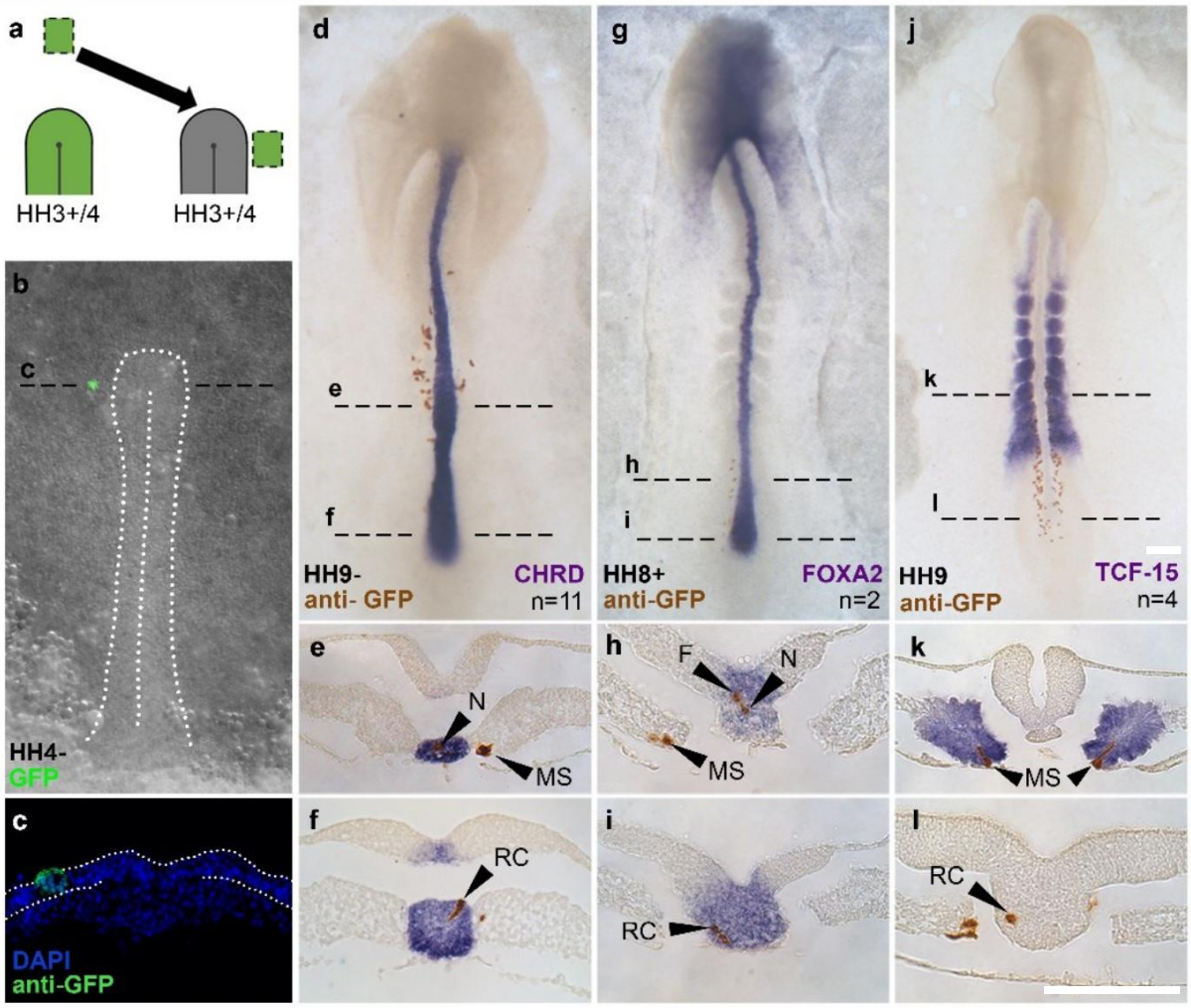

Figure 3.15 Anterior epiblast contributes to axial tissues and expresses appropriate markers when forced to transit through the node

A. Scheme illustrating the transplant of anterior epiblast from transgenic GFP donor to a region lateral to the node in WT host. **B.** Widefield fluorescence microscopy showing HH3+ host embryo after graft. **C.** Transverse section of embryo after graft. White dashed line highlights epiblast. **D-L.** Whole mount in situ hybridization and immunostaining of embryos cultured overnight after epiblast graft illustrated in A. Shows expression of node, notochord and somite markers CHRD (D-F), FOXA2 (G-I) and TCF-15 (Paraxis) (J-L). N=notochord, MS=medial somite, RC=resident cell, F=floorplate. Experiment performed by Tatiana Solovieva. Images of wholemount embryos represent a region around 2 mm x 5mm. Scale bars, 200μm.

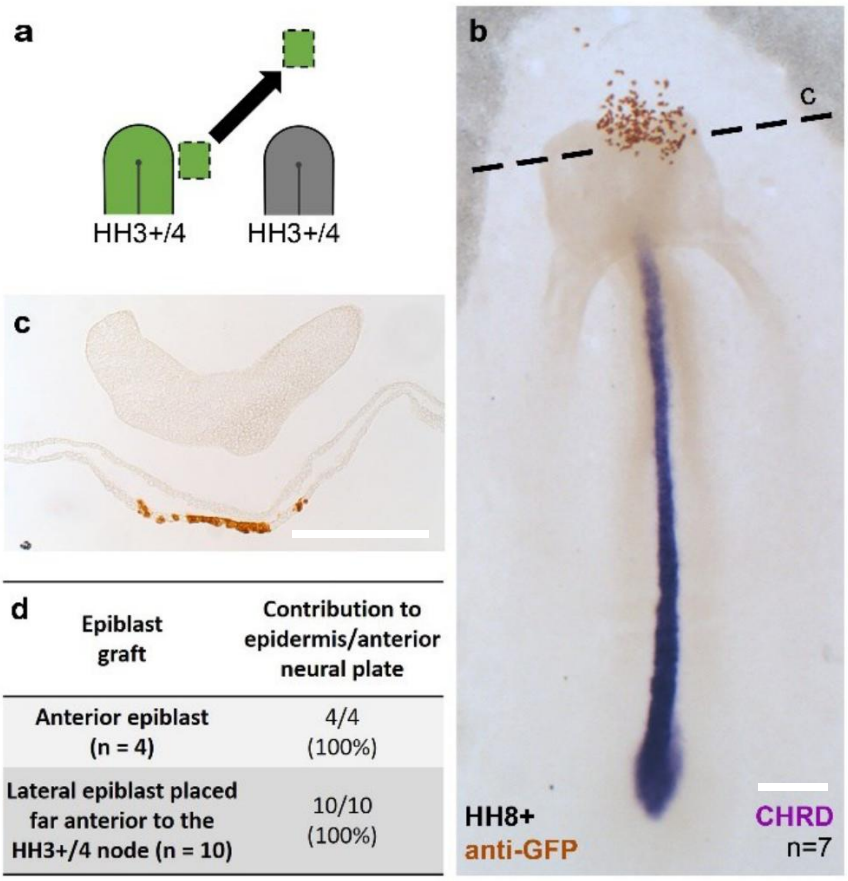

d

Epiblast graft	Contribution to epidermis/anterior neural plate
Anterior epiblast (n = 4)	4/4 (100%)
Lateral epiblast placed far anterior to the HH3+/4 node (n = 10)	10/10 (100%)

Figure 3.16 Cells that would normally enter the node have plasticity and contribute to other tissues if they do not enter the node

A. Scheme illustrating transplant of epiblast lateral to node from transgenic GFP donor to a region anterior to the node in WT host. **B.** Whole mount in situ hybridization and immunostaining of an embryo cultured overnight after epiblast graft illustrated in A. Shows expression of node and notochord marker CHRD. Black dashed line shows location of transverse section shown in C. **C.** Transverse section showing lack of expression of CHRD in transplanted cells contributing to epidermis. **D.** Table comparing contribution of grafted cells in anterior to anterior vs lateral to anterior grafts. Experiment performed by Tatiana Solovieva. Images of wholemount embryos represent a region around 2 mm x 5mm. Scale bars, 200μm.

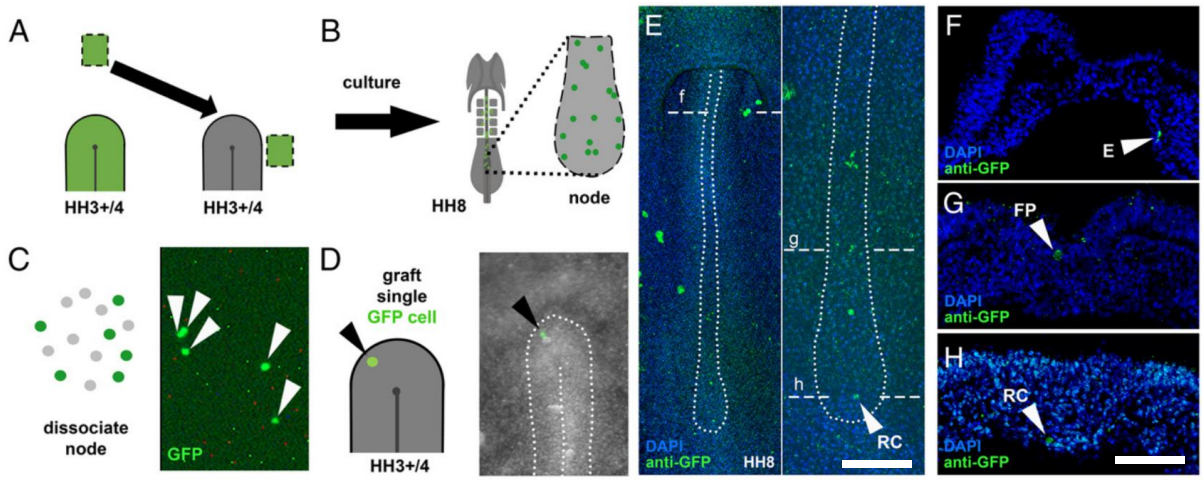

Figure 3.17 Regrafting of resident cells demonstrates their ability to self-renew
A-B. Scheme showing initial steps of regrafting experiment, where an anterior to lateral graft was performed using stage HH3+/4 embryos and then the host embryo was cultured to stage HH8-10. **C.** The node of the HH8-10 host was then removed and dissociated and single resident GFP+ cell was selected. **D.** The single GFP+ cell was then regrafted into a second HH3+/4 host. **E.** Widefield fluorescence images of immunostained HH8 host embryo after being regrafted with a single GFP+ node cell, showing the presence of a resident cell in the node as well as GFP+ cells along the axis. Dashed white lines indicate the position of transverse sections shown in **F-H**. E=endoderm, FP=floorplate, RC=resident cell. Experiment performed by Tatiana Solovieva. Scale bars, 100μm.

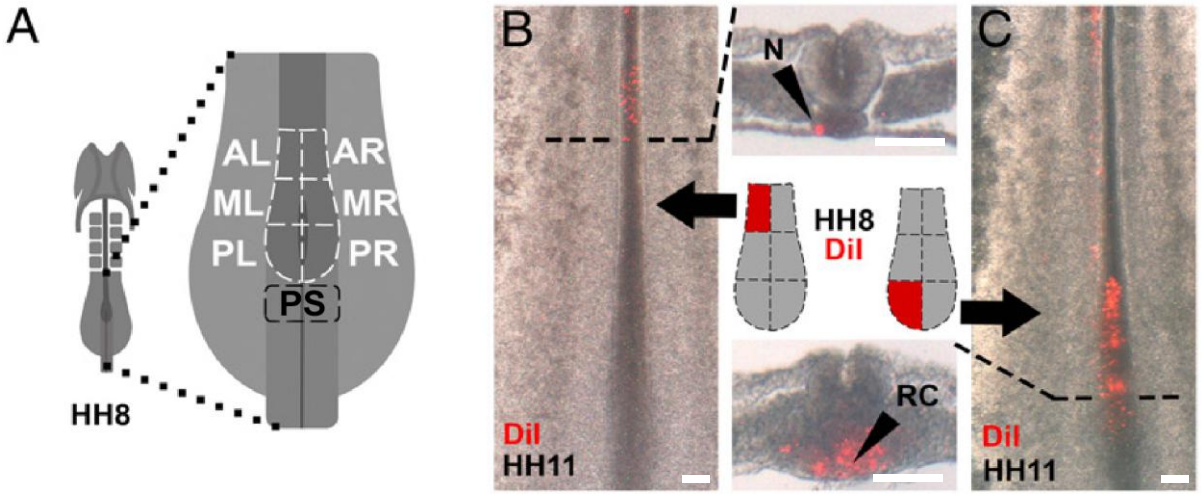

D

DiI-labeled region	Tissue contribution of DiI-labeled cells after culture (% of embryos)							
	Anterior streak	Caudal node	CNH	Notochord	Floorplate	PSM/ medial somite	Neural plate	Endoderm
AL (n = 3)	0	0	0	100	100	33	100	33
AR (n = 2)	0	0	0	100	100	50	0	50
ML (n = 5)	0	0	80	100	100	100	60	20
MR (n = 4)	0	0	50	100	100	75	50	25
PL (n = 4)	0	50	50	75	50	100	50	25
PR (n = 3)	0	100	100	100	100	100	0	33
PS (n = 3)	100	100	100	100	66	100	33	33

Figure 3.18 Lineage tracing suggests that cells of the posterior node remain resident

A. Scheme showing the subdivision of the node into subregions. AL, AR = anterior left and right respectively, ML, MR = middle left and right respectively, PL, PR = posterior left and right respectively. PS = primitive streak, just caudal of the posterior node. **B.** Fluorescence images of an embryo where anterior left of the node was labelled with DiI and cultured to HH11, showing labelled cells have exited the node and contributed to axial tissues. **C.** Embryo where the posterior left of the node was labelled with DiI and cultured to HH11, showing labelled cells contributing to axial tissues, the chordoneural hinge, but also a significant population of cells remaining resident in the posterior node. **D.** Table showing the contribution of each region of the node after culture. Experiment performed by Tatiana Solovieva. Scale bars, 100μm.

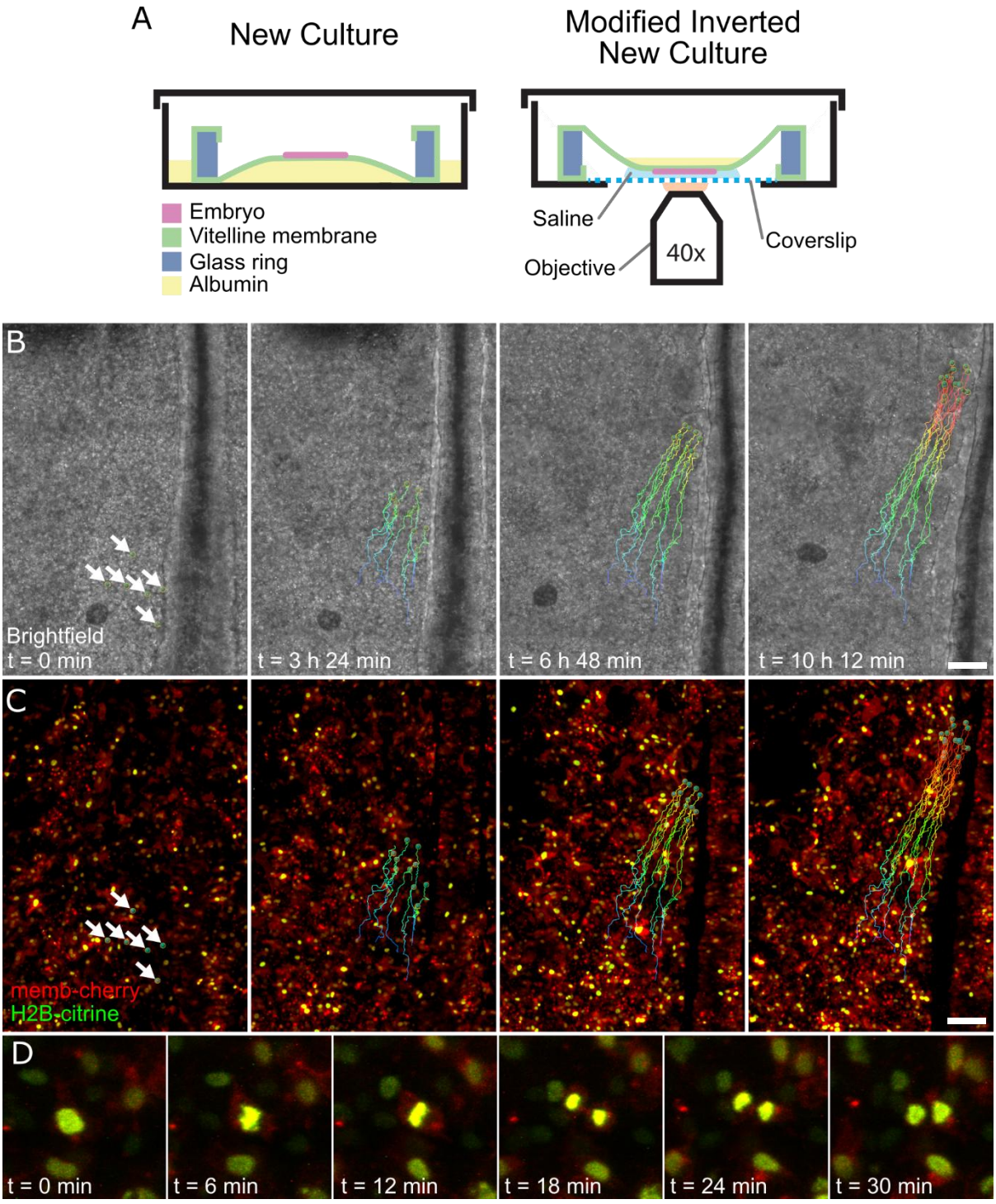

Figure 3.19 Developing a protocol for high spatial and temporal resolution live imaging of chick embryos

A. Scheme showing a modified, inverted New culture set up. **B-C** Example of tracking a group of cells that contributing to the same somite as they transit through the PSM. White arrows highlight the starting position of tracked cells. **D.** Example of cell division, highlighting the spatial and temporal resolution required for accurate cell tracking. Scale bars, 100µm.

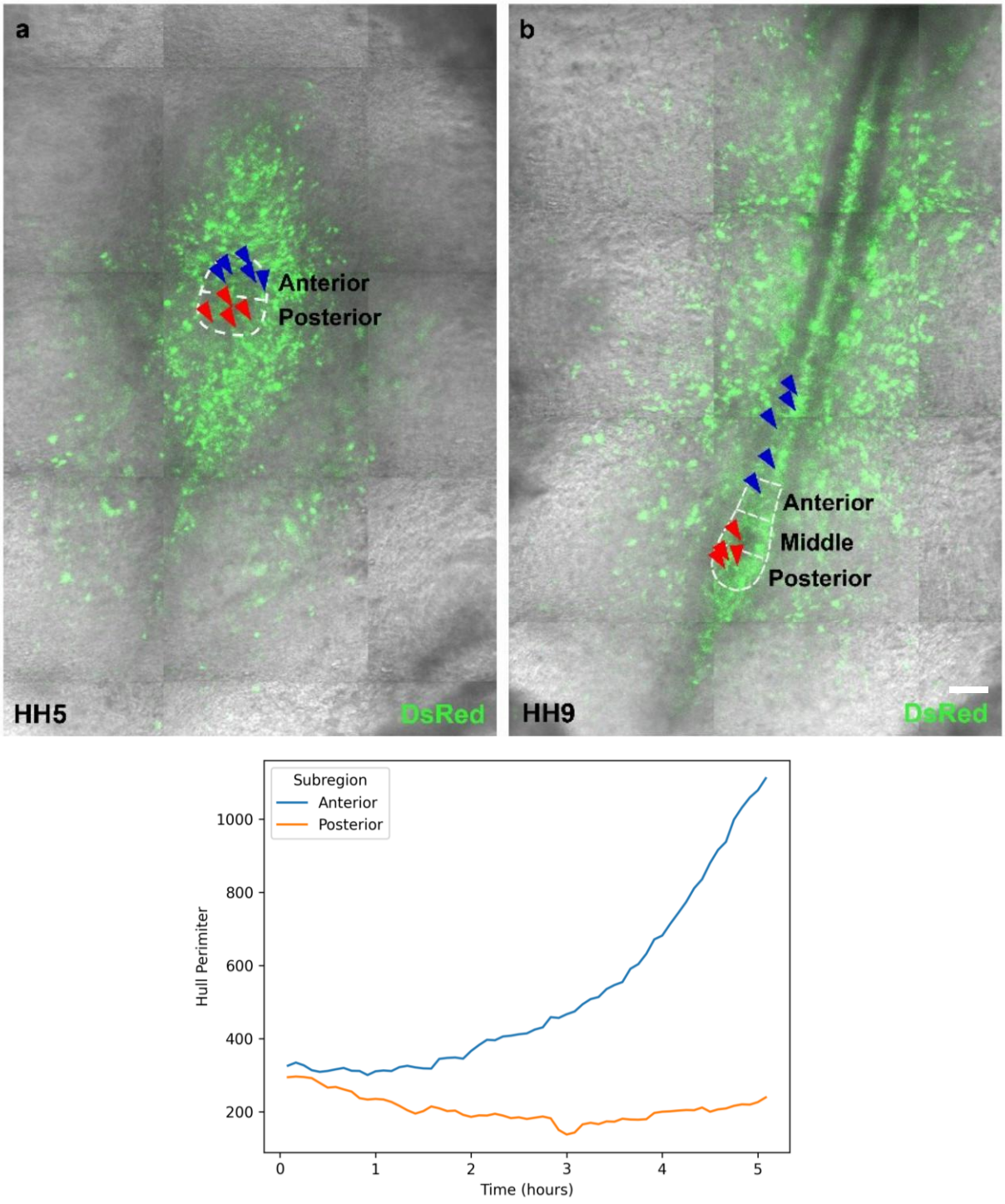

Figure 3.20 Live imaging shows that cells of the posterior node remain resident. **A-B.** Stills from Supplementary Movie 2, showing a mosaic of cells labelled with DsRed (pseudo-colour encoded as green) and the regressing node (dashed white outline) segmented and divided into anterior, middle and posterior sub-regions (dashed white lines). The position of tracked cells from the anterior node (blue arrows) and posterior node (red arrows) are shown at stage HH5 (a) and HH9 (b). **C.** Plot showing the perimeter of the convex hull containing all cells of anterior and posterior

regions of the node over time. Shows the convex hull of anterior cells increasing over time as they are spread across axial tissues, whereas the area of the convex hull of posterior cells remains relatively constant in size as they remain resident in the node. Scale bars, 100μm.

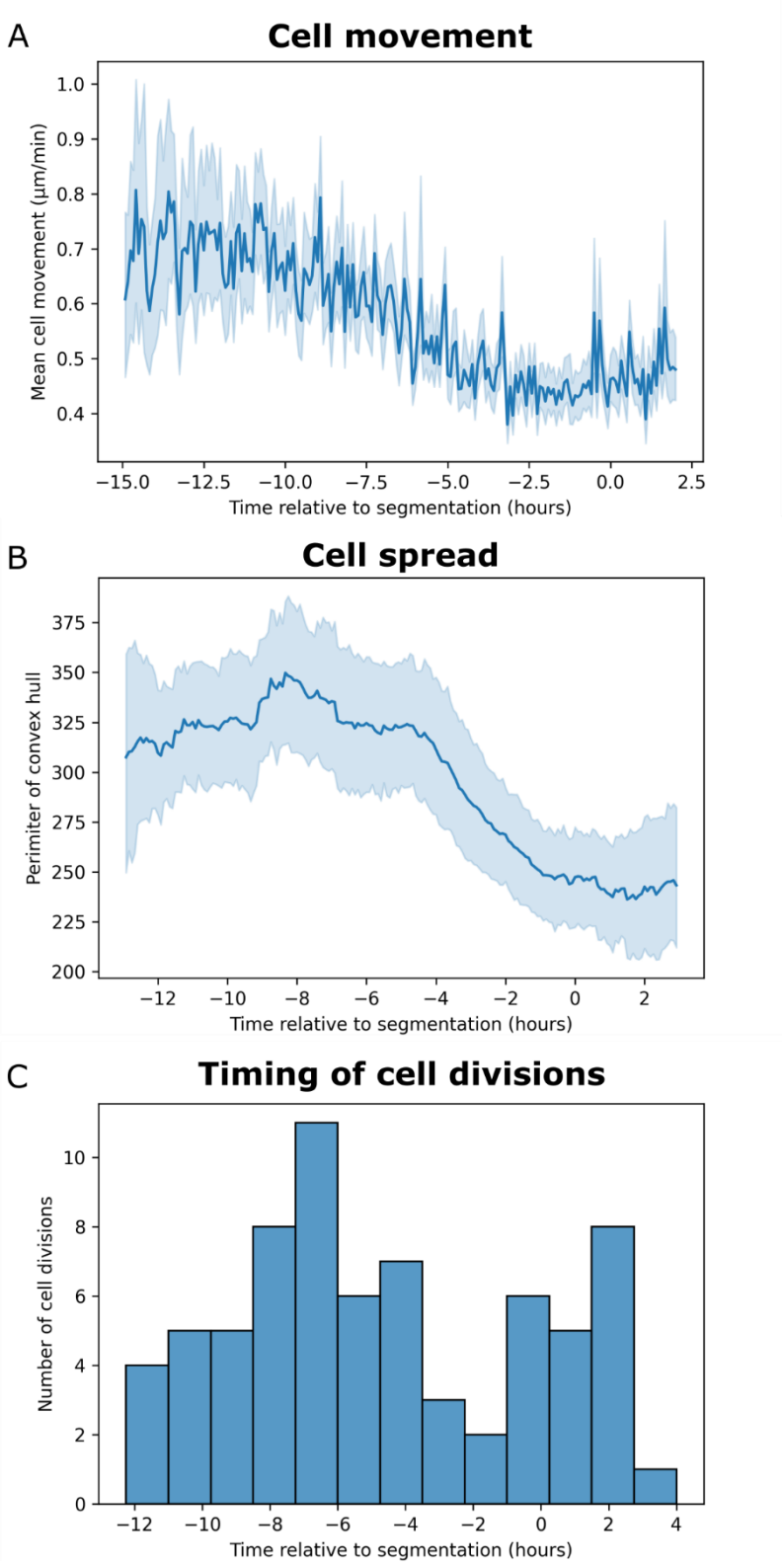

Figure 3.21 Analysis of cell movement and divisions in the PSM

A. Plot showing cell movement relative to the time of segmentation (3 embryos, 116 cells). **B.** A convex hull enclosing the cells of each somite was created and its perimeter measured. The average perimeter of each hull was then plotted relative to the time of segmentation (3 embryos, 116 cells). **C.** Histogram showing the frequency of cell divisions relative to the time of segmentation (3 embryos, 71 cells).

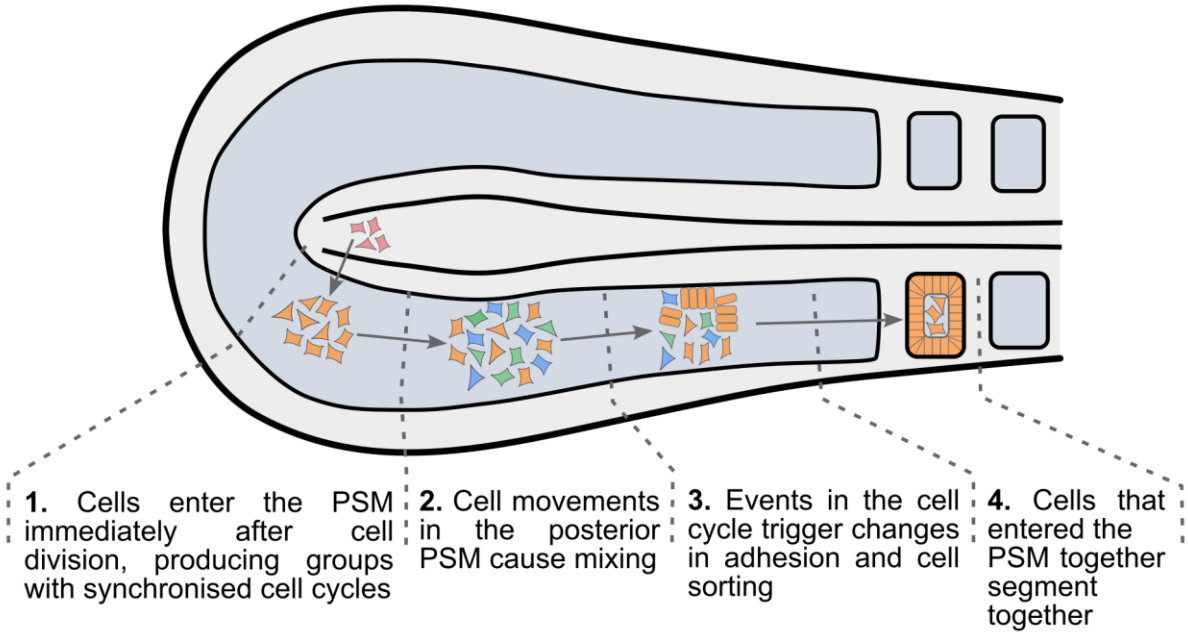

Figure 3.22 Scheme of proposed events in the PSM leading up to segmentation

3.4. Discussion

3.4.1. Cellular events in PSM

There have been several studies exploring cellular behaviours in different regions of the PSM leading up to segmentation. One report suggests that the anterior third of the PSM is where the onset of epithelialisation begins (Duband et al., 1987), with the posterior two thirds remaining mesenchymal. A difference in the timing of epithelialisation between the dorsal and ventral PSM has also been reported (Bellairs, 1979), with the dorsal epithelialising earlier. The same has been reported for the medial-lateral axis, with the medial epithelialising first (Kulesa and Fraser, 2002; Martins et al., 2009). Our data presented here suggest that certain domains of the PSM begin epithelialising much earlier than previously reported (Bellairs, 1979, 1963; Duband et al., 1987; Kulesa and Fraser, 2002; Martins et al., 2009), with SEM images showing that the dorsal PSM shows signs of epithelialisation as early as 40% of the PSM length. However, the order of epithelialisation is largely consistent with previous observations, with dorsal epithelialisation consistently preceding ventral, and the medial consistently preceding the lateral. There have been contradictory reports as to whether the anterior or posterior half of newly forming somites epithelialises first, with some studies suggesting the posterior region epithelialises first (Duband et al., 1987; Kulesa and Fraser, 2002; Kulesa et al., 2007) and others the anterior side (Beloussov and Naumidi, 1983; Martins et al., 2009). Our observations did not reveal a significant difference, suggesting that the two regions epithelialise at approximately the same rate.

In contrast to earlier published SEM images of the PSM (Meier, 1984), we were unable to detect a prepatterning to the PSM in the form of somitomeres. In the anterior PSM we observed cell arrangements which approximated the next 1-3 prospective somites, but this is in stark contrast to previous reports of 10-12 somitomeres spanning the length of the PSM. This further supports the proposal that the somitomeres are artefacts of the fixation and sample preparation process (Wood and Thorogood, 1994).

Paraxis (TCF-15) is expressed in the anterior PSM and somites and is associated with the epithelialisation of the PSM because in paraxis mutants the PSM never epithelialises, displaying a segmented arrangement, but remaining mesenchymal (Burgess et al., 1996, 1995; Kulesa et al., 2007). However, this is not consistent with

our results showing that the first signs of PSM epithelialisation can be seen at 40% of the PSM length, which is much earlier than Paraxis expression has been detected.

Some studies have suggested that the neural tube and ectoderm are necessary to induce epithelialisation (Correia and Conlon, 2000; Lash and Yamada, 1986; Packard and Jacobson, 1976; Šošić et al., 1997), which is consistent with our observations of the dorsal and medial PSM epithelialising first. Although the importance of the ectoderm and neural tube is debated, some studies showed that the PSM epithelialises autonomously as long as the surrounding fibronectin matrix remains intact (Rifes et al., 2007). Other studies suggest that Wnt6 is responsible for inducing epithelialisation (Schmidt et al., 2004) and that the role of Paraxis may lie in the maintenance of epithelialisation, with its activity being downstream of Wnt6 and β-catenin signalling (Linker et al., 2005). These data are consistent with our observations, given the expression of Wnt6 in the ectoderm and neural tube (Hollyday et al., 1995; Parr et al., 1993; Rodríguez-Niedenführ et al., 2003; Schubert et al., 2002). It has been suggested that epithelialisation of the PSM may be triggered by lateral induction (Nelemans et al., 2020). It is plausible that epithelialisation is initially triggered by Wnt6 secreted by the ectoderm and neural tube and that the ventral and lateral domains epithelialise later as a result of lateral induction from neighbouring cells.

3.4.2. Our observations and models of somite formation

As outlined in the introduction of this chapter, there are several problems with the clock and wavefront model, including the results of heat shock experiments (Cooke, 1978; Elsdale et al., 1976; Keynes and Stern, 1988; Primmett et al., 1989, 1988; Roy et al., 1999), somites continuing to form in Notch mutants (Conlon et al., 1995; de la Pompa et al., 1997; Oginuma et al., 2010), in the absence of oscillatory gene expression (Dias et al., 2014), somite scaling and different regions of the PSM epithelialising at different rates (Bellairs, 1979; Kulesa and Fraser, 2002; Martins et al., 2009), and the order in which the occipital somites form (Hamburger and Hamilton, 1951).

Our data presented here further confounds the issue of the timing of epithelialisation in each axis of the PSM. The original clock and wavefront model posits that the output of the model would be a signal triggering cells of the PSM to undergo a rapid and synchronised epithelialisation (Cooke and Zeeman, 1976). However, our detailed

analysis of PSM epithelialisation, through SEM imaging and examination of markers of epithelialisation, revealed a gradual epithelialisation occurring over many hours and in some domains lasting over half the length of the PSM. It is not clear how a clock and wavefront style model could coordinate this protracted epithelialisation, along with its staggered onset between dorsal, ventral, medial and lateral domains. Furthermore, inhibition of Notch signalling did not significantly alter the timing or order of epithelialisation events in the PSM, further indicating that this process is regulated by another mechanism. Another observation that is not explained by the clock and wavefront model is the behaviour of the core cells, which do not epithelialise at any point. However, this is a common oversight of most models of somite formation and could be explained for example by proposing that the core cells originate from a separate population that simply does not respond to certain signals.

A previous observation that appears incompatible with the clock and wavefront model are the repeated segmentation anomalies that are produced in heat shock experiments (Cooke, 1978; Primmett et al., 1988). The cell cycle model was proposed to explain these observations (Collier et al., 2000; Primmett et al., 1989; Stern et al., 1988), and suggests the PSM is organised with cells in age order and they segment together based on shared timing of cell cycle events. This was supported by pharmacological perturbations, such as with treatment with L-Phenylalanine, that interfere with the cell cycle. These cell cycle perturbations induced similar, repeating segmentation anomalies as the heat shock experiments (Primmett et al., 1989). The original model suggested the cell cycle event that triggers groups of cells to segment might be one cell cycle before segmentation, which is roughly 10 hours. This timing is more in line with the onset of epithelialisation we observed in the PSM, although this varies from one region to another, ranging from a little over 10 hours before segmentation in the dorsal PSM to as little as 5 hours in the lateral PSM. Our data showed that cells of the PSM divide around the same time, approximately 8 hours prior to segmentation, which also matched the time cells start aggregating according to our cell tracking data. Although there were two peaks in the frequency of cell divisions, they are not sharp peaks, suggesting there could be variation in the cell cycle timing in each region of the PSM, which could account for the differences in the onset of epithelialisation in each region.

Reaction-diffusion models, such as the one proposed by Meinhardt (1982), suggest that cells responding to a morphogen gradient while oscillating between two cellular states could generate a segmented pattern. The PORD model proposes similar, but rather than a morphogen gradient, relies on diffusion of a local repressor to establish segments. If the two oscillating states are epithelial and mesenchymal, then this might explain the clusters of epithelial cells we observed in the dorsal PSM at 40-50% PSM length, as these models rely on neighbouring cells inducing an opposing state to create travelling waves, but this is not compatible with our observations in the anterior PSM, which is primarily epithelial. If the oscillating cellular state is interpreted as expression of a 'clock' gene switching on and off, then these reaction diffusion models struggle with the same observations that the clock and wavefront model cannot explain, such as segmentation in the absence of Notch signalling and the staggered epithelialisation of different domains of the PSM.

3.4.3. Are epithelialisation and boundary formation controlled by separate mechanisms?

It is possible that the epithelialisation of the PSM and the formation of somite boundaries (as well as rostral and caudal halves) are controlled by two independent mechanisms. This would be consistent with several observations, such as our data showing that when Notch signalling is inhibited, epithelialisation proceeds largely unchanged despite the absence of oscillating gene expression. Previously published observations in Paraxis mutants show the PSM continues to segment despite failing to epithelialise (Burgess et al., 1996, 1995; Kulesa et al., 2007). Our data show that inhibition of Notch signalling also results in unstable boundaries between somites and a lack of rostral-caudal polarity. The ability of somites to form in the absence of 'proper' boundaries is plausible given that epithelial rosettes form as self-organising, intermediate structures in a variety of morphogenetic processes (Harding et al., 2014) and ectopic somites have been shown to form simultaneously in a self-organising fashion (Dias et al., 2014). Here we observed that epithelialisation of the PSM occurs asynchronously across different domains of the PSM, with approximately 5 hours between the onset of epithelialisation in the dorsal and lateral domains. Given this difference in timing, it seems unlikely that the mechanism that coordinates the onset of epithelialisation could be the same as the one that controls boundary formation, which occurs every 90 minutes. It is therefore plausible that epithelialisation is

triggered via a mechanism such as Wnt6 secretion from the neural tube and ectoderm, or events in the cell cycle, while somite boundaries are specified by an alternate mechanism relying on oscillatory gene expression such as a clock and gradient or PORD model. The behaviour of the occipital somites partially fits this hypothesis. The first pair of somites to form are the second pair along the anterior-posterior axis. The first and third pair form almost simultaneously after the second pair, with the fourth pair onwards forming sequentially. The first somite to display rostral-caudal polarity is the third somite (Schrägle et al., 2004), which coincides with the onset of somites forming sequentially in an anterior to poster manner with rostral-caudal polarity. The out of sequence and simultaneous formation of the first three somite pairs can be explained by the formation of epithelial rosettes in a self-organising manner upon epithelialisation. However, if the first three somites are entirely self-organising and lack true boundaries, our observations predict these boundaries would be unstable leading to merging and splitting of these somites, which is not observed. How the posterior half of the third somite pair acquires caudal identity also remains unanswered. Finally, this proposal does not provide an explanation for the repeated anomalies observed in heat-shock experiments.

3.4.4. The core cells

The core cells are a feature of amniote somites and are not present in anamniotes such as zebrafish and frog, whose somites possess a different cellular organisation. The mechanism by which core cells arise has not been well studied and few models of somite formation attempt to describe how they emerge. It is possible they are intrinsically different from other cells of the PSM, or that differences at the time of segmentation result in some cells being allocated to the core. Live imaging shows that cells of the somite core can contribute to the epithelial rosette (Kulesa et al., 2007; Kulesa and Fraser, 2002; Martins et al., 2009). When embryos are stretched somites have been observed to split, with authors proposing that core cells epithelialise to reform the rosette structure (Nelemans et al., 2020). Conversely, cells of the somite core are also believed to result from cells of the epithelial rosette ingressing into the core (Martins et al., 2009; Wong et al., 1993). These results suggest that core cells possess similar properties to other cells in the PSM and have the potential to epithelialise and form part of the rosette. Our results support this, suggesting that rather than sorting, it is the cells at the centre of the PSM that are enclosed as cells in

the outer regions epithelialise. However, because our data are primarily fixed embryos, it isn't clear if there is any dynamic exchange or "shuttling" between core cells and other domains, a possibility supported by previous studies that reported extensive cell mixing in the posterior PSM (Bénazéraf et al., 2017, 2010; M. A. J. Selleck and Stern, 1991; Stern et al., 1988).

Using hybridization chain reaction (HCR) to detect rostral (EphA4) and caudal (Uncx4.1) markers, we observed that the expression boundaries of these markers change over time. Before segmentation, EphA4 spans a region larger than one somite half, but as segmentation proceeds, Uncx4.1 expression becomes dominant, occupying a larger region than EphA4. Additionally, the boundary between the two expression domains is not perpendicular to the coronal plane. Shuttling between the core and epithelial regions, as well as core cell fate not being fixed (Kulesa et al., 2007; Martins et al., 2009; Senthinathan et al., 2012) is consistent with the wide variety of tissues the core cells contribute to, including myotome, sclerotome, the annulus fibrosus of the intervertebral discs and intervertebral joints (Huang et al., 1996, 1994; Mestres and Hinrichsen, 1976; Mittapalli et al., 2005).

3.4.5. Origin of somite cells from a resident stem cell population in the node

We also examined the origin of cells that contribute to the PSM and the possibility that a resident stem cell population exists in the node. Most of the research on resident cells in the node has relied on population-level studies (Cambray and Wilson, 2007, 2002; Charrier et al., 1999; McGrew et al., 2008; Tam and Tan, 1992), with only a few using single-cell fate mapping (Forlani et al., 2003; Lawson et al., 1991; M. A. J. Selleck and Stern, 1991). The ability of these cells to self-renew has not been robustly demonstrated and their origin remains unclear. It is also unknown whether they represent a sub population that is present when the node forms, or if the node is instructive, inducing a stem-cell and resident behaviour in cells that transit through it. Using single cell grafts, we were able to demonstrate the ability of the node to induce stem-cell behaviour in cells of the epiblast that would typically contribute to other parts of the embryo and not enter the node. Our use of live imaging and cell tracking indicates that resident cells are likely situated in the posterior part of the node. This observation is consistent with mouse studies where fate mapping revealed that labelled cells stay at the border between the node and the primitive streak during axis formation (Cambray and Wilson, 2007; Wymeersch et al., 2019). This is further

supported by grafts of the anterior node (where resident cells have not been reported), into the posterior node, showing that grafted cells contribute to the chordoneural hinge and tailbud mesoderm (Cambray and Wilson, 2007), suggesting the caudal region of the node can impart resident behaviour. However, since groups of cells were transplanted, this does not confirm if these cells are self-renewing. Removing the posterior node in both chick and mouse models disrupts elongation of the body axis, further highlighting its importance in axial development (Charrier et al., 1999; Wymeersch et al., 2019). Our single-cell grafts in the posterior node reveal that self-renewing resident cells exist in both the dorsal and ventral regions. In mouse studies, BrdU staining indicates that dorsal node cells divide rapidly, whereas ventral cells are mostly quiescent, except near the caudal end (Bellomo et al., 1996; Wymeersch et al., 2019). Although a regional variation in proliferation rate does not appear to be clearly defined in chick embryos, the finding that resident cells occur in both regions is consistent with observations in the mouse node. In summary, our results demonstrate that the node is capable of directing cells to adopt a resident, self-renewing state through at least stage HH8, and this ability may extend into later developmental stages, including the tailbud phase. The findings presented here are expanded upon in Solovieva et al., (2022) by using scRNAseq to explore the molecular properties of cells in the node. GFP labelled cells were grafted lateral to the node at stage HH4 and later, any GFP labelled cells present in posterior, middle and anterior regions of the node at HH8 were collected and processed for scRNAseq. Principal component analysis identified a cluster of cells in the posterior node with a distinct identity from cells of the middle and anterior node. Of the 37 genes enriched in this cluster, 31 of them are associated with the G2/M phase of the cell cycle, suggesting this cluster of cells are actively preparing to divide. This, along with posterior enrichment of Wnt, FGF and Notch pathway genes associated with stem cell niches, offers additional evidence for the presence of a resident stem cell niche in the posterior node.

Chapter 4. Conclusion

This thesis aimed to explore the cellular and molecular mechanisms underlying two important processes in early development. To achieve this, we used a combination of high-resolution fixed imaging and live imaging, making a number of novel observations in two model systems.

4.1.1. Mechanotransduction during early embryogenesis

We identified a novel role for Lamin-A/C as a mechanosensor in the preimplantation embryo. We showed that the organization of the nuclear lamina changes in response to cytoskeletal forces that occur during the segregation of cells into inner and outer positions. These changes appeared to be mediated by phosphorylation of Lamin-A/C, directing it from the lamina to the nucleoplasm. By manipulating actomyosin contractility we observed corresponding changes in Lamin-A/C localisation. These changes in Lamin-A/C correlated with Yap localisation and Cdx2 expression. Knockdown of Lamin-A/C resulted in a loss of inner and outer cell identity as assessed by Yap and Cdx2 expression, suggesting a causal link between Lamin-A/C expression and inner-outer cell identity. We then explored the mechanism by which Lamin-A/C might direct cell identity during lineage segregation. We observed that in inner cells there is a dense F-actin meshwork in the cytoplasm and in outer cells the actin nucleator Formin-2 is sequestered in the nucleus. Knockdown of Lamin-A/C suggests that Formin-2 sequestration occurs in a Lamin-A/C dependent manner, showing a mechanism by which Lamin-A/C might regulate actin organisation. We then showed that this dense F-actin meshwork in the cytoplasm of inner cells appears to stabilise Amot, causing Yap phosphorylation and preventing Cdx2 expression. We also observed similar patterns of Lamin-A/C and Amot expression in human blastocysts, as well as similar patterns of actin organisation. Manipulation of actomyosin contractility in human embryos also resulted in corresponding changes to Lamin-A/C organisation, although we were unable to obtain enough human embryos to demonstrate this with statistical significance.

4.1.2. Cellular dynamics during somitogenesis

We used SEM imaging and immunofluorescence to examine the epithelialisation of the PSM, observing that the onset of epithelialization in the PSM is much earlier than previously reported. The epithelialisation is also staggered between different regions

of the PSM, with the dorsal epithelialising first, followed by the medial, ventral and finally the lateral PSM. Treatment with a Notch inhibitor showed that somite formation proceeded in the absence of oscillating gene expression, and did not affect the epithelialisation dynamics in the PSM. However, inhibition of Notch did cause a loss of rostral-caudal polarity in the somites as well as increased variability in the size of somites. Live imaging revealed that in Notch inhibited embryos, somites appear to form normally, then split and merge with neighbouring somites, suggesting that Notch inhibition causes a loss of somite boundaries. Live imaging and cell tracking showed that there is cell cycle synchronisation in the PSM with a peak in cells entering mitosis eight hours before segmentation. We demonstrated that Hensen's node has the ability induce stem cell properties and resident behaviour in cells that enter it. The node was also able to impart this behaviour on epiblast cells that would never normally enter the node. By regrafting single cells into a second host embryo we were also able to demonstrate the ability of these cells to self-renew. Live imaging and cell tracking also identified these resident cells reside in the posterior of the node.

4.1.3. Limitations of the study

Microscopy is a powerful technique in developmental biology that allows us to observe the processes that unfold during development through fixed snapshots and live imaging. It allows the measurement of many properties of cells and tissues, including the expression and localisation of proteins, physical parameters such as shape and size, as well as the ability to infer the mobility of proteins and transcription factor binding dynamics with techniques such as FRAP and FCS. However, if microscopy is the sole method used then it is also limited, as any observations remain purely correlative. Only through well designed experiments and targeted manipulations can causality begin to be established. Although we aimed to establish causality in our pathway where Lamin-A/C guides lineage segregation, several factors could still confound our conclusions. Actin appears to play a role both upstream and downstream of Lamin-A/C which makes causality particularly difficult to establish, and many of our methods of manipulating actomyosin contractility are likely to have non-specific effects, especially on polarity. Similarly, our observations about the relationship between cell cycle timing and segmentation are currently only correlative. Another limitation of our work performed in the mouse is that our measurements of mechanical forces were all indirect.

4.1.4. Future perspectives

To better establish causality in our Lamin-A/C pathway, it would be useful to apply direct mechanical forces to embryos and observe downstream changes in Lamin-A/C. This could be achieved using magnetic tweezers or through atomic force microscopy. These tools would also allow us to make direct measurements of cortex stiffness. Another potential tool for measuring membrane stiffness, with the advantage of being non-invasive, would be via mechanosensitive fluorescent reporters (Chen et al., 2023). These would also allow us to correlate changes in membrane stiffness with Lamin-A/C expression in real time. Our current study is primarily limited to events at the 16-cell stage. In future work it would be interesting to examine Lamin-A/C's role in blastocysts, where cells are exposed to the mechanical stresses of cavity expansion (Domingo-Muelas et al., 2023).

In our work in the chick embryo we attempted to perform long term cell tracking to trace cells from the time they entered the PSM up to the point of segmentation. Although we succeeded in live imaging for 18 hours, this was not long enough to trace the origin of segmenting cells due to arrested or abnormal development. If this is the result of phototoxicity, then a less phototoxic imaging modality such multiphoton, spinning disk or light-sheet microscopy may be gentler and allow for longer imaging. We observed a correlation between cell cycle timing and segmentation in our study, but it would be use to try to establish a causal link between them. This may be possible with agents such as CDK inhibitors to slow or arrest the cell cycle and CHK1/CHK2 inhibitors to accelerate it and observe the effects on the timing of segmentation. It would be interesting to combine these manipulations with cell cycle reporters such as FUCCI (Bajar et al., 2016; Sugiyama et al., 2014) to further explore cell cycle dynamics in PSM.

Supplementary Movies

Supplementary Movie 1

Live-imaging of cleavage divisions during the transition from 4-cell to 8-cell stage and from 8-cell to 16-cell stages. Embryos were microinjected with mRNA encoding Utrophin-GFP allowing for 3D segmentation and calculation of cell sphericity. 3D segmentation is overlaid with a colour map of local curvature.

Supplementary Movie 2

Live imaging showing a mosaic of cells labelled with DsRed (pseudo-colour encoded as green). Selected cells originating in the anterior node at HH5 are highlighted in blue and cells originating from the posterior node are highlighted in red. A white dashed line highlights the outline of the node and its division into anterior and posterior regions.

References

Ajduk, A., Zernicka-Goetz, M., 2016. Polarity and cell division orientation in the cleavage embryo: from worm to human. Mol. Hum. Reprod. 22, 691–703. https://doi.org/10.1093/molehr/gav068

Almonacid, M., Al Jord, A., El-Hayek, S., Othmani, A., Coulpier, F., Lemoine, S., Miyamoto, K., Grosse, R., Klein, C., Piolot, T., Mailly, P., Voituriez, R., Genovesio, A., Verlhac, M.-H., 2019. Active Fluctuations of the Nuclear Envelope Shape the Transcriptional Dynamics in Oocytes. Developmental Cell 51, 145-157.e10. https://doi.org/10.1016/j.devcel.2019.09.010

Amano, M., Ito, M., Kimura, K., Fukata, Y., Chihara, K., Nakano, T., Matsuura, Y., Kaibuchi, K., 1996. Phosphorylation and Activation of Myosin by Rho-associated Kinase (Rho-kinase). Journal of Biological Chemistry 271, 20246–20249. https://doi.org/10.1074/jbc.271.34.20246

Andrés, V., González, J.M., 2009. Role of A-type lamins in signaling, transcription, and chromatin organization. Journal of Cell Biology 187, 945–957. https://doi.org/10.1083/jcb.200904124

Aragona, M., Panciera, T., Manfrin, A., Giulitti, S., Michielin, F., Elvassore, N., Dupont, S., Piccolo, S., 2013. A Mechanical Checkpoint Controls Multicellular Growth through YAP/TAZ Regulation by Actin-Processing Factors. Cell 154, 1047–1059. https://doi.org/10.1016/j.cell.2013.07.042

Arekatla, G., Trenzinger, C., Reimann, A., Loeffler, D., Kull, T., Schroeder, T., 2023. Optogenetic manipulation identifies the roles of ERK and AKT dynamics in controlling mouse embryonic stem cell exit from pluripotency. Developmental Cell 58, 1022-1036.e4. https://doi.org/10.1016/j.devcel.2023.04.013

Aulehla, A., Wehrle, C., Brand-Saberi, B., Kemler, R., Gossler, A., Kanzler, B., Herrmann, B.G., 2003. Wnt3a plays a major role in the segmentation clock controlling somitogenesis. Developmental cell 4, 395–406. https://doi.org/10.1016/s1534-5807(03)00055-8

Aulehla, A., Wiegraebe, W., Baubet, V., Wahl, M.B., Deng, C., Taketo, M., Lewandoski, M., Pourquié, O., 2008. A β-catenin gradient links the clock and wavefront systems in mouse embryo segmentation. Nature Cell Biology 10, 186–193. https://doi.org/10.1038/ncb1679

Bajar, B.T., Lam, A.J., Badiee, R.K., Oh, Y.-H., Chu, J., Zhou, X.X., Kim, N., Kim, B.B., Chung, M., Yablonovitch, A.L., Cruz, B.F., Kulalert, K., Tao, J.J., Meyer, T., Su, X.-D., Lin, M.Z., 2016. Fluorescent indicators for simultaneous reporting of all four cell cycle phases. Nat Methods 13, 993–996. https://doi.org/10.1038/nmeth.4045

Bango Da Cunha Correia, R.F., 2018. Optimising light-sheet microscopy for high resolution live imaging of the early development of chick embryos (Doctoral Thesis). University of Dundee.

Becker, A.J., McCulloch, E.A., Till, J.E., 1963. Cytological Demonstration of the Clonal Nature of Spleen Colonies Derived from Transplanted Mouse Marrow Cells. Nature 197, 452–454. https://doi.org/10.1038/197452a0

Bellairs, R., 1979. The mechanism of somite segmentation in the chick embryo. Development 51, 227–243. https://doi.org/10.1242/dev.51.1.227

Bellairs, R., 1963. The Development of Somites in the Chick Embryo. Development 11, 697–714. https://doi.org/10.1242/dev.11.4.697

Bellomo, D., Lander, A., Harragan, I., Brown, N.A., 1996. Cell proliferation in mammalian gastrulation: The ventral node and notochord are relatively

quiescent. Dev. Dyn. 205, 471–485. https://doi.org/10.1002/(SICI)1097-0177(199604)205:4%3C471::AID-AJA10%3E3.0.CO;2-4
Beloussov, L.V., Naumidi, I.I., 1983. Cell contacts and rearrangements preceding somitogenesis in chick embryo. Cell Differentiation 12, 191–204. https://doi.org/10.1016/0045-6039(83)90028-3
Bénazéraf, B., Beaupeux, M., Tchernookov, M., Wallingford, A., Salisbury, T., Shirtz, Amelia, Shirtz, Andrew, Huss, D., Pourquié, O., François, P., Lansford, R., 2017. Multiscale quantification of tissue behavior during amniote embryo axis elongation. Development dev.150557. https://doi.org/10.1242/dev.150557
Bénazéraf, B., Francois, P., Baker, R.E., Denans, N., Little, C.D., Pourquié, O., 2010. A random cell motility gradient downstream of FGF controls elongation of an amniote embryo. Nature 466, 248–252. https://doi.org/10.1038/nature09151
Bénazéraf, B., Pourquié, O., 2013. Formation and Segmentation of the Vertebrate Body Axis. Annual Review of Cell and Developmental Biology 29, 1–26. https://doi.org/10.1146/annurev-cellbio-101011-155703
Ben-Zvi, D., Barkai, N., 2010. Scaling of morphogen gradients by an expansion-repression integral feedback control. Proc. Natl. Acad. Sci. U.S.A. 107, 6924–6929. https://doi.org/10.1073/pnas.0912734107
Ben-Zvi, D., Fainsod, A., Shilo, B., Barkai, N., 2014. Scaling of dorsal-ventral patterning in the *Xenopus laevis* embryo. BioEssays 36, 151–156. https://doi.org/10.1002/bies.201300136
Bhavna, R., 2019. Segmentation clock dynamics is strongly synchronized in the forming somite. Developmental Biology. https://doi.org/10.1016/j.ydbio.2019.03.008
Bone, C.R., Starr, D.A., 2016. Nuclear migration events throughout development. Journal of Cell Science 129, 1951–1961. https://doi.org/10.1242/jcs.179788
Bortier, H., Vakaet, L.C.A., 1992. Fate mapping the neural plate and the intraembryonic mesoblast in the upper layer of the chicken blastoderm with xenografting and time-lapse videography. Development 116, 93–97. https://doi.org/10.1242/dev.116.Supplement.93
Bougaran, P., Bautch, V.L., 2024. Life at the crossroads: the nuclear LINC complex and vascular mechanotransduction. Front. Physiol. 15, 1411995. https://doi.org/10.3389/fphys.2024.1411995
Bronner-Fraser, M., 1986. Analysis of the early stages of trunk neural crest migration in avian embryos using monoclonal antibody HNK-1. Developmental biology 115, 44–55. https://doi.org/10.1016/0012-1606(86)90226-5
Bronner-Fraser, M., Stern, C., 1991. Effects of mesodermal tissues on avian neural crest cell migration. Developmental Biology 143, 213–217. https://doi.org/10.1016/0012-1606(91)90071-A
Burgess, R., Cserjesi, P., Ligon, K.L., Olson, E.N., 1995. Paraxis: A Basic Helix-Loop-Helix Protein Expressed in Paraxial Mesoderm and Developing Somites. Developmental Biology 168, 296–306. https://doi.org/10.1006/dbio.1995.1081
Burgess, R., Rawls, A., Brown, D., Bradley, A., Olson, E.N., 1996. Requirement of the paraxis gene for somite formation and musculoskeletal patterning. Nature 384, 570–573. https://doi.org/10.1038/384570a0
Busch, A., Kiel, T., Heupel, W.-M., Wehnert, M., Hübner, S., 2009. Nuclear protein import is reduced in cells expressing nuclear envelopathy-causing lamin A mutants. Experimental Cell Research 315, 2373–2385. https://doi.org/10.1016/j.yexcr.2009.05.003

Buxboim, A., Swift, J., Irianto, J., Spinler, K.R., Dingal, P.C.D.P., Athirasala, A., Kao, Y.-R.C., Cho, S., Harada, T., Shin, J.-W., Discher, D.E., 2014. Matrix Elasticity Regulates Lamin-A,C Phosphorylation and Turnover with Feedback to Actomyosin. Current Biology 24, 1909–1917. https://doi.org/10.1016/j.cub.2014.07.001

Cambray, N., Wilson, V., 2007. Two distinct sources for a population of maturing axial progenitors. Development 134, 2829–2840. https://doi.org/10.1242/dev.02877

Cambray, N., Wilson, V., 2002. Axial progenitors with extensive potency are localised to the mouse chordoneural hinge. Development 129, 4855–4866. https://doi.org/10.1242/dev.129.20.4855

Campellone, K.G., Welch, M.D., 2010. A nucleator arms race: cellular control of actin assembly. Nat Rev Mol Cell Biol 11, 237–251. https://doi.org/10.1038/nrm2867

Cantwell, H., Dey, G., 2022. Nuclear size and shape control. Seminars in Cell & Developmental Biology 130, 90–97. https://doi.org/10.1016/j.semcdb.2021.10.013

Carrieri, F.A., Murray, P.J., Ditsova, D., Ferris, M.A., Davies, P., Dale, J.K., 2019. CDK1 and CDK2 regulate NICD1 turnover and the periodicity of the segmentation clock. EMBO reports e46436. https://doi.org/10.15252/embr.201846436

Chaigne, A., Campillo, C., Gov, N.S., Voituriez, R., Sykes, C., Verlhac, M.H., Terret, M.E., 2015. A narrow window of cortical tension guides asymmetric spindle positioning in the mouse oocyte. Nat Commun 6, 6027. https://doi.org/10.1038/ncomms7027

Chapman, S.C., Collignon, J., Schoenwolf, G.C., Lumsden, A., 2001. Improved method for chick whole-embryo culture using a filter paper carrier. Developmental dynamics : an official publication of the American Association of Anatomists 220, 284–9. https://doi.org/10.1002/1097-0177(20010301)220:3%253C284::AID-DVDY1102%253E3.0.CO;2-5

Charrier, J.B., Teillet, M.A., Lapointe, F., Le Douarin, N.M., 1999. Defining subregions of Hensen's node essential for caudalward movement, midline development and cell survival. Development 126, 4771–4783. https://doi.org/10.1242/dev.126.21.4771

Chen, F., Ma, L., Parrini, M.C., Mao, X., Lopez, M., Wu, C., Marks, P.W., Davidson, L., Kwiatkowski, D.J., Kirchhausen, T., Orkin, S.H., Rosen, F.S., Mayer, B.J., Kirschner, M.W., Alt, F.W., 2000. Cdc42 is required for PIP2-induced actin polymerization and early development but not for cell viability. Current Biology 10, 758–765. https://doi.org/10.1016/S0960-9822(00)00571-6

Chen, X., Bayard, F., Gonzalez-Sanchis, N., Pamungkas, K.K.P., Sakai, N., Matile, S., 2023. Fluorescent Flippers: Small-Molecule Probes to Image Membrane Tension in Living Systems. Angewandte Chemie 135, e202217868. https://doi.org/10.1002/ange.202217868

Christ, B., Huang, R., Scaal, M., 2004. Formation and differentiation of the avian sclerotome. Anat Embryol 208. https://doi.org/10.1007/s00429-004-0408-z

Christ, B., Jacob, H.J., Jacob, M., 1974. [Somitogenesis in the chick embryo. Determination of the segmentation direction]. Verh Anat Ges 68, 573–579.

Collier, J.R., Mcinerney, D., Schnell, S., Maini, P.K., Gavaghan, D.J., Houston, P., Stern, C.D., 2000. A cell cycle model for somitogenesis: mathematical formulation and numerical simulation. Journal of theoretical biology 207, 305–16. https://doi.org/10.1006/jtbi.2000.2172

Conlon, R. a, Reaume, a G., Rossant, J., 1995. Notch1 is required for the coordinate segmentation of somites. Development (Cambridge, England) 121, 1533–45.

Cook, G.M., Sousa, C., Schaeffer, J., Wiles, K., Jareonsettasin, P., Kalyanasundaram, A., Walder, E., Casper, C., Patel, S., Chua, P.W., Riboni-Verri, G., Raza, M., Swaddiwudhipong, N., Hui, A., Abdullah, A., Wajed, S., Keynes, R.J., 2020. Regulation of nerve growth and patterning by cell surface protein disulphide isomerase. eLife 9, e54612. https://doi.org/10.7554/eLife.54612

Cooke, J., 1978. Somite abnormalities caused by short heat shocks to pre-neurula stages of *Xenopus laevis*. Development 45, 283–294. https://doi.org/10.1242/dev.45.1.283

Cooke, J., 1975. Control of somite number during morphogenesis of a vertebrate, Xenopus laevis. Nature 254, 196–199. https://doi.org/10.1038/254196a0

Cooke, J., Zeeman, E.C., 1976. A clock and wavefront model for control of the number of repeated structures during animal morphogenesis. Journal of Theoretical Biology 58, 455–476. https://doi.org/10.1016/S0022-5193(76)80131-2

Correia, K.M., Conlon, R.A., 2000. Surface ectoderm is necessary for the morphogenesis of somites. Mechanisms of Development 91, 19–30. https://doi.org/10.1016/S0925-4773(99)00260-9

Cotterell, J., Robert-Moreno, A., Sharpe, J., 2015. A Local, Self-Organizing Reaction-Diffusion Model Can Explain Somite Patterning in Embryos. Cell Systems 1, 257–269. https://doi.org/10.1016/j.cels.2015.10.002

Crick, F., 1970. Diffusion in Embryogenesis. Nature 225, 420–422. https://doi.org/10.1038/225420a0

Crisp, M., Liu, Q., Roux, K., Rattner, J.B., Shanahan, C., Burke, B., Stahl, P.D., Hodzic, D., 2006. Coupling of the nucleus and cytoplasm: Role of the LINC complex. The Journal of Cell Biology 172, 41–53. https://doi.org/10.1083/jcb.200509124

Dale, J.K., Maroto, M., Dequeant, M.-L., Malapert, P., McGrew, M., Pourquie, O., 2003. Periodic Notch inhibition by Lunatic Fringe underlies the chick segmentation clock. Nature 421, 275–278. https://doi.org/10.1038/nature01244

Davies, J.A., Cook, G.M.W., Stern, C.D., Keynes, R.J., 1990. Isolation from chick somites of a glycoprotein fraction that causes collapse of dorsal root ganglion growth cones. Neuron 4, 11–20. https://doi.org/10.1016/0896-6273(90)90439-M

Davy, A., Soriano, P., 2007. Ephrin-B2 forward signaling regulates somite patterning and neural crest cell development. Developmental Biology 304, 182–193. https://doi.org/10.1016/j.ydbio.2006.12.028

de la Pompa, J.L., Wakeham, A., Correia, K.M., Samper, E., Brown, S., Aguilera, R.J., Nakano, T., Honjo, T., Mak, T.W., Rossant, J., Conlon, R. a, 1997. Conservation of the Notch signalling pathway in mammalian neurogenesis. Development (Cambridge, England) 124, 1139–48.

Delaune, E.A., François, P., Shih, N.P., Amacher, S.L., 2012. Single-Cell-Resolution Imaging of the Impact of Notch Signaling and Mitosis on Segmentation Clock Dynamics. Developmental Cell 23, 995–1005. https://doi.org/10.1016/j.devcel.2012.09.009

Dequeant, M.-L., Glynn, E., Gaudenz, K., Wahl, M., Chen, J., Mushegian, A., Pourquie, O., 2006. A Complex Oscillating Network of Signaling Genes Underlies the Mouse Segmentation Clock. Science 314, 1595–1598. https://doi.org/10.1126/science.1133141

Dessaud, E., Ribes, V., Balaskas, N., Yang, L.L., Pierani, A., Kicheva, A., Novitch, B.G., Briscoe, J., Sasai, N., 2010. Dynamic Assignment and Maintenance of Positional Identity in the Ventral Neural Tube by the Morphogen Sonic

Hedgehog. PLoS Biol 8, e1000382. https://doi.org/10.1371/journal.pbio.1000382
Dessaud, E., Yang, L.L., Hill, K., Cox, B., Ulloa, F., Ribeiro, A., Mynett, A., Novitch, B.G., Briscoe, J., 2007. Interpretation of the sonic hedgehog morphogen gradient by a temporal adaptation mechanism. Nature 450, 717–720. https://doi.org/10.1038/nature06347
Dexter, T.M., Allen, T.D., Lajtha, L.G., 1977. Conditions controlling the proliferation of haemopoietic stem cells in vitro. Journal Cellular Physiology 91, 335–344. https://doi.org/10.1002/jcp.1040910303
Dias, a. S., de Almeida, I., Belmonte, J.M., Glazier, J. a., Stern, C.D., 2014. Somites Without a Clock. Science 343, 791–795. https://doi.org/10.1126/science.1247575
Diaz-Cuadros, M., Wagner, D.E., Budjan, C., Hubaud, A., Tarazona, O.A., Donelly, S., Michaut, A., Al Tanoury, Z., Yoshioka-Kobayashi, K., Niino, Y., Kageyama, R., Miyawaki, A., Touboul, J., Pourquié, O., 2020. In vitro characterization of the human segmentation clock. Nature. https://doi.org/10.1038/s41586-019-1885-9
Dietrich, J.-E., Hiiragi, T., 2007. Stochastic patterning in the mouse pre-implantation embryo. Development 134, 4219–4231. https://doi.org/10.1242/dev.003798
Diez del Corral, R., Olivera-Martinez, I., Goriely, A., Gale, E., Maden, M., Storey, K., 2003. Opposing FGF and Retinoid Pathways Control Ventral Neural Pattern, Neuronal Differentiation, and Segmentation during Body Axis Extension. Neuron 40, 65–79. https://doi.org/10.1016/S0896-6273(03)00565-8
Dirks, R.M., Pierce, N.A., 2004. Triggered amplification by hybridization chain reaction. Proc. Natl. Acad. Sci. U.S.A. 101, 15275–15278. https://doi.org/10.1073/pnas.0407024101
Domingo-Muelas, A., Skory, R.M., Moverley, A.A., Ardestani, G., Pomp, O., Rubio, C., Tetlak, P., Hernandez, B., Rhon-Calderon, E.A., Navarro-Sánchez, L., García-Pascual, C.M., Bissiere, S., Bartolomei, M.S., Sakkas, D., Simón, C., Plachta, N., 2023. Human embryo live imaging reveals nuclear DNA shedding during blastocyst expansion and biopsy. Cell 186, 3166-3181.e18. https://doi.org/10.1016/j.cell.2023.06.003
Donnaloja, F., Jacchetti, E., Soncini, M., Raimondi, M.T., 2019. Mechanosensing at the Nuclear Envelope by Nuclear Pore Complex Stretch Activation and Its Effect in Physiology and Pathology. Front. Physiol. 10, 896. https://doi.org/10.3389/fphys.2019.00896
Dorner, D., Vlcek, S., Foeger, N., Gajewski, A., Makolm, C., Gotzmann, J., Hutchison, C.J., Foisner, R., 2006. Lamina-associated polypeptide 2α regulates cell cycle progression and differentiation via the retinoblastoma–E2F pathway. The Journal of Cell Biology 173, 83–93. https://doi.org/10.1083/jcb.200511149
Driesch, H., 1892. Entwicklungsmechanisiche Studien, I. Der Werth der beiden ersten FurchungszeHen in der Echinodermentwicklung. Experimentelle Erzeugen von Theil-und Doppelbildung. Z. Wiss. Zool. 53, 160–184.
Driever, W., Nüsslein-Volhard, C., 1988. The bicoid protein determines position in the Drosophila embryo in a concentration-dependent manner. Cell 54, 95–104. https://doi.org/10.1016/0092-8674(88)90183-3
Duband, J.L., Dufour, S., Hatta, K., Takeichi, M., Edelman, G.M., Thiery, J.P., 1987. Adhesion molecules during somitogenesis in the avian embryo. The Journal of cell biology 104, 1361–74. https://doi.org/10.1083/jcb.104.5.1361

Dubrulle, J., McGrew, M.J., Pourquié, O., 2001. FGF Signaling Controls Somite Boundary Position and Regulates Segmentation Clock Control of Spatiotemporal Hox Gene Activation. Cell 106, 219–232. https://doi.org/10.1016/S0092-8674(01)00437-8

Dubrulle, J., Pourquié, O., 2004. fgf8 mRNA decay establishes a gradient that couples axial elongation to patterning in the vertebrate embryo. Nature 427, 419–422. https://doi.org/10.1038/nature02216

Dumont, J., Million, K., Sunderland, K., Rassinier, P., Lim, H., Leader, B., Verlhac, M.-H., 2007. Formin-2 is required for spindle migration and for the late steps of cytokinesis in mouse oocytes. Developmental Biology 301, 254–265. https://doi.org/10.1016/j.ydbio.2006.08.044

Dupont, S., Morsut, L., Aragona, M., Enzo, E., Giulitti, S., Cordenonsi, M., Zanconato, F., Le Digabel, J., Forcato, M., Bicciato, S., Elvassore, N., Piccolo, S., 2011. Role of YAP/TAZ in mechanotransduction. Nature 474, 179–183. https://doi.org/10.1038/nature10137

Elosegui-Artola, A., Andreu, I., Beedle, A.E.M., Lezamiz, A., Uroz, M., Kosmalska, A.J., Oria, R., Kechagia, J.Z., Rico-Lastres, P., Le Roux, A.-L., Shanahan, C.M., Trepat, X., Navajas, D., Garcia-Manyes, S., Roca-Cusachs, P., 2017. Force Triggers YAP Nuclear Entry by Regulating Transport across Nuclear Pores. Cell 171, 1397-1410.e14. https://doi.org/10.1016/j.cell.2017.10.008

Elsdale, T., Pearson, M., Whitehead, M., 1976. Abnormalities in somite segmentation following heat shock to *Xenopus* embryos. Development 35, 625–635. https://doi.org/10.1242/dev.35.3.625

Ernkvist, M., Aase, K., Ukomadu, C., Wohlschlegel, J., Blackman, R., Veitonmäki, N., Bratt, A., Dutta, A., Holmgren, L., 2006. p130-Angiomotin associates to actin and controls endothelial cell shape. The FEBS Journal 273, 2000–2011. https://doi.org/10.1111/j.1742-4658.2006.05216.x

Eyal-Giladi, H., Kochav, S., 1976. From cleavage to primitive streak formation: A complementary normal table and a new look at the first stages of the development of the chick. Developmental Biology 49, 321–337. https://doi.org/10.1016/0012-1606(76)90178-0

Fagotto, F., 2014. The cellular basis of tissue separation. Development (Cambridge) 141, 3303–3318. https://doi.org/10.1242/dev.090332

Fierro-González, J.C., White, M.D., Silva, J.C., Plachta, N., 2013. Cadherin-dependent filopodia control preimplantation embryo compaction. Nat Cell Biol 15, 1424–1433. https://doi.org/10.1038/ncb2875

Forlani, S., Lawson, K.A., Deschamps, J., 2003. Acquisition of Hox codes during gastrulation and axial elongation in the mouse embryo. Development 130, 3807–3819. https://doi.org/10.1242/dev.00573

Forsberg, H., Crozet, F., Brown, N.A., 1998. Waves of mouse Lunatic fringe expression, in four-hour cycles at two-hour intervals, precede somite boundary formation. Current Biology 8, 1027–1030. https://doi.org/10.1016/S0960-9822(07)00424-1

Frohnert, C., Schweizer, S., Hoyer-Fender, S., 2011. SPAG4L/SPAG4L-2 are testis-specific SUN domain proteins restricted to the apical nuclear envelope of round spermatids facing the acrosome. Molecular Human Reproduction 17, 207–218. https://doi.org/10.1093/molehr/gaq099

Furukawa, K., Hotta, Y., 1993. cDNA cloning of a germ cell specific lamin B3 from mouse spermatocytes and analysis of its function by ectopic expression in

somatic cells. The EMBO Journal 12, 97–106. https://doi.org/10.1002/j.1460-2075.1993.tb05635.x
Gammill, L.S., Gonzalez, C., Gu, C., Bronner-Fraser, M., 2006. Guidance of trunk neural crest migration requires neuropilin 2/semaphorin 3F signaling. Development 133, 99–106. https://doi.org/10.1242/dev.02187
Garcia-Martinez, V., Alvarez, I.S., Schoenwolf, G.C., 1993. Locations of the ectodermal and nonectodermal subdivisions of the epiblast at stages 3 and 4 of avian gastrulation and neurulation. Journal of Experimental Zoology 267, 431–446. https://doi.org/10.1002/jez.1402670409
Gierer, A., Meinhardt, H., 1972. A theory of biological pattern formation. Kybernetik 12, 30–39. https://doi.org/10.1007/BF00289234
Göb, E., Schmitt, J., Benavente, R., Alsheimer, M., 2010. Mammalian Sperm Head Formation Involves Different Polarization of Two Novel LINC Complexes. PLoS ONE 5, e12072. https://doi.org/10.1371/journal.pone.0012072
Gonzalez, N.P., Tao, J., Rochman, N.D., Vig, D., Chiu, E., Wirtz, D., Sun, S.X., 2018. Cell tension and mechanical regulation of cell volume. Molecular Biology of the Cell 29, 2591–2600. https://doi.org/10.1091/mbc.E18-04-0213
Green, J.B.A., Sharpe, J., 2015. Positional information and reaction-diffusion: two big ideas in developmental biology combine. Development 142, 1203–1211. https://doi.org/10.1242/dev.114991
Gregor, T., Tank, D.W., Wieschaus, E.F., Bialek, W., 2007a. Probing the Limits to Positional Information. Cell 130, 153–164. https://doi.org/10.1016/j.cell.2007.05.025
Gregor, T., Wieschaus, E.F., McGregor, A.P., Bialek, W., Tank, D.W., 2007b. Stability and Nuclear Dynamics of the Bicoid Morphogen Gradient. Cell 130, 141–152. https://doi.org/10.1016/j.cell.2007.05.026
Grill, S.W., 2011. Growing up is stressful: biophysical laws of morphogenesis. Current Opinion in Genetics & Development 21, 647–652. https://doi.org/10.1016/j.gde.2011.09.005
Guilluy, C., Osborne, L.D., Van Landeghem, L., Sharek, L., Superfine, R., Garcia-Mata, R., Burridge, K., 2014. Isolated nuclei adapt to force and reveal a mechanotransduction pathway in the nucleus. Nat Cell Biol 16, 376–381. https://doi.org/10.1038/ncb2927
Guo, Z., Yao, J., Zheng, X., Cao, J., Lv, X., Gao, Z., Guo, S., Li, H., Guan, D., Li, Long, Qin, D., Li, D., Wang, X., Tan, M., Zhang, J., Zhang, Y., Wang, B., Bu, W., Li, J., Zhao, X., Meng, F., Feng, Y., Li, Lei, Du, J., Fan, Y., 2025. Cavity oscillation drives pattern formation in early mammalian embryos. Cell Reports 44, 115342. https://doi.org/10.1016/j.celrep.2025.115342
Gurskaya, N.G., Verkhusha, V.V., Shcheglov, A.S., Staroverov, D.B., Chepurnykh, T.V., Fradkov, A.F., Lukyanov, S., Lukyanov, K.A., 2006. Engineering of a monomeric green-to-red photoactivatable fluorescent protein induced by blue light. Nat Biotechnol 24, 461–465. https://doi.org/10.1038/nbt1191
Hamburger, V., Hamilton, H.L., 1951. A series of normal stages in the development of the chick embryo. Journal of Morphology 88, 49–92. https://doi.org/10.1002/jmor.1050880104
Han, C., Yan, D., Belenkaya, T.Y., Lin, X., 2005. *Drosophila* glypicans Dally and Dally-like shape the extracellular Wingless morphogen gradient in the wing disc. Development 132, 667–679. https://doi.org/10.1242/dev.01636

Hao, H., Starr, D.A., 2019. SUN/KASH interactions facilitate force transmission across the nuclear envelope. Nucleus 10, 73–80. https://doi.org/10.1080/19491034.2019.1595313
Haque, F., Lloyd, D.J., Smallwood, D.T., Dent, C.L., Shanahan, C.M., Fry, A.M., Trembath, R.C., Shackleton, S., 2006. SUN1 Interacts with Nuclear Lamin A and Cytoplasmic Nesprins To Provide a Physical Connection between the Nuclear Lamina and the Cytoskeleton. Molecular and Cellular Biology 26, 3738–3751. https://doi.org/10.1128/MCB.26.10.3738-3751.2006
Harada, T., Swift, J., Irianto, J., Shin, J.-W., Spinler, K.R., Athirasala, A., Diegmiller, R., Dingal, P.C.D.P., Ivanovska, I.L., Discher, D.E., 2014. Nuclear lamin stiffness is a barrier to 3D migration, but softness can limit survival. Journal of Cell Biology 204, 669–682. https://doi.org/10.1083/jcb.201308029
Harding, M.J., McGraw, H.F., Nechiporuk, A., 2014. The roles and regulation of multicellular rosette structures during morphogenesis. Development 141, 2549–2558. https://doi.org/10.1242/dev.101444
Harfe, B.D., Scherz, P.J., Nissim, S., Tian, H., McMahon, A.P., Tabin, C.J., 2004. Evidence for an Expansion-Based Temporal Shh Gradient in Specifying Vertebrate Digit Identities. Cell 118, 517–528. https://doi.org/10.1016/j.cell.2004.07.024
Hatada, Y., Stern, C.D., 1994. A fate map of the epiblast of the early chick embryo. Development (Cambridge, England) 120, 2879–89.
Hertwig, O., 1876. Beiträge zur kenntniss der bildung, befruchtung und theilung des thierischen Eies. Morphologisches Jahrbuch 1, 347–434.
Hieda, M., 2017. Implications for Diverse Functions of the LINC Complexes Based on the Structure. Cells 6, 3. https://doi.org/10.3390/cells6010003
Hinsch, G.W., Hamilton, H.L., 1956. The developmental fate of the first somite of the chick. Anat. Rec. 125, 225–245. https://doi.org/10.1002/ar.1091250206
Hirano, M., Ando, R., Shimozono, S., Sugiyama, M., Takeda, N., Kurokawa, H., Deguchi, R., Endo, K., Haga, K., Takai-Todaka, R., Inaura, S., Matsumura, Y., Hama, H., Okada, Y., Fujiwara, T., Morimoto, T., Katayama, K., Miyawaki, A., 2022. A highly photostable and bright green fluorescent protein. Nat Biotechnol 40, 1132–1142. https://doi.org/10.1038/s41587-022-01278-2
Hirate, Y., Hirahara, S., Inoue, K., Kiyonari, H., Niwa, H., Sasaki, H., 2015. Par-aPKC-dependent and -independent mechanisms cooperatively control cell polarity, Hippo signaling, and cell positioning in 16-cell stage mouse embryos. Dev Growth Differ 57, 544–556. https://doi.org/10.1111/dgd.12235
Hirate, Y., Hirahara, S., Inoue, K., Suzuki, A., Alarcon, V.B., Akimoto, K., Hirai, T., Hara, T., Adachi, M., Chida, K., Ohno, S., Marikawa, Y., Nakao, K., Shimono, A., Sasaki, H., 2013. Polarity-Dependent Distribution of Angiomotin Localizes Hippo Signaling in Preimplantation Embryos. Current Biology 23, 1181–1194. https://doi.org/10.1016/j.cub.2013.05.014
Ho, C.Y., Jaalouk, D.E., Vartiainen, M.K., Lammerding, J., 2013. Lamin A/C and emerin regulate MKL1–SRF activity by modulating actin dynamics. Nature 497, 507–511. https://doi.org/10.1038/nature12105
Ho, C.Y., Lammerding, J., 2012. Lamins at a glance. Journal of Cell Science 125, 2087–2093. https://doi.org/10.1242/jcs.087288
Hodge, R.G., Ridley, A.J., 2016. Regulating Rho GTPases and their regulators. Nat Rev Mol Cell Biol 17, 496–510. https://doi.org/10.1038/nrm.2016.67

Hodzic, D.M., Yeater, D.B., Bengtsson, L., Otto, H., Stahl, P.D., 2004. Sun2 Is a Novel Mammalian Inner Nuclear Membrane Protein. Journal of Biological Chemistry 279, 25805–25812. https://doi.org/10.1074/jbc.M313157200

Hollyday, M., McMahon, J.A., McMahon, A.P., 1995. Wnt expression patterns in chick embryo nervous system. Mechanisms of Development 52, 9–25. https://doi.org/10.1016/0925-4773(95)00385-E

Holtfreter, J., 1938. Differenzierungspotenzen isolierter Teile der Urodelengastrula. W. Roux' Archiv f. Entwicklungsmechanik 138, 522–656. https://doi.org/10.1007/BF00573814

Houchmandzadeh, B., Wieschaus, E., Leibler, S., 2002. Establishment of developmental precision and proportions in the early Drosophila embryo. Nature 415, 798–802. https://doi.org/10.1038/415798a

Huang, R., Zhi, Q., Neubuser, A., Miiller, T.S., Brand-Saberi, B., Christ, B., Wilting, J., 1996. Function of Somite and Somitocoele Cells in the Formation of the Vertebral Motion Segment in Avian Embryos. Cells Tissues Organs 155, 231–241. https://doi.org/10.1159/000147811

Huang, R., Zhi, Q., Wilting, J., Christ, B., 1994. The fate of somitocoele cells in avian embryos. Anatomy and Embryology 190, 243–250. https://doi.org/10.1007/BF00234302

Hubaud, A., Regev, I., Mahadevan, L., Pourquié, O., 2017. Excitable Dynamics and Yap-Dependent Mechanical Cues Drive the Segmentation Clock. Cell 171, 668-682.e11. https://doi.org/10.1016/j.cell.2017.08.043

Huelsmann, S., Ylänne, J., Brown, N.H., 2013. Filopodia-like Actin Cables Position Nuclei in Association with Perinuclear Actin in Drosophila Nurse Cells. Developmental Cell 26, 604–615. https://doi.org/10.1016/j.devcel.2013.08.014

Ihalainen, T.O., Aires, L., Herzog, F.A., Schwartlander, R., Moeller, J., Vogel, V., 2015. Differential basal-to-apical accessibility of lamin A/C epitopes in the nuclear lamina regulated by changes in cytoskeletal tension. Nature Mater 14, 1252–1261. https://doi.org/10.1038/nmat4389

Ikenoya, M., Hidaka, H., Hosoya, T., Suzuki, M., Yamamoto, N., Sasaki, Y., 2002. Inhibition of Rho-kinase-induced myristoylated alanine-rich C kinase substrate (MARCKS) phosphorylation in human neuronal cells by H-1152, a novel and specific Rho-kinase inhibitor. Journal of Neurochemistry 81, 9–16. https://doi.org/10.1046/j.1471-4159.2002.00801.x

Inomata, H., Shibata, T., Haraguchi, T., Sasai, Y., 2013. Scaling of Dorsal-Ventral Patterning by Embryo Size-Dependent Degradation of Spemann's Organizer Signals. Cell 153, 1296–1311. https://doi.org/10.1016/j.cell.2013.05.004

Izpisúa-Belmonte, J.C., De Robertis, E.M., Storey, K.G., Stern, C.D., 1993. The homeobox gene goosecoid and the origin of organizer cells in the early chick blastoderm. Cell 74, 645–659. https://doi.org/10.1016/0092-8674(93)90512-O

Jacob, M., Wachtler, F., Jacob, H.J., Christ, B., 1986. On the Problem of Metamerism in the Head Mesenchyme of Chick Embryos, in: Bellairs, R., Ede, D.A., Lash, J.W. (Eds.), Somites in Developing Embryos. Springer US, Boston, MA, pp. 79–89. https://doi.org/10.1007/978-1-4899-2013-3_7

Jacobson, A.G., Meier, S., 1984. Morphogenesis of the head of a newt: Mesodermal segments, neuromeres, and distribution of neural crest. Developmental Biology 106, 181–193. https://doi.org/10.1016/0012-1606(84)90074-5

Johnson, M., Ziomek, C., 1981. The foundation of two distinct cell lineages within the mouse morula. Cell 24, 71–80. https://doi.org/10.1016/0092-8674(81)90502-X

Joubin, K., Stern, C.D., 1999. Molecular Interactions Continuously Define the Organizer during the Cell Movements of Gastrulation. Cell 98, 559–571. https://doi.org/10.1016/S0092-8674(00)80044-6

Jouve, C., Palmeirim, I., Henrique, D., Beckers, J., Gossler, A., Ish-Horowicz, D., Pourquié, O., 2000. Notch signalling is required for cyclic expression of the hairy-like gene HES1 in the presomitic mesoderm. Development (Cambridge, England) 127, 1421–9.

Kaur, G., Costa, M.W., Nefzger, C.M., Silva, J., Fierro-González, J.C., Polo, J.M., Bell, T.D.M., Plachta, N., 2013. Probing transcription factor diffusion dynamics in the living mammalian embryo with photoactivatable fluorescence correlation spectroscopy. Nat Commun 4, 1637. https://doi.org/10.1038/ncomms2657

Kerszberg, M., Wolpert, L., 2007. Specifying Positional Information in the Embryo: Looking Beyond Morphogens. Cell 130, 205–209. https://doi.org/10.1016/j.cell.2007.06.038

Kerszberg, M., Wolpert, L., 2000. A clock and trail model for somite formation, specialization and polarization. Journal of theoretical biology 205, 505–10. https://doi.org/10.1006/jtbi.2000.2085

Keynes, R.J., Stern, C.D., 1988. Mechanisms of vertebrate segmentation. Development (Cambridge, England) 103, 413–429.

Keynes, R.J., Stern, C.D., 1984. Segmentation in the vertebrate nervous system. Nature 310, 786–789. https://doi.org/10.1038/310786a0

Kimura, K., Ito, M., Amano, M., Chihara, K., Fukata, Y., Nakafuku, M., Yamamori, B., Feng, J., Nakano, T., Okawa, K., Iwamatsu, A., Kaibuchi, K., 1996. Regulation of Myosin Phosphatase by Rho and Rho-Associated Kinase (Rho-Kinase). Science 273, 245–248. https://doi.org/10.1126/science.273.5272.245

Koblar, S.A., Krull, C.E., Pasquale, E.B., McLennan, R., Peale, F.D., Cerretti, D.P., Bothwell, M., 2000. Spinal motor axons and neural crest cells use different molecular guides for segmental migration through the rostral half-somite. J. Neurobiol. 42, 437–447. https://doi.org/10.1002/(SICI)1097-4695(200003)42:4%253C437::AID-NEU5%253E3.0.CO;2-O

Kochin, V., Shimi, T., Torvaldson, E., Adam, S.A., Goldman, A., Pack, C.-G., Melo-Cardenas, J., Imanishi, S.Y., Goldman, R.D., Eriksson, J.E., 2014. Interphase phosphorylation of lamin A. Journal of Cell Science jcs.141820. https://doi.org/10.1242/jcs.141820

Kondo, S., Miura, T., 2010. Reaction-Diffusion Model as a Framework for Understanding Biological Pattern Formation. Science 329, 1616–1620. https://doi.org/10.1126/science.1179047

Korotkevich, E., Niwayama, R., Courtois, A., Friese, S., Berger, N., Buchholz, F., Hiiragi, T., 2017. The Apical Domain Is Required and Sufficient for the First Lineage Segregation in the Mouse Embryo. Developmental Cell 40, 235-247.e7. https://doi.org/10.1016/j.devcel.2017.01.006

Kremers, G.-J., Goedhart, J., Van Munster, E.B., Gadella, T.W.J., 2006. Cyan and Yellow Super Fluorescent Proteins with Improved Brightness, Protein Folding, and FRET Förster Radius. Biochemistry 45, 6570–6580. https://doi.org/10.1021/bi0516273

Krieg, M., Arboleda-Estudillo, Y., Puech, P.-H., Käfer, J., Graner, F., Müller, D.J., Heisenberg, C.-P., 2008. Tensile forces govern germ-layer organization in zebrafish. Nat Cell Biol 10, 429–436. https://doi.org/10.1038/ncb1705

Kulesa, P.M., Fraser, S.E., 2002. Cell Dynamics During Somite Boundary Formation Revealed by Time-Lapse Analysis. Science 298, 991–995. https://doi.org/10.1126/science.1075544
Kulesa, P.M., Schnell, S., Rudloff, S., Baker, R.E., Maini, P.K., 2007. From segment to somite: Segmentation to epithelialization analyzed within quantitative frameworks. Developmental Dynamics 236, 1392–1402. https://doi.org/10.1002/dvdy.21199
Kumaran, R.I., Muralikrishna, B., Parnaik, V.K., 2002. Lamin A/C speckles mediate spatial organization of splicing factor compartments and RNA polymerase II transcription. The Journal of Cell Biology 159, 783–793. https://doi.org/10.1083/jcb.200204149
Lambert, M.W., 2019. The functional importance of lamins, actin, myosin, spectrin and the LINC complex in DNA repair. Exp Biol Med (Maywood) 244, 1382–1406. https://doi.org/10.1177/1535370219876651
Lammerding, J., Fong, L.G., Ji, J.Y., Reue, K., Stewart, C.L., Young, S.G., Lee, R.T., 2006. Lamins A and C but Not Lamin B1 Regulate Nuclear Mechanics. Journal of Biological Chemistry 281, 25768–25780. https://doi.org/10.1074/jbc.M513511200
Lander, A.D., 2011. Pattern, Growth, and Control. Cell 144, 955–969. https://doi.org/10.1016/j.cell.2011.03.009
Lash, J.W., Yamada, K.M., 1986. The Adhesion Recognition Signal of Fibronectin: A Possible Trigger Mechanism for Compaction During Somitogenesis, in: Bellairs, R., Ede, D.A., Lash, J.W. (Eds.), Somites in Developing Embryos. Springer US, Boston, MA, pp. 201–208. https://doi.org/10.1007/978-1-4899-2013-3_16
Lawson, K.A., Meneses, J.J., Pedersen, R.A., 1991. Clonal analysis of epiblast fate during germ layer formation in the mouse embryo. Development 113, 891–911. https://doi.org/10.1242/dev.113.3.891
Lee, H.C., Hastings, C., Oliveira, N.M.M., Pérez-Carrasco, R., Page, K.M., Wolpert, L., Stern, C.D., 2022. 'Neighbourhood watch' model: embryonic epiblast cells assess positional information in relation to their neighbours. Development 149, dev200295. https://doi.org/10.1242/dev.200295
Leeuwenhoek, A.V., 1679. Observationes D. Anthonii Lewenhoeck, de natis e semine genitali animalculis. Phil. Trans. R. Soc. 12, 1040–1046. https://doi.org/10.1098/rstl.1677.0068
Lele, T.P., Dickinson, R.B., Gundersen, G.G., 2018. Mechanical principles of nuclear shaping and positioning. Journal of Cell Biology 217, 3330–3342. https://doi.org/10.1083/jcb.201804052
Leung, C.Y., Zernicka-Goetz, M., 2013. Angiomotin prevents pluripotent lineage differentiation in mouse embryos via Hippo pathway-dependent and -independent mechanisms. Nat Commun 4, 2251. https://doi.org/10.1038/ncomms3251
Li, L., Xie, T., 2005. STEM CELL NICHE: Structure and Function. Annu. Rev. Cell Dev. Biol. 21, 605–631. https://doi.org/10.1146/annurev.cellbio.21.012704.131525
Lim, H.Y.G., Alvarez, Y.D., Gasnier, M., Wang, Y., Tetlak, P., Bissiere, S., Wang, H., Biro, M., Plachta, N., 2020. Keratins are asymmetrically inherited fate determinants in the mammalian embryo. Nature 585, 404–409. https://doi.org/10.1038/s41586-020-2647-4
Lim, T.M., Lunn, E.R., Keynes, R.J., Stern, C.D., 1987. The differing effects of occipital and trunk somites on neural development in the chick embryo. Development 100, 525–533. https://doi.org/10.1242/dev.100.3.525

Lin, F., Worman, H.J., 1993. Structural organization of the human gene encoding nuclear lamin A and nuclear lamin C. Journal of Biological Chemistry 268, 16321–16326. https://doi.org/10.1016/S0021-9258(19)85424-8

Linker, C., Lesbros, C., Gros, J., Burrus, L.W., Rawls, A., Marcelle, C., 2005. β-catenin-dependent Wnt signalling controls the epithelial organisation of somites through the activation of paraxis. Development 132, 3895–3905. https://doi.org/10.1242/dev.01961

Lityagina, O., Dobreva, G., 2021. The LINC Between Mechanical Forces and Chromatin. Front. Physiol. 12, 710809. https://doi.org/10.3389/fphys.2021.710809

Lomakin, A.J., Cattin, C.J., Cuvelier, D., Alraies, Z., Molina, M., Nader, G.P.F., Srivastava, N., Sáez, P.J., Garcia-Arcos, J.M., Zhitnyak, I.Y., Bhargava, A., Driscoll, M.K., Welf, E.S., Fiolka, R., Petrie, R.J., De Silva, N.S., González-Granado, J.M., Manel, N., Lennon-Duménil, A.M., Müller, D.J., Piel, M., 2020. The nucleus acts as a ruler tailoring cell responses to spatial constraints. Science 370, eaba2894. https://doi.org/10.1126/science.aba2894

Lu, H., Hesse, M., Peters, B., Magin, T.M., 2005. Type II keratins precede type I keratins during early embryonic development. European Journal of Cell Biology 84, 709–718. https://doi.org/10.1016/j.ejcb.2005.04.001

Lucchetta, E.M., Vincent, M.E., Ismagilov, R.F., 2008. A Precise Bicoid Gradient Is Nonessential during Cycles 11–13 for Precise Patterning in the Drosophila Blastoderm. PLoS ONE 3, e3651. https://doi.org/10.1371/journal.pone.0003651

Maekawa, M., Ishizaki, T., Boku, S., Watanabe, N., Fujita, A., Iwamatsu, A., Obinata, T., Ohashi, K., Mizuno, K., Narumiya, S., 1999. Signaling from Rho to the Actin Cytoskeleton Through Protein Kinases ROCK and LIM-kinase. Science 285, 895–898. https://doi.org/10.1126/science.285.5429.895

Maître, J.-L., Niwayama, R., Turlier, H., Nédélec, F., Hiiragi, T., 2015. Pulsatile cell-autonomous contractility drives compaction in the mouse embryo. Nat Cell Biol 17, 849–855. https://doi.org/10.1038/ncb3185

Mäntylä, E., Montonen, T., Azzari, L., Mattola, S., Hannula, M., Vihinen-Ranta, M., Hyttinen, J., Vippola, M., Foi, A., Nymark, S., Ihalainen, T.O., 2023. Iterative immunostaining combined with expansion microscopy and image processing reveals nanoscopic network organization of nuclear lamina. MBoC 34, br13. https://doi.org/10.1091/mbc.E22-09-0448

Manu, Surkova, S., Spirov, A.V., Gursky, V.V., Janssens, H., Kim, A.-R., Radulescu, O., Vanario-Alonso, C.E., Sharp, D.H., Samsonova, M., Reinitz, J., 2009. Canalization of Gene Expression in the Drosophila Blastoderm by Gap Gene Cross Regulation. PLoS Biol 7, e1000049. https://doi.org/10.1371/journal.pbio.1000049

Martins, G.G., Rifes, P., Amaândio, R., Rodrigues, G., Palmeirim, I., Thorsteinsdóttir, S., 2009. Dynamic 3D cell rearrangements guided by a fibronectin matrix underlie somitogenesis. PLoS ONE 4. https://doi.org/10.1371/journal.pone.0007429

Mathis, L., Kulesa, P.M., Fraser, S.E., 2001. FGF receptor signalling is required to maintain neural progenitors during Hensen's node progression. Nat Cell Biol 3, 559–566. https://doi.org/10.1038/35078535

Matsuda, M., Yamanaka, Y., Uemura, M., Osawa, M., Saito, M.K., Nagahashi, A., Nishio, M., Guo, L., Ikegawa, S., Sakurai, S., Kihara, S., Maurissen, T.L., Nakamura, M., Matsumoto, T., Yoshitomi, H., Ikeya, M., Kawakami, N.,

Yamamoto, T., Woltjen, K., Ebisuya, M., Toguchida, J., Alev, C., 2020. Recapitulating the human segmentation clock with pluripotent stem cells. Nature 580, 124–129. https://doi.org/10.1038/s41586-020-2144-9
Matz, M.V., Fradkov, A.F., Labas, Y.A., Savitsky, A.P., Zaraisky, A.G., Markelov, M.L., Lukyanov, S.A., 1999. Fluorescent proteins from nonbioluminescent Anthozoa species. Nat Biotechnol 17, 969–973. https://doi.org/10.1038/13657
McGrew, M.J., Sherman, A., Lillico, S.G., Ellard, F.M., Radcliffe, P.A., Gilhooley, H.J., Mitrophanous, K.A., Cambray, N., Wilson, V., Sang, H., 2008. Localised axial progenitor cell populations in the avian tail bud are not committed to a posterior Hox identity. Development 135, 2289–2299. https://doi.org/10.1242/dev.022020
McHale, P., Rappel, W.-J., Levine, H., 2006. Embryonic pattern scaling achieved by oppositely directed morphogen gradients. Phys. Biol. 3, 107–120. https://doi.org/10.1088/1478-3975/3/2/003
Meier, S., 1984. Somite formation and its relationship to metameric patterning of the mesoderm. Cell Differentiation 14, 235–243. https://doi.org/10.1016/0045-6039(84)90012-5
Meier, S., 1979. Development of the chick embryo mesoblast. Developmental Biology 73, 25–45. https://doi.org/10.1016/0012-1606(79)90135-0
Meilhac, S.M., Adams, R.J., Morris, S.A., Danckaert, A., Le Garrec, J.-F., Zernicka-Goetz, M., 2009. Active cell movements coupled to positional induction are involved in lineage segregation in the mouse blastocyst. Developmental Biology 331, 210–221. https://doi.org/10.1016/j.ydbio.2009.04.036
Meinhardt, H., 2009. The Algorithmic Beauty of Sea Shells, The Virtual Laboratory. Springer Berlin Heidelberg, Berlin, Heidelberg. https://doi.org/10.1007/978-3-540-92142-4
Meinhardt, H., 1982. Models of biological pattern formation, 2. print. ed. Acad. Press, London.
Meinhardt, H., 1978. Space-dependent cell determination under the control of a morphogen gradient. Journal of Theoretical Biology 74, 307–321. https://doi.org/10.1016/0022-5193(78)90078-4
Mestres, P., Hinrichsen, K., 1976. Zur Histogenese des Somiten beim Hühnchen. Development 36, 669–683. https://doi.org/10.1242/dev.36.3.669
Miao, Y., Diaz-Cuadros, M., Pourquié, O., 2023. Modeling Human Paraxial Mesoderm Development with Pluripotent Stem Cells, in: Methods in Molecular Biology. Springer US, New York, NY. https://doi.org/10.1007/7651_2023_507
Mittapalli, V.R., Huang, R., Patel, K., Christ, B., Scaal, M., 2005. Arthrotome: A specific joint forming compartment in the avian somite. Developmental Dynamics 234, 48–53. https://doi.org/10.1002/dvdy.20502
Mongera, A., Rowghanian, P., Gustafson, H.J., Shelton, E., Kealhofer, D.A., Carn, E.K., Serwane, F., Lucio, A.A., Giammona, J., Campàs, O., 2018. A fluid-to-solid jamming transition underlies vertebrate body axis elongation. Nature 561, 401–405. https://doi.org/10.1038/s41586-018-0479-2
Moore, R.P., Fogerson, S.M., Tulu, U.S., Yu, J.W., Cox, A.H., Sican, M.A., Li, D., Legant, W.R., Weigel, A.V., Crawford, J.M., Betzig, E., Kiehart, D.P., 2022. Superresolution microscopy reveals actomyosin dynamics in medioapical arrays. MBoC 33, ar94. https://doi.org/10.1091/mbc.E21-11-0537
Murray, J.D. (Ed.), 2002. Mathematical Biology: I. An Introduction, Interdisciplinary Applied Mathematics. Springer New York, New York, NY. https://doi.org/10.1007/b98868

Nakamura, T., Mine, N., Nakaguchi, E., Mochizuki, A., Yamamoto, M., Yashiro, K., Meno, C., Hamada, H., 2006. Generation of Robust Left-Right Asymmetry in the Mouse Embryo Requires a Self-Enhancement and Lateral-Inhibition System. Developmental Cell 11, 495–504. https://doi.org/10.1016/j.devcel.2006.08.002

Nakaya, Y., Kuroda, S., Katagiri, Y.T., Kaibuchi, K., Takahashi, Y., 2004. Mesenchymal-Epithelial Transition during Somitic Segmentation Is Regulated by Differential Roles of Cdc42 and Rac1. Developmental Cell 7, 425–438. https://doi.org/10.1016/j.devcel.2004.08.003

Nelemans, B.K.A., Schmitz, M., Tahir, H., Merks, R.M.H., Smit, T.H., 2020. Somite Division and New Boundary Formation by Mechanical Strain. iScience 23, 100976. https://doi.org/10.1016/j.isci.2020.100976

New, D.A.T., 1955. A New Technique for the Cultivation of the Chick Embryo in vitro. Journal of Embryology & Experimental Morphology 3, 320–331.

Nishimura, Y., Shi, S., Zhang, F., Liu, R., Takagi, Y., Bershadsky, A.D., Viasnoff, V., Sellers, J.R., 2021. The formin inhibitor SMIFH2 inhibits members of the myosin superfamily. Journal of Cell Science 134, jcs253708. https://doi.org/10.1242/jcs.253708

Nishioka, N., Inoue, K., Adachi, K., Kiyonari, H., Ota, M., Ralston, A., Yabuta, N., Hirahara, S., Stephenson, R.O., Ogonuki, N., Makita, R., Kurihara, H., Morin-Kensicki, E.M., Nojima, H., Rossant, J., Nakao, K., Niwa, H., Sasaki, H., 2009. The Hippo Signaling Pathway Components Lats and Yap Pattern Tead4 Activity to Distinguish Mouse Trophectoderm from Inner Cell Mass. Developmental Cell 16, 398–410. https://doi.org/10.1016/j.devcel.2009.02.003

Niwa, H., Toyooka, Y., Shimosato, D., Strumpf, D., Takahashi, K., Yagi, R., Rossant, J., 2005. Interaction between Oct3/4 and Cdx2 Determines Trophectoderm Differentiation. Cell 123, 917–929. https://doi.org/10.1016/j.cell.2005.08.040

Ochoa-Espinosa, A., Yu, D., Tsirigos, A., Struffi, P., Small, S., 2009. Anterior-posterior positional information in the absence of a strong Bicoid gradient. Proc. Natl. Acad. Sci. U.S.A. 106, 3823–3828. https://doi.org/10.1073/pnas.0807878105

Oginuma, M., Takahashi, Y., Kitajima, S., Kiso, M., Kanno, J., Kimura, A., Saga, Y., 2010. The oscillation of Notch activation, but not its boundary, is required for somite border formation and rostral-caudal patterning within a somite. Development 137, 1515–1522. https://doi.org/10.1242/dev.044545

Ohashi, K., Nagata, K., Maekawa, M., Ishizaki, T., Narumiya, S., Mizuno, K., 2000. Rho-associated Kinase ROCK Activates LIM-kinase 1 by Phosphorylation at Threonine 508 within the Activation Loop. Journal of Biological Chemistry 275, 3577–3582. https://doi.org/10.1074/jbc.275.5.3577

Ordahl, C.P., Le Douarin, N.M., 1992. Two myogenic lineages within the developing somite. Development 114, 339–353. https://doi.org/10.1242/dev.114.2.339

Osmanagic-Myers, S., Dechat, T., Foisner, R., 2015. Lamins at the crossroads of mechanosignaling. Genes Dev. 29, 225–237. https://doi.org/10.1101/gad.255968.114

Packard, D.S., Jacobson, A.G., 1976. The influence of axial structures on chick somite formation. Developmental Biology 53, 36–48. https://doi.org/10.1016/0012-1606(76)90207-4

Packard, D.S., Meier, S., 1984. Morphological and experimental studies of the somitomeric organization of the segmental plate in snapping turtle embryos. Development 84, 35–48. https://doi.org/10.1242/dev.84.1.35

Packard, D.S., Meier, S., 1983. An experimental study of the somitomeric organization of the avian segmental plate. Developmental Biology 97, 191–202. https://doi.org/10.1016/0012-1606(83)90076-3

Palmeirim, I., Henrique, D., Ish-Horowicz, D., Pourquié, O., 1997. Avian hairy gene expression identifies a molecular clock linked to vertebrate segmentation and somitogenesis. Cell 91, 639–48. https://doi.org/10.1016/S0092-8674(00)80451-1

Palmieri, S.L., Peter, W., Hess, H., Schöler, H.R., 1994. Oct-4 Transcription Factor Is Differentially Expressed in the Mouse Embryo during Establishment of the First Two Extraembryonic Cell Lineages Involved in Implantation. Developmental Biology 166, 259–267. https://doi.org/10.1006/dbio.1994.1312

Panáková, D., Sprong, H., Marois, E., Thiele, C., Eaton, S., 2005. Lipoprotein particles are required for Hedgehog and Wingless signalling. Nature 435, 58–65. https://doi.org/10.1038/nature03504

Panciera, T., Azzolin, L., Cordenonsi, M., Piccolo, S., 2017. Mechanobiology of YAP and TAZ in physiology and disease. Nat Rev Mol Cell Biol 18, 758–770. https://doi.org/10.1038/nrm.2017.87

Parr, B.A., Shea, M.J., Vassileva, G., McMahon, A.P., 1993. Mouse *Wnt* genes exhibit discrete domains of expression in the early embryonic CNS and limb buds. Development 119, 247–261. https://doi.org/10.1242/dev.119.1.247

Patterson, G.H., Lippincott-Schwartz, J., 2002. A Photoactivatable GFP for Selective Photolabeling of Proteins and Cells. Science 297, 1873–1877. https://doi.org/10.1126/science.1074952

Peter, M., Kitten, G.T., Lehner, C.F., Vorburger, K., Bailer, S.M., Maridor, G., Nigg, E.A., 1989. Cloning and sequencing of cDNA clones encoding chicken lamins A and B1 and comparison of the primary structures of vertebrate A- and B-type lamins. Journal of Molecular Biology 208, 393–404. https://doi.org/10.1016/0022-2836(89)90504-4

Piatkowska, A.M., Adhikari, K., Moverley, A.A., Turmaine, M., Glazier, J.A., Plachta, N., Evans, S.E., Stern, C.D., 2023. Sequential changes in cellular properties accompanying amniote somite formation. Journal of Anatomy 242, 417–435. https://doi.org/10.1111/joa.13791

Piccolo, S., Sasai, Y., Lu, B., De Robertis, E.M., 1996. Dorsoventral Patterning in Xenopus: Inhibition of Ventral Signals by Direct Binding of Chordin to BMP-4. Cell 86, 589–598. https://doi.org/10.1016/S0092-8674(00)80132-4

Polezhaev, A.A., 1992. A mathematical model of the mechanism of vertebrate somitic segmentation. Journal of Theoretical Biology 156, 169–181. https://doi.org/10.1016/S0022-5193(05)80671-X

Pomp, O., Lim, H.Y.G., Skory, R.M., Moverley, A.A., Tetlak, P., Bissiere, S., Plachta, N., 2022. A monoastral mitotic spindle determines lineage fate and position in the mouse embryo. Nat Cell Biol 24, 155–167. https://doi.org/10.1038/s41556-021-00826-3

Prasher, D.C., Eckenrode, V.K., Ward, W.W., Prendergast, F.G., Cormier, M.J., 1992. Primary structure of the Aequorea victoria green-fluorescent protein. Gene 111, 229–233. https://doi.org/10.1016/0378-1119(92)90691-H

Primmett, D.R., Norris, W.E., Carlson, G.J., Keynes, R.J., Stern, C.D., 1989. Periodic segmental anomalies induced by heat shock in the chick embryo are associated with the cell cycle. Development (Cambridge, England) 105, 119–30.

Primmett, D.R., Stern, C.D., Keynes, R.J., 1988. Heat shock causes repeated segmental anomalies in the chick embryo. Development (Cambridge, England) 104, 331–9.
Psychoyos, D., Stern, C.D., 1996. Fates and migratory routes of primitive streak cells in the chick embryo. Development (Cambridge, England) 122, 1523–34.
Ramkumar, N., Baum, B., 2016. Coupling changes in cell shape to chromosome segregation. Nat Rev Mol Cell Biol 17, 511–521. https://doi.org/10.1038/nrm.2016.75
Rasolonjanahary, M., Vasiev, B., 2018. Scaling of Morphogenetic Patterns, in: Dubrulle, J. (Ed.), Morphogen Gradients, Methods in Molecular Biology. Springer New York, New York, NY, pp. 263–280. https://doi.org/10.1007/978-1-4939-8772-6_15
Rasolonjanahary, M., Vasiev, B., 2016. Scaling of morphogenetic patterns in reaction-diffusion systems. Journal of Theoretical Biology 404, 109–119. https://doi.org/10.1016/j.jtbi.2016.05.035
Razafsky, D., Wirtz, D., Hodzic, D., 2014. Nuclear Envelope in Nuclear Positioning and Cell Migration, in: Schirmer, E.C., De Las Heras, J.I. (Eds.), Cancer Biology and the Nuclear Envelope, Advances in Experimental Medicine and Biology. Springer New York, New York, NY, pp. 471–490. https://doi.org/10.1007/978-1-4899-8032-8_21
Reversade, B., De Robertis, E.M., 2005. Regulation of ADMP and BMP2/4/7 at Opposite Embryonic Poles Generates a Self-Regulating Morphogenetic Field. Cell 123, 1147–1160. https://doi.org/10.1016/j.cell.2005.08.047
Rickmann, M., Fawcett, J.W., Keynes, R.J., 1985. The migration of neural crest cells and the growth of motor axons through the rostral half of the chick somite. Journal of Embryology and Experimental Morphology VOL. 90, 437–455.
Riddle, R.D., Johnson, R.L., Laufer, E., Tabin, C., 1993. Sonic hedgehog mediates the polarizing activity of the ZPA. Cell 75, 1401–1416. https://doi.org/10.1016/0092-8674(93)90626-2
Rifes, P., Carvalho, L., Lopes, C., Andrade, R.P., Rodrigues, G., Palmeirim, I., Thorsteinsdóttir, S., 2007. Redefining the role of ectoderm in somitogenesis: a player in the formation of the fibronectin matrix of presomitic mesoderm. Development 134, 3155–3165. https://doi.org/10.1242/dev.003665
Rodríguez-Niedenführ, M., Dathe, V., Jacob, H.J., Pröls, F., Christ, B., 2003. Spatial and temporal pattern of Wnt-6 expression during chick development. Anat Embryol 206, 447–451. https://doi.org/10.1007/s00429-003-0322-9
Roy, M.N., Prince, V.E., Ho, R.K., 1999. Heat shock produces periodic somitic disturbances in the zebrafish embryo. Mechanisms of Development 85, 27–34. https://doi.org/10.1016/S0925-4773(99)00039-8
Samarage, C.R., White, M.D., Álvarez, Y.D., Fierro-González, J.C., Henon, Y., Jesudason, E.C., Bissiere, S., Fouras, A., Plachta, N., 2015. Cortical Tension Allocates the First Inner Cells of the Mammalian Embryo. Developmental Cell 34, 435–447. https://doi.org/10.1016/j.devcel.2015.07.004
Sanaki-Matsumiya, M., Matsuda, M., Gritti, N., Nakaki, F., Sharpe, J., Trivedi, V., Ebisuya, M., 2022. Periodic formation of epithelial somites from human pluripotent stem cells. Nat Commun 13, 2325. https://doi.org/10.1038/s41467-022-29967-1
Sasai, Y., Lu, B., Steinbeisser, H., De Robertis, E.M., 1995. Regulation of neural induction by the Chd and Bmp-4 antagonistic patterning signals in Xenopus. Nature 376, 333–336. https://doi.org/10.1038/376333a0

Sasaki, H., 2017. Roles and regulations of Hippo signaling during preimplantation mouse development. Develop. Growth Differ. 59, 12–20. https://doi.org/10.1111/dgd.12335
Sato, Y., Takahashi, Y., 2005. A novel signal induces a segmentation fissure by acting in a ventral-to-dorsal direction in the presomitic mesoderm. Developmental Biology 282, 183–191. https://doi.org/10.1016/j.ydbio.2005.03.007
Sato, Y., Yasuda, K., Takahashi, Y., 2002. Morphological boundary forms by a novel inductive event mediated by Lunatic fringe and Notch during somitic segmentation. Development (Cambridge, England) 129, 3633–44.
Schmidt, C., Christ, B., Maden, M., Brand-Saberi, B., Patel, K., 2001. Regulation of *Epha4* expression in paraxial and lateral plate mesoderm by ectoderm-derived signals. Developmental Dynamics 220, 377–386. https://doi.org/10.1002/dvdy.1117
Schmidt, C., Stoeckelhuber, M., McKinnell, I., Putz, R., Christ, B., Patel, K., 2004. Wnt 6 regulates the epithelialisation process of the segmental plate mesoderm leading to somite formation. Developmental Biology 271, 198–209. https://doi.org/10.1016/j.ydbio.2004.03.016
Schoenwolf, G.C., Garcia-Martinez, V., Dias, M.S., 1992. Mesoderm movement and fate during avian gastrulation and neurulation. Developmental dynamics : an official publication of the American Association of Anatomists 193, 235–48. https://doi.org/10.1002/aja.1001930304
Schofield, R., 1978. The relationship between the spleen colony-forming cell and the haemopoietic stem cell. Blood Cells 4, 7–25.
Schrägle, J., Huang, R., Christ, B., Pröls, F., 2004. Control of the temporal and spatial Uncx4.1 expression in the paraxial mesoderm of avian embryos. Anatomy and Embryology 208, 323–332. https://doi.org/10.1007/s00429-004-0404-3
Schubert, F.R., Mootoosamy, R.C., Walters, E.H., Graham, A., Tumiotto, L., Münsterberg, A.E., Lumsden, A., Dietrich, S., 2002. Wnt6 marks sites of epithelial transformations in the chick embryo. Mechanisms of Development 114, 143–148. https://doi.org/10.1016/S0925-4773(02)00039-4
Schuh, M., 2011. An actin-dependent mechanism for long-range vesicle transport. Nat Cell Biol 13, 1431–1436. https://doi.org/10.1038/ncb2353
Schwarz, Q., Maden, C.H., Davidson, K., Ruhrberg, C., 2009. Neuropilin-mediated neural crest cell guidance is essential to organise sensory neurons into segmented dorsal root ganglia. Development 136, 1785–1789. https://doi.org/10.1242/dev.034322
Selleck, M.A., Stern, C.D., 1991. Fate mapping and cell lineage analysis of Hensen's node in the chick embryo. Development (Cambridge, England) 112, 615–26. https://doi.org/10.1242/dev.063834
Selleck, M.A.J., Stern, C.D., 1992. Evidence for Stem Cells in the Mesoderm of Hensen's Node and Their Role in Embryonic Pattern Formation, in: Bellairs, R., Sanders, E.J., Lash, J.W. (Eds.), Formation and Differentiation of Early Embryonic Mesoderm. Springer US, Boston, MA, pp. 23–31. https://doi.org/10.1007/978-1-4615-3458-7_3
Selleck, M.A.J., Stern, C.D., 1991. Fate mapping and cell lineage analysis of Hensen's node in the chick embryo. Development 112, 615–626. https://doi.org/10.1242/dev.112.2.615
Senthinathan, B., Sousa, C., Tannahill, D., Keynes, R., 2012. The generation of vertebral segmental patterning in the chick embryo. Journal of Anatomy 220, 591–602. https://doi.org/10.1111/j.1469-7580.2012.01497.x

Shaner, N.C., Campbell, R.E., Steinbach, P.A., Giepmans, B.N.G., Palmer, A.E., Tsien, R.Y., 2004. Improved monomeric red, orange and yellow fluorescent proteins derived from Discosoma sp. red fluorescent protein. Nat Biotechnol 22, 1567–1572. https://doi.org/10.1038/nbt1037

Sheng, G., Dos Reis, M., Stern, C.D., 2003. Churchill, a Zinc Finger Transcriptional Activator, Regulates the Transition between Gastrulation and Neurulation. Cell 115, 603–613. https://doi.org/10.1016/S0092-8674(03)00927-9

Shevelyov, Y.Y., Ulianov, S.V., 2019. The Nuclear Lamina as an Organizer of Chromosome Architecture. Cells 8, 136. https://doi.org/10.3390/cells8020136

Shi, J., Chen, Q., Li, X., Zheng, X., Zhang, Y., Qiao, J., Tang, F., Tao, Y., Zhou, Q., Duan, E., 2015. Dynamic transcriptional symmetry-breaking in pre-implantation mammalian embryo development revealed by single-cell RNA-seq. Development dev.123950. https://doi.org/10.1242/dev.123950

Shi, X., Yin, Z., Ling, B., Wang, L., Liu, C., Ruan, X., Zhang, W., Chen, L., 2017. Rho differentially regulates the Hippo pathway by modulating the interaction between Amot and Nf2 in the blastocyst. Development dev.157917. https://doi.org/10.1242/dev.157917

Shin, J.-W., Spinler, K.R., Swift, J., Chasis, J.A., Mohandas, N., Discher, D.E., 2013. Lamins regulate cell trafficking and lineage maturation of adult human hematopoietic cells. Proc. Natl. Acad. Sci. U.S.A. 110, 18892–18897. https://doi.org/10.1073/pnas.1304996110

Shumaker, D.K., Lopez-Soler, R.I., Adam, S.A., Herrmann, H., Moir, R.D., Spann, T.P., Goldman, R.D., 2005. Functions and dysfunctions of the nuclear lamin Ig-fold domain in nuclear assembly, growth, and Emery–Dreifuss muscular dystrophy. Proc. Natl. Acad. Sci. U.S.A. 102, 15494–15499. https://doi.org/10.1073/pnas.0507612102

Shumaker, D.K., Solimando, L., Sengupta, K., Shimi, T., Adam, S.A., Grunwald, A., Strelkov, S.V., Aebi, U., Cardoso, M.C., Goldman, R.D., 2008. The highly conserved nuclear lamin Ig-fold binds to PCNA: its role in DNA replication. The Journal of Cell Biology 181, 269–280. https://doi.org/10.1083/jcb.200708155

Sick, S., Reinker, S., Timmer, J., Schlake, T., 2006. WNT and DKK Determine Hair Follicle Spacing Through a Reaction-Diffusion Mechanism. Science 314, 1447–1450. https://doi.org/10.1126/science.1130088

Siminovitch, L., McCulloch, E.A., Till, J.E., 1963. The distribution of colony-forming cells among spleen colonies. J. Cell. Comp. Physiol. 62, 327–336. https://doi.org/10.1002/jcp.1030620313

Slack, J.M.W., 1983. From Egg to Embryo: Regional Specification in Early Development, 2nd ed. Cambridge University Press. https://doi.org/10.1017/CBO9780511525322

Solovieva, T., Lu, H.-C., Moverley, A., Plachta, N., Stern, C.D., 2022. The embryonic node behaves as an instructive stem cell niche for axial elongation. Proc. Natl. Acad. Sci. U.S.A. 119, e2108935119. https://doi.org/10.1073/pnas.2108935119

Sonnen, K.F., Lauschke, V.M., Uraji, J., Falk, H.J., Petersen, Y., Funk, M.C., Beaupeux, M., François, P., Merten, C.A., Aulehla, A., 2018. Modulation of Phase Shift between Wnt and Notch Signaling Oscillations Controls Mesoderm Segmentation. Cell 172, 1079-1081.e12. https://doi.org/10.1016/j.cell.2018.01.026

Šošić, D., Brand-Saberi, B., Schmidt, C., Christ, B., Olson, E.N., 1997. Regulation of Paraxis Expression and Somite Formation by Ectoderm- and Neural Tube-

Derived Signals. Developmental Biology 185, 229–243. https://doi.org/10.1006/dbio.1997.8561
Spemann, H., 1903. Entwickelungsphysiologische Studien am Triton-Ei. Archiv f\:ur Entwicklungsmechanik der Organismen 16, 551–631. https://doi.org/10.1007/BF02301267
Spemann, H., Mangold, H., 1924. über Induktion von Embryonalanlagen durch Implantation artfremder Organisatoren. Archiv f mikr Anat u Entwicklungsmechanik 100, 599–638. https://doi.org/10.1007/BF02108133
Spratt, N.T., 1947. Regression and shortening of the primitive streak in the explanted chick blastoderm. J. Exp. Zool. 104, 69–100. https://doi.org/10.1002/jez.1401040105
Starr, D.A., Fischer, J.A., 2005. KASH ’n Karry: The KASH domain family of cargo-specific cytoskeletal adaptor proteins. BioEssays 27, 1136–1146. https://doi.org/10.1002/bies.20312
Starr, D.A., Han, M., 2002. Role of ANC-1 in Tethering Nuclei to the Actin Cytoskeleton. Science 298, 406–409. https://doi.org/10.1126/science.1075119
Steinberg, M.S., 2007. Differential adhesion in morphogenesis: a modern view. Current Opinion in Genetics & Development 17, 281–286. https://doi.org/10.1016/j.gde.2007.05.002
Stern, C.D., 2005. Neural induction: old problem, new findings, yet more questions. Development 132, 2007–2021. https://doi.org/10.1242/dev.01794
Stern, C.D., 1993. Avian embryos, in: Stern, C.D., Holland, P.W.H. (Eds.), Essential Developmental Biology. Oxford University PressOxford, pp. 45–54. https://doi.org/10.1093/oso/9780199634231.003.0006
Stern, C.D., Fraser, S.E., Keynes, R.J., Primmett, D.R., 1988. A cell lineage analysis of segmentation in the chick embryo. Development (Cambridge, England) 104 Suppl, 231–44.
Stern, C.D., Ireland, G.W., 1981. An integrated experimental study of endoderm formation in avian embryos. Anatomy and Embryology 163, 245–263. https://doi.org/10.1007/BF00315703
Stern, C.D., Keynes, R.J., 1987. Interactions between somite cells: the formation and maintenance of segment boundaries in the chick embryo. Development (Cambridge, England) 99, 261–72.
Stewart, M.P., Helenius, J., Toyoda, Y., Ramanathan, S.P., Muller, D.J., Hyman, A.A., 2011. Hydrostatic pressure and the actomyosin cortex drive mitotic cell rounding. Nature 469, 226–230. https://doi.org/10.1038/nature09642
Straight, A.F., Cheung, A., Limouze, J., Chen, I., Westwood, N.J., Sellers, J.R., Mitchison, T.J., 2003. Dissecting Temporal and Spatial Control of Cytokinesis with a Myosin II Inhibitor. Science 299, 1743–1747. https://doi.org/10.1126/science.1081412
Streit, A., Berliner, A.J., Papanayotou, C., Sirulnik, A., Stern, C.D., 2000. Initiation of neural induction by FGF signalling before gastrulation. Nature 406, 74–78. https://doi.org/10.1038/35017617
Streit, A., Stern, C.D., 2001. Combined Whole-Mount in Situ Hybridization and Immunohistochemistry in Avian Embryos. Methods 23, 339–344. https://doi.org/10.1006/meth.2000.1146
Strumpf, D., Mao, C.-A., Yamanaka, Y., Ralston, A., Chawengsaksophak, K., Beck, F., Rossant, J., 2005. Cdx2 is required for correct cell fate specification and differentiation of trophectoderm in the mouse blastocyst. Development 132, 2093–2102. https://doi.org/10.1242/dev.01801

Sugiyama, M., Saitou, T., Kurokawa, H., Sakaue-Sawano, A., Imamura, T., Miyawaki, A., Iimura, T., 2014. Live Imaging-Based Model Selection Reveals Periodic Regulation of the Stochastic G1/S Phase Transition in Vertebrate Axial Development. PLoS Computational Biology 10. https://doi.org/10.1371/journal.pcbi.1003957

Swift, J., Ivanovska, I.L., Buxboim, A., Harada, T., Dingal, P.C.D.P., Pinter, J., Pajerowski, J.D., Spinler, K.R., Shin, J.-W., Tewari, M., Rehfeldt, F., Speicher, D.W., Discher, D.E., 2013. Nuclear Lamin-A Scales with Tissue Stiffness and Enhances Matrix-Directed Differentiation. Science 341, 1240104. https://doi.org/10.1126/science.1240104

Tam, P.P.L., Meier, S., Jacobson, A.G., 1982. Differentiation of the Metameric Pattern in the Embryonic Axis of the Mouse. Differentiation 21, 109–122. https://doi.org/10.1111/j.1432-0436.1982.tb01203.x

Tam, P.P.L., Tan, S.-S., 1992. The somitogenetic potential of cells in the primitive streak and the tail bud of the organogenesis-stage mouse embryo. Development 115, 703–715. https://doi.org/10.1242/dev.115.3.703

Till, J.E., McCulloch, E.A., Siminovitch, L., 1964. A stochastic model of stem cell proliferation, based on the growth of spleen colony-forming cells. Proc. Natl. Acad. Sci. U.S.A. 51, 29–36. https://doi.org/10.1073/pnas.51.1.29

Turing, A.M., 1952. The chemical basis of morphogenesis. Philosophical Transactions of the Royal Society of London. Series B, Biological Sciences 237, 37–72. https://doi.org/10.1098/rstb.1952.0012

Van Steensel, B., Belmont, A.S., 2017. Lamina-Associated Domains: Links with Chromosome Architecture, Heterochromatin, and Gene Repression. Cell 169, 780–791. https://doi.org/10.1016/j.cell.2017.04.022

Veenvliet, J.V., Bolondi, A., Kretzmer, H., Haut, L., Scholze-Wittler, M., Schifferl, D., Koch, F., Guignard, L., Kumar, A.S., Pustet, M., Heimann, S., Buschow, R., Wittler, L., Timmermann, B., Meissner, A., Herrmann, B.G., 2020. Mouse embryonic stem cells self-organize into trunk-like structures with neural tube and somites. Science 370, eaba4937. https://doi.org/10.1126/science.aba4937

Venturini, V., Pezzano, F., Català Castro, F., Häkkinen, H.-M., Jiménez-Delgado, S., Colomer-Rosell, M., Marro, M., Tolosa-Ramon, Q., Paz-López, S., Valverde, M.A., Weghuber, J., Loza-Alvarez, P., Krieg, M., Wieser, S., Ruprecht, V., 2020. The nucleus measures shape changes for cellular proprioception to control dynamic cell behavior. Science 370, eaba2644. https://doi.org/10.1126/science.aba2644

Violette, M.I., Madan, P., Watson, A.J., 2006. Na+/K+-ATPase regulates tight junction formation and function during mouse preimplantation development. Developmental Biology 289, 406–419. https://doi.org/10.1016/j.ydbio.2005.11.004

Voiculescu, O., Papanayotou, C., Stern, C.D., 2008. Spatially and temporally controlled electroporation of early chick embryos. Nat Protoc 3, 419–426. https://doi.org/10.1038/nprot.2008.10

von Ebner, V., 1888. Urwirbel und Neugliederung der Wirbelsäule. Sitzungsber Akad Wiss Wien 3, 194–206.

Vorburger, K., Lehner, C.F., Kitten, G.T., Eppenberger, H.M., Nigg, E.A., 1989. A second higher vertebrate B-type lamin. Journal of Molecular Biology 208, 405–415. https://doi.org/10.1016/0022-2836(89)90505-6

Ward, L., Evans, S.E., Stern, C.D., 2017. A resegmentation-shift model for vertebral patterning. Journal of Anatomy 230, 290–296. https://doi.org/10.1111/joa.12540

Wicklow, E., Blij, S., Frum, T., Hirate, Y., Lang, R.A., Sasaki, H., Ralston, A., 2014. HIPPO Pathway Members Restrict SOX2 to the Inner Cell Mass Where It Promotes ICM Fates in the Mouse Blastocyst. PLoS Genet 10, e1004618. https://doi.org/10.1371/journal.pgen.1004618

Wiedermann, G., Bone, R.A., Silva, J.C., Bjorklund, M., Murray, P.J., Dale, J.K., 2015. A balance of positive and negative regulators determines the pace of the segmentation clock. eLife 4, e05842. https://doi.org/10.7554/eLife.05842

Wilhelmsen, K., Ketema, M., Truong, H., Sonnenberg, A., 2006. KASH-domain proteins in nuclear migration, anchorage and other processes. Journal of Cell Science 119, 5021–5029. https://doi.org/10.1242/jcs.03295

Williams, L.W., 1910. The somites of the chick. Am. J. Anat. 11, 55–100. https://doi.org/10.1002/aja.1000110103

Wolf, C.M., Wang, L., Alcalai, R., Pizard, A., Burgon, P.G., Ahmad, F., Sherwood, M., Branco, D.M., Wakimoto, H., Fishman, G.I., See, V., Stewart, C.L., Conner, D.A., Berul, C.I., Seidman, C.E., Seidman, J.G., 2008. Lamin A/C haploinsufficiency causes dilated cardiomyopathy and apoptosis-triggered cardiac conduction system disease. Journal of Molecular and Cellular Cardiology 44, 293–303. https://doi.org/10.1016/j.yjmcc.2007.11.008

Wolpert, L., 1969. Positional information and the spatial pattern of cellular differentiation. Journal of Theoretical Biology 25, 1–47. https://doi.org/10.1016/S0022-5193(69)80016-0

Wong, GeneK., Bagnall, KeithM., Berdan, RobertC., 1993. The immediate fate of cells in the epithelial somite of the chick embryo. Anat Embryol 188. https://doi.org/10.1007/BF00190138

Wong, X., Loo, T.-H., Stewart, C.L., 2021. LINC complex regulation of genome organization and function. Current Opinion in Genetics & Development 67, 130–141. https://doi.org/10.1016/j.gde.2020.12.007

Wood, A., Thorogood, P., 1994. Patterns of cell behaviour underlying somitogenesis and notochord formation in intact vertebrate embryos. Developmental Dynamics 201, 151–167. https://doi.org/10.1002/aja.1002010206

Wymeersch, F.J., Skylaki, S., Huang, Y., Watson, J.A., Economou, C., Marek-Johnston, C., Tomlinson, S.R., Wilson, V., 2019. Transcriptionally dynamic progenitor populations organised around a stable niche drive axial patterning. Development dev.168161. https://doi.org/10.1242/dev.168161

Yamaguchi, M., Yoshimoto, E., Kondo, S., 2007. Pattern regulation in the stripe of zebrafish suggests an underlying dynamic and autonomous mechanism. Proc. Natl. Acad. Sci. U.S.A. 104, 4790–4793. https://doi.org/10.1073/pnas.0607790104

Yaman, Y.I., Ramanathan, S., 2023. Controlling human organoid symmetry breaking reveals signaling gradients drive segmentation clock waves. Cell 186, 513-527.e19. https://doi.org/10.1016/j.cell.2022.12.042

Yanagida, A., Corujo-Simon, E., Revell, C.K., Sahu, P., Stirparo, G.G., Aspalter, I.M., Winkel, A.K., Peters, R., De Belly, H., Cassani, D.A.D., Achouri, S., Blumenfeld, R., Franze, K., Hannezo, E., Paluch, E.K., Nichols, J., Chalut, K.J., 2022. Cell surface fluctuations regulate early embryonic lineage sorting. Cell 185, 777-793.e20. https://doi.org/10.1016/j.cell.2022.01.022

Yoshioka-Kobayashi, K., Matsumiya, M., Niino, Y., Isomura, A., Kori, H., Miyawaki, A., Kageyama, R., 2020. Coupling delay controls synchronized oscillation in the segmentation clock. Nature 580, 119–123. https://doi.org/10.1038/s41586-019-1882-z

Youn, B.W., Malacinski, G.M., 1981. Comparative analysis of amphibian somite morphogenesis: cell rearrangement patterns during rosette formation and myoblast fusion. Development 66, 1–26. https://doi.org/10.1242/dev.66.1.1
Zhao, Z.W., White, M.D., Alvarez, Y.D., Zenker, J., Bissiere, S., Plachta, N., 2017. Quantifying transcription factor–DNA binding in single cells in vivo with photoactivatable fluorescence correlation spectroscopy. Nat Protoc 12, 1458–1471. https://doi.org/10.1038/nprot.2017.051
Zhuang, Y., Shi, X., 2023. Expansion microscopy: A chemical approach for super-resolution microscopy. Current Opinion in Structural Biology 81, 102614. https://doi.org/10.1016/j.sbi.2023.102614